CRANFIELD UNIVERSITY

Amirmasoud Soltani

Low Cost Integration of Electric Power-Assisted Steering (EPAS) with Enhanced Stability Program (ESP)

School of Aerospace, Transport and Manufacturing
Automotive Engineering Centre

PhD
Academic Year: 2013 - 2014

Supervisor: Prof. Francis Assadian
October 2014

CRANFIELD UNIVERSITY

School of Aerospace, Transport and Manufacturing
Automotive Engineering Centre

PhD

Academic Year 2013 - 2014

Amirmasoud Soltani

Low Cost Integration of Electric Power-Assisted Steering (EPAS) with Enhanced Stability Program (ESP)

Supervisor: Prof. Francis Assadian
October 2014

This thesis is submitted in partial fulfilment of the requirements for the degree of PhD

ABSTRACT

Vehicle Dynamics Control (VDC) systems (also known as *Active Chassis systems*) are mechatronic systems developed for improving vehicle comfort, handling and/or stability. Traditionally, most of these systems have been individually developed and manufactured by various suppliers and utilised by automotive manufacturers. These decentralised control systems usually improve one aspect of vehicle performance and in some cases even worsen some other features of the vehicle.

Although the benefit of the stand-alone VDC systems has been proven, however, by increasing the number of the active systems in vehicles, the importance of controlling them in a coordinated and integrated manner to reduce the system complexity, eliminate the possible conflicts as well as expand the system operational envelope, has become predominant. The subject of **Integrated Vehicle Dynamics Control (IVDC)** for improving the overall vehicle performance in the existence of several VDC active systems has recently become the topic of many research and development activities in both academia and industries

Several approaches have been proposed for integration of vehicle control systems, which range from the simple and obvious solution of networking the sensors, actuators and processors signals through different protocols like CAN or FlexRay, to some sort of complicated multi-layered, multi-variable control architectures. In fact, development of an integrated control system is a challenging multidisciplinary task and should be able to reduce the complexity, increase the flexibility and improve the overall performance of the vehicle.

The aim of this thesis is to develop a low-cost control scheme for integration of Electric Power-Assisted Steering (EPAS) system with Enhanced Stability Program (ESP) system to improve driver comfort as well as vehicle safety. In this dissertation, a systematic approach toward a modular, flexible and reconfigurable control architecture for integrated vehicle dynamics control systems is proposed which can be implemented in real time environment with

low computational cost. The proposed control architecture, so named “Integrated Vehicle Control System (IVCS)”, is customised for integration of EPAS and ESP control systems.

IVCS architecture consists of three cascade control loops, including high-level vehicle control, low-level (steering torque and brake slip) control and smart actuator (EPAS and EHB) control systems. The controllers are designed based on Youla parameterisation (closed-loop shaping) method. A fast, adaptive and reconfigurable control allocation scheme is proposed to coordinate the control of EPAS and ESP systems. An integrated ESP & ESP HiL/RCP system including the real EPAS and Electro Hydraulic Brake (EHB) smart actuators integrated with a virtual vehicle model (using CarMaker/HiL®) with driver in the loop capability is designed and utilised as a rapid control development platform to verify and validate the developed control systems in real time environment.

Integrated Vehicle Dynamic Control is one of the most promising and challenging research and development topics. A general architecture and control logic of the IVDC system based on a modular and reconfigurable control allocation scheme for redundant systems is presented in this research. The proposed fault tolerant configuration is applicable for not only integrated control of EPAS and ESP system but also for integration of other types of the vehicle active systems which could be the subject of future works.

Keywords:

Integrated vehicle Dynamics Control, Control Allocation, Reconfigurable & Fault tolerant control system, Youla parameterisation, Multi-layer control architecture, daisy-chain method, EPAS control system, ESP control system, Wheel slip control system, HiL simulation and validation.

ACKNOWLEDGEMENTS

I would like to express my sincerest gratitude to my supervisor, Professor Francis Assadian, who has been instrumental to me throughout this project. He has forever changed my life, and I cannot begin thank him enough for his help and support. I hope that I can one day reciprocate the liveliness, enthusiasm and supportiveness that Professor Assadian has shown to me. This project would not have been possible without him.

I feel very fortunate to have been given the opportunity to work closely with Dr. Sajjad Fekriasl. I have learned so much from Sajjad's remarkable knowledge and experience on control system theory and design.

I must also extend my thanks to all of the staff within the Automotive Engineering Centre, particularly the Phd and Msc students who have worked with me over the past couple of years. Many thanks to MSc student, Carlos Moralles, whose hardworking and support have come to value with the implementation of HiL.

A special thanks to Ali Al-Safi and Tracy Al-Safi for donating their time in assisting with editing and proofreading this thesis,

Finally to my family. My kind and wonderful wife, Tayebe, who has been without a doubt my greatest and strongest support. There are no words that can truly convey my love and thanks to her. Without her, none of this would have been achievable, and I am so lucky to have been able to count and depend on her. To my three daughters, Somaye, Zahra and Sara and my sons-in-law, Farhad and Adam for their kindness and understanding, and who always managed to raise my spirits when I was feeling down.

I dedicate this thesis in loving memory of my mother, Mansoureh.

I miss you and love you dearly.

TABLE OF CONTENTS

LIST OF FIGURES

LIST OF TABLES

LIST OF EQUATIONS

LIST OF ABBREVIATIONS

A

ABS	Anti-Lock Brake System
ADAS	Advanced Driver Assistance Systems
AFS	Active Front Steering
IVCS	Advanced Global Chassis Control
ARC	Active Roll Control

B

BBW	Brake By Wire

C

CA	Control Allocation
CAN	Controller Area Network

D

DoF	Degrees of Freedom

E

ECU	Electronic Control Unit
EHB	Electro Hydraulic Brake
EPAS	Electric Power-Assisted Steering
ESP	Enhanced Stability Program

H

HiL	Hardware in the Loop
HPAS	Hydraulic Power-Assisted Steering
HMI	Human Machine Interface

I

IVCS	Integrated Vehicle Control System
IVDC	Integrated Vehicle Dynamic Control

M

MBD	Model Based Development
MiL	Model in the Loop
MIMO	Multi Input Multi Output

O

OEM	Original Equipment Manufacturer

P

PRM	Process Reference Model

R

RCP	Rapid Control Prototyping
RHP	Right Half s Plane, including the imaginary axis
RTI	Real Time Interface

S

SBC	Sensotronic Brake Control
SBW	Steer By Wire
SIG	Automotive Special Interest Group
SiL	Software in the Loop
SISO	Single Input Single Output
SUD	System Under Development

T

TCS	Traction Control System

V

VDC	Vehicle Dynamics Control

1 Introduction

Among several existing systems in today's vehicles, the *Vehicle Dynamics Control (VDC) systems* (also known as *Active chassis systems* systems), such as EPAS, ABS, ESP, ARC, etc., are mechatronic systems developed to improve the vehicle dynamics behaviour during different driving conditions. These control systems receive inputs from several sources (such as driver, road and environment); measure the vehicle motion states (through sensors measurement or by estimation); and generate appropriate commands to the chassis control smart actuators to improve vehicle comfort, handling, manoeuvrability and/or stability. Because of current advancement in automotive ECUs, sensors and actuators technologies, the cost of embedded systems in vehicles is continuously reducing, meanwhile their performance is improving. Subsequently, the numbers of chassis control systems utilised in the vehicles (even in the low-cost vehicles) are growing fast in recent years (Heißing & Ersoy, 2011).

Traditionally, most of the vehicle active systems are individually developed and provided to the automotive manufacturers from different suppliers. Although the benefit of the stand-alone VDC systems has been proven (Robert Bosch GmbH, 2011), however, by increasing the number of the embedded systems in vehicles, the importance of controlling them in a coordinated and integrated manner to reduce the system complexity, eliminate the possible conflicts as well as expand the system operational envelope, become predominant. The subject of **Integrated Vehicle Dynamics Control (IVDC)** for improving the overall vehicle performance in the existence of several VDC active systems has recently become the topic of many research and development activities in both academia and industries (Yu, Li, & Crolla, 2008).

This dissertation is aimed at proposing a systematic approach for development of a "low-cost", coordinated and reconfigurable IVDC system. Here, "low-cost" refers to low "processing" cost, so the aim is to design an integrated control system that could be executed in real time by employing low cost processor (ECU). The proposed integrated control system has several interesting features

such as flexible, modular, coordinated, adaptive, reconfigurable and fault-tolerant. Flexible means the proposed control architecture is not limited to any specific control design method. It is possible to employ various (linear or nonlinear) control design methods in each control loop in a systematic approach. Modular means the proposed control architecture is not limited to any specific actuators and/or control objectives. It provides a flexible framework for designing several customised IVDC systems within the existing (general) architecture. Coordination refers to the possibility of controlling of all the available actuation resources towards the same overall control objectives, while (active) fault-tolerance is the property of the control system that ensures control objectives are best achieved even in case of some of the actuators failure (Wang, 2007). Last but not least, adaptive means the control system could be adjusted for better performance if some external conditions such as road surface coefficient of friction are changed.

To prove this concept, the proposed control architecture is customised for integration of two stand-alone VDC systems, namely EPAS and ESP. The system objective is to provide driver comfort as well as vehicle safety. Several high-level and Low-level control loops are designed based on Youla-Parameterisation (closed-loop shaping) method. A fast control allocation algorithm based on the daisy-chain method is proposed for steering and brake allocation. Performance of the designed control system is validated through simulation in each design stage. To validate the performance of the integrated control system in real time environment, a Hardware-in-the-Loop (HiL) system is designed and developed. The integrated EPAS & ESP HiL configuration includes real steering and brake actuators in conjunction with a virtual high fidelity real time vehicle model (run in a dSPACE ds1006 simulator), real driver in the loop, and dSPACE MicroAutoBox as rapid control prototyping platform. The proposed control architecture is implemented in real time and its performance is validated through HiL testing.

In this chapter, the project motivations, the research goals, contributions, an outline of the dissertation as well as the literature survey are presented.

1.1 Motivation

Increasing the number of vehicle dynamics active systems, at times, make the vehicle essentially redundant (or over-actuated). This means that the available control authorities are more than the number states that are intended to be controlled (Oppenheime, Doman, & Bolender, 2006, June). For example, it is possible to alter the vehicle yaw rate (i.e. one controlled state) by either (front) steering and/or (individual) braking actuations (i.e. five independent actuators). The system redundancy makes the control system design more complex and the standard SISO control design methods are not directly applicable (Bodson M. , 2002). Existence of redundancy in the system could cause some conflict among actuators or might degrade the performance of the system, which is not suitable. However, if the redundant actuators could be exploited in a coordinated manner, over-actuation can offer the opportunity to improve safety, reliability and performance of the system (Zhang & Jiang, 2008).

The systematic approach to deal with the control of (linear or nonlinear) systems with redundant and constrained actuation, so called “Control Allocation” (CA), is a relatively new subject of research and originated from aircraft and marine vessel control system design (Johansen & Fossen, 2012). The modularity of design scheme, flexibility of using control design method and the possibility of considering actuators dynamics and constraints make the control allocation a very powerful, practical and promising approach in control design problem of over-actuated systems. There has recently been increasing interest in application of control allocation methodologies in design of complicated automotive control systems such as integrated vehicle dynamics systems (Wang & Longoria, 2006) or hybrid (electric) vehicles (Yu, Zinger, & Bose, 2011).

To implement the control allocation scheme for achieving overall IVDC objectives, one should consider several factors such as, the nonlinear and complex behaviour of tyre forces, environmental parameters changes (mainly road-tyre coefficient of friction), and actuators dynamics and constraints. A well-designed control allocation scheme could provide several benefits to an IVDC

system. It results in a coordinated usage of all the available actuation resources that could improve the overall vehicle dynamic performance. The control allocation scheme could be designed reconfigurable to make the system fault tolerant in case of the actuator failure/degradation. Moreover, it is possible to employ adaptive algorithms in CA scheme to consider system parameters changes (such as road conditions), which make the CA scheme more attractive for implementation in vehicle. In theory, control allocation can reach to an optimal solution, but usually with numbers of iterations (Bodson M. , 2002). Therefore, real time implementation of control allocation for practical applications is a challenging task (Johansen & Fossen, 2012).

1.2 Research Goal

By assuming the presence of several vehicle dynamic smart actuators in a vehicle, the objective of an IVDC system is to improve vehicle handling, manoeuvrability, and/or stability through optimum utilisation of the actuators in a coordinated manner (Yu, Li, & Crolla, 2008, September). The goal of the research is to develop a low-cost, integrated, adaptive and reconfigurable control system to utilise all the available actuation resources, namely, tyre lateral and longitudinal forces, in a coordinated manner to meet the integrated vehicle dynamic control objectives. In the present thesis, it is assumed that Electric Power-Assisted Steering (EPAS) and independent four-wheel brake (EHB) module are the existing actuators in the vehicle. More specifically, the integrated steering and brake control system objectives are defined as follow:

- providing driver comfort in normal driving conditions;
- improving vehicle handling in mild stability condition and
- maintaining vehicle stability in severe stability (tyre saturation) condition.

The control system should be executable in real-time environment with low computational cost, which would be suitable for implementation in vehicle.

Development of the proposed system is based on well-accepted Model Based Design (MBD) approach and V development process (VDI 2206, 2004) which is one of the most widely acceptable approaches for developing mechatronic

systems (Isermann R. , 2005). It consists of several seamless steps (and feedbacks) starting from requirement definition and ending up with field tests and validation on the vehicle. By considering the fact that IVDC systems are essentially over-actuated, a modified V process to include CA scheme for over-actuated systems is presented in this thesis.

By adopting the newly proposed modified control design process, a multilayer hierarchical control structure consists of target generator, high level controllers, control allocation, low level controllers, smart actuators controllers and a supervisory control system is presented. To prove the concept, the proposed general multilayer control structure is customised for the case of lateral motion control in the presence of steering and brake smart actuators (EPAS and EHP systems).

The high-level (vehicle dynamics) and low-level (smart actuators) control loops are designed based on Youla parameterisation approach, which leads to several simple yet robust controller systems. A fast, adaptive daisy-chain control allocation scheme is proposed to effectively allocate the high level forces and torque demand to low level smart actuators (here steering and brake) in a coordinated and reconfigurable manner.

As an integral part of the seamless V design process, the stability and performance of the designed control system should be validated in each step through various Model in the Loop (MiL) and Hardware in the Loop (HiL) testing. Therefore, an integrated steering and Brake HiL setup/ test rig with driver-in-the-loop capability is designed and implemented. The HiL test results of the proposed integrated control system, confirms the expected performance of the IVDC system (in a real time environment) and present improvements on the system operational envelope even under adverse driving conditions.

This research is focused on design and validation of an integrated control system, so the required inputs to the system including vehicle motions (yaw rate and sideslip), tyre-road friction coefficient, tyre slip and self-aligning moment are assumed available through (sensors) measurement and/or estimation (see (Ahn, Peng, & Tseng, 2012; van Zanten A. , 2000; Hsu Y. , 2009) for example).

1.3 Mechatronic Systems Development

As a result of increasing the number and the capabilities of microprocessors, sensors and actuators that are being embedded in most of today's engineering systems (so called mechatronic systems), the functionalities, complexities and level of integration of these products evolve considerably. Development of mechatronic systems is a complicated multidisciplinary task and often requires contribution from diverse technical disciplines. In a systemic approach to product development process, the product considered as a system encompasses three domains, namely, 'product', 'process' and 'organisation' (Eppinger & Salminen, 2001). The *product* is described as the final outcome of the development; the *process* refers to the whole chain of activities related to the product development; and the *organisation* denotes all the organisational infrastructures engaged in the development process. A successful development is performed based on the synthesis and managing each individual domain as well as their interactions. To deal with the complexity of the system, the systemic approach to development includes decomposition of the system into several sub-systems with respect to these three domains

The *Product* could be considered as a hierarchical composition of several sub-systems, and these in turn may be further composed of sub-assemblies and/or components (Eppinger & Salminen, 2001). For example, a vehicle is a product comprising of several sub-systems such as chassis, powertrain, body, infotainment and so on. The chassis sub-system, in turn, is a composition of several sub-systems like steering, brakes, wheels, suspension. Traditionally the chassis sub-systems are comprised of several mechanical components with a few interactions between them, whereas, the modern vehicle dynamic active systems are complex integrated systems consisting of several hardware, software, microprocessors and mechanical components.

The *process* refers to the whole chain of development activities and comprises of several stages such as idea generation, prototyping, commercialising, and production, etc. Each stage could be hierarchically decomposed into phases or sub-processes and then into tasks, activities and work units in the lowest level.

Finally, the product development *organisation* is decomposed into teams (within the company's boundary or among several collaborating companies such as Original Equipment Manufacturers (OEMs) and Suppliers and these in turn may be further decomposed into working groups and individual assignments (Eppinger & Salminen, 2001).

It is clear that these three domains are strongly interrelated to each other in any product development project; however, we focus mainly on the product and process aspects of the development in this dissertation. We also should emphasise that in the product lifecycle, the process of prototype development is clearly distinct from the product development for mass production (Aslaksen & Belcher, 1992). The aim of this dissertation is to propose a new low-cost concept for integration of Electric Power Assist Steering (EPAS) with Enhanced Stability Program (ESP) systems and to prove it through prototyping and Hardware in the Loop (HIL) testing, so we only consider the relevant process, methods and tools in this research.

Model Based Development (MBD), formulated as V-model, is one of the well-known and widely accepted systemic approaches to product development considering the product and process domains. (Aslaksen & Belcher, 1992). The V-model probably originates from system engineering and software development; however, this approach was adopted for mechatronic product development (Isermann R. , 2008; VDI 2206, 2004) as well as for development of automotive embedded systems (Nazareth & Siwy, 2013). The V-model addresses tree main steps toward product development including *System Decomposition*, *System Implementation* and *System Integration* as shown schematically in Figure 1-1 (Holtmann, Meyer, & Meyer, 2011). The process consists of several feedback loops, such as Model-in-the-Loop (MIL), Software-in-the-Loop (SIL) and Hardware-in-the-Loop (HIL), to reduce the development time and cost by ensuring that the verification and validation are taking place in the early stages of development (Bringmann & Krämer, 2008).

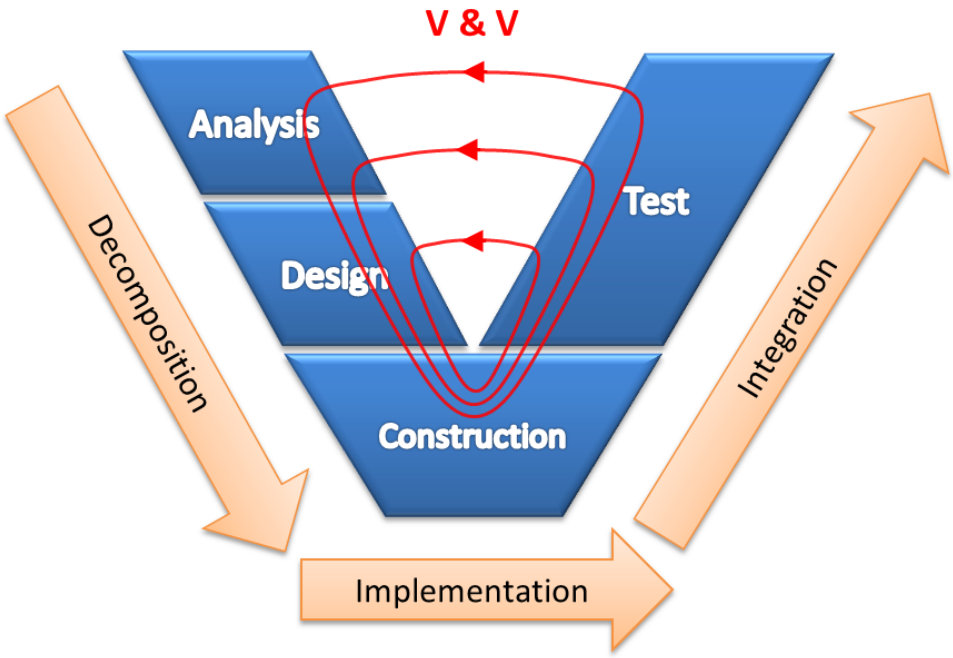

Figure 1-1: The V-Model (Holtmann, Meyer, & Meyer, 2011)

Recently, the consensus of the car manufacturers within the Automotive Special Interest Group (SIG) initiated the "Automotive SPICE® Process Reference Model (PRM)" in which ten engineering processes are defined as essential steps towards an automotive embedded system development (Automotive SIG, 2010). These engineering steps have been studied and represented graphically on a V-model diagram for the automotive systems having software and hardware sub-systems (Holtmann, Meyer, & Meyer, 2011). In this dissertation, we propose a modified version of the V-model for development of integrated control systems with emphasis on control allocation for redundant systems.

1.3.1 System decomposition

The development process starts with the *analysis* phase and is then followed by the *design* phase (see the left part of the V-model in Figure 1-1). The development process starts with abstract and textual descriptions of the requirements, followed by translating them into technical specifications and then continues with detailed model-based system engineering design solutions (Nazareth & Siwy, 2013).

1.3.1.1 System Analysis

In the system analysis phase, the functional and non-functional requirements of the system are specified and then translated into technical specifications. According to the Automotive SPICE® RPM, the system analysis phase consists of the *requirement elicitation* and the *requirement analysis* steps (Automotive SIG, 2010).

The requirement elicitation (which is also referred to as *customer requirements*) is a textual documentation of the system behaviour extracted from customer's needs and requirements analysis (Automotive SIG, 2010). The requirements are usually written in natural language and consist of two types of documents: the *functional requirements* which define the system anticipated functionalities and the *non-functional requirements* which define how these functionalities are expected to be performed. The non-functional requirements are the system qualitative behaviours such as price, fault tolerant, flexibility, robustness, scalability and so on (Glinz, 2007, October).

The requirements analysis (also referred to as *System Specification*) is the process of translating the customer requirements into a set of technical specifications that will guide the design of the system (Automotive SIG, 2010). The requirements are usually written in an informal language (what the user expects from the system) whereas the specifications are written in more formal and technical language and sometimes contain references to the standards and engineering norms (Loucopoulos & Karakostas, 1995).

1.3.1.2 System design

System Design is a systematic process by which a technical solution for the system under development (SUD) is derived to satisfy the specified requirements (Ertas, 1996). The output of the design phase is being used in the system implementation and integration phases whereas the system specifications and requirements are being used for system validation and verification.

There are several methodologies that have been proposed for the design process of a system (Ertas, 1996). VDI 2206 is a widely-accepted guideline (including design stages) for mechatronic system development (VDI 2206, 2004) and Automotive SPICE® Process Reference Model (RPM) is a procedure developed by a joint group of top automotive manufacturers to unify and evaluate the process of embedded system development among automotive industries (Automotive SIG, 2010). The using of Model Based Development (MBD) methodology together with the V-model development process is a well-accepted approach for control system development (Nicolescu & Mosterman, 2010). In the MBD approach, the mathematical formulation of the system dynamics are modelled and represented graphically in order to provide a common environment across different engineering disciplines, which lead to a simplified and more efficient design process. Moreover, the low-level machine codes can be seamlessly generated from the models causing a dramatic reduction in time and cost required for system implementation and testing.

By taking the Model-Based development approach, a modified V-model for control system design of redundant systems is proposed in this dissertation. The proposed design process consists of five main steps and several feedback loops as shown in Figure 1-2.The main steps towards designing a (redundant) control system are as follow:

1. System architectural design
2. System modelling
3. High-Level Control Design
4. Control Allocation
5. Low-Level Control Design

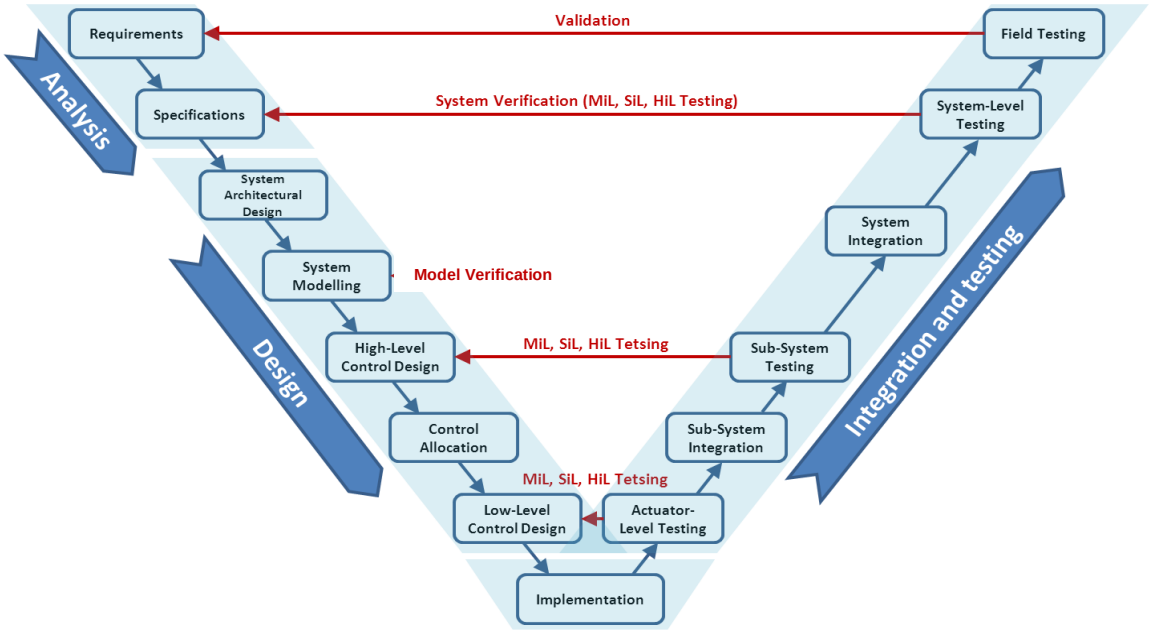

Figure 1-2: : V-model for redundant system control system design

By considering the final product as a controlled plant (here, a vehicle), which has been equipped with several sensors, actuators and controllers, the purpose of the *system architectural design* is to define the main building blocks of the control system, design the system topology, specify the control logics among them and assign each block's functionalities based on the system specifications (Gordon, Howell, & Brandao, 2003).

In the *system modelling* step, the conceptual and mathematical representations of the system dynamics are derived. The system modelling is the key step in model-based design (MBD) approach. To deal with the model complexity, the system dynamics could be decomposed into several hierarchical layers: the top layer is the (linear or non-linear) model of plant dynamics and the (linear or non-linear) models of actuators dynamics located in the following sub-layers. The accuracy of the derived models shall be verified by analysing the simulation results before using these models in the next control development stages (Bringmann & Krämer, 2008).

The purpose of the *high-level control development* is to design a feedback control law to make the top level model (plant dynamics) output track the desired reference value asymptotically. The output of the high-level controller is

a set of virtual force and moments without specifying how to generate them through the actual redundant actuators. In other word, to design the high-level control, the rigid body plant dynamics is considered and any actuator (low-level) dynamics is ignored.

In the real world these forces and moments are not generated directly, but through several actuators and effectors equipped in the system. Effectors are mechanical devices that can be used in order to generate time-varying mechanical forces and moments on the mechanical systems. Actuators are electromechanical devices that are used to control the magnitude and/or direction of forces and moments generated by the individual effectors (Johansen & Fossen, 2012). In case of system redundancy (i.e. the number of the available actuators is greater than the number of the generalised forces and moments intended to be controlled in the high-level control) a *Control Allocation (CA)* scheme can be employed to optimally distribute the virtual forces and moments in to each available actuator considering both actuation amplitude and rate constraints.

By assuming the output of control allocation as a reference for each of the available actuators and by considering the actuator dynamics, a control law is employed such that for any smooth reference path, the output of the low-level controllers will track the reference values asymptotically.

1.3.2 System integration and testing

The Integration phase will take place after the completion of the design phase and can be defined as the process of incorporating the subsystems and components in order to satisfy the requirements and specifications given at the initial stages of the development process. The system integration steps can be considered as the opposite direction of the system decomposition (see Figure 1-1). The integration strategies are mainly formalised in the system architectural design stage. A well-designed integrated system is a complex system with high-level interactions between the sub-systems in comparison to a simple parallel architecture in which the active systems are working with several stand-alone controllers. Integration can provide several benefits such as

performance improvement, conflict reduction, fault tolerant capabilities, system flexibility, adaptation and cost reduction (Gordon, Howell, & Brandao, 2003). There are many different ways through system integration, but in general they can be categorised into two main approaches as follows (Isermann R. , 2008; Koehn, Eckrich, Smakman, & Schaffert, 2006):

- *Hardware integration* is referring to a range of engineering solutions that could lead the existing sensors, actuators and microcontrollers to become more centralised, more accessible to all the system or more embedded into the mechanical process (Koehn, Eckrich, Smakman, & Schaffert, 2006). The Integration of the microprocessor with sensor lead to smart-sensors development, and integrated microcontroller and actuator are referred as smart-actuator (Isermann R. , 2008). Electrical signals integration can be performed through several well-established network communication protocols such as CAN, LIN or FlexRay buses (Leen & Heffernan, 2002).
- *Software integration* is a broad subject referring to the integration of functional objectives, control authorities, decision making, and information processing (Isermann R. , 2008). The main goal of the system functional integration is to achieve the desired global tasks through coordinated control of all the available sub-systems/resources (Wang, 2007). Functional integration is the most important and obvious stimulus for chassis control system integration (Koehn, Eckrich, Smakman, & Schaffert, 2006). The *control integration* is referring to the various methods of designing integrated control systems which could be achieved by employing advance linear or nonlinear control law designs, and it may include the solution for the control tasks integration such as control allocation, control optimisation, control adaptation or rule based decision making algorithms. Integration of information processing is the other potential field of integration in which the required information for the system operation are provided through different algorithms such as on-line state estimation, state recognition or fault diagnosis as shown in Figure 1-3) (Isermann R. , 2008).

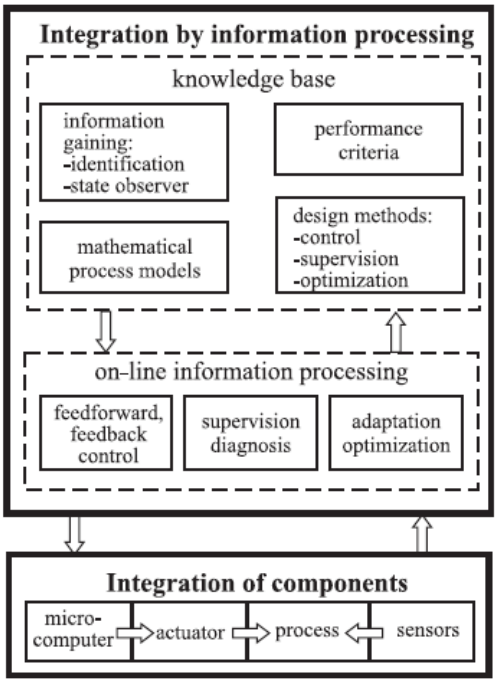

Figure 1-3: Integration of mechatronic systems: Hardware Integration and Software Integration (Isermann R. , 2008)

The Model Based Development process incorporates several feedback loops during the system integration phase as shown in Figure 1-2. The objective of these tasks, so called, Verification and Validation (V&V), is to test out the System under Development (SUD) to ensure the control system is designed correctly (i.e. meet the specifications) and also the customer requirements are satisfied (Aslaksen & Belcher, 1992). More specifically, the 'Model in the Loop' (MiL) stands for the off-line simulation and verification of the system models and controllers which are developed at different stages of the design process (see Figure 1-2). The 'Software in the Loop' (SiL) is the real time simulation software codes which are automatically generated from the developed models during the implantation phase; and in the 'Hardware in the loop' (HiL) testing, the plant model and physical components are commanded by control algorithms in a real time test system (Bringmann & Krämer, 2008).

The global structure of the proposed integrated vehicle dynamics control system is presented in the next section and it will be employed for development of an

integrated system based on steering and brake actuation. The development process consists of four main phases of ‘analysis, ‘design’, ‘implementation’, and ‘test’, as described in the section 1.3.1 . More specifically, the *analysis* and *design* phases are discussed in the following sections as well as in Chapters 4, 5, and 6, and the system *implementation* and *testing* phases are discussed in Chapter 7.

1.4 Literature Review

A brief literature survey about stand-alone EPAS systems, stand-alone ESP systems, integrated vehicle dynamics systems and integrated steering and brake systems are presented in this section. More in-depth literature reviews, for different subjects of the research, are also provided in each relevant chapter.

1.4.1 Stand-alone EPAS Systems

Electric Power-Assisted Steering (EPAS) is a smart actuator which provides an electronically controlled superposition of an assisting torque to the vehicle steering system. The main objective of an EPAS is to provide driver comfort by augmenting the steering torque (Burton, 2003) however, recent developments showed that the EPAS could also be employed to enhance the vehicle stability (Kurishige, et al., 2002; McCann, 2000; Motoyama, 2008).

EPAS is working based on steering torque overlay by means of an electric motor attached to the steering column, rack or pinion. “Power Assist” is the main function of an EPAS when it is being utilised to reduce driver steering wheel effort for his/her comfort. The amount of torque assist to be provided is proportional to the driver steering torque input, which is calculated through a characteristic curve[1]. Moreover, the EPAS control system can be designed in such a way that the electric motor provides different steering torque in various driving conditions to improve steering feel, vehicle stability or manoeuvrability (Heißing & Ersoy, 2011). Some of the well-known EPAS functionalities are pointed out in the following paragraphs.

[1] Basic EPAS characteristic curve is very similar to the HPAS boost curve (Heißing & Ersoy , 2011).

Delivering variable steering torque as a function of vehicle speed is one of the earliest functionalities that have been added to the basic assist functionality of the EPAS. To reduce the amount of the provided steering assist when increasing the vehicle speed, the basic EPAS boost curve is extended to accommodate vehicle speed as an additional input to the steering torque look up table (Kim & Song, 2002). This will increase the vehicle damping which helps the driver to keep control of the vehicle at high-speed manoeuvers (Milliken & Milliken, 1995).

In order to improve the overall feel and response of the steering, which is of crucial importance for the driver, two closed loop algorithms, so called, “Active Return” and “Active Damping”, have been proposed and implemented by General Motors (Bitar, Bolourchi, Colosky, Colosky, & Etienne, 1999). These functions take the steering dynamics and friction into consideration. Steering wheel angle, steering wheel angular velocity and the driver steering torque are the feedback signals to the algorithms. The aim of active return algorithm is to compensate internal friction (or build tolerances) of the steering system which prevent the steering wheel to return to the exact position. The Damping Algorithm prevents the steering “free control” oscillations that usually happen at high vehicle speeds and allows for the steering wheel to come back to centre in a damped way (Badawy, Zuraski, Bolourchi, & Chandy, 1999).

The existence of vehicle networking communicating protocols such as CAN or FlexRay, provide the opportunity of exchanging data between EPAS and other existing vehicle dynamics systems such as ABS, ESP, TCS, and so on. This makes it possible to determine the ideal power assist torque for a given situation by using not only the parameters such as velocity, steering angle, and steering torque, but also by taking into account the other existing vehicle dynamics sensors (such as yaw rate sensor) (Burton, 2003).

The driver receives information from the road via steering wheel haptic feedback (Toffin, Reymond, Kemeny, & Droulez, 2007). For the vehicle equipped with Electric Power-Assisted Steering system, it is possible to provide the driver with much realistic road surface condition information by evaluating

the signal noise associated with certain yaw rates and lateral accelerations within a certain frequency range (through a lead compensator) and transmit this information to the driver (McCann, 2000).

Superimposed steering torque allows the vehicle's dynamic control system to alter steering torque to improve vehicle stability, if a critical driving situation is detected (Yuhara, Horiuchi, Iijima, Shimizu, & Asanuma, 1997; Kurishige, Tanaka, Inoue, Tsutsumi, & Kifuku, 2002). Steering torque overlay is particularly suitable in oversteering situations. In case of forthcoming oversteer, a superimposed steering system can actively reduce the vehicle's steer torque (and angle), thereby decreasing the yaw rate and preventing vehicle spin-out (Liu, Nagai, & Raksincharoensak, 2008). As the tyres have already been saturated in terminal understeer situation, the steering torque (angle) superimposed cannot provide any effective driving improvement in these circumstances.

Having electrically controlled torque on steering enables the implementation of numerous additional functionalities. As an example, EPAS systems can be used to compensate for the negative effects of gust winds on vehicle tracking (Burton, 2003). Electric Power-Assisted Steering system is a vital part of several Advanced Driver Assistance Systems (ADAS) such as lane departure avoidance (Minoiu Enache, Netto, Mammar, & Lusetti, 2009), lane keeping (Ishida & Gayko, 2004, June) or parallel park assist (Fehrenbach, Hoetzel, Tschiskale, & Weber, 2000).

Steer-By-Wire (SBW) systems is the next generation of steering systems in which the steering wheel is mechanically detached from the steering rack and an angle actuator (usually attached to the steering rack) translate the driver's input into a steering motion at the front wheels . To provide the haptic feedback torque to the driver, a separate actuator generates a freely definable torque on the steering wheel (Amberkar, Bolourchi, Demerly, & Millsap, 2004). SBW provides a number of new features and advantages such as increasing packaging freedom, improving passive safety, enabling adjustable steering behaviour and also steering (torque / angle) intervention for vehicle dynamic

control and lane-/road keeping (Yih & Gerdes, 2005). The steering system of the future will be purely electric and will feature full by-wire capabilities, however, due to the fact that the vehicle's steering is a safety critical system, steer-by-wire systems are subject to additional requirements and design challenges with respect to reliability, system monitoring, and fail-safe behaviour (Heißing & Ersoy, 2011).

1.4.2 Stand-alone ESP Systems

Enhanced Stability Program (ESP)[2] is an active system to improve the safety of a vehicle by detecting and reducing loss of handling by application of differential braking between the right and left wheels (Rajamani, 2012). The main task of ESP is to limit the vehicle yaw rate and sideslip in order to prevent vehicle spin (van Zanten A. , 2000). ESP functionality is based on control of tyre longitudinal slip at each individual wheel. ABS (Anti-lock Braking System) was the first commercialised slip control technology (Heißing & Ersoy, 2011). The object of ABS is to provide maximum (straight line) braking force by preventing the wheels from locking during braking. ABS controls the tyre slip by regulating the brake pressure in each wheel. While the ABS aim is to control the slip of each individual wheel, ESP systems can be considered as an advancement of the ABS concept, as its task is to adjust the vehicle's motion if there is a risk of vehicle instability. ESP continuously monitors the vehicle's lateral states (i.e. yaw rate and sideslip) by means of vehicle motions sensors, together with the driver's steering angle input by means of steering wheel angle sensor (attached to the steering column). The vehicle instability situation is detected by comparing the intended (reference) with the actual direction of motion of the vehicle. When ESP detects loss of steering control, it automatically applies brake force (by modulating the brake pressure) to individual wheels to help "steer" the vehicle to the direction that the driver intends to turn, such as the outer front wheel to counter oversteer or the inner rear wheel to counter

[2] Also referred as Electronic Stability Control (ESC), Electronic Stability Program (ESP) or Dynamic Stability Control (DSC)

understeer. The system may also reduce the engine torque, which provides an added stabilisation effect (Robert Bosch GmbH, 2011).

ESP system consists of a hydraulic modulator, a control unit and several sensors[3] which determine and evaluate the driving situation. Conventional ABS and ESP systems have several on/off switching valves to modulate the brake pressure (Robert Bosch GmbH, 2011). In recent years, a new continuous hydraulic modulating system, so called Electro Hydraulic Braking (EHB) system, has been developed by Bosch in which the brake pressure is continuously controlled in each wheel (Robert Bosch GmbH, 2011). The ultimate advancement on brake control technologies will be a completely “dry” braking system, so called Brake-By-Wire (BBW) system, in which the entire hydraulic actuation system is replaced with electro-mechanical actuation system. Employing the electric actuators provide higher actuation bandwidth, more precise control over the tyre longitudinal force, extra braking functionalities as well as lower maintenance cost due to eliminating the hydraulic piping and actuation. Even though electromechanical BBW system has several advantages over traditional hydraulic braking systems, they are not yet employed in series production vehicles due to number of unsolved problems mainly from safety and reliability aspects of the system (Heißing & Ersoy, 2011).

ESP control architecture is a two level cascade control system consisting of a higher level controller and a lower level controller (Rajamani, 2012). In the high level controller the current lateral motions of the vehicle (i.e. the vehicle yaw rate and sideslip) is compared with the desired lateral motion and a desired yaw moment is calculated. The yaw moment which is calculated by the high-level controller is based on Direct Yaw Control (DYC) concept (Shibahata, Shimada, & Tomari., 1993). To achieve the objectives of tracking yaw rate and sideslip angle, several control design methodologies such as sliding mode control (Yi, Chung, Kim, & Yi, 2003; Uematsu & Gerdes, 2002; Mokhiamar & Abe, 2004), Riccati method (van Zanten, Erhardt, Pfaff, Kost, Hartmann, & Ehret, 1996),

[3] The vehicle motion sensors for ESP system consist of a yaw rate sensor, a lateral acceleration sensor, and four wheel speed sensors (Tseng, Ashrafi, Madau, Brown, & Recker, 1999).

model-matching control technique (Nagai, Shino, & Gao, 2002), or H_∞ control system (Hirano, Harada, Ono, & Takanami, 1993) have been proposed in the literatures.

The objective of low level control is to ensure that the desired value of yaw moment (output of the high-level controller) is indeed obtained from the differential braking actuation. It consist of a allocation scheme to relate the total value of the yaw moment to the individual tyre longitudinal force and also an individual wheel slip control law to make sure that the desired longitudinal tyre force is achieved through wheel slip control (van Zanten A. , 2000). Design of a slip control system is a challenging task, because of the complex nature of the tyre behaviours and variable dynamics of the system. Several linear and nonlinear control design approaches have been proposed in the literatures, ranging from linear and nonlinear PID control system (Jiang & Gao, 2001), fuzzy logic (Mauer, 1995), gain scheduling (Johansen, Petersen, Kalkkuhl, & Ludemann, 2003) to some sort of nonlinear methodologies such as sliding mode (Drakunov, Ozguner, Dix, & Ashrafi, 1995) and Lyapunov-based (Savaresi & Tanelli, 2010) control design approaches.

ESP control system relies on several measured signals from the existing sensors and also other values, such as vehicle sideslip angle, vehicle lateral velocity, tyres lateral and normal forces or tyre-road coefficient of friction, which are not readily available. Vehicle estate estimation algorithms are an essential part of any ESP system (Tseng, Ashrafi, Madau, Brown, & Recker, 1999). To estimate the required values, Kalman filter approach has widely been employed (van Zanten, Erhardt, Pfaff, Kost, Hartmann, & Ehret, 1996).

1.4.3 Integrated Vehicle Dynamics Systems

The problem of steering and brake integration can be considered as a special case in the broader subject of integrated vehicle dynamics control systems, whereby increasing the number of ECUs, sensors and actuators in today's vehicle, becomes one of most important topics of research and development in the vehicle industry (Yu, Li, & Crolla, 2008).

Several approaches have been proposed for integration of vehicle control systems which range from the obvious solution of networking the (sensors, actuators, and ECUs) signals through well-known communication protocols such as CAN or FlexRay (Navet & Simonot_Lion, 2008) to some sort of complicated multi-layered, multivariable control architectures (Shladover, 1995; Trachtler, 2004). A multivariable control system is introduced in (Assadian & Aneke, 2006) for integration of active differential and active roll control system and the results were compared with optimisation technique. Fuzzy logic (Karbalaei, Ghaffari, Kazemi, & Tabatabaei, 2007) and rule-based approaches (Smakman, 2000) are among the most popular methods for synchronising of various vehicle dynamic systems (Gordon, Howell, & Brandao, 2003).

In fact, development of an integrated vehicle dynamics control system is a challenging task as it should be able to reduce the complexity, increase the flexibility and improve the overall performance of the vehicle (Gordon, Howell, & Brandao, 2003). From a practical point of view, development of the most integrated control system requires a close collaboration between vehicle manufactureres (so called OEMs) and their suppliers. Therefore, any proposed solution should respect the intellectual property rights of both sides and also make a clear distinction between the roles, responsibilites and deliverables of each party in a joint development process (Navet & Simonot_Lion, 2008). A well organised yet flexible control structure for the integrated vehicle dynamics system can provide good co-ordination between OEM and its suppliers. This would not only reduce the development efforts and prevent probable confilcts, but also could considerably decrease the time and cost of the development process.

Control allocation methodology is a systematic approach towards a coordinated and flexible solution for integration of over-actuated systems (Oppenheimer, Doman, & Bolender, 2011). The control allocation scheme has recently been proposed for solving some automotive control problems such as integrated vehicle dynamics (Laine, 2007) or energy management in electric vehicles (Chen & Wang, 2012). Control allocation performs an optimised and

coordinated employment of all the existing actuation resources (here steering and brake actuators) in an IVDC system that could lead to improve the overall vehicle dynamic performance (Wang & Longoria, 2006). Successful implementation of a control allocation scheme to achieve overall IVDC objectives is a challenging task (Johansen & Fossen, 2012). Vehicle dynamics as well as tyre forces exhibit nonlinear behaviours in stability conditions, which make the control allocation scheme nonlinear (see for example, (Tjønnås, 2008)). Whilst driving, the vehicle parameters, such as tyre normal forces or road-tyre coefficient of friction, are subject to continuous change. It is possible to employ adaptive algorithms in CA scheme to consider system parameter changes. An adaptive control allocation scheme could dynamically allocate the optimum forces to each of the available actuators in different driving conditions, which make the CA scheme more attractive for implementation in vehicles (Davidson, Lallman, & Bundick, 2001, July). The possibility of including actuators dynamics and constraints in control allocation formulation provides a great advantage for this approach, especially in practical applications (Durham, 1993). Moreover, the control allocation scheme could be designed reconfigurable to make the system fault tolerant in case of the actuator failure/degradation (Zhang & Jiang, 2008).

1.4.4 Integration of EPAS and ESP system

A comprehensive literature review on integrated lateral vehicle dynamics control was performed by (Manning & Crolla, 2007). Interestingly, most of the published research on integration of steering and brake to improve vehicle stability are based on AFS system for steering actuation. The reason might arise from the fact that AFS is an *angle* actuator (rather than EPAS, which is a *torque* actuator). Unlike the steering torque input, the relationship between steering angle input and vehicle states output (such as yaw rate, sideslip or lateral acceleration) are straightforward and have been extensively studied in the literatures (Milliken & Milliken, 1995), even for the nonlinear vehicle model in unstable situation (van Zanten, Erhardt, Pfaff, Kost, Hartmann, & Ehret, 1996; Mammar & Koenig, 2002). On the other hand, the transfer function between

steering torque input and vehicle dynamics response (such as yaw rate, sideslip or lateral acceleration) includes the vehicle dynamics, steering dynamics and self-aligning moment feedback to the driver. Moreover, as AFS system provides 2 degrees of freedom on wheel angles actuation (Klier & Reinelt, 2004), it is possible to design a control system that differentiates between steering primary task, so called “path following task”, and its secondary task to stabilise the vehicle, so called “disturbance attenuation task” (Ackermann, 1997). In Electric Power-Assisted Steering, however, any change in steering wheel torque is immediately being felt and reacted to by the driver through his/her neuromuscular dynamics, which will eventually influence vehicle dynamic responses (Pick & Cole, 2003). Because of the complexity of system dynamics, design of the stability control system based on EPAS is more challenging than AFS.

The main drawback on using AFS is in the fact that this additional actuator brings extra cost and complexity to the vehicle, which might be tolerable only for luxury cars. On the other hand, employing EPAS for vehicle stability improvement has no extra (hardware) cost to the vehicle, as the ever increasing number of today’s produced vehicles are being equipped with Electric Power-Assisted Steering system, instead of hydraulic types (Burton, 2003). This important fact about EPAS, makes it attractive as a low cost solution for integrated vehicle stability improvement (and other vehicle assistance systems).

1.5 Research Contribution

This dissertation presents a systematic approach toward development of a flexible and low cost control architecture for integrated vehicle dynamics control systems. To prove the concept, an integrated vehicle dynamics control system for Electric Power-Assisted Steering (EPAS) and Enhanced Stability Program (ESP) systems is designed and validated through simulation and real time HiL testing. The contributions of this research are:

1. Introducing a modified procedure for control design of over-actuated mechatronic systems by comprising the control allocation scheme into standard V design process.

2. Proposing a multi-layer structure for integrated vehicle dynamics control system; including supervisory control, high-level control, control allocation, low-level control and smart actuator control modules, so called IVCS system.
3. Developing a customised version of IVCS system for integration of EPAS with ESP in a coordinated manner to meet the defined vehicle dynamics systems requirements and specifications.
4. Designing of three novel simple yet robust high-level SISO control systems based on Youla-parameterization (closed-loop shaping) method for vehicle planar motions (i.e. longitudinal velocities, lateral velocity, and yaw rate) tracking controls.
5. Proposing an adaptive and reconfigurable control allocation scheme for integration of EPAS with ESP based on daisy-chain method. The solution is fast and could be executed in real time with low processing cost, which is the main advantage of the proposed method over the existing control allocations suggested for IVDC.
6. Designing of a novel low level control system for EPAS based on self-aligning moment feedback, by using Youla-parameterisation method. By assuming that the estimation of self-aligning moment is available, it is possible to control tyre lateral force without a need of knowing tyre slip angle (which is difficult to measure or estimate in practice).
7. Designing of a novel low level brake control system based on wheel slip feedback, by employing Youla-parameterisation method and considering the complete brake system dynamics and constraints.
8. Designing , Developing and implementing an elaborated Hardware in the Loop (HiL) test rig for Rapid Control Prototyping (RCP) and validation of integrated steering and brake control systems, including real driver in the loop coupled with a high fidelity virtual vehicle model (driving simulator).
9. Implementing IVCS system with real EPAS and SBC EHB smart actuators in real time environment rapid control prototyping environment. Validation of the simulation results by experimental test using the hardware in the loop (HiL) facility.

1.6 Dissertation Outline

An introduction and literature review of the research topics were presented in this chapter. The outline of the following chapters is summarised below:

Chapter 2 presents a general multilayer architecture for integrated vehicle dynamic control system (so called IVCS system). Based on the requirement and specification of the system, a customised control structure for integration of EPAS with ESP is proposed.

The relevant mathematical model of the system, including the vehicle model, tyre model, steering and brake dynamics are derived in Chapter 3. The steady state response of the linear vehicle model is being employed for deriving the reference values of the control system. The accuracy of the proposed vehicle model is investigated by comparing with the simulation results of CarMaker® as a validated off-the-shelf high-fidelity vehicle dynamic model.

Chapter 4 discusses the required control theories for design of the proposed control systems. More specifically, system linearisation, MIMO control systems decoupling, performance specification of linear time-invariant SISO control system in frequency domain and closed loop shaping control design method based on Youla parameterisation, are presented. By employing these subjects, the high level closed loop control system for asymptotic tracking of desired vehicle lateral motions are designed and validated by simulation.

Chapter 5 explains the control allocation concepts and implementation. A fast and flexible control allocation scheme for integrated EPAS and ESP system based on daisy-chain method is proposed. The method is capable of executing in real-time environment with low-cost processors. The accuracy, efficiency and advantages of the proposed control allocation scheme is verified by comparing the simulation results with a numerical optimisation solution (interior point method) and also with traditional steering and brake allocation methods.

The design of novel low-level control systems for steering and brake actuation is presented in Chapter 6. More specifically, it consists of a low level control system for EPAS consists of a DC motor (torque) Youla controller, a closed loop

steering torque Youla control system based on self-aligning moment feedback, and an closed loop brake pressure control based on tyre slip feedback for each individual wheel. Moreover, the new EPAS control system to provides driver comfort in normal driving conditions is also presented in this chapter.

Chapter 7 focuses on the HiL design and implementation, as well as the control system validation through HiL testing. The general structure and (hardware and software) components of a HiL system are introduced and then the various steps toward design of the integrated EPAS and ESP HiL system are explained. The developed HiL is then employed for validation of the proposed integrated control system. The validation results are presented at the end of this chapter.

Conclusion and some proposal for future work are put forward in Chapter 8.

2 System Architecture

2.1 Integrated Vehicle Control System (IVCS)

The global chassis control system can be defined as an integrated control system to combine and supervise all controllable sub-systems affecting vehicle dynamic response (Gordon, Howell, & Brandao, 2003). The objective of the system is to provide a means of safe and comfortable driving conditions by controlling the vehicle motion along its six rigid-body Degrees of Freedom (DoF), i.e. three linear motions (longitudinal, lateral and vertical velocities) and three angular velocities (roll, yaw and pitch) as shown in Figure 2-1. To achieve this task, the system should determine the desired motions by considering the driver intent (through steering, brake and accelerator request inputs); observe the vehicle, road and environment conditions and provide the designated global objective (comfort / safety or agility) through utilisation of available vehicle dynamic smart actuators in a coordinated manner.

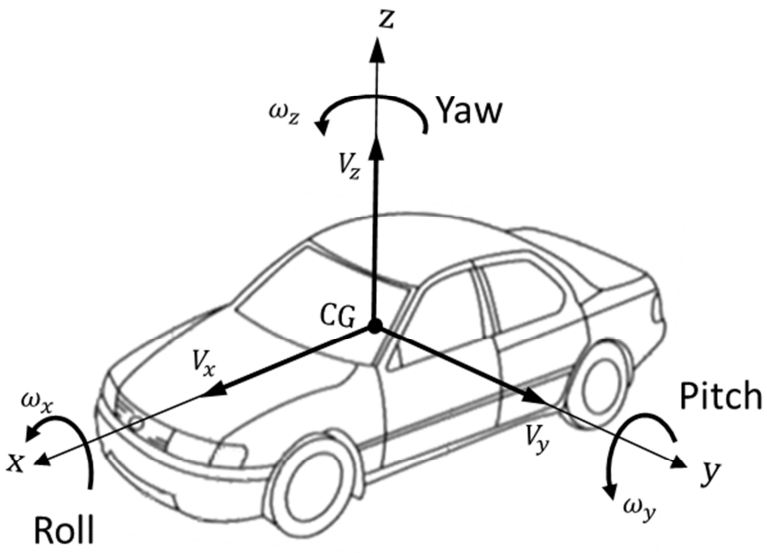

Figure 2-1: Vehicle Axis System (ISO 8855-2011)

2.1.1 IVCS architecture

The objective of the proposed integrated vehicle dynamic control system is providing a functional integration of several existing vehicle dynamic active systems in a coordinated and reconfigurable manner. The system architecture is designed based on a hierarchical multi-layered design approach (Gordon, Howell, & Brandao, 2003) and hereinafter called 'Advanced Global Chassis Control' (IVCS) system.

The IVCS architecture consists of six different layers (Assadian F. , 2012) as shown in Figure 2-2. The system global task is to control all possible linear and angular motions of the vehicle along three spatial directions (x, y and z) in a coordinated manner. The intended vehicle motions are defined in the first layer and provide as reference value to the vehicle dynamic controllers in the lower layers. The system has two functional modes (Safety and Comfort) and based on the driving conditions and vehicle state recognition, it decides to operate in either comfort or safety mode. Having the reference motion values known from the first layer, the high-level vehicle dynamics control task (placed in the third layer), is to derive the appropriate generalised forces and moments along three axes. This forces the vehicle to follow the reference motion path asymptotically. The high-level controller may consists of a set of up to six Single Input Single Output (SISO) vehicle motion controllers (Wang & Longoria, 2006) or several Multi-Input Multi-Output (MIMO) controller as proposed in some literature (Assadian & Aneke, 2006; Horiuchi, Okada, & Nohtomi, 1999; Chen, Xiao, Liu, Zu, & Zhou , 2011). The proposed flexible architecture gives the possibility of changing the number and type of body controllers based on the system global objectives and available actuators. The outputs of the body controllers are the vehicle generalised forces and moments, which are then optimally distributed among several low-level vehicle dynamic controllers in layer 4. The low level control actions are fulfilled through several vehicle dynamics actuators implemented in the vehicle and work in conjunction with vehicle dynamics traditional sub-systems like steering, brake, suspension and so on (layer 5 and 6 in Figure 2-2).

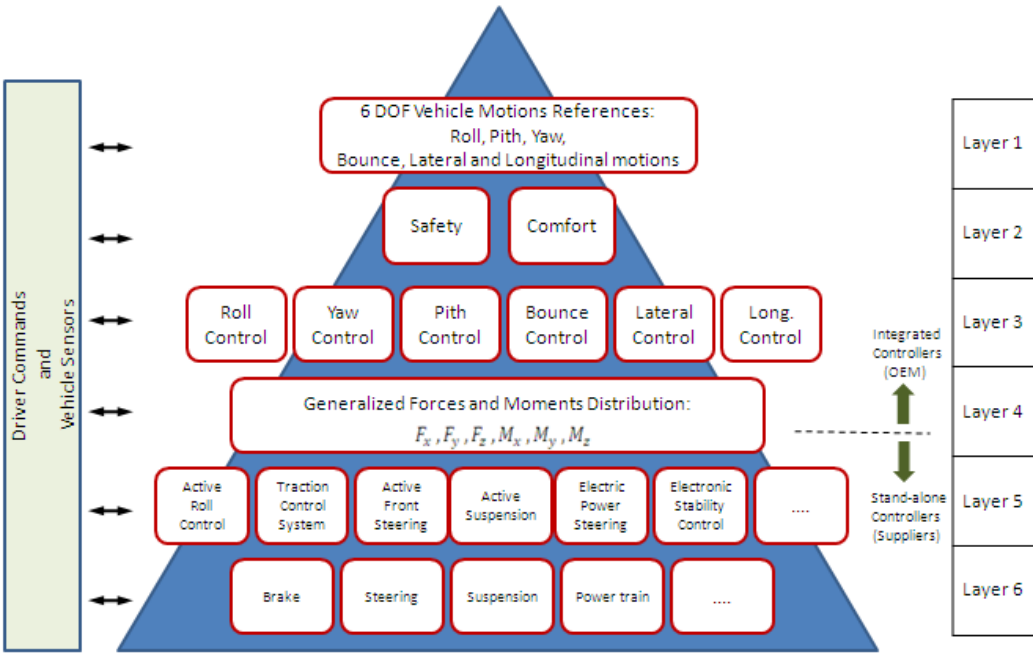

Figure 2-2: Multi-layered Architecture of IVCS system

Detailed description of the IVCS system layers are as follows:

Layer 1. **Driver Evaluator Layer (Vehicle Motion Reference Values):** The objective of a global chassis control system is to provide a means of safe and comfortable driving conditions by controlling the vehicle motions along its 6 spatial DoF, i.e.: roll, pitch, yaw, bounce, longitudinal and lateral velocities. In the first layer, the desired vehicle dynamics behaviours, i.e. the desired values of vehicle linear and angular motions in the direction of x, y and z axes, $\mathbf{x_d} = [V_{x,d} \quad V_{y,d} \quad V_{z,d} \quad \omega_{x,d} \quad \omega_{y,d} \quad \omega_{z,d}]^T$, are defined. The vehicle dynamic behaviour in different driving and environments is one of the important features of a vehicle as the drivers (and passengers) are usually sensitive to it (Gillespie , 1992). While most of the vehicle dynamic behaviours in traditional vehicle dynamic systems are fixed and characterised by the mechanical specifications of the passive sub-systems, using the vehicle dynamics control systems gives the opportunity to modify some dynamic characteristics of the vehicle by altering the control system reference values. The possibility of

shaping the vehicle dynamic behaviour is one of the major advantages of vehicle dynamic active systems over traditional mechanical (passive) systems (Heißing & Ersoy, 2011). Model Reference approach is the most common and acceptable method for defining the vehicle dynamic reference values (Rajamani, 2012; Mokhiamar & Abe, 2004; van Zanten, Erhardt, Pfaff, Kost, Hartmann, & Ehret, 1996) where the dynamic behaviour of an idealised vehicle model is considered as the reference value input to the vehicle dynamic controllers. The desired dynamic behaviour can be obtained by altering some of the vehicle model parameters (such as tyre cornering stiffness), so it can be considered as tuning knobs for vehicle dynamic control system designers.

Layer 2. **Control Mode Decision Layer:** Based on different driving conditions, the task of the IVCS system is defined as providing driver comfort, or providing vehicle safety. The main decision regarding activation of each control mode (safety or comfort) is made based on the vehicle state recognition. In normal driving conditions, the comfort mode is activated. While in severe driving conditions, vehicle safety is the priority. Changing the control mode can be fulfilled by changing the reference values (first layer) and/or control systems in conjunction with some advanced switching techniques to ensure that smooth transition between the controllers will take place (Asarin, Bournez, Dang, Maler, & Pnueli, 2000; Boada, Boada, & Diaz, 2005). The decision mode is fulfilled by recognition of the vehicle state based on the parameters measurement or estimation. Despite the existence of several sensors in today's vehicle to measure the parameters such as vehicle lateral acceleration, longitudinal acceleration, yaw rate, wheel speed and so on; there are some vehicle parameters such as tyre forces, tyre self-aligning moment, tyre-road friction coefficients and vehicle sideslip which their measurements are difficult or unfeasible. Proper algorithms for robust

estimating the vehicle parameters that could not be measured are implemented and employed as virtual sensors in this layer.

Layer 3. **High-Level Controllers Layer (Generalised Forces and Moments Calculation):** The main goal of IVCS system is to control the vehicle motions, $\mathbf{x} = [V_x \quad V_y \quad V_z \quad \omega_x \quad \omega_y \quad \omega_z]^T$, to follow the reference values, $\mathbf{x_d}$, which was set in the first layer. Based on Newton's second law, and by assuming the vehicle as a moving rigid- body, the vehicle motions are directly related to the forces and moments applied to the vehicle's centre of gravity in three axes directions, (see Figure 2-3). The general form of the vehicle dynamic in state space form can be represented as

$$\dot{\mathbf{x}} = \mathbf{f}(\mathbf{x}, t) + \mathbf{g}(\mathbf{x}, t)\,\boldsymbol{\tau} \tag{2-1}$$

$$\mathbf{y} = \mathbf{l}(\mathbf{x}, t) \tag{2-2}$$

where $\mathbf{f}$, $\mathbf{g}$ and $\mathbf{l}$ are functions, t is time, $\mathbf{x} \in \mathbb{R}^{\boldsymbol{n}}$ is the vehicle state vector , $\mathbf{y} \in \mathbb{R}^{\boldsymbol{m}}$ is the output vector that has to be controlled and $\boldsymbol{\tau} \in \mathbb{R}^{\boldsymbol{m}}$ is the input vector of generalised forces and moments at the vehicle's centre of gravity. In a general form, the vector $\boldsymbol{\tau}$ consists of all the forces and moments in three spatial directions,

$$\boldsymbol{\tau} = [F_x \quad F_y \quad F_z \quad M_x \quad M_y \quad M_z]^T \tag{2-3}$$

however, due to several practical reasons such as system cost or actuator limitations, usually some of these forces and moments are chosen to be controlled. The objective of the high-level control law is to calculate the values of the generalised forces and moments, $\boldsymbol{\tau}_c$, which impose the vehicle motion, $\mathbf{x}$, to follow the desired values, $\mathbf{x_d}$. The high-level control law, $\mathbf{k}_{\mathrm{H}}(\mathbf{x}, t)$, can be written as

$$\boldsymbol{\tau}_c = \mathbf{k}_{\mathrm{H}}(\mathbf{x}, t) \tag{2-4}$$

By ignoring the actuator dynamics, it is assumed that the output of the controller , $\boldsymbol{\tau}_c$, is equal to the virtual plant input, i.e. $\boldsymbol{\tau} = \boldsymbol{\tau}_\mathbf{c}$ .The high-level control law could be either a parallel set of up to six close-loop (linear or non-linear) SISO controllers, or several (liner or non-linear) MIMO controller (Gordon, Howell, & Brandao, 2003; Chen, Xiao, Liu, Zu, & Zhou , 2011). The feedback values (vehicle states) for the control loops are provided by real sensor measurements and virtual sensor estimations as well.

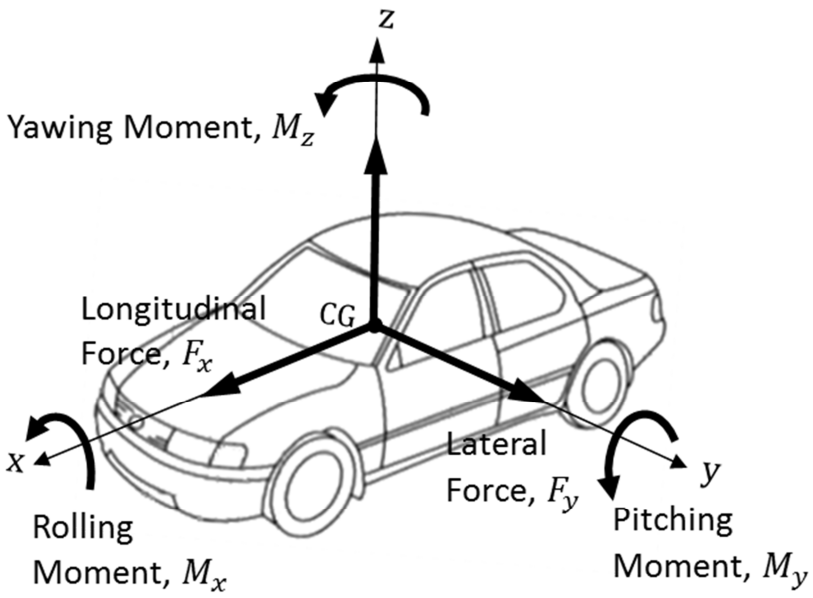

Figure 2-3 Generalised forces and moments on vehicle

Layer 4. Control Allocation Layer: In practice, it is impossible that the generalised forces and moments to be directly applied to the vehicle's centre of gravity. Except the aerodynamic forces, all the forces and moments necessary to control the vehicle are only produced through the road tyre interactions (Jazar, 2008). So the tyres are considered to be the sole vehicle dynamics effectors existing in the vehicle (Johansen & Fossen, 2012). The relation between generalised forces and moments on the vehicle level (body coordinate system) and the forces and moments on the tyre level (tyre coordinate system) can be derived from the vehicle/tyre

kinematic relation (Kiencke & Nielsen, 2005) and could be represented in the form of

$$\boldsymbol{\tau} = \mathbf{B}\mathbf{u} \tag{2-5}$$

where $\mathbf{B} \in \mathbb{R}^{m \times p}$ is the effectiveness matrix, $\mathbf{u} \in \mathbb{R}^{p}$ is the vector of control inputs at the tyre level (actuators input) and p is the number of the available actuators in the system.

To control the magnitude and/or direction of the tyre forces, most of today's vehicles are equipped with several (smart) actuators such as: Electric Power-Assisted Steering (EPAS), Anti-Lock Braking System (ABS), Active Front Steering (AFS), Traction Control System (TCS), Active Suspension and so on. The control allocation can be formulated as follows: given the value of generalised forces and moments, $\boldsymbol{\tau} \in \mathbb{R}^{m}$, and effectiveness matrix , $\mathbf{B} \in \mathbb{R}^{m \times p}$, find the value of actuator control input, $\mathbf{u} \in \mathbb{R}^{p}$. If the matrix $\mathbf{B}$ is square (i.e. $p = m$) and invertible (non-singular), the solution of the above control allocation problem is

$$\mathbf{u} = \mathbf{B}^{-1}\boldsymbol{\tau} \tag{2-6}$$

However, if the number of the available actuators is greater than the number of the controlled states (i.e. $p > m$) the system called redundant (or over-actuated) and the control allocation solution is ill-posed as the inverse of $\mathbf{B}$ is not unique. In case of system redundancy, the objective of control allocation is to find the 'best' way for distributing the generalised forces and moments (output of the previous layer) among several existing smart actuators so that the sum of the forces and moments which are generated by the actuators always be equal to the required generalised forces and moments. The control allocation plays an important role in characterising the overall performance of an integrated vehicle dynamic system (Wang & Longoria, 2006). Several approaches such

as model predictive control (Chang, 2007), optimal control (Härkegard & Glad, 2005), linear optimisation (Oppenheimer & Doman, 2006), nonlinear optimisation (Wang, 2007), artificial neural network and fuzzy rule-based (Gordon, Howell, & Brandao, 2003) methods have been proposed to solve the control allocation problem in recent years. In this dissertation, the vehicle dynamics control allocation is formulated as a constrained linear optimisation problem and a fast and direct solution based on daisy-chain methods (Bodson M. , 2002; Oppenheimer & Doman, 2006) are proposed. The performance and robustness of the proposed method is validated by simulation (MiL) and HiL testing, as explained in Chapter 5 and 7 respectively.

Layer 5. **Low-Level Controllers Layer:** In this layer, the control laws for the existing low-level vehicle dynamic control systems (smart actuators) such as ABS, EPAS, TCS, active suspension and so on, are designed. By considering the optimally distributed values of control input vector, $\mathbf{u}$, as references for each smart actuator controller, the control task for each of these stand-alone active systems is to follow these reference values asymptotically. The control laws may consist of feedback or feed-forward controls considering the actuator dynamics as well as their constraints. In case of closed-loop control, the feedback signals are provided by measurement and/or estimation.

Layer 6. **Smart Actuators Layer:** The vehicle dynamics smart actuators are mechanically attached to the associated traditional vehicle dynamics sub-systems such as steering, brake, suspension, powertrain. Each vehicle dynamic actuator is equipped with its own effectors (so called low-level effectors). These are the electromechanical devices such as electric motor, hydraulic valve that are used for generating or controlling the magnitude or direction of each actuator's forces or moments and controlled by smart actuator controllers. The actuators

controllers placed in the lowest loop in this cascade control system. The actuation references are the low-level values such as force, torque or hydraulic pressure which are calculated from the previous layer and the feedback signals are in most cases provided by each actuator's real or virtual sensors.

2.1.2 Integrated EPAS and ESP system architecture

In the previous section a general form of the IVCS architecture is introduced assuming the control authority over the vehicle's 6 rigid-body motions. However, for several technical and/or economic reasons (such as customer requirement, system cost, actuators availability or actuators physical limitations), most integrated vehicle dynamics control systems are designed to control only some of the vehicle's DoF. The modularity and flexibility of the proposed IVCS system structure enables us to design a customised control system solution based on the required vehicle global features (i.e. system requirements and specifications).

The analysis and design of an integrated control system can be performed based on three different methodologies, namely: Top-down, bottom-up, hybrid approaches (Gordon, Howell, & Brandao, 2003). In a top-down approach, similar to the above described IVCS system, the system requirements are first defined and then the system specification and architecture, including the requisite number and specification of the actuators are designed to meet the requirements. However, in a bottom-up approach the high level requirements and specifications of the system are defined based on the 'pre-determined' number, type and specifications of low-level actuators. In both top-down and bottom-up approaches, it is assumed that each layer is only interacting with its neighbouring layers which in reality are not the case. Because of high degree of interaction among different layers, any practical design would involve a combination of a top-down and a bottom-up approach (so called hybrid approach) (Gordon, Howell, & Brandao, 2003).

In this dissertation, it is assumed that the EHB hydraulic value modulation unit (independent wheel braking) and EPAS (torque assisted front steering) are the

only existing vehicle dynamics actuators in the vehicle. It is further assumed that the mechanical components of the sub-systems have already been designed, so that their mechanical specifications are known and fixed. By these assumptions, and adopting the hybrid design approach, the design objective is limited to the control system development of an integrated vehicle dynamics system with the control authority only on vehicle planar motion. Based on the process presented in section 1.3.1, the development starts with the system requirements and specification definition and then conducted by the system architectural design, which are the subject of the following sections.

2.1.2.1 System Requirements

System Requirements are the textual documentation determined from the customer's needs and requirements. The functional and non-functional requirements of the SUD (in this thesis) are defined as follows:

A: Functional Requirements:

1. *The vehicle is intended to be equipped with EPAS and EHB systems.*
2. *There is no other vehicle dynamic active system that will be added to the vehicle.*
3. *The system should provide a means of driver comfort in case of normal driving conditions.*
4. *The system should provide a means of vehicle safety in case of vehicle instability.*
5. *The system application should cover all the range of driving conditions.*
6. *The only available sensors in the vehicle are those belong to EPAS and EHB systems.*
7. *No other sensor will be added to the vehicle.*

B: Non-functional Requirements

8. *The system should be implemented with Low Cost.*
9. *The system should be Robust against environmental, and vehicle parameters changes.*
10. *The system should be fault tolerant (fail-safe).*

2.1.2.2 System Specifications

System specifications are the translation of requirements into technical terms. By analysing the above-defined system requirements, the technical specifications for the SUD are derived as follows:

1. *The desired vehicle linear and angular motions are derived from steady-state response of a bicycle model.*
2. *The vehicle equipped with EPAS, provides control authority over front tyre self-aligning moment. The vehicle lateral velocity as well as yaw rate should be controlled by altering tyre self-aligning moment through steering system.*
3. *The vehicle equipped with EHB brake intervention system, provides continuous control authority over four lines hydraulic brake pressure.*
4. *Each tyre longitudinal forces should be controlled by means of controlling the corresponding tyre longitudinal slip.*
5. *In case of brake intervention, the vehicle yaw rate should be controlled by individual wheel braking (ESP functionality).*
6. *There is no direct control over vertical, roll and pitch motions.*
7. *In conclusion, the motions for vehicle dynamic control are limited to longitudinal, lateral, and yaw motions, i.e. vehicle planar motion.*
8. *The EPAS will reduce the driver steering wheel torque in normal driving conditions to provide the driver comfort.*
9. *For maintaining driver comfort and also reducing tyre wear, the steering base stability has the priority over the brake base stability in mild stability condition.*
10. *In the situation that the steering based stability is unable to stabilise the vehicle (hazardous stability condition), the brake based stability system (ESP) should be activated and is predominant.*
11. *In case of oversteering situation, the EPAS has to reduce the steering torque accordingly to recover the vehicle stability.*
12. *Because of the front tyre saturation, there is no control authority over steering in terminal understeering situation. Therefore, in terminal understeering situation, the EPAS based stability system will not work.*

13. *The lateral acceleration, longitudinal acceleration, yaw rate, wheel speed, hydraulic brake pressure, vehicle speed, steering column torque and EPAS electric motor current are the available signals provided through the sensor measurements.*
14. *The other required vehicle parameters such as front tyre self-aligning moment, road-tyre coefficient of friction, and vehicle sideslip should be estimated accurately and robustly.*
15. *The integrated control system has to be reconfigurable so the EPAS and EHB can work in a redundant manner to provide fault tolerance.*
16. *The mechanical systems are assumed fixed. In order to reduce the system cost, the control algorithms could be run on inexpensive processors, i.e. need less computational efforts.*
17. *The control system has to be robust against system structured and unstructured uncertainties and adaptive to external parameters (such as road surface coefficient of friction or vehicle parameters) variations.*

2.1.3 System architecture

A customized version of the IVCS system to provide a coordinated control over the ESP and EPAS smart actuators to meet the system specifications is proposed in this section. The system consists of 6 layers similar to general IVCS architecture, however, layer 1 and 2 are placed in *supervisory control* block, layers 3 and 4 are put in *high-level control* block, and layers 5 is sited in *low-level control* block and layer 6 is in the smart actuator control block, as shown in Figure 2-4.

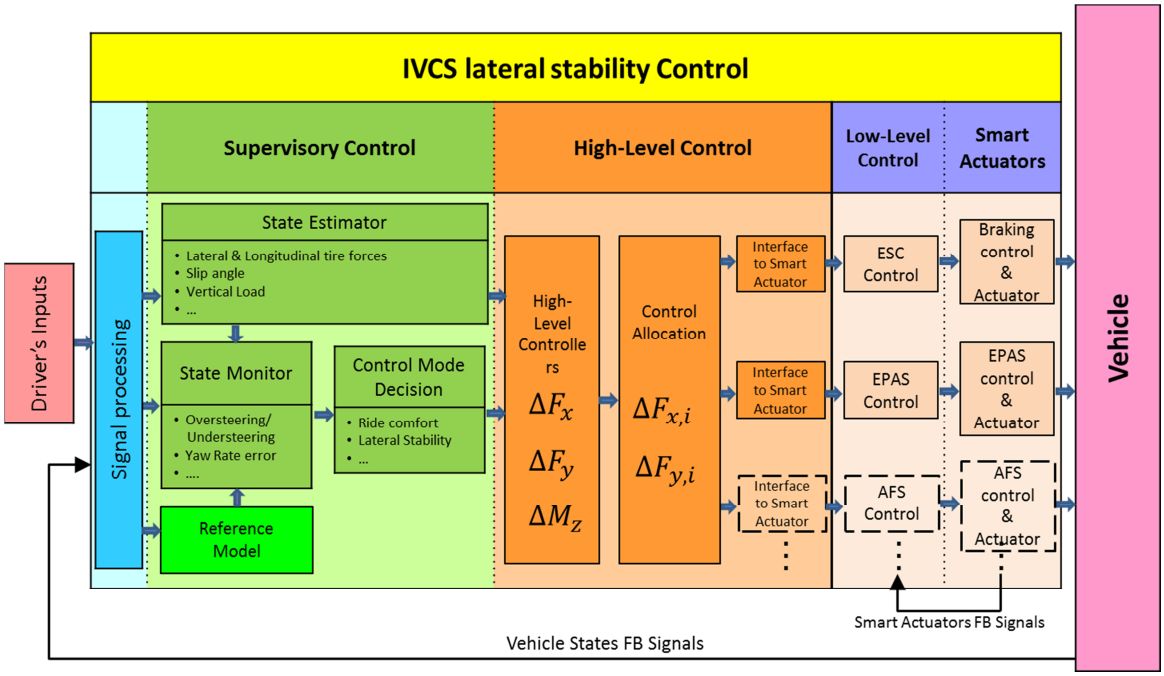

Figure 2-4: Structure of IVCS system for planar motion control

More detailed descriptions of the layers are as follows:

Layer 1. By assumption of having the control authority exclusively on the steering (torque) and brake (slip), the control task are limited to vehicles' 'yaw', 'lateral' and 'longitudinal' motions, so called vehicle planar motions. We don't have any direct control over the vehicle's roll, pitch and bounce because of the actuator limitation. The lateral vehicle dynamics system can be constructed based on vehicle's yaw velocity (so-called yaw rate) control as well as vehicle sideslip (ratio of lateral velocity to longitudinal velocity) control (Gillespie , 1992; Rajamani, 2012), so the high-level control system states vector is $\mathbf{x} = [V_x \quad V_y \quad \omega_z]^T$. The model reference approach is adopted to derive the reference values, in which, the steady state behaviour of a two DoF vehicle model (so called bicycle model) is used to drive the reference values (Rajamani, 2012; van Zanten, Erhardt, Pfaff, Kost, Hartmann, & Ehret, 1996). This layer is shown as the "*Reference Model"* block in Figure 2-4.

Layer 2. The second layer consists of three modules, so called the "*State Estimator"*, the "*State Monitor"* and the "*Control Mode Decision"*

blocks (see also Figure 2-2). In the absence of some real sensor measurement (due to practical limitation or for cost reduction), we have to use several robust estimation methods to 'virtually' measure the required vehicle parameters. More specifically, there is a need for estimation of tyre self-aligning moment (Hsu Y. , 2009), vehicle sideslip (van Zanten A. , 2000) and tyre-road coefficient of friction (Ahn, Peng, & Tseng, 2012). Estimation algorithms are employed in the *State Estimator* block.

In the *State Monitor* block, the existing states of the vehicle are compared with reference values to identify three different driving conditions: normal driving, mild and hazardous stability conditions. In stability conditions, the over-steering/Understeering situation is also determined. Normal driving conditions (on dry road, with coefficient of friction $\mu = 1$) stands for the lateral acceleration range from zero up to $0.4g$, which corresponds to tyre's linear region (Smakman, 2000). The lateral accelerations from $0.4g$ up to $0.6g$ is the tyre non-linear working range which is here featured as mild stability condition. Higher lateral accelerations up to maximum saturation limit (i.e $a_y = g$) is characterised as hazardous stability condition (Milliken & Milliken, 1995) .

In normal driving conditions, the control task is to provide the driver comfort while in mild and hazardous conditions the vehicle stability is the priority. In the comfort mode, the driver steering (torque) trigger the EPAS assist block to generate the relevant assist torque for the sake of driver comfort (Zaremba, Liubakka, & Stuntz, 1998; Post, 1995), whereas, the driver's command on braking goes directly to the slip control system. When the vehicle tends to move to an unstable region (limited stability) (Takahashi, 2004), the control system switches to mild stability mode, in which the IVCS system will try to stabilise the vehicle by reducing the magnitude of the assist torque and even more by producing a counter steering torque to the steering wheel (Liu, et al, 2008; McCann, 2000; Tanaka, et al, 2007). If the

amount of driver's steering correction will not be sufficient to stabilise the vehicle, the control mode switch to hazardous stability mode, which represents autonomous brake intervention (Chang, 2007; Ono, et al, 2006). In hazardous mode, the brake control plays the major role because of the steering limitation. The control mode switching will provide by means of a (bumpless) rule-based approach (Asarin, et al, 2000).

Layer 3. Based on Newton's second law, the derivative of vehicle planar motions, $\dot{\mathbf{x}} = \begin{bmatrix} \dot{V}_x & \dot{V}_y & \dot{V}_z \end{bmatrix}^T$, are proportional to the planar generalised forces and moments, i.e. longitudinal and lateral forces and yaw moment, so the generalised forces and moment vector is

$$\boldsymbol{\tau} = [F_x \quad F_y \quad M_z]^T \tag{2-7}$$

The high-level controllers consist of three closed loop control laws on vehicle's states which will be activated in case of mild or hazardous stability conditions. The output of the controllers are the values of the vector $\boldsymbol{\tau}$ which will stabilise the vehicle if they are applied at the vehicle's centre of gravity (ignoring actuators dynamics). There are several (SISO or MIMO) control laws that have been proposed for the vehicle yaw rate and sideslip control which range from PID controllers (Shibahata, Progress and future direction of Chassis control technology, 2005) to more advanced controllers like sliding mode control (Furukawa & Abe, 1997; Rajamani, 2012), fuzzy logic control (Chen, Dao, & Lin, 2010) or H-infinity control (Hirano, Harada, Ono, & Takanami, 1993; Horiuchi, Okada, & Nohtomi, 1999). In this dissertation a novel high-level control law is developed by employing the Youla parameterisation control design approach. (Youla, Jabr , & Bongiorno Jr, 1976)

Layer 4. Considering the steering and brakes as the only available actuators in the vehicle, the low-level control authorises are available only on the front tyres lateral forces, $\Delta F_{y,i}$, $i = 1,2$ (through front steering intervention) and the four tyres longitudinal forces, $\Delta F_{x,i}$, $i = 1,2,3,4$

(through 4 wheels brake intervention) where $i = 1,2,3,4$ indices stands for *front left*, *front right*, *rear left* and *rear right* tyres respectively. The control input vector can be defined as

$$\mathbf{u} = [\Delta F_{x,1} \quad \Delta F_{y,1} \quad \Delta F_{x,2} \quad \Delta F_{y,2} \quad \Delta F_{x,3} \quad \Delta F_{x,4}]^T \tag{2-8}$$

As the number of generalised forces and moments ($\boldsymbol{\tau} \in \mathbb{R}^3$) is less than the number of available actuators ($\mathbf{u} \in \mathbb{R}^6$), so the system is redundant (over-actuated) and based on known values of $\boldsymbol{\tau}$,there is not a unique or a direct solution for vector $\mathbf{u}$.The optimum distribution of generalised yaw moment (on the vehicle level) to the relevant actuators forces and moments (on the tyre level) is employed by solving a constrained optimisation problem. A fast, reconfigurable and adaptive control allocation solution is proposed in this dissertation. The proposed control allocation provides several properties to the integrated control system to address the required specifications defined in section 3.2.2, such as low cost execution, fault tolerance and adaptation to vehicle and/or environment parameters changes.

Layer 5. The proposed integrated vehicle dynamics control system is based on steering (torque) and brake (pressure) intervention by means of the EPAS (steering torque control) and EHB (brake hydraulic pressure control) actuators. By assuming: the front tyres lateral forces and the four tyres longitudinal force as the low-level control states; the EPAS, EHB as the controlled plants; and the output of the control allocation block, $\mathbf{u}$, as the reference tracks; the (low-level) control objectives are to design a set of low-level control laws by considering the actuators dynamics such that the output of the plants follow the reference values asymptotically. One closed loop controller based on steering self-aligning moment feedback and four (similar) closed loop controller based on (each) tyre longitudinal slip feedback are designed and implemented in this layer.

Layer 6. Each smart actuator has been equipped with its means of force or moment generating system (so called, low-level effectors). More

specifically, the EPAS generates steering torque by means of an electric motor attached to the steering column (or pinion or rack) and EHB generates longitudinal tyre forces by generating (or changing) the hydraulic pressure on the brake pad through a set of hydraulic valves and an electric pump actuation (Robert Bosch GmbH, 2011). The objective of the (actuator level) control system in this layer is to control the magnitude and/or direction of the forces or moments produced by the electromechanical effectors associated with each actuator such that it follows the reference values from the previous layer asymptotically. These effectors includes DC electric motor closed loop current controller for EPAS (Hu, 2008) and a continuous hydraulic pressure control on four wheels braking for EHB systems (Van Zanten, 2002).

By considering the proposed architecture and various layers of the integrated vehicle dynamics system, as discussed above, the top building blocks of the proposed IVCS system in Simulink® environment are presented in Figure 2-5.

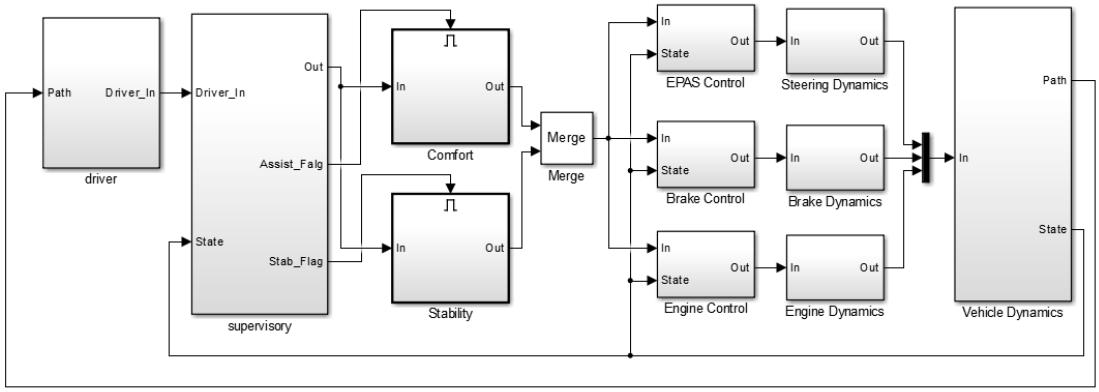

Figure 2-5: Top layer of Simulink® blocks of the customized IVCS system

3 System Modelling

Based on the V-model, introduced in the previous chapter, the design phase starts with *System modelling*[4] in which the conceptual and mathematical representations of the system dynamics are constructed. From a control design point of view, the model should be complete to ideally capture the fundamental dynamics of the system and remain simple enough to provide a basis for model based control development. If a model includes sufficient fidelity, then the control performance can be evaluated through simulation and the risk and cost associated with experimental validation will be reduced considerably. (Gerdes & Hedrick, 1999)

The modelling starts with systematic decomposition, in which the control system is considered as a hierarchical composition of several layers of sub-systems. The Simulink® blocks of the IVCS system dynamics, including vehicle dynamics, as well as steering, brake (and engine) dynamics are highlighted in Figure 3-1.

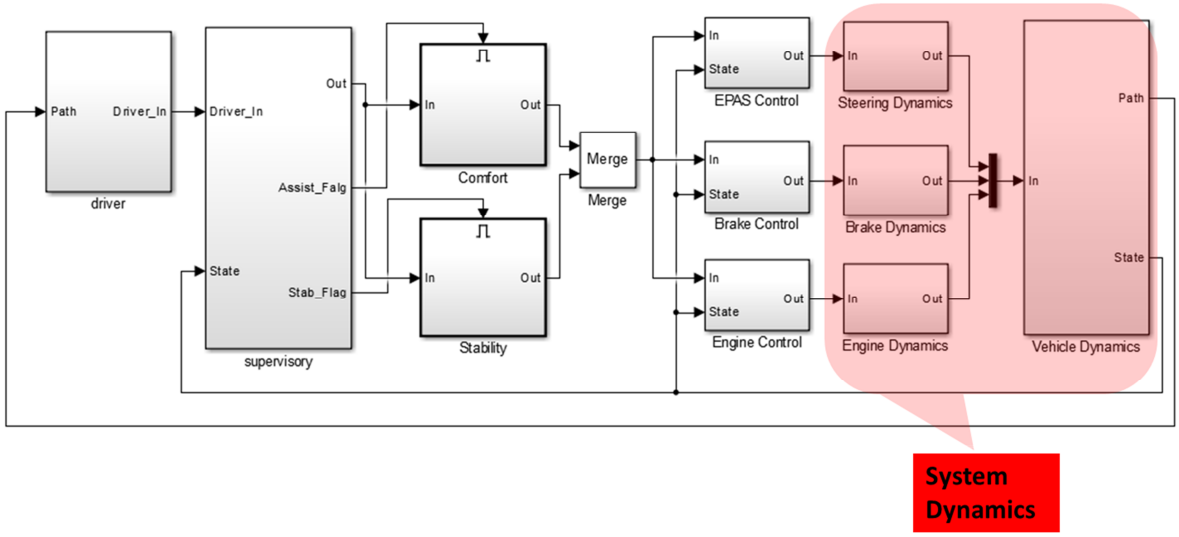

Figure 3-1: The IVCS system dynamics Simulink® blocks

The mathematical modelling of the system dynamics including the vehicle, steering and brake dynamics are presented in this chapter.

[4] see Figure 1-1

3.1 Vehicle coordinate systems

Ground vehicle is a complex three-dimensional moving system composed of several connected rigid bodies. To describe and calculate vehicle's states, including its inputs and outputs such as displacements, velocities, accelerations and forces, it is often required to employ various reference frames (Karnopp, 2013). The following three types of right-handed Cartesian coordinate systems are employed in this dissertation:

- **The Earth-Fixed Coordinate System:** is a fixed coordinate system with its axis attached to the ground and the X-Y surface lies on the ground plane, as shown in Figure 3-2.
- **The Body Coordinate System:** is a rotating coordinate system attached to the vehicle and its origin is at the vehicle's centre of gravity, with the x-axis pointed toward the direction of vehicle travel. This is the most important reference frame in vehicle dynamics analysis as all vehicle motions and forces are defined with reference to this coordinate system (Kiencke & Nielsen, 2005). In this work, we adopt ISO 8855 sign convention for body coordinate system as shown in Figure 3-2 (ISO 8855-2011)

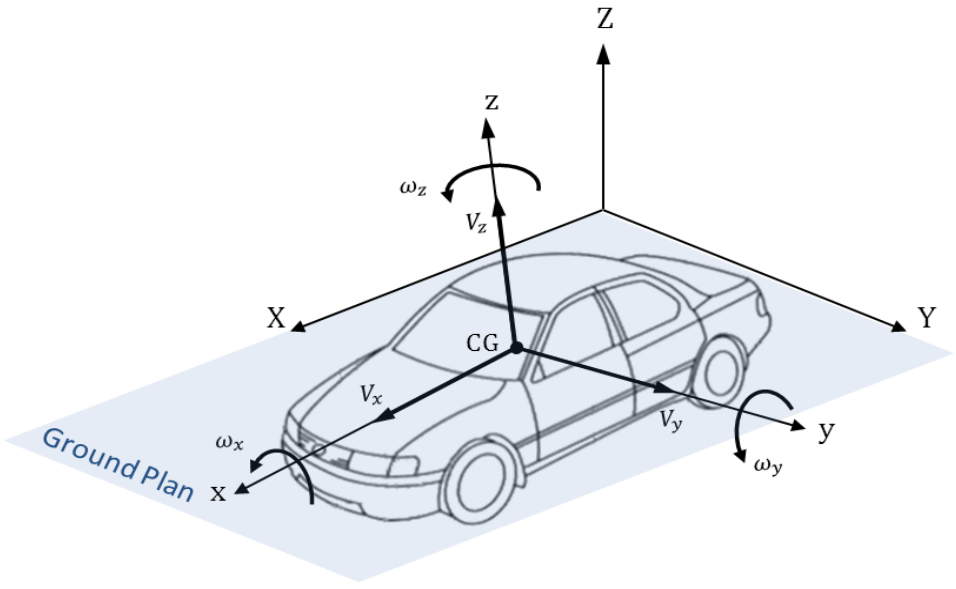

Figure 3-2: The earth fixed and the body coordinate systems

- **The Tyre Coordinate System:** is a coordinate system attached to the tyre, its origin is at the centre of tyre-road contact patch and the z-axis is

perpendicular to the road surface. For the tyre coordinate system, ISO 8855 sign convention is adopted, as shown in Figure 3-3 (ISO 8855-2011).

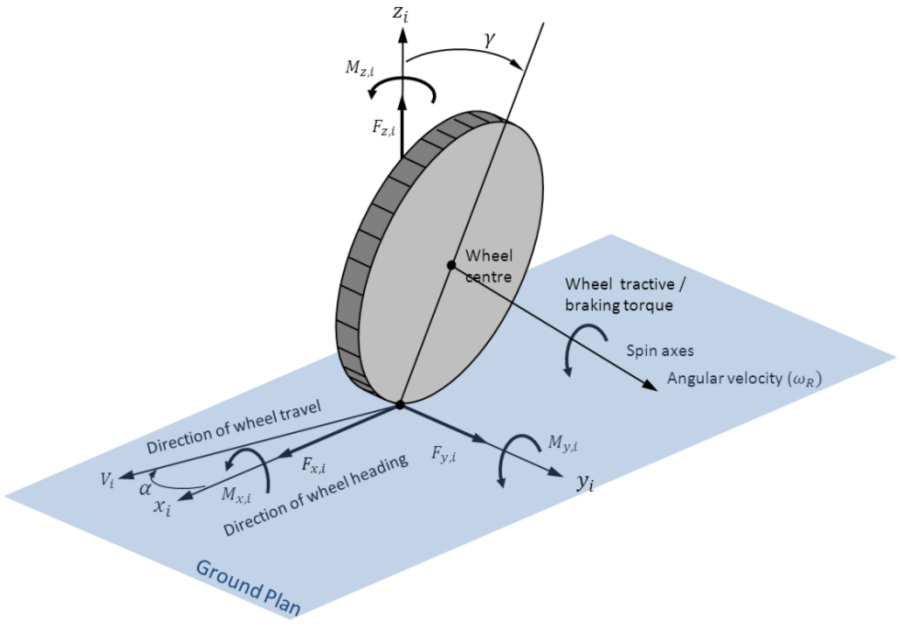

Figure 3-3: ISO Tyre Coordinate System

3.2 Vehicle model

By assuming the vehicle system as a rigid moving body, the vehicle's equation of motions can be derived in earth fixed coordinate system by applying Euler's first and second laws as:

$$\mathbf{F} = \frac{\mathrm{d}\mathbf{P}}{\mathrm{dt}} \tag{3-1}$$

$$\mathbf{M} = \frac{\mathrm{d}\mathbf{H}}{\mathrm{dt}} \tag{3-2}$$

(note: vectors and matrixes quantities are denoted by bold font in this report), where $\mathbf{F} = [F_x \quad F_y \quad F_z]^{\boldsymbol{T}}$ and $\mathbf{M} = [M_x \quad M_y \quad M_z]^{\boldsymbol{T}}$ are the vectors of forces and moments applied at the vehicle's centre of gravity respectively. $\mathbf{P}$ and $\mathbf{H}$ are the vectors of linear and angular momentum respectively:

$$\mathbf{P} = m\mathbf{V} \tag{3-3}$$

$$\mathbf{H} = \mathbf{I\Omega} \tag{3-4}$$

where $\mathbf{V} = [V_x \quad V_y \quad V_z]^{\boldsymbol{T}}$ is the vehicle linear velocity vector, $\mathbf{\Omega} = [\omega_x \quad \omega_y \quad \omega_z]^{\boldsymbol{T}}$ is the angular velocity vector, m is the vehicle's (sprung and unsprung) mass lumped at the centre of gravity and $\mathbf{I}$ is the vehicle's mass moment of inertia:

$$\mathbf{I} = \begin{bmatrix} I_x & I_{xy} & I_{xz} \\ I_{yx} & I_y & I_{yz} \\ I_{zx} & I_{zy} & I_z \end{bmatrix} \tag{3-5}$$

which is a tensor (i.e. $I_{xy} = I_{yx}$, $I_{xz} = I_{zx}$, $I_{zy} = I_{yz}$). By assuming a constant mass and inertia for the vehicle, Eqs. (3-1) and (3-2) can be rewritten in the form

$$\mathbf{F} = \frac{\mathrm{d}\mathbf{P}}{\mathrm{dt}} = m\frac{\mathrm{d}\mathbf{V}}{\mathrm{dt}} \tag{3-6}$$

$$\mathbf{M} = \frac{\mathrm{d}\mathbf{H}}{\mathrm{dt}} = \mathbf{I}\frac{\mathrm{d}\mathbf{\Omega}}{\mathrm{dt}} \tag{3-7}$$

which are the equations of vehicle's motion in the earth fixed coordinate system; however, it is convenient to describe the equations of motion in body coordinate system (Kiencke & Nielsen, 2005). The fundamental relation between time derivatives of an arbitrary vector $\mathbf{P} = \begin{bmatrix} P_x & P_y & P_z \end{bmatrix}^T$ in a fixed coordinate system and of those in a moving frame rotating with angular velocity $\mathbf{\Omega} = [\omega_x \quad \omega_y \quad \omega_z]^{\boldsymbol{T}}$ is as follows (Karnopp, 2013):

$$\frac{\mathrm{d}\mathbf{P}}{\mathrm{dt}} = \frac{\partial \mathbf{P}}{\partial \mathrm{t}} + \mathbf{\Omega} \times \mathbf{P} \tag{3-8}$$

where the italicized $\partial/\partial t$ represents a derivative in the body rotating frame and $\mathbf{\Omega} \times \mathbf{P}$ is the cross vector product of $\mathbf{\Omega}$ and $\mathbf{A}$:

$$\mathbf{\Omega} \times \mathbf{P} = \begin{bmatrix} \omega_y P_z - \omega_z P_y & \omega_z P_x - \omega_x P_z & \omega_x P_y - \omega_y P_x \end{bmatrix}^T \tag{3-9}$$

Eq. (3-6) can be rewritten in body coordinate system by employing Eq. (3-8) as follows:

$$\mathbf{F} = m\frac{d\mathbf{V}}{d\mathrm{t}} + m\boldsymbol{\Omega} \times \mathbf{V} \tag{3-10}$$

or as components:

$$\begin{aligned} F_x &= m\left(\frac{dV_x}{dt} + \omega_y V_z - \omega_z V_y\right) \\ F_y &= m\left(\frac{dV_y}{dt} + \omega_z V_x - \omega_x V_z\right) \\ F_z &= m\left(\frac{dV_z}{dt} + \omega_x V_y - \omega_y V_x\right) \end{aligned} \tag{3-11}$$

and the moment Eq. (3-2) becomes:

$$\mathbf{M} = \mathbf{I} \times \frac{d\boldsymbol{\Omega}}{d\mathrm{t}} + \boldsymbol{\Omega} \times (\mathbf{I}\boldsymbol{\Omega}) \tag{3-12}$$

By neglecting I_{xy}, I_{xz}, I_{yz} (principal axes assumption), the components of moment equations are:

$$\begin{aligned} M_x &= I_x\frac{d\omega_x}{dt} + I_z\omega_y\omega_z - I_y\omega_z\omega_y \\ M_y &= I_y\frac{d\omega_y}{dt} + I_x\omega_z\omega_x - I_z\omega_x\omega_z \\ M_z &= I_z\frac{d\omega_z}{dt} + I_y\omega_x\omega_y - I_x\omega_y\omega_x \end{aligned} \tag{3-13}$$

which are the well-known Euler's equations of motion.

Eqs. (3-10) and (3-12) may be rearranged for the purposes of simulation or control development as:

$$\dot{\mathbf{V}} = -\boldsymbol{\Omega} \times \mathbf{V} + \frac{1}{m}\mathbf{F} \tag{3-14}$$

$$\dot{\boldsymbol{\Omega}} = \mathbf{I}^{-1}(\boldsymbol{\Omega} \times \mathbf{I}\boldsymbol{\Omega}) + \mathbf{I}^{-1}\mathbf{M} \tag{3-15}$$

or in general state-space form as:

$$\dot{\mathbf{x}} = f(\mathbf{x}) + g(\mathbf{x})\boldsymbol{\tau} \tag{3-16}$$

where f and g are functions, $\mathbf{x}$ is the vector of system states and $\boldsymbol{\tau}$ is the generalised forces and moments vector (system input), i.e.

$$\mathbf{x} = [V_x \quad V_y \quad V_z \quad \omega_x \quad \omega_y \quad \omega_z]^T \tag{3-17}$$

$$\boldsymbol{\tau} = [F_x \quad F_y \quad F_z \quad M_x \quad M_y \quad M_z]^T \tag{3-18}$$

We note that the above equations are simplified in-so-far as they ignore the interaction of sprung and unsprung masses. Moreover, we have assumed six degrees of freedom here but actual problems may involve additional states associated with suspension dynamics, wheels dynamics, tyres deflection and so on. These additional degrees of freedom may be added to form more general dynamical equations.

As we focus on the vehicle planar motion in this dissertation, the vehicle vertical motion V_z and the angular motion in the roll ω_x and pitch ω_y directions, mainly influenced by suspension and road banking are neglected. Therefore, the control authority is limited to longitudinal and lateral accelerations as well as the yaw rate so the Eqs. (3-12) and (3-14) are simplified as

$$\begin{bmatrix} \dot{V}_x \\ \dot{V}_y \\ \dot{\omega}_z \end{bmatrix} = \begin{bmatrix} V_y\omega_z \\ -V_x\omega_z \\ 0 \end{bmatrix} + \begin{bmatrix} 1/M & 0 & 0 \\ 0 & 1/M & 0 \\ 0 & 0 & 1/I_z \end{bmatrix} \begin{bmatrix} F_x \\ F_y \\ M_z \end{bmatrix} \tag{3-19}$$

which again can be represented in the form of Eq. (3-16). These nonlinear, coupled differential equations, usually denoted as the control-oriented vehicle dynamic model (Wang, 2007), capture the dominant vehicle dynamics in x-y plane and can be integrated in time (for the purpose of simulation) or could be employed for high-level (linear or nonlinear) control system development. To design a linear control system, the Eq. (3-19) should be linearised around some operating points, as discussed in the next chapter.

3.3 Chassis model

In a ground vehicle, the generalised forces and moments, required to create/change the vehicle motions (Eq. (3-16)), are generated through the

forces and moments exerted on the tyres by the road. The relationship between the forces and moments on the tyre contact patch (in tyre coordinate system) and the vehicle forces and moments at the centre of gravity (in body coordinate system) can be represented in general form as:

$$\boldsymbol{\tau} = \mathbf{B}\mathbf{u} \tag{3-20}$$

where the $\mathbf{B}$ is the so called effectiveness matrix, $\mathbf{u}$ is the vector of *tyres* forces and moments and $\boldsymbol{\tau}$ is the vector of the *vehicle* generalised forces and moment as presented in the previous section.

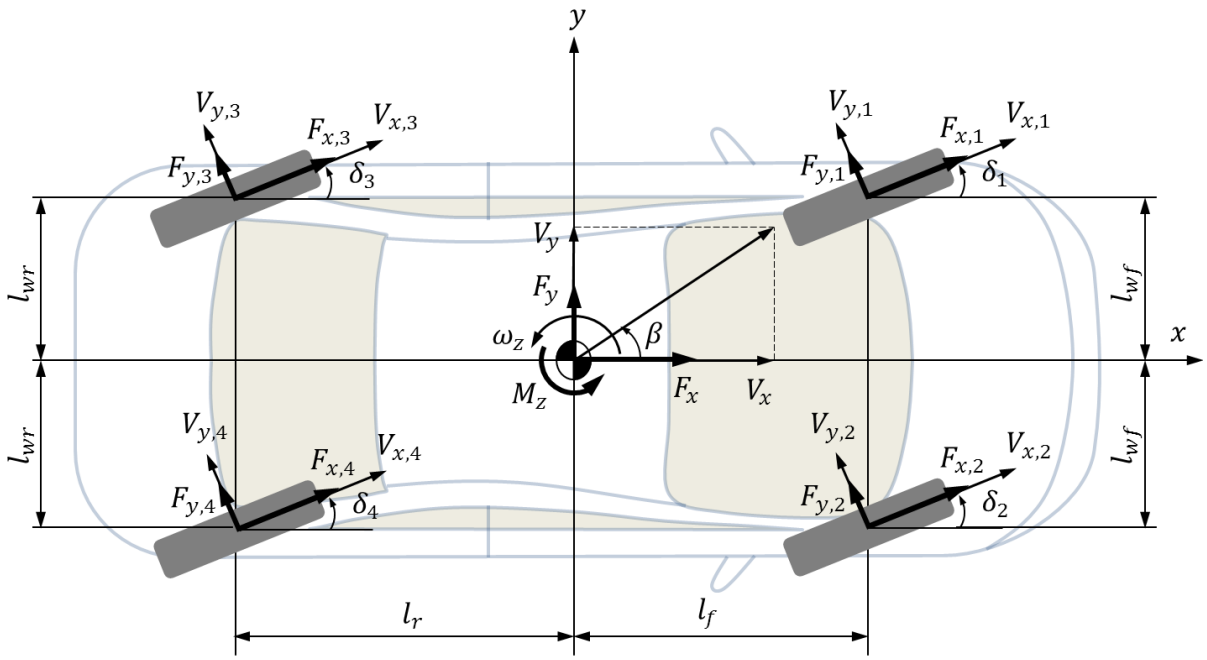

Figure 3-4: The vehicle planar dynamics

For the vehicle planar motion, as shown in Figure 3-4, the generalised forces and moments vector (3-18) reduce to (see (3-19)):

$$\boldsymbol{\tau} = \begin{bmatrix} F_x \\ F_y \\ M_z \end{bmatrix}, \qquad \boldsymbol{\tau} \in \mathbb{R}^{3\times 1} \tag{3-21}$$

and in case of four wheels steering, braking and driving, there exist control authorities over longitudinal and lateral forces for all four tyres, i.e.

$$\mathbf{u} = \begin{bmatrix} F_{x,i} \\ F_{y,i} \end{bmatrix} \quad , \quad i = 1,2,3,4 \quad , \quad \mathbf{u} \in \mathbb{R}^{8\times 1} \tag{3-22}$$

where the indices 1,2,3,4 are referring to the Front Left (FL), Front Right (FR), Rear Left (RL) and Rear Right (RR) wheels respectively, as shown in Figure 3-4. The effectiveness matrix $\mathbf{B} \in \mathbb{R}^{\mathbf{3\times 8}}$ can be defined as (Jonasson, 2009):

$$\mathbf{B} = \mathbf{AT} \tag{3-23}$$

where $\mathbf{A} \in \mathbb{R}^{\mathbf{3\times 8}}$ can be derived from vehicle kinematics

$$\mathbf{A} = \begin{bmatrix} 1 & 0 & 1 & 0 & 1 & 0 & 1 & 0 \\ 0 & 1 & 0 & 1 & 0 & 1 & 0 & 1 \\ -l_{wf} & l_f & l_{wf} & l_f & -l_{wr} & -l_r & l_{wr} & -l_r \end{bmatrix} \tag{3-24}$$

and $\mathbf{T} \in \mathbb{R}^{\mathbf{8\times 8}}$ is the transformation matrix for rotating tyre force vector about the z axis (Kiencke & Nielsen, 2005)

$$\mathbf{T} = \mathrm{diag}(\mathbf{T_i}) \quad , \quad \mathbf{T_i} = \begin{bmatrix} \cos\delta_i & -\sin\delta_i \\ \sin\delta_i & \cos\delta_i \end{bmatrix} \quad , \quad i = 1,2,3,4 \tag{3-25}$$

The tyre forces are functions of tyre slip and slip angle which themselves are functions of tyre and vehicle velocities, as will be discussed in the following sections. The relationship between the vehicle velocities at the vehicle centre of gravity (in body coordinate system) and the velocities at the centre of tyre contact patch (in tyre coordinate system) can be represented in general form as:

$$\mathbf{v} = \mathbf{T}_v\mathbf{x} \tag{3-26}$$

where $\mathbf{x}$ is the vehicle velocity vector at the centre of gravity, $\mathbf{v}$ is the tyres velocity vector and $\mathbf{T}_v$ is the transformation matrix from the body coordinate system to the tyre coordinate system.

In case of planar motion, as shown in Figure 3-4, the tyre velocities include the vehicle velocity at the centre of gravity and the motion about the vertical vehicle axis. The vehicle velocity vector $\mathbf{x}$ is:

$$\mathbf{x} = \begin{bmatrix} V_x \\ V_y \\ \omega_z \end{bmatrix} \quad , \qquad \mathbf{x} \in \mathbb{R}^{3\times 1} \tag{3-27}$$

and $\mathbf{v}$ is the vector of translational velocities in each tyre, i.e.

$$\mathbf{v} = \begin{bmatrix} V_{x,i} \\ V_{y,i} \end{bmatrix} \quad , \; i = 1,2,3,4 \; , \; \mathbf{v} \in \mathbb{R}^{8\times 1} \tag{3-28}$$

Here we ignore the tyre rotational velocities. The transformation matrix $\mathbf{T_v} \in \mathbb{R}^{\mathbf{8\times 3}}$ can be derived from vehicle kinematics as (Kiencke & Nielsen, 2005):

$$\mathbf{T_v} = \mathbf{T}^T \mathbf{A}^T \tag{3-29}$$

where $\mathbf{A}^T$ is the transpose of matrix $\mathbf{A}$, and

$$\mathbf{T}^T = \mathrm{diag}(\mathbf{T}^T{}_{\boldsymbol{i}}) \quad , \quad \mathbf{T}^T{}_{\boldsymbol{i}} = \begin{bmatrix} \cos\delta_i & \sin\delta_i \\ -\sin\delta_i & \cos\delta_i \end{bmatrix} \quad , \; i = 1,2,3,4 \tag{3-30}$$

The above mentioned relationship of the forces and velocities for the vehicle planar motions can be further reduced based on the number of available actuators on the vehicle. For example, in case of front wheel steering: $\delta_1 = \delta_2 = \delta$ and $\delta_3 = \delta_4 = 0$ (i.e. $\sin\delta_3 = \sin\delta_4 = 0$ and $\cos\delta_3 = \cos\delta_4 = 1$) and by assumption of $l_{wf} = l_{wr} = l_w$, Eq. (3-23) is simplified, and the components of Eq. (3-20) can be represented as follows:

$$F_x = \left(F_{x,1}+F_{x,2}\right)\cos\delta - \left(F_{y,1}+F_{y,2}\right)\sin\delta + F_{x,3} + F_{x,4} \tag{3-31}$$

$$F_y = \left(F_{x,1}+F_{x,2}\right)\sin\delta + \left(F_{y,1}+F_{y,2}\right)\cos\delta + F_{y,3} + F_{y,4} \tag{3-32}$$

$$\begin{aligned} M_z = {} & l_f\left\{\left(F_{x,1}+F_{x,2}\right)\sin\delta + \left(F_{y,1}+F_{y,2}\right)\cos\delta\right\} - l_r\left(F_{y,3}+F_{y,4}\right) \\ & - l_w\left\{\left(F_{x,1}-F_{x,2}\right)\cos\delta - \left(F_{y,1}-F_{y,2}\right)\sin\delta + \left(F_{x,3}-F_{x,4}\right)\right\} \end{aligned} \tag{3-33}$$

By substituting these forces and moments into Eq. (3-19), the well-known planar equation of motions of the vehicle body obtained as (Rajamani, 2012)

$$\dot{V}_x = V_y\omega_z + \frac{1}{m}\left[\left(F_{x,1}+F_{x,2}\right)\cos\delta - \left(F_{y,1}+F_{y,2}\right)\sin\delta + F_{x,3} + F_{x,4}\right] \tag{3-34}$$

$$\dot{V}_y = -V_x\omega_z + \frac{1}{m}\left[\left(F_{x,1}+F_{x,2}\right)\sin\delta + \left(F_{y,1}+F_{y,2}\right)\cos\delta + F_{y,3} + F_{y,4}\right] \tag{3-35}$$

$$\begin{aligned}\dot{\omega}_z = \frac{1}{I_z}\Big[l_f\left\{\left(F_{x,1}+F_{x,2}\right)\sin\delta + \left(F_{y,1}+F_{y,2}\right)\cos\delta\right\} - l_r\left(F_{y,3}+F_{y,4}\right) \\ - l_w\left\{\left(F_{x,1}-F_{x,2}\right)\cos\delta - \left(F_{y,1}-F_{y,2}\right)\sin\delta + \left(F_{x,3}-F_{x,4}\right)\right\}\Big]\end{aligned} \tag{3-36}$$

The above equations represent the nonlinear two-track vehicle model which can be employed for simulation and control system development purposes. A more simplified “linear” single track vehicle model, known as bicycle model, suitable for vehicle lateral dynamics and stability analysis can be found in Appendix B. The bicycle model is a reasonable mathematical representation of vehicle behaviour especially for lateral motion dynamics and several important vehicle dynamics performance measures have been derived from this model (Milliken & Milliken, 1995; Pacejka, 2006)

From Eq. (3-26), the components of tyre velocities in case of front wheel steering are

$$\begin{aligned}V_{x1} &= (V_x - \omega_z l_w)\cos\delta + \left(V_y + \omega_z l_f\right)\sin\delta \\ V_{y1} &= -(V_x - \omega_z l_w)\sin\delta + \left(V_y + \omega_z l_f\right)\cos\delta \\ V_{x2} &= (V_x + \omega_z l_w)\cos\delta + \left(V_y + \omega_z l_f\right)\sin\delta \\ V_{y2} &= -(V_x + \omega_z l_w)\sin\delta + \left(V_y + \omega_z l_f\right)\cos\delta \\ V_{x3} &= (V_x - \omega_z l_w) \\ V_{y3} &= \left(V_y - \omega_z l_r\right) \\ V_{x4} &= (V_x + \omega_z l_w) \\ V_{y4} &= \left(V_y - \omega_z l_r\right)\end{aligned} \tag{3-37}$$

In the above equations, the tyre longitudinal and lateral forces are unknown, so for concluding the vehicle model it is necessary to construct a reliable tyre mathematical model to relate tyre kinematics to its kinetics.

3.4 Tyre model

Pneumatic tyres are perhaps the most important, but difficult to model, component in vehicle dynamics studies. Except for the inertial and aerodynamic forces, all the forces and moments applied to the vehicles are from the forces and moments generated at the tyre-road contact patch (Pacejka, 2006). The tyre forces and moments play a fundamental role in vehicle dynamics control system, as the vehicle longitudinal, lateral and vertical motions are ultimately controlled by the tyre forces (Heißing & Ersoy, 2011). Tyres are considered to be the sole (high level) vehicle dynamics effectors in a vehicle and all the chassis systems such as steering, brake and suspension are mechanically connected to the (wheels and) tyres to affect the magnitude and/or direction of the tyre forces.

The analysis of tyre forces and moments is a difficult task due to the tyre's complex nature and nonlinear behaviour. There exist several tyre models which have been developed for different applications and with different levels of fidelity and accuracy (see (Pacejka, 2006) for example).

3.4.1 Tyre forces and moments

During vehicle driving, tyres are subjected to four types of (usually simultaneous) loading, known as: free rolling, braking / acceleration, cornering and vertical force transfer loads (Heißing & Ersoy, 2011). As a result of the friction between the tyre and road surface, three forces and three moments are developed at the tyre-road contact patch. Longitudinal (Tractive) Force $F_{x,i}$, Lateral (Cornering) Force $F_{y,i}$ and Normal Force $F_{z,i}$ are the three components of the resultant forces as well as Overturning Moment $M_{x,i}$, Rolling Resistance Moment $M_{y,i}$ and Self-Aligning Moment $M_{z,i}$ are the three components of the resultant moments exerted on a tyre from the road in the x, y and z directions respectively, as shown in Figure 3-3 (ISO 8855-2011).

In case of free rolling (no braking or accelerating and/or cornering), rolling resistance is the main force acting on a tyre. Rolling resistance is an important parameter in vehicle fuel consumption studies, which is not the subject of this work. Moreover, overturning moment is usually ignored in vehicle dynamics control as its magnitude is small compared to tractive or braking forces during critical manoeuvres (Wang, 2007).

In addition to the above mentioned steady-state force and moments, tyres present several transient and oscillatory dynamics behaviours when the frequency of lateral and yaw excitation are no longer small (Pacejka,2006). It should be noted that the tyre models that have been presented and employed in this thesis don't include the transient behaviour, as the steady-state tyre models are sufficient for braking and turning control study of a vehicle (Gillespie , 1992). However, the final validation of the proposed control system through HiL simulation involves using of CarMaker® software, which considers the dynamic property of the tyre[5].

3.4.1.1 Tyre Longitudinal Force

By employing a braking (or tractive) torque to a pneumatic tyre, the tyre tread elements start to deflect and lead the tyre to travel less (or more) than its free rolling situation. The difference between a tyre straight rolling speed and its travel speed, known as (longitudinal) slip, results in the development of a negative (or positive) longitudinal force at the tyre-ground contact patch (Wong, 2008). There are various definitions for longitudinal slip in publications; however, the following definition for the tyre longitudinal slip is adopted in this work (Robert Bosch GmbH, 2011) :

$$\lambda_A = 1 - \frac{V_{x,i}}{R_{dyn}\omega_R} \qquad \text{during acceleration} \qquad (3\text{-}38)$$

$$\lambda_B = \frac{R_{dyn}\omega_R}{V_{x,i}} - 1 \qquad \text{during braking} \qquad (3\text{-}39)$$

[5] See chapter 7 for more detailed explanations of HiL testing and validation.

where $V_{x,i}$ is the forward speed of the tyre centre (contain vehicle longitudinal, lateral velocities and yaw rate as discussed in the previous section), R_{dyn} is the tyre dynamic rolling radius and ω_R is the angular velocity of the tyre, as shown in Figure 3-3. According to definitions (3-38) and (3-39), the slip is always negative in braking, starts from zero and reaches to -1 when a tyre is locked ($\omega_R = 0$); and the slip is always positive in acceleration, starts from zero and reaches to 1 when a tyre is spinning but the translational speed of the tyre is zero, as shown in Figure 3-5.

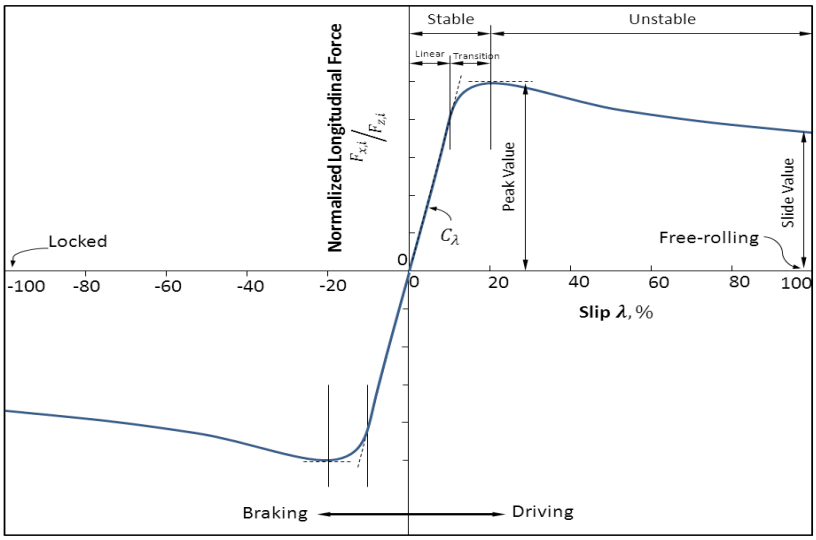

Figure 3-5: Variation of longitudinal force with slip

In the absence of any lateral forces and under typical tractive (or braking) conditions, the tyre longitudinal force $F_{x,i}$ is a function of the tyre slip λ_i, tyre-road coefficient of friction μ_i and tyre normal force $F_{z,i}$ (see Figure 3-5) :

$$F_{x,i} = f(\lambda_i, \mu_i, F_{z,i}) \tag{3-40}$$

At the initial stage, slip is mainly developed as a result of elastic deformation of the tyre tread and the relationship between the longitudinal force and slip is linear with a slope known as tyre longitudinal stiffness $C_{\lambda,i}$, such as:

$$F_{x,i} = C_{\lambda,i} \cdot \lambda_i \qquad \text{for } |\boldsymbol{\lambda_i}| < 10\% \sim 30\% \tag{3-41}$$

where the longitudinal stiffness is

$$C_{\lambda,i} = \left.\frac{dF_{x,i}}{d\lambda_i}\right|_{\lambda_i=0\%} \tag{3-42}$$

By further increasing (decreasing) of tractive (braking) torque, the tyre longitudinal force increases (decreases) but some parts of the tyre tread start to slide on the ground, so the relationship between the longitudinal forces and the slip becomes nonlinear. The maximum longitudinal force $F_{x,i}$ is usually reached at the absolute slip value of approximately 10% - 30% depending on the road surface type (Heißing & Ersoy, 2011). For the values of absolute slip beyond the maximum point, the longitudinal force reduces from the peak value to the pure sliding value, as shown in Figure 3-5, which results in an unstable condition. The longitudinal force value at the maximum point is $\mu_p F_{z,i}$ and for the pure sliding is determined by $\mu_s F_{z,i}$,where $F_{z,i}$ is the normal force on the tyre and μ_p and μ_s are the peak and sliding values of the coefficient of road adhesion, respectively (Wong, 2008).

3.4.1.2 Tyre Lateral Force

Lateral force (also known as side forces or cornering forces) is crucial to control the vehicle lateral motion in turns, and also to overcome external forces such as wind gusts or road banking. The lateral forces $F_{y,i}$ are generated mainly due to lateral deformation of the tyre in the tyre-ground contact patch. Tyre slip angle α_i is defined as the angle of tyre deformation, or in other words, it is the angle between the wheel heading direction and its actual travelling direction ($V_{t,i}$) as shown in Figure 3-6 (see also Figure 3-3), i.e.

$$\alpha_i = \tan^{-1}\frac{V_{y,i}}{|V_{x,i}|} \tag{3-43}$$

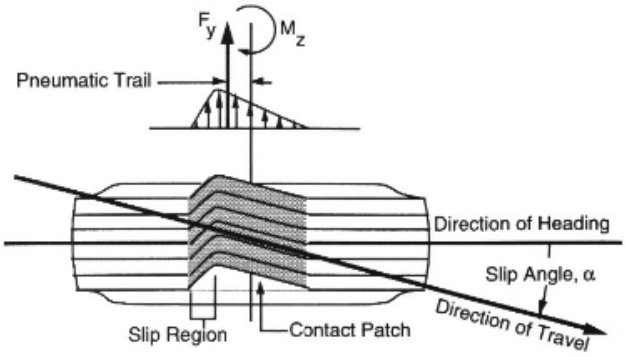

Figure 3-6: Generation of lateral forces and self-aligning moment due to slip angle (Gillespie , 1992)

By assuming small steering angle δ_i ($\sin\delta_i = \delta_i$ and $\cos\delta_i = 1$), the simplified version of equations (3-37) for the slip angle for each tyre (in case of 4WS) can be expressed as (Karnopp, 2013):

$$\alpha_1 = \delta_1 - \tan^{-1}\left(\frac{V_y + \omega_z\, l_f}{V_x - \omega_z\, l_w}\right)$$

$$\alpha_2 = \delta_2 - \tan^{-1}\left(\frac{V_y + \omega_z\, l_f}{V_x + \omega_z\, l_w}\right)$$

$$\alpha_3 = \delta_3 - \tan^{-1}\left(\frac{V_y - \omega_z\, l_f}{V_x + \omega_z\, l_w}\right)$$

$$\alpha_4 = \delta_4 - \tan^{-1}\left(\frac{V_y - \omega_z\, l_f}{V_x + \omega_z\, l_w}\right) \qquad (3\text{-}44)$$

In the absence of any longitudinal forces and under typical steering conditions, the lateral force is a function of tyre side angle, road coefficient of friction, normal force and the vehicle speed, however, the dependency on speed can generally be ignored (Robert Bosch GmbH, 2011) :

$$F_{y,i} = f\left(\alpha, \mu, F_{z,i}\right) \qquad (3\text{-}45)$$

For small slip angles (usually less than 3 - 4 degrees on dry road (Heißing & Ersoy, 2011), a linear relationship exists between lateral force and slip angle with a slope known as tyre cornering stiffness C_α such as

$$F_{y,i} = C_\alpha \cdot \alpha \qquad \text{for } |\alpha| < 3° \sim 4° \tag{3-46}$$

where the cornering stiffness is

$$C_\alpha = \left.\frac{dF_{y,i}}{d\alpha}\right|_{\alpha=0°} \tag{3-47}$$

By increasing the tyre slip angle, the lateral force increases at a lower rate and it reaches a maximum value, as shown in Figure 3-7, where the tyre begins sliding laterally as a result of limited friction on the road. In this region, a nonlinear relationship exists between tyre lateral force and slip angle and the equation (3-46) is no longer valid.

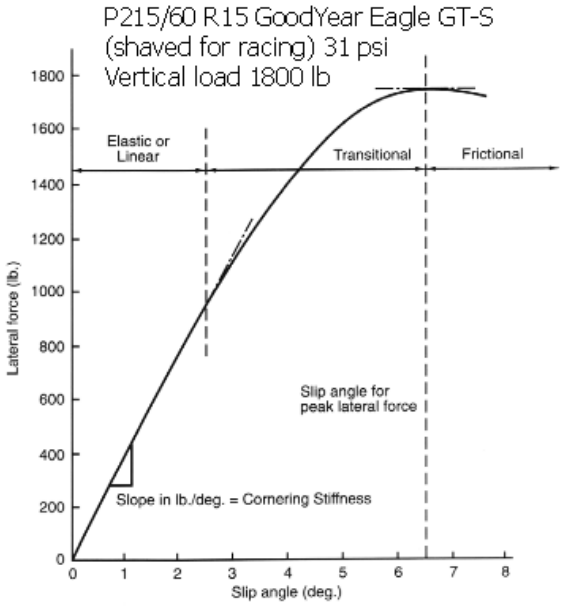

Figure 3-7: Cornering stiffness and lateral force character (Milliken & Milliken, 1995)

The cornering stiffness plays an important role in steady-state and transient handling characteristics of a vehicle (Wong, 2008) and it is a function of several parameters, such as: tyre properties (size, type, width, tread and so on), tyre pressure and the road condition (Gillespie , 1992). The cornering stiffness may change during the driving on different road conditions or different manoeuvres. For example, when the vehicle turns the tyre pressure in the outside wheels

increases as a result of weight transfer, and this can lead to change in the cornering stiffness. Fortunately, such variations are normally less than 10% and are still valid for most robust steering controllers (Stéphant, Charara, & Meizel, 2004). In contrast to tyre cornering stiffness, the tyre nonlinear behaviour and more importantly the maximum achievable tyre force are sensitive to variation of the tyre normal force as well as the change to the road surface (such as dry, wet, and so on) (Pacejka, 2006) .

3.4.1.3 Tyre Self-Aligning Moment

The shear force generated in the contact patch of a tyre operating at a slip angle does not have a symmetric pattern, so the effective lateral force $F_{y,i}$ does not apply at the centre of the tyre contact patch but at a distance known as the tyre pneumatic trial t_p (see Figure 3-8). As a result, a torque $M_{z,i}$ about the steer axis is generated which is called the self-aligning moment (or aligning torque) (Pacejka, 2006).

In addition to the pneumatic trail, the steering system geometry also provides a level arm for the lateral force, called mechanical trial t_m. Mechanical trial is a result of inclination of the tyre plane from the x-z plane which is known as caster angle. To calculate the tyre self-aligning moment $M_{z,i}$, the values of tyre pneumatic trial t_p and mechanical trail t_m should be known as

$$M_{z,i} = (t_p + t_m) \cdot F_{y,i} \tag{3-48}$$

The pneumatic trail is a function of tyre slip angle, tyre cornering stiffness and maximum achievable lateral force whereas; mechanical trail t_m depends only on steering geometry. The magnitude of mechanical trail is usually small in comparison to pneumatic trial, so we ignore it in calculations of self-aligning moment for the sake of simplicity (Hsu Y. , 2009).

The tyre self-aligning moment initially increases with the increment of slip angle up to a maximum value at a given slip angle. Any additional increment of the tyre slip angle, lateral force moves toward the centre of the contact patch (and finally saturates) so the self-aligning moment decreases and finally vanishes

once the tyre lateral forces reaches the limit of tyre adhesion, as shown in Figure 3-8 (Pacejka, 2006). The self-aligning moment has characteristics that reaches to its maximum point before the lateral force saturates; this phenomenon can be used for early detection of the vehicle instability as discussed in the following chapters (Ono, Asano, & Koibuchi, 2004).

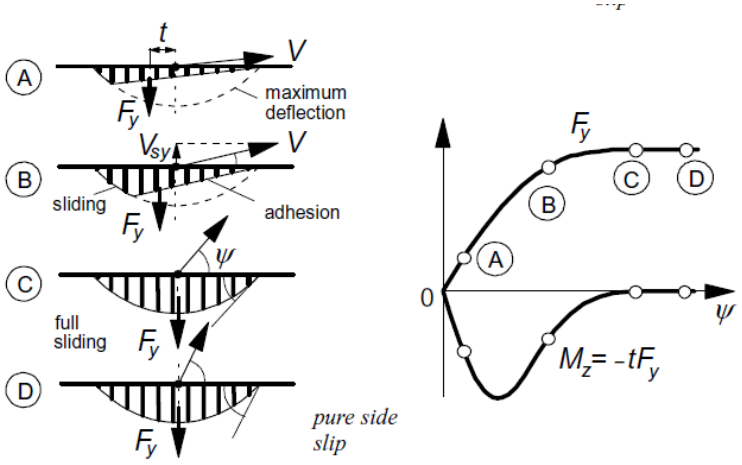

Figure 3-8: Lateral force and self-aligning moment at different slip condition (Pacejka, 2006)

The self-aligning moment is one the vehicle parameters that is sensed by the driver through steering system feedback and has an important effect on the steering 'feel' (Blundell & Harty, 2004). The self-aligning moment has also a small contribution on the total yaw moment generation on a vehicle. Although, the influence of the self-aligning moment on vehicle stability through its contribution on yaw moment generation is not considerable, its major effect on the steering system reaction may have a more substantial impact on vehicle handling (Gillespie , 1992). It should be noted that under normal driving conditions, the effect of self-aligning moment is to resist any turning motion, so it has an understeer consequence on vehicle handling (Gillespie , 1992). In other words, the tyre self-aligning moment can only help the driver to stabilise an oversteered vehicle.

3.4.1.4 Friction circle

So far, the pure longitudinal and lateral forces of a tyre have been studied. However, quite often a tyre is operated under conditions of the simultaneous

lateral and longitudinal slip such as acceleration in cornering or braking while steering. In general, employing longitudinal slip will reduce the available cornering force for a given slip angle, and conversely, employing slip angle will reduce the available longitudinal force for a given slip condition as shown in Figure 3-9 (Pacejka, 2006).

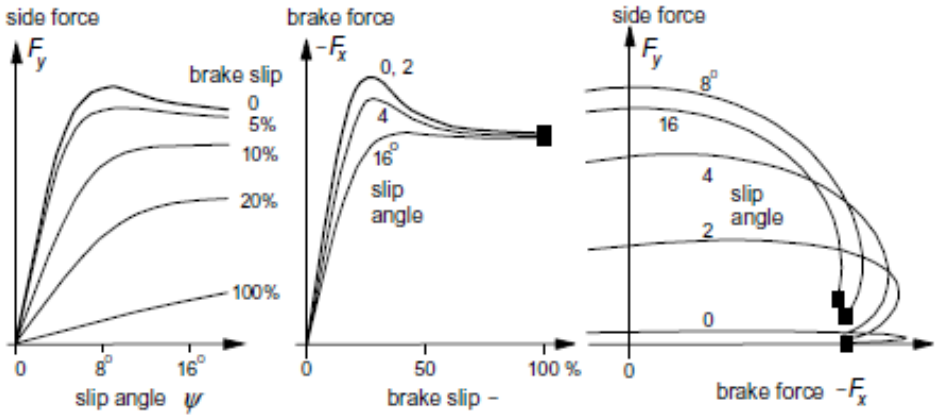

Figure 3-9: Variation of longitudinal and lateral forces with longitudinal slip and slip angle (Pacejka, 2006)

One of the simplest yet useful theories for predicating the maximum available force in the presence of combined slip and slip angle is based on the friction circle concept. Here it is assumed that the maximum friction behaviour of a tyre is independent of the slip direction and the resultant tyre force in any case may not exceed the maximum value of $\mu F_{z,i}$, as shown in Figure 3-10. By employing the friction circle theory, a degree of tyre grip utilisation in any direction, can be defined as follows:

$$\varepsilon = \frac{\sqrt{{F_{y,i}}^2 + {F_{x,i}}^2}}{\mu F_{z,i}} \tag{3-49}$$

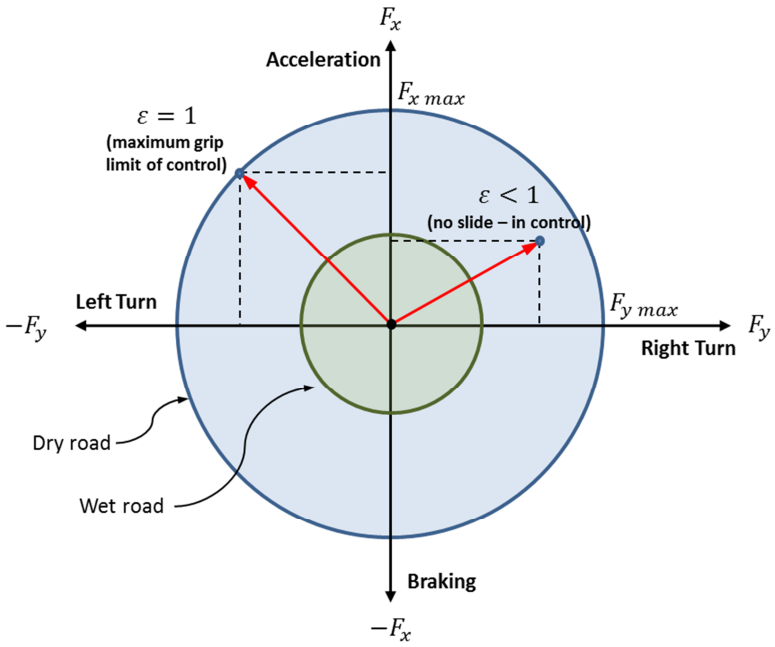

Figure 3-10: Friction Circle

Tyre grip is a very important parameter in vehicle stability analysis: for a given slip and slip angle, $\varepsilon < 1$ means that the tyre is within the friction circle and is in control, by increasing the tyre slip or slip angle, tyre reaches to the point of maximum grip $(\varepsilon = 1)$ so the tyre is in limit of sliding and control. The tyre grip determines the maximum amount of the force that could be generated by a tyre (Milliken & Milliken, 1995). As the radius of the friction circle is equal to $\mu F_{z,i}$, so the maximum achievable force on a tyre (corresponds to a point of $\varepsilon = 1$) dependent on the road coefficient of friction as well as the tyre normal force (see Figure 3-10). By considering the fact that the tyres are the only (high level) vehicle dynamics effectors in a vehicle, the tyre grip margin is one of the main constraints in a vehicle dynamics control allocation scheme.

3.4.1.5 Tyre Normal Force

The tyre normal load $\boldsymbol{F_{z,i}}$ plays an important role in determining the maximum force capability of a tyre as the tyre longitudinal and lateral forces are strongly dependent on the normal force, as shown in the previous sections. The normal forces on a tyre consists of two parts, namely the static and the dynamic loads. The static load is the vehicle weight distribution on each wheel when the vehicle

is at rest, while, the dynamic load is the effect of vehicle load transfer due to longitudinal and lateral accelerations when the vehicle is moving. By assuming the total sprung and unsprung mass as a single mass $\boldsymbol{m}$ and neglecting the roll effect (i.e. suspension effects are not considered), the normal force on each wheel of a vehicle (as shown in Figure 3-4) can be estimated from the following equations (Milliken & Milliken, 1995):

$$
\begin{aligned}
F_{z,1} &= \left[\frac{1}{2}mg\frac{l_r}{(l_f+l_r)}\right] - \left[\frac{1}{2}ma_x\frac{h}{(l_f+l_r)}\right] - \left[\frac{1}{4}ma_y\frac{h}{l_w}\right] \\
F_{z,2} &= \left[\frac{1}{2}mg\frac{l_r}{(l_f+l_r)}\right] - \left[\frac{1}{2}ma_x\frac{h}{(l_f+l_r)}\right] + \left[\frac{1}{4}ma_y\frac{h}{l_w}\right] \\
F_{z,3} &= \left[\frac{1}{2}mg\frac{l_r}{(l_f+l_r)}\right] + \left[\frac{1}{2}ma_x\frac{h}{(l_f+l_r)}\right] - \left[\frac{1}{4}ma_y\frac{h}{l_w}\right] \\
F_{z,4} &= \left[\frac{1}{2}mg\frac{l_r}{(l_f+l_r)}\right] + \left[\frac{1}{2}ma_x\frac{h}{(l_f+l_r)}\right] + \left[\frac{1}{4}ma_y\frac{h}{l_w}\right]
\end{aligned}
\tag{3-50}
$$

where h is the height of vehicle's centre of gravity. In the above equations, the first term represents the vehicle weight distribution on each wheel (static load), the second term is the load transfer due to longitudinal acceleration and the third term is the load transfer as a result of lateral acceleration (dynamic loads).

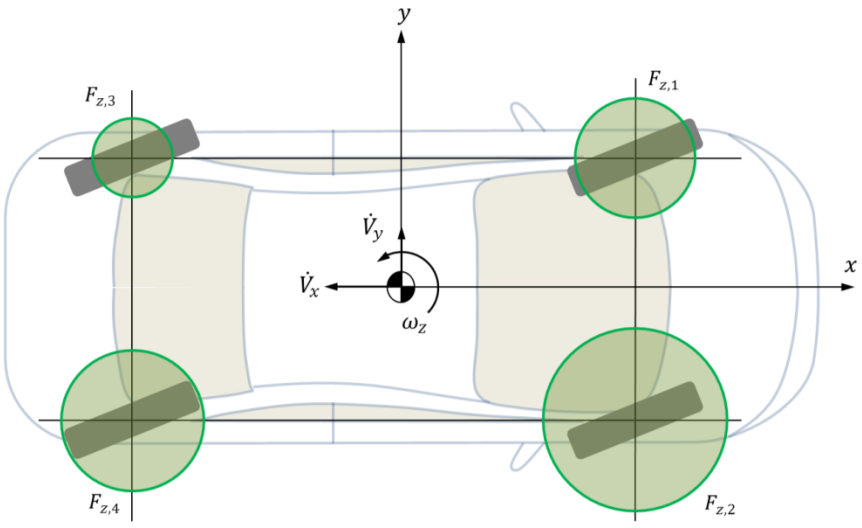

Figure 3-11: Normal forces on the four tyres for a vehicle in left hand cornering

From the above equations, it is clear that the normal loads on the four tyres are not the same when the vehicle is subject to longitudinal and/or lateral acceleration. For example, Figure 3-11 shows an illustration of normal forces for a vehicle during braking in a turn (i.e. subject to simultaneous longitudinal (braking) and lateral forces). For this specific manoeuvre, the highest normal force is applied to the front right tyre and the normal load on the rear left tyre is very low. By assuming a similar coefficient of friction for all the four tyres, the radius of friction circle (i.e. maximum achievable force) on a tyre is determined by its normal force.

3.4.2 Tyre models

As discussed in the previous sections, the linear functions of tyre forces are valid only for small values of slip and slip angle. However, to investigate the vehicle dynamics at or near the stability limit, it is necessary to model the tyre nonlinear behaviour. There exist several tyre models for different applications which can be categorised as physical (such as HSRI, Brush and Fiala models), semi-empirical (like Magic Formula, Dugoff and TMeasy) and empirical methods (Kiébré, 2010). The physical methods are more appropriate for control system development rather than empirical and semi-empirical methods due to their simplicity, accuracy and capability of real time calculation (Heißing & Ersoy, 2011). In this dissertation, we make use of three tyre models namely, Brush, Burckhardt and Pacejka's Magic formulas that have been widely accepted in vehicle dynamics and control investigations (Pacejka, 2006). More specifically, the Pacejka tyre model is employed in the 7-DoF vehicle model[6], Brush model is used for tyre self-aligning moment estimation and the slip control system is developed based on Burckhardt tyre model.

[6] This is an internally developed vehicle model, consist of 3-DoF vehicle planar dynamics (introduced in section 3.3) and four independent wheels dynamics (introduced in section3.6.2). The model was mainly used for control system (MiL) validation in this thesis. See sections 3.7, 4.6.2 and 5.6 for more detail.

3.4.2.1 Brush tyre model

Brush tyre model is an analytical tyre model which has been widely used in several vehicle dynamic analysis and control developments (Pacejka & Sharp, 1991; Ono, Asano, & Koibuchi, 2004; Mokhiamar & Abe, 2004). This model idealised the tyre as a carcase and relies on the assumption that tyre brushes can deform under the axle load to develop the slip on the contact patch. It is further assumed a parabolic pressure distribution along the contact patch and a constant coefficient of friction of the sliding rubber (Pacejka, 2006). The Brush model formulation for pure lateral force is

$$F_{y,i} = \begin{cases} -C_\alpha \tan\alpha + \frac{C_\alpha^2}{3}|\tan\alpha|\tan\alpha\, I_f - \frac{C_\alpha^3}{27}\tan^3\alpha\, I_f^2 & \text{If } |\alpha| \le \alpha_{sl} \\ -\frac{1}{I_f}\operatorname{sgn}\alpha & \text{else} \end{cases} \quad (3\text{-}51)$$

where

$$I_f = \frac{1}{\mu F_z}$$

$$\alpha_{sl} = \tan^{-1}\left(\frac{3}{C_\alpha I_f}\right)$$

in the above formulation, α_{sl} is the slip angle at which the tyre has lost lateral adhesion .Also, with an estimate of cornering stiffness, we only need to estimate the I_f and it is the inverse of maximum lateral force. Similarly, the relationships for longitudinal force in case of pure slip as well as the tyre model for combined slip are also available (Pacejka & Sharp, 1991).

Almost all tyre models propose formulations for direct or indirect calculation of the self-aligning moment. Indirect methods require calculating the pneumatic trial based on the relevant lateral force tyre model. However, in some cases the accuracy of pneumatic trail model is not the same as the lateral force models (Laws, Gadda, Kohn, Yih, Gerdes, & Milroy, 2005). In this dissertation we select a simple yet accurate model for pneumatic trial called ‘affine’ formula (Hsu & Gerdes, 2008) as:

$$t_p = \begin{cases} t_{p0} - \dfrac{t_{p0} C_\alpha}{3} |\tan \alpha| I_f & \text{If } |\alpha| \le \alpha_{sl} \\ 0 & \text{else} \end{cases} \tag{3-52}$$

In this formula the pneumatic trial begins at an initial trial length t_{p0} and vanishes when tyres lose their lateral adhesion. The plot of t_p (normalized by t_{p0}) for different coefficient of frictions is shown in Figure 3-12 (Hsu Y. , 2009).

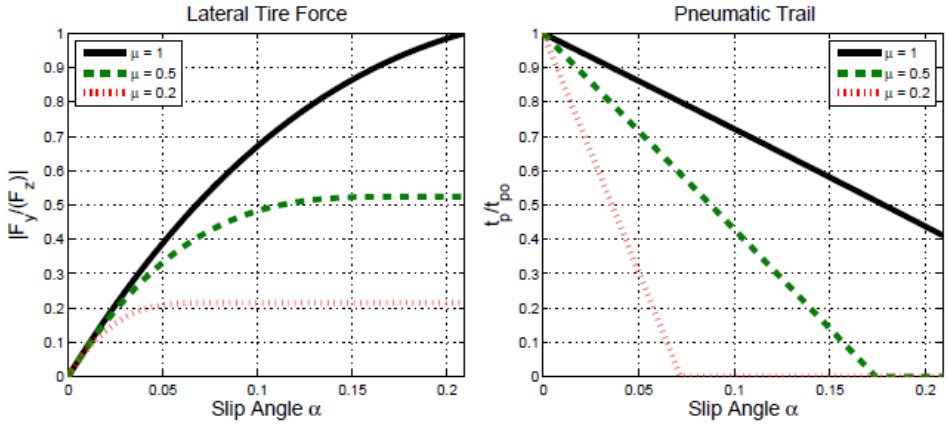

Figure 3-12: Comparison of Lateral Force and Pneumatic Trail (Hsu Y. , 2009)

By using the Brush tyre model for lateral force (equation (3-51)) and the linear pneumatic trail model (equation (3-52)), ignoring the mechanical trail, the tyre self-aligning moment before fully sliding can be obtained from equation (3-48) as:

$$\begin{aligned} M_{z,i} = &-\left(t_{p0} - \frac{t_{p0} C_\alpha}{3} |\tan \alpha| I_f\right) \\ &\times \left(-C_\alpha \tan \alpha + \frac{C_\alpha^2}{3} |\tan \alpha| \tan \alpha \, I_f - \frac{C_\alpha^3}{27} \tan^3 \alpha \, I_f^2\right) \end{aligned} \tag{3-53}$$

After full sliding, the self-aligning moment reduces to:

$$M_{z,i} = \frac{t_m}{I_f} \operatorname{sgn} \alpha \tag{3-54}$$

3.4.2.2 Burckhardt Tyre Model

Burckhardt Tyre Model is a simple model which is derived empirically based solely on steady-state experimental data (Burckhardt, 1993). This model provide the normalised longitudinal force as a function of tyre slip and velocity in the form of

$$F_{x,i}(\lambda_i, V)/F_{z,i} = \left(c_1\left(1 - e^{-c_2\lambda_i}\right) - c_3\lambda_i\right)e^{-c_4 V} \tag{3-55}$$

where $c_1, \ldots, c_4$ are constants.

Alternatively, Burckhardt (Burckhardt, 1993) proposes a simple, velocity-independent model as follows

$$F_{x,i}(\lambda_i)/F_{z,i} = c_1\left(1 - e^{-c_2\lambda_i}\right) - c_3\lambda_i \tag{3-56}$$

With the exception of wet cobblestones, the model exhibit a very precise match to the measured data, and has been widely employed for development of vehicle longitudinal control systems such as ABS and TCS (Savaresi & Tanelli, 2010; Kiencke & Nielsen, 2005).

Note that the model has only three parameters. By changing the values of these three parameters, many different tyre–road friction conditions can be modelled. The parameters of Burckhardt tyre model for different road surfaces are presented in Table 3-1 (Burckhardt, 1993).

Table 3-1: Values of the Burckhardt tyre model coefficients

Road Surface	c_1	c_2	c_3
Asphalt, dry	1.2801	23.99	0.52
Asphalt, wet	0.857	33.822	0.347
Concrete, dry	1.1973	25.168	0.5373
Cobblestone, dry	1.3713	6.4565	0.6691
Snow	0.1946	94.129	0.0646
Ice	0.05	306.39	0

3.4.2.3 Magic Formula tyre model

Pacejka's Magic Formula is one of the most well-known semi-empirical tyre models commonly used in vehicle dynamics simulations and analyses (Kiencke & Nielsen, 2005). The Magic formula is constructed based on the similarity method and produce tyre characteristics that are closely matched to the measured data (Pacejka, 2006; Wong, 2008). Several versions of Pacejka tyre models exist (Kiébré, 2010), however, we use the following form of the model in the case of pure longitudinal slip or lateral slip angle

$$Y(x) = Dsin\{C\ tan^{-1}[B(1-E)Kx + E\,tan^{-1}(BKx)]\} \quad (3\text{-}57)$$

where $Y(x)$ represents the tyre normalised longitudinal force, lateral force or self-aligning moment. Typical values of the coefficients used in the Eq. (**3-57**) for predicating the longitudinal and lateral forces are given in Table 3-2 (Brach & Brach, 2009).

It should be noted that in the above formulation, zero camber is assumed so the tyre horizontal and vertical shifts due to camber angle are ignored. The magnitude of the tyre longitudinal and lateral forces for different road surfaces with various tyre-road friction coefficients and also for different tyre normal loads can be derived by multiplying the normalised values given by Eq. (3-57**)** to the appropriate value of F_z . The typical value of the road coefficient of friction μ for dry concrete or asphalt surface is $= 0.8 \sim 0.9$, for the wet surface is $\mu = 0.5 \sim 0.7$, for the hard snow surface is $\mu = 0.3 \sim 0.5$ and for icy surface is about $\mu = 0.1 \sim 0.3$ (Wong, 2008). For low cost control implementations in a vehicle, the road-tyre friction coefficient should be robustly observed or estimated in real time. There are several algorithms proposed in the literature for estimation of unmeasurable vehicle parameters such as tyre-road coefficient of friction (Ahn, Peng, & Tseng, 2012).

Table 3-2: Values of the coefficients in the Magic formula

Force	x	B	C	D	E	K
Longitudinal	s	1/15	1.5	1.0	0.30	100.0
Lateral	$2\alpha/\pi$	8/75	1.5	1.0	0.60	100.0

The tyre longitudinal and lateral forces in the case of combined slip and slip angle (i.e. combined cornering and braking) can be determined by employing the friction circle theory to the pure longitudinal and lateral tyre forces. The following formulation for (normalised) combined tyre forces, known as Nicolas-Comstock-Brach (NCB) equation, is being employed in some vehicle dynamics software packages, and in this dissertation (Brach & Brach, 2000):

$$F_{x,i}(\alpha, s) = \frac{F_{x,i}(s)F_{y,i}(\alpha)s}{\sqrt{s^2{F_{y,i}}^2(\alpha) + {F_{x,i}}^2(s)\tan^2\alpha}} \frac{\sqrt{s^2{C_\alpha}^2 + (1-s)^2\cos^2\alpha{F_{x,i}}^2(s)}}{sC_\alpha} \quad (3\text{-}58)$$

$$F_{y,i}(\alpha, s) = \frac{F_{x,i}(s)F_{y,i}(\alpha)\tan\alpha}{\sqrt{s^2{F_{y,i}}^2(\alpha) + {F_{x,i}}^2(s)\tan^2\alpha}} \frac{\sqrt{(1-s)^2\cos^2\alpha\,{F_{y,i}}^2(\alpha) + {C_s}^2\sin^2\alpha}}{C_s\sin\alpha} \quad (3\text{-}59)$$

A three dimensional surface plot of the normalised tyre forces for combined slip and slip angle is shown Figure 3-13. It is verified in (Brach & Brach, 2009) that the Eqs. (3-58**)** and (3-59**)** reduce to Eq. (3-57**)**, in case of pure cornering or braking.

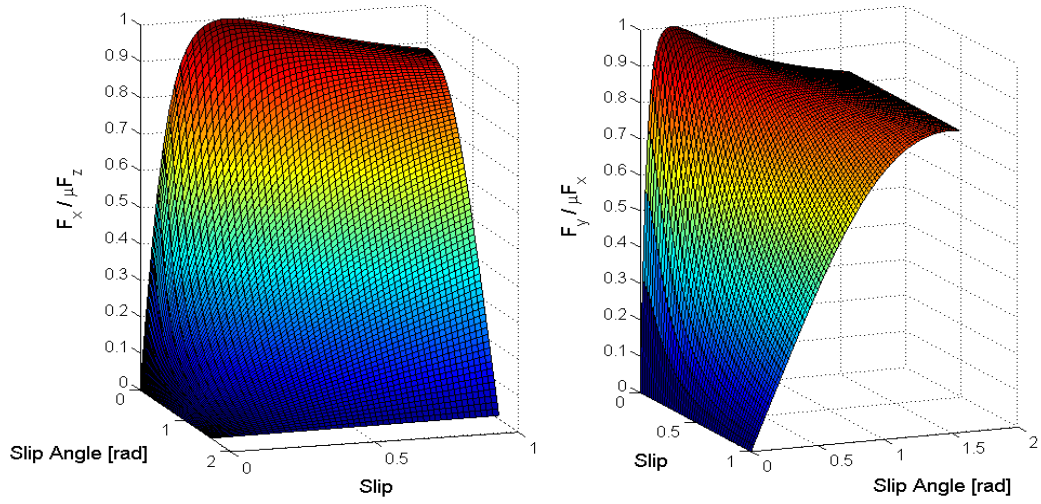

Figure 3-13: Normalised longitudinal and lateral tyre forces for combined slip ad slip angle (Pacejka model)

3.5 Vehicle steady state and transient response

The simple 2 DoF bicycle model, presented in appendix A, provides a suitable mathematical tool to analyse the steady state and transient behaviour of the vehicle in different driving conditions. In the bicycle model, the vehicle yaw rate and sideslip (or lateral velocity) are the two system states whereas the steering angle is the only input to the vehicle (see Eqs. (A-7)and (A-8) for example). Various vehicle dynamics stability and performance measures are defined based on the yaw rate and sideslip responses of the vehicle subject to steering input (Milliken & Milliken, 1995).

Eq. (A-9) (in Appendix A) represents the bicycle model in state-space form. Any linear system represented in state-space form of

$$\dot{\mathbf{x}} = \mathbf{A}\mathbf{x} + \mathbf{B}\mathbf{u}$$

$$\mathbf{y} = \mathbf{C}\mathbf{x} + \mathbf{D}\mathbf{u}$$

can also be described in transfer function form (in Laplace domain) as

$$\mathbf{y}(s) = \mathbf{T}(s)\mathbf{u}(s) \tag{3-60}$$

where $\mathbf{T}(s)$ is the (output to input) transfer function matrix, derived from the following equation (Antsaklis & Michel, 1997)

$$\mathbf{T}(s) = \frac{\mathbf{y}(s)}{\mathbf{u}(s)} = [\mathbf{C}(s\mathbf{I} - \mathbf{A})^{-\mathbf{1}}\mathbf{B} + \mathbf{D}] \tag{3-61}$$

Employing Eq. (3-61) in the state-space representation of the bicycle model (Eq. (A-9)), the transfer functions of yaw rate and sideslip output to steering angle input can be derived as

$$\begin{bmatrix}\beta \\ r\end{bmatrix} = \frac{1}{s^2 - (A_{11} + A_{22})s + (A_{11}A_{22} - A_{12}A_{21})} \begin{bmatrix}B_1 s + (B_2 A_{12} - B_1 A_{22}) \\ B_2 s + (B_1 A_{21} - B_2 A_{11})\end{bmatrix} [\delta] \tag{3-62}$$

The denominator (the characteristic equations) of the both yaw rate and sideslip transfer functions are the same and it is of second order. The characteristic equation which describes the dynamic behaviour of the vehicle can be written as

$$s^2 + 2\zeta\omega_n\, s + \omega_n^2$$

where ω_n and ζ representing the natural frequency and damping ratio of the system, respectively. Therefore the transient behaviour and the stability of the vehicle is determined by two parameters ω_n and ζ (which correspond to the location of the two poles of the system in the s plane) (Ogata, 2010).

From Eq. (3-62) one can conclude that

$$\omega_n^2 = A_{11}A_{22} - A_{12}A_{21}$$

$$2\zeta\omega_n = -(A_{11} + A_{22})$$

and by substituting the values A_{11}, A_{12}, A_{21} and $A_{22}$from Eq. (A-9),

$$\omega_n^2 = \left(\frac{C_f C_r l^2}{m I_z {V_x}^2}\right) - \left(\frac{C_f l_f - C_r l_r}{I_z}\right) \tag{3-63}$$

$$2\zeta\omega_n = \frac{m\left(C_f l_f^2 + C_r l_r^2\right) + I_z\left(C_f + C_r\right)}{m I_z V_x} \tag{3-64}$$

It is worth noting that although the yaw rate and sideslip responses have identical natural frequency and damping (as they have the same characteristic equation in their denominators), their transient specifications (such as rise time, over shoot and so on) are different and determined by their numerators. From Eq. (3-62), the numerator of yaw rate transfer function is $B_2 s + (B_1 A_{21} - B_2 A_{11})$, which can be derived from Eq. (A-9) as:

$$\left(\frac{C_f l_f}{I_z}\right) s + \left(\frac{C_f C_r l}{m I_z V_x}\right) \tag{3-65}$$

Eq. (3-65) is always positive, therefore, has one real root in the left-half s plane (which is the zero of yaw rate transfer function): the vehicle is minimum-phase with respect to yaw rate response.

Similarly, the numerator of sideslip transfer function from Eq. (3-62) is $B_1 s + (B_2 A_{12} - B_1 A_{22})$, and can be derived from Eq. (A-9) as:

$$\left(\frac{C_f}{m V_x}\right) s + \left(\frac{C_f C_r l_r l}{m I_z V_x^2} - \frac{C_f l_f}{I_z}\right) \tag{3-66}$$

The root of Eq. (3-66) is real, but is negative if $V_x > \sqrt{C_r l_r l / m l_f}$. In this case, the zero of sideslip transfer function is in the right-half s plane; therefore, the system is non-minimum-phase with respect to sideslip response. Existence of zero in the right-half s plane causes delay in the system and should be considered in case of sideslip control system design[7].

The natural frequency and damping ratio, as defined above, can be observed as the parameters that are related to various dynamic specifications of the vehicle (Milliken & Milliken, 1995). For example, the well-known understeer gradient (or understeer factor) $\overline{K}$ is defined as (Gillespie , 1992)

$$\overline{K} = \frac{mg}{l}\left(\frac{l_r}{C_f} - \frac{l_f}{C_r}\right) \tag{3-67}$$

[7] See Section 5 for more discussion on the effect of pole and zero on the system behaviour and the control design approach to provide stability and performance specification.

The undamped natural frequency, Eq. (3-63), in terms of understeer gradient is

$$\omega_n^2 = \left(\frac{C_f C_r l}{m I_z {V_x}^2}\right)\left(lg + \bar{K}{V_x}^2\right)$$

The first term defines the natural frequency of the neutral steer vehicle (multiplied by g) which is a function of vehicle speed, whereas, the second term modifies this frequency upward or downward for understeer or oversteer vehicles accordingly[8] and is independent of speed.

The undamped natural frequency is that frequency at which the system would oscillate if the damping were decreased to zero. If the linear system has any amount of damping ζ, the natural frequency which can be observed in reality is the damped natural frequency ω_d which is always lower than the undamped natural frequency ω_n as

$$\omega_d = \omega_n\sqrt{1-\zeta^2} \qquad \text{for} \qquad (0 < \zeta \leq 1) \tag{3-68}$$

For underdamped system ($0 < \zeta < 1$), an increase in damping ratio would reduce the damped natural frequency; for critically damped system ($\zeta = 1$), and overdamped system ($\zeta > 1$) the response will not oscillate (Ogata, 2010). It is interesting to note that, neutral steer vehicles are very nearly critically damped; understeer vehicles are underdamped at all speeds whereas oversteer vehicles are overdamped (Milliken & Milliken, 1995).

The transient and steady-state specifications of a passenger car are presented in Table 3-3. The natural frequency and damping for yaw rate and sideslip response are the same, however, the transient specifications such as rise time, overshoot, etc; are different, as discussed above.

[8] Recall the understeer gradient is positive for understeer vehicles, zero for neutral steer vehicles and negative for oversteer vehicles.

Table 3-3: The vehicle transient and steady-state specifications

$m = 1253\ (kg)$, $I_z = 1957(kg\ m^2)$, $l_f = 1.0(m)$, $l_r = 1.5(m)$ $C_f = 48701$, $Cr = 45836\ (Nm/rad)$	$V_x = 20\ m/s$		$V_x = 30\ m/s$		$V_x = 40\ m/s$	
	r	β	r	β	r	β
Undamped natural frequency, ω_n, rad/sec	4.95	4.95	4.07	4.07	3.72	3.72
Damping Ratio, ζ	0.77	0.77	0.63	0.63	0.52	0.52
Damped Natural Frequency, ω_d, rad/sec	3.14	3.14	3.17	3.17	3.19	3.19
Rise time, t_r, sec	0.25	0.45	0.20	0.46	0.16	0.44
Peak time, t_p, sec	0.58	1.08	0.54	1.04	0.55	1.05
Maximum Overshoot, M_r, %	7.80	2.39	26.3	8.2	50.7	15.3
DC gain,	4.65	-0.67	4.58	-1.27	4.12	-1.65

Figure 3-14 shows the variation of undamped natural frequency, damping ratio and damped natural frequency with speed for the specified vehicle. The vehicle exhibits underdamped (and understeer) behaviour. The undamped natural frequency and damping ratio are decreasing with vehicle speed; however, vehicle (damped) natural frequency is almost constant for high velocities (which is around 3.2 rad/sec). Higher values of the natural frequencies are also reported for various (commercial and race) cars (Milliken & Milliken, 1995); in this thesis, we adopt the magnitude of 6.28 rad/sec (1Hz) as a common natural frequency (bandwidth) of passenger vehicles (plant bandwidth)

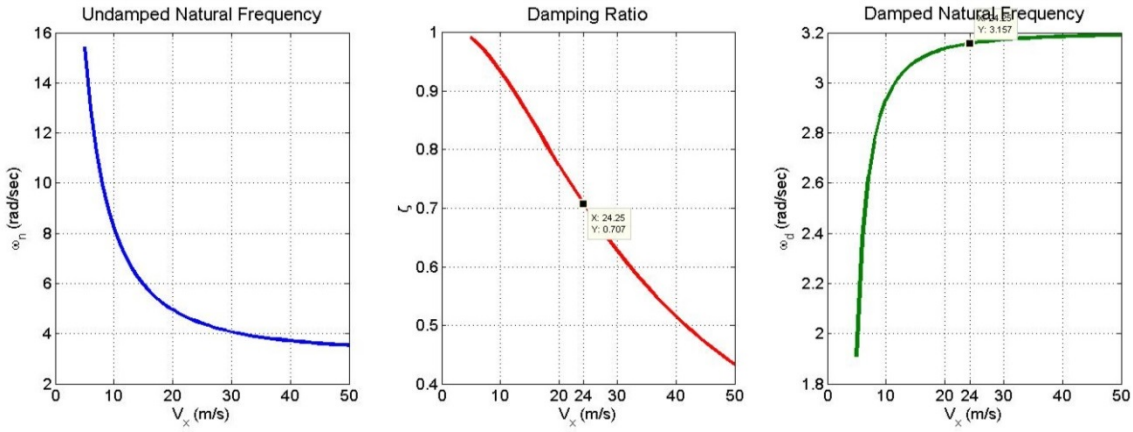

Figure 3-14: Variation of vehicle natural frequencies and damping ratio with speed

In addition to the transient response of the vehicle, the steady-state values of yaw rate and sideslip are important both in vehicle dynamics studies (Pacejka, 2006) and vehicle dynamics control design (Rajamani, 2012). In vehicle dynamics control design, the steady state values of yaw rate and sideslip are considered as the reference (target) values and one of the control system objectives is to track these target values asymptotically (Mokhiamar & Abe, 2004).

To derive the steady-state values one can calculate the DC gain of the state space representation of the system. DC gain is the transfer function value at the frequency $s = 0$, therefore, from Eq. (3-61) the DC gain $\mathbf{K}$ can be derived as

$$\mathbf{K} = \mathbf{T}(0) = \mathbf{D} - \mathbf{C}\mathbf{A}^{-1}\mathbf{B} \tag{3-69}$$

From the bicycle model, represented by Eq. (A-9), the DC gain values for the yaw rate and sideslip are

$$\begin{bmatrix} \beta_{ss} \\ r_{ss} \end{bmatrix} = \frac{1}{(A_{11}A_{22} - A_{12}A_{21})} \begin{bmatrix} (B_2A_{12} - B_1A_{22}) \\ (B_1A_{21} - B_2A_{11}) \end{bmatrix} [\delta] \tag{3-70}$$

By substituting the elements of matrix $\mathbf{A}$ and $\mathbf{B}$ into Eq. (3-70) and after some simplification, the steady-state value of yaw rate is derived as

$$r_{ss} = \frac{V}{l + \frac{mV^2}{l}\left(\frac{l_r}{C_f} - \frac{l_f}{C_r}\right)}\delta \tag{3-71}$$

The characteristic speed V_{Char} is defined as (Gillespie , 1992)

$$V_{char} = \sqrt{\frac{gl}{\overline{K}}} \tag{3-72}$$

where g denotes the gravitational acceleration. The steady-state value of yaw rate in terms of characteristic speed is

$$r_{ss} = \frac{V}{l\left(1 + \left(\frac{V}{V_{Char}}\right)^2\right)}\delta \tag{3-73}$$

It should be noted that the vehicle yaw rate response to steering angle reaches a maximum at the characteristic speed for understeer vehicles (Milliken & Milliken, 1995). This explains another cause for using steady state yaw rate as a target value for the yaw rate controller.

Similarly, the steady-state sideslip can be derived form (3-70) as

$$\beta_{ss} = \frac{l_r - \frac{mV^2}{l}\frac{l_f}{C_r}}{l\left(1 + \left(\frac{V}{V_{Char}}\right)^2\right)}\delta \tag{3-74}$$

As the maximum lateral acceleration of the vehicle is limited by the maximum adhesion between the tyre and the road,

$$\left|a_y\right| \leq |\mu . g| \tag{3-75}$$

therefore, the desired yaw rate and sideslip (as defined by Eqs. (3-73) and (3-74)) cannot always be achieved. The following values are suggested for the maximum value (upper bound) of the yaw rate and sideslip targets (Rajamani, 2012)

$$r_{upper\_bound} = 0.85\frac{\mu g}{V} \tag{3-76}$$

$$\beta_{upper\_bound} = \tan^{-1}(0.02\,\mu g) \tag{3-77}$$

3.6 Chassis control systems model

The chassis control systems encompass all the active systems (smart actuators) associated with steering, brake and suspension which can affect the longitudinal, lateral and vertical dynamic behaviours of a vehicle. These active systems can be further classified into handling (safety) control, ride comfort control and driver assistance control systems based on their primary vehicle dynamic domains as well as their primary functions (Heißing & Ersoy, 2011). It is assumed that the Electric Power-Assisted Steering (EPAS) and active brake force intervention (EHB) are the only chassis control systems available in the vehicle (see section 3-1). A brief description of these systems and their mathematical models are presented in the following sections.

3.6.1 Electric Power-Assisted Steering (EPAS) Model

3.6.1.1 EPAS System Overview

It was shown in section 3.4.1.2 that the tyre lateral forces are generated as a result of tyre slip angle. In a ground vehicle, the steering is the main system dealing with the lateral vehicle dynamics and has the function of transferring the driver input steering angle/torque to the front wheels in order to provide overall directional control of the vehicle (Gillespie , 1992).

A column type Electric Power-Assisted Steering, as shown in Figure 3-15, consists of an electric motor attached to the steering column through a reduction gear, a torque sensor, a current sensor and an Electric Control Unit (ECU). The amount of the torque applied by the driver to the steering wheel is measured by a torque sensor mounted in between the steering wheel and steering column. Based on the measured driver torque, the EPAS ECU calculates the additional torque required to turn the wheels and control the electric motor to ensure that the requested torque is generated by the electric motor. The current sensor measures the motor current and provides the feedback signal to the ECU controller to close the motor current control loop.

The generated torque by the electric motor will be superimposed to the driver input torque based on the driving mode: In normal driving conditions (comfort mode) the EPAS always adds torque to the steering system, whereas in stability mode the torque may be added or subtracted (Motoyama, 2008).

3.6.1.2 EPAS Model

The Electric Power-Assisted Steering system can be modelled with a number of masses lumped together with spring and dampers (and friction) elements. The full order (complete) model of an EPAS system is proposed in (Badawy, et al., 1999), however, it is possible to reduce the order of the models by combining two or more of the masses into one, and also ignoring the compliances that has little effects to the overall dynamics of the system. Validity of the reduced order can be verified by analysing the frequency response of the system: It is shown in (Badawy, et al., 1999) that the ignored elements in the reduced order model only affect the higher frequency modes of the system (greater than system cut off frequency), which are usually unimportant to the fundamental behaviour of the system and are dominated by lower frequency modes

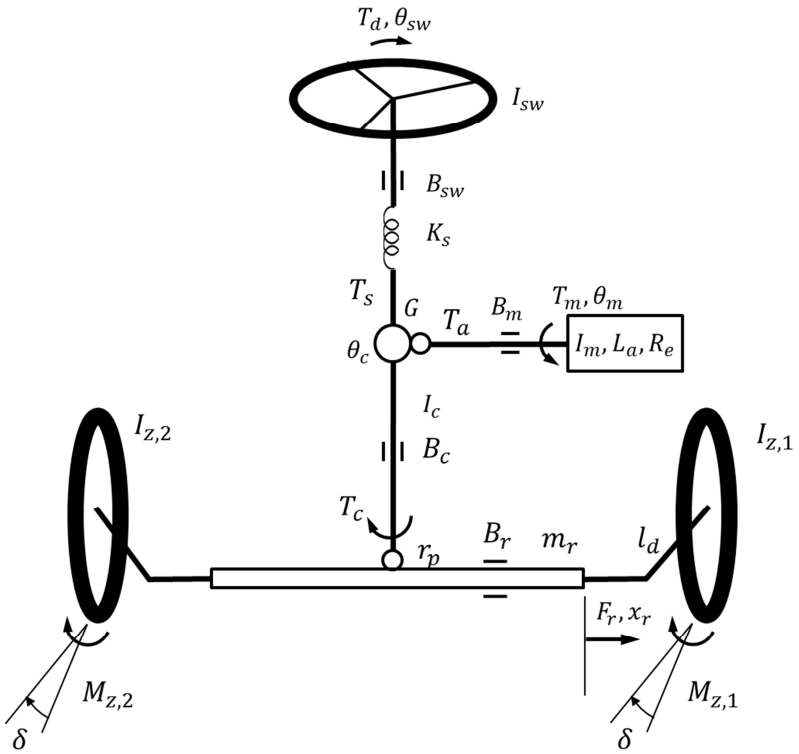

Figure 3-15: EPAS dynamic model

A well accepted model of an EPAS is showing in Figure 3-15 (Badawy, et al., 1999; Chen, et al., 2008) in which, the steering wheel is modelled by an inertia (I_{sw}), the torque sensor is modelled by a spring (K_s) and a damper (B_{sw}). The DC electric motor is connected to the steering column via a reduction gear G and its electrical parts are modelled by inductance (L_a) and resistance (R_a) and the mechanical parts by shaft inertia (I_m) and damper (B_m). The column consists of an inertia I_c, and a damping B_c and is connected to the rack by a rack and pinion mechanism with the pinion radius of r_p. It is assumed that the rack has a mass of m_r and a damping of B_r. The rack is attached to the vehicle wheel by drop link mechanism which has the length of l_d .The rack force F_r multiplied to the drop link (moment arm) generate a moment $M_{w,i}$ $(i = 1,2)$ around the z axis at each front wheels to overcome the inertial torque, which is the product of the wheel inertia, $I_{z,i}$,and the wheel angular acceleration, $\ddot{\delta}$ and also the front tyres self-aligning moment $M_{z,i}$ $(i = 1,2)$. It should be noted that in this steering model the effect of suspension kinematics and compliance are not considered.

The governing equations for the described EPAS system are (Chen, et al., 2008; Zaremba, et al., 1998):

- The steering wheel dynamics:

$$I_{sw}\ddot{\theta}_{sw} + B_{sw}\dot{\theta}_{sw} = T_d - T_s \tag{3-78}$$

$$T_s = K_s(\theta_{sw} - \theta_c) \tag{3-79}$$

$$I_{sw}\ddot{\theta}_{sw} + B_{sw}\dot{\theta}_{sw} + K_s\theta_{sw} - K_sN\delta = T_d \tag{3-80}$$

$$N = l_d/r_p \tag{3-81}$$

- The DC electric motor dynamics:

$$I_m\ddot{\theta}_m + B_m\dot{\theta}_m = T_m - T_a \tag{3-82}$$

$$T_m = k_t i_a \tag{3-83}$$

$$I_m\ddot{\theta}_m + B_m\dot{\theta}_m = k_t i_a - T_a \tag{3-84}$$

$$L_a\frac{di_a}{dt} + R_a i_a + K_e\dot{\theta}_m = u \tag{3-85}$$

- The steering column dynamics:

$$I_c\ddot{\theta}_c + B_c\dot{\theta}_c = T_s + GT_a - T_c \tag{3-86}$$

$$\theta_c = N \times \delta \tag{3-87}$$

- The steering rack dynamics:

$$m_r\ddot{x}_r + B_r\dot{x}_r = F_r - \frac{1}{l_d}\left(T_{w,1} + T_{w,2}\right) \tag{3-88}$$

$$x_r = l_d \times \delta \tag{3-89}$$

$$F_r = T_c/r_p \tag{3-90}$$

- The wheel (lateral) dynamics :

$$I_{z,i}\ddot{\delta} = T_{w,i} - M_{z,i} \qquad i = 1,2 \tag{3-91}$$

Combining equations (3-86), (3-87), (3-81), (3-88), (3-89), (3-90) and (3-91) yields the following equation for the column, rack and wheel dynamics:

$$I_{eq}\ddot{\delta} + B_{eq}\dot{\delta} = T_s + GT_a - \frac{1}{N}T_{sat} \tag{3-92}$$

where

$$I_{eq} = \frac{1}{N}\left[N^2 I_c + (I_{z,1} + I_{z,2}) + l_d^2 m_r\right] \tag{3-93}$$

$$B_{eq} = \frac{1}{N}\left[N^2 B_c + l_d^2 B_r\right] \tag{3-94}$$

and T_{sat} is the total self-aligning moment of the front left and front tyres

$$T_{sat} = M_{z,1} + M_{z,2} \tag{3-95}$$

From equation (3-48**)** (and by ignoring the mechanical trail), the self-aligning moment for each tyre is the product of tyre lateral force to pneumatic trail:

$$M_{z,i} = t_{p,i} \times F_{y,i}$$

so the equation (3-95) can be written as a function of the (front) tyre lateral forces :

$$T_{sat} = \left(t_{p,1} \cdot F_{y,1} + t_{p,2} \cdot F_{y,2}\right) \tag{3-96}$$

For the linear bicycle model, presented in appendix A, the self-aligning moments of the left and right tyres are equal, therefore, the front tyres (total) self-aligning moment is

$$T_{sat} = 2t_p C_{\alpha f} \alpha_f = 2t_p C_{\alpha f}(\delta - \beta - \frac{l_f}{V_x}\omega_z) \tag{3-97}$$

and the equation (3-96**)** can be written as:

$$I_{eq}\ddot{\delta} + B_{eq}\dot{\delta} + 2t_p C_{\alpha f}\delta = T_s + GT_a + 2t_p C_{\alpha f}\beta + \frac{2t_p C_{\alpha f} l_f}{V_x}\omega_z \tag{3-98}$$

The equations (3-80), (3-84), (3-85) and (3-98) represent the complete EPAS (linear) model including with vehicle dynamics. The system has two inputs as driver torque (T_d) and motor voltage (u) and two outputs as vehicle yaw rate (ω_z) and sideslip (β), which can be presented in block diagram as Figure 3-16.

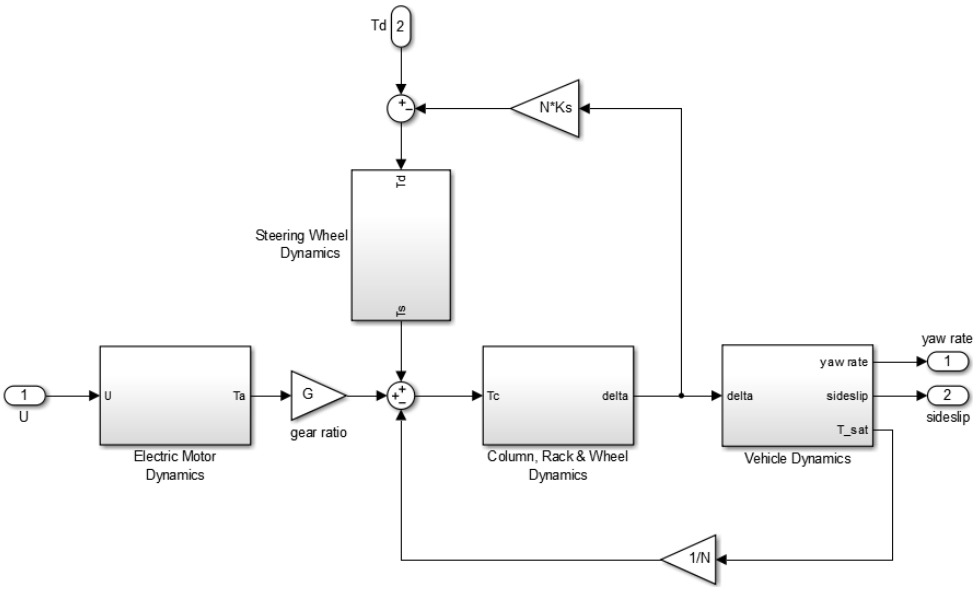

Figure 3-16: EPAS and vehicle dynamics block diagram

It should be noted that this linear model was derived by employing the linear bicycle model, which is based on several simplifying assumptions as discussed in the previous chapters. The main advantage of this model is its linearity, which makes it suitable and valid for linear control system design. One should also note that, to derive a linear dynamics model for EPAS, the steering nonlinearities such as friction, is ignored. The friction term will be added as a feed-forward term to the closed loop controller, as will be presented in Chapter 6. The parameters of the EPAS system which is employed in this research is indicated in Appendix B.

3.6.2 Wheel dynamics

In section 3.4.1.1 the relationship between the applied tractive / braking torque to the wheel and the generated longitudinal force on the tyre was discussed without considering the dynamics of the rotating tyre/wheel, however, in case of high longitudinal tyre slip (such as hard braking), wheel dynamics often constitute a dominant part (Jonasson, 2009). The wheel dynamics can be modelled by constructing the wheel free body diagram as shown in Figure 3-17. Here the effect of rolling resistance is ignored and it is assumed that the wheel has rotational moment of inertia $J_{y,i}$ along the y axis (axis of spin) and is subject

to tractive or braking torque $T_{w,i}$ at the wheel hub (centre) as well as the longitudinal force $F_{x,i}$ at the centre of tyre-ground contact patch.

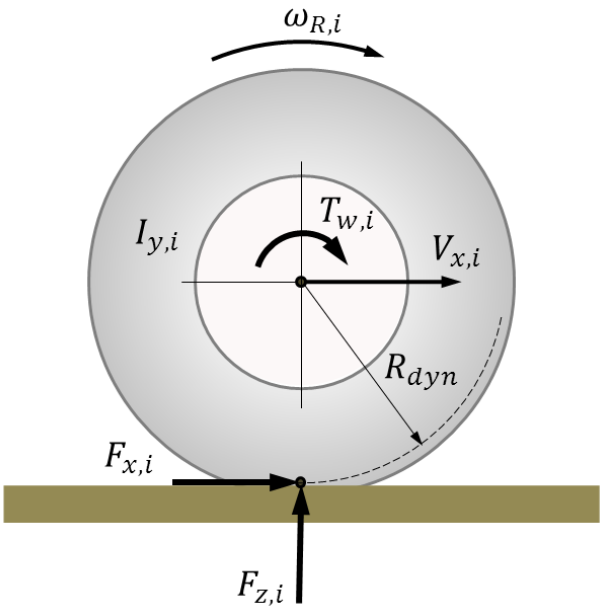

Figure 3-17: wheel free body diagram

For each wheel, the equation of rotational motion can be derived as

$$J_{y,i}\dot{\omega}_{R,i} = T_{w,i} - R_{dyn}F_{x,i} \qquad i \in \{1,2,3,4\} \tag{3-99}$$

where $i = 1,2,3,4$ representing the front left, front right, rear left and rear right wheels respectively.

3.6.3 Brake Model

In passenger vehicles, the required braking torque about the wheel spin axis to change the slip ratio and subsequent braking forces is produced by a hydraulic brake mechanism. In the passive (or standard) brakes, the driver input brake pedal force is amplified by a vacuum booster and then transformed to hydraulic pressure and distributed to four wheel-brake cylinder assemblies by the master cylinder mechanism. The wheel-brake assembly consists of calliper pistons, brake pads and brake discs, which transform hydraulic pressure to braking torque. However, in the active braking systems, such as (conventional) ABS or ESP, the hydraulic pressure (partially or totally) build up by a hydraulic

modulator unit connected in between the brake master cylinder and the wheel-brake cylinders. The hydraulic modulator unit actively modulate the hydraulic pressure on each wheel and consist of 8 or 12 solenoid valves, a plunger pump, a reservoir chamber, a damper, a pressure sensor and an ECU. (Robert Bosch GmbH, 2011).

The basic arrangement of a hydraulic brake system is modelled from fundamental principles of incompressible hydraulic flow: the braking torque T_b is proportional to the acting brake line pressure P on the calliper piston (Gerdes & Hedrick, 1999). The braking torque in each wheel is developed as the result of friction force between brake pads and brake discs (Limpert, 2011):

$$T_{wb,i} = n\mu_b F_n R_d \tag{3-100}$$

where n is the number of brake pads, μ_b is the coefficient of friction between the brake pads and the disc, F_n is the normal brake force applied to the brake pad and R_d is the radius of the pad centre from the wheel centre. Here, the coefficient of friction μ_b is assumed constant; however, this is a simplification as this coefficient is a function of several variable among which temperature plays a significant role (Limpert, 2011). The normal force on the brake pad is developed by application of hydraulic line pressure on the brake pad surface area so the braking torque on each wheel can be calculated by the following equation (Blundell & Harty, 2004):

$$T_{wb,i} = n\mu_b P_l A R_d \eta_c \eta_p \tag{3-101}$$

where A is the brake pad area, P_l is the hydraulic line pressure, η_c is wheel cylinder efficiency, to consider the hydraulic line pressure losses and η_p is pedal level efficiency which includes the efficiency of the master cylinder. Typical values for the pedal level efficiency, η_p, is 0.8 and for the wheel-brake cylinder efficiency, η_c, is 0.98 for disc brakes (Limpert, 2011).

Note that in derivation of Eqs. (3-100) and (3-101) a static brake pad friction model is assumed, i.e., the braking torque $T_{wb,i}$ is computed from the measured brake pressure $P_{l,i}$. The brake pads friction coefficient is in general not perfectly

constant over the brake life, as it varies mainly due to brake usage. However, the variation of the braking dynamic behaviour is in general might be considered as an uncertainty which could be compensated by the closed loop control system[9].

The dynamic response of the hydraulic brake system is normally modelled by a first order time lag transfer function between input and output variables. The time delay to build up pressure in the hydraulic line is very small and is typically less than 0.1 to 0.2 sec (Limpert, 2011).

Considering the time lag τ_{cal} for line pressure build up, the relationship between hydraulic line pressure and wheel brake torque is

$$T_{wb,i} = K_{b,i} P_{l,i} \left(\frac{1}{\tau_{cal} s + 1} \right) \tag{3-102}$$

It is shown in (Gerdes & Hedrick, 1999) that this simple linear model exhibits a right balance between fidelity and simplicity for brake control system development applications. The detailed modelling of ABS and ESP hydraulic modulator valves can be found in (van Zanten, et al., 1996) for example, and are not presented here.

3.7 Vehicle Model Validation

The model development often involves several inevitable trade-offs between completeness and simplicity. As the construction of a model (especially for control design purpose) often involves several levels of simplification and abstraction, the outputs of the model deviate to a greater or lesser extent from the real values. Having concerns about the reliability of the simulation outputs, *fidelity* is defined as the measure of degree to which a model reproduces the state and behaviour of the real system. To ensure the appropriate level of fidelity, some criteria should be defined with respect to a prior knowledge, standards or perceptions of the system behaviour (Gross, 1999). The process of verification of the model against the fidelity criteria is known as model

[9] Design of the closed loop brake control system is presented in section 6.3.2.

validation. The traditional method of validation is to evaluate the reaction of the model to measured data and compare it with actual test results (Kiencke & Nielsen, 2005). By introducing high fidelity off-the-shelf simulation packages in recent years, it is possible to employ these validated models as a reliable virtual test platform for the purpose of validation (Kathrin, et al., 2012). The list of the vehicle models employed in this thesis can be summarised in Table 3-4 below.

Table 3-4: The list of vehicle models employed in the thesis

Name	DoF	Equations	Purpose	Developer
Bicycle Model	2	(A-7) & (A-8)	Reference Generator	By Author
7 DoF Model	7	(3-34), (3-35) & (3-36) (3-58) & (3-59) (3-99)	Control system MiL validation	By Author
CarMaker® Version 4.0.6	14	CarMaker® Reference Manual (IPG Automotive GmbH, 2013)	Validation of 7DoF Model Control system HiL validation	IPG Automotive GmbH

To validate a vehicle model one can employ several driving manoeuvres and test scenarios which have been defined by automotive manufacturers or certification bodies, covering the open loop and closed loop (driver included) tests, such as:

Longitudinal vehicle dynamics behaviour:

- *Straight ahead braking and accelerating driving*
- μ-split braking (ISO 14521)

Lateral vehicle dynamics behaviour:

- *Step steer (ISO 7401)*
- *Sine input*
- *Sine with dwell (FMSS126)*
- *Sine Sweep (0-4 Hz) (ISO 7401)*

- *Constant Radius Test (ISO 4138)*
- Lane Change (ISO 3888)

It should be noted that the above standard test procedures (or any other legislation standards) need to be simplified before being employed in model validation as they include many specifications that are not directly relevant to simulation. Selection of the proper driving manoeuvres are based on the dynamic variables of the model to be validated: For the longitudinal vehicle dynamics validation, the open loop '*Straight ahead braking and accelerating driving'* and for lateral vehicle dynamics validation, '*Step steer*' and '*Sine input*' manoeuvres would be suitable (Kiencke & Nielsen, 2005).

As a part of the model validation effort in this dissertation, the simulation results of the proposed 7-DoF vehicle model were compared with an off-the-shelf vehicle dynamics simulation package, CarMaker® form IPG Automotive GmbH. IPG CarMaker® employs a complex 14 degrees of freedom vehicle dynamics model and can produce response characteristics comparable with experimental data taken from real vehicles. Interestingly, IPG CarMaker® has been successfully employed for simulation based homologation of different active safety systems (Kathrin, et al., 2012).

The following lateral dynamics manoeuvres are selected for simulation:

1) High mu surface, step steer, low speed (**Step60_mu1.0_V65**): at road coefficient of friction $\mu = 1.0$, a 60° step steer will apply within 1 second to the vehicle which have initial longitudinal speed of 65 Kph, the manoeuvre will be performed off-throttle.
2) High mu surface, step steer, high speed (**Step60_mu1.0_V100**): the same conditions as previous manoeuvre but with the longitudinal velocity of 100 Kph.
3) Low mu surface, step steer, low speed (**Step60_mu0.2_V20**): at road coefficient of friction $\mu = 0.2$, a 60° step steer will be applied within 1 second to the vehicle which have initial longitudinal speed of 20 Kph, and the manoeuvre will be performed on-throttle.

4) High mu surface, step steer, high speed (**Step60_mu0.2_V50**): the same condition as previous manoeuvre but with the longitudinal velocity of 50 Kph.
5) In the second group of manoeuvres, the steering command is changed to a sinusoidal input with amplitude of 60° and period of 2 sec. The rest of the driving conditions are similar to previously defined manoeuvers. (Nominated as: **Sin60_mu1.0_V65**, **Sin60_mu1.0_V100**, **Sin60_mu0.2_V20** and **Sin60_mu0.2_V50,** respectively).

The control inputs for the step steer and sinusoidal steer manoeuvers (as described above) are plotted in Figure 3-18.

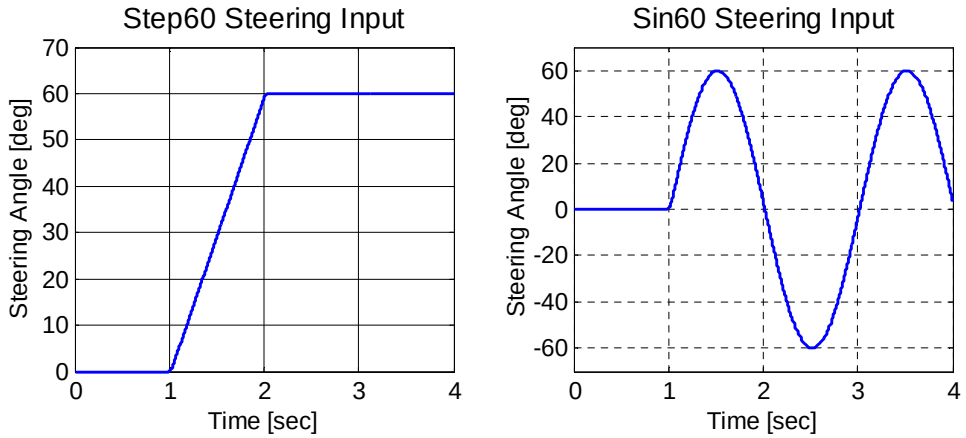

Figure 3-18: Control Input for Step60 and sin60 manoeuvers

In the following figures, the simulation results of the proposed 7-DoF vehicle model (using combined magic formula tyre model, as presented in section 3.4.3 by Eqs. (3-58) & (3-59)) are compared to IPG CarMaker® results, for various step and sinusoidal steer input manoeuvers. The vehicle data set for Peugeot 206CC was selected from CarMaker® vehicle library (Demo_Peogeot_206CC). The corresponding vehicle parameters for 7-DoF vehicle model are indicated in Appendix A. One should note that the CarMaker® model is a fully validated vehicle model including suspension Kinematics and Compliance, engine model, extensive tyre models all tyre, with all real car geometries such as wheel caster and camber, and so on; including all 6 degree of freedoms motions of the

vehicle body. The 7-DoF vehicle model, on the other hand, just considers the vehicle planar motion, as described in previous sections.

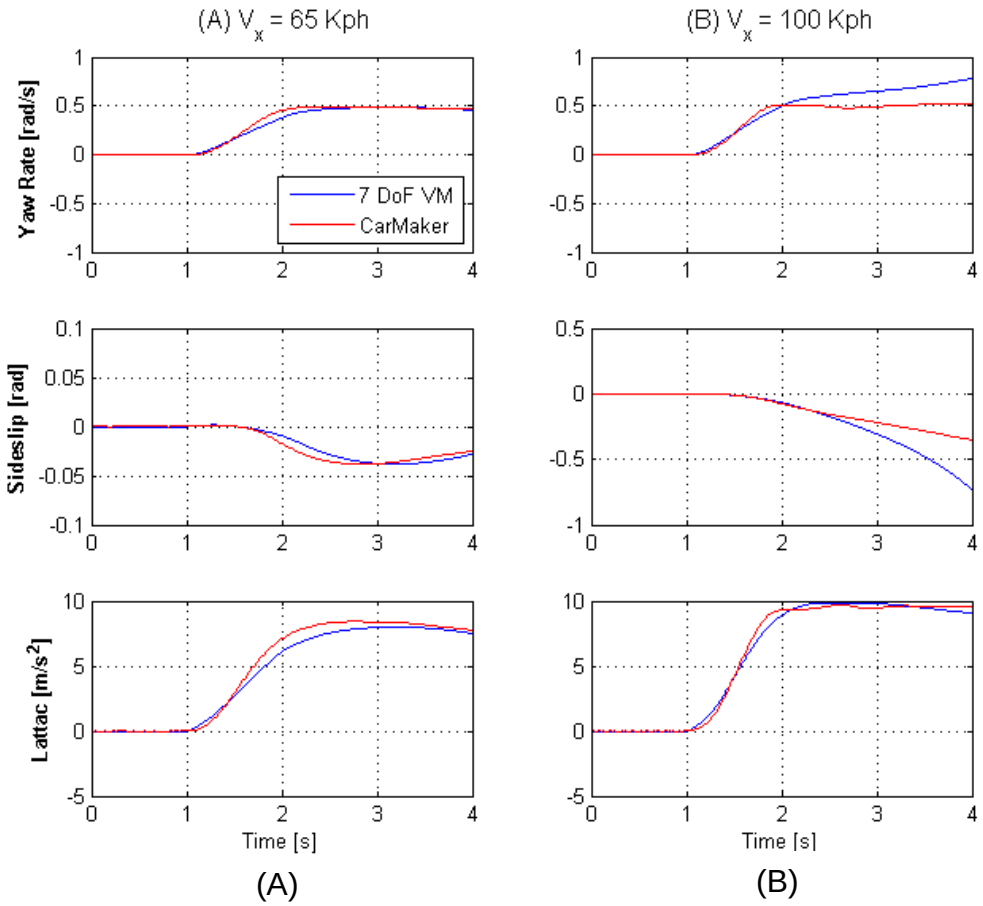

Figure 3-19: Vehicle response comparison between 7-DoF Vehicle Model and CarMaker® for 60° steering Step Inputs, μ=1.0, Off-Throttle

The comparative simulation results for step steer input manoeuvres at high mu surface (Step60_mu1.0_V65 and Step60_mu1.0_V100) are shown in Figure 3-19. At longitudinal velocity of 65 Kph, the vehicle is stable and the simulation results obtained from 7 DoF vehicle model is a good match to CarMaker® outcome. Increasing the vehicle speed to 100 Kph makes the vehicle unstable (spin out - oversteer) as confirmed by yaw rate and sideslip responses in Figure 3-19 (B). The simulation results of CarMaker® show more oversteering behaviour than 7-DoF vehicle model, which might be due to roll effect (Milliken & Milliken, 1995). However, the lateral acceleration in both models are almost identical.

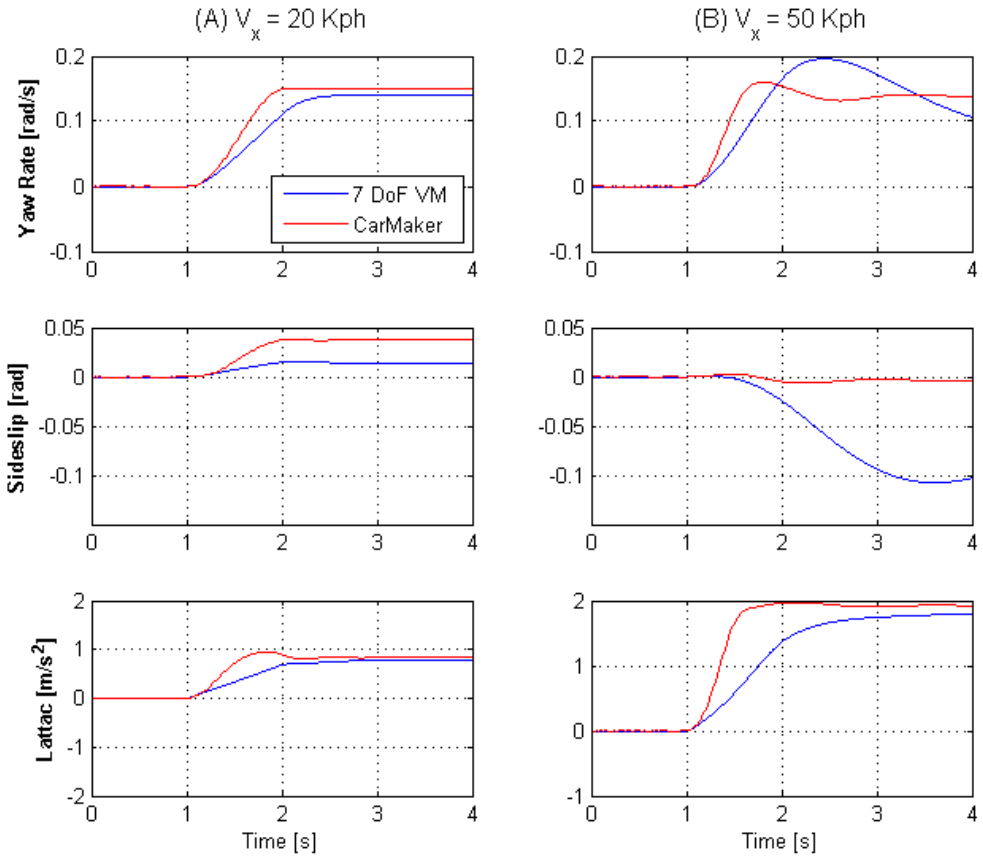

(A) (B)

Figure 3-20: Vehicle response comparison between 7 DoF Vehicle Model and CarMaker® for 60° steering Step Inputs, μ=0.2, On-Throttle

Similarly, the comparative simulation results for step steer input manoeuvres at low mu surface (Step60_mu0.2_V20 and Step60_mu0.2_V50) are shown in Figure 3-20. At longitudinal velocity of 20 Kph, the vehicle is stable and the simulation results for yaw rate and lateral acceleration from both models are matched well to each other, however, the 7-DoF vehicle exhibits slower (and more damped) transient response than carmaker. Moreover the sideslip results of 7-DoF model is lower than CarMaker® result, as shown in Figure 3-20(A). By increasing the vehicle speed to 50 Kph, the difference between the results of two models becomes higher, as shown in Figure 3-20(B). The main reasons might be from the accuracy of the tyre model that we used in our 7-DoF vehicle model. It seems that the combined Pacejka tyre model, as presented in section 3.4.3, is less accurate than the CarMaker® tyre model at low slip and sideslip values.

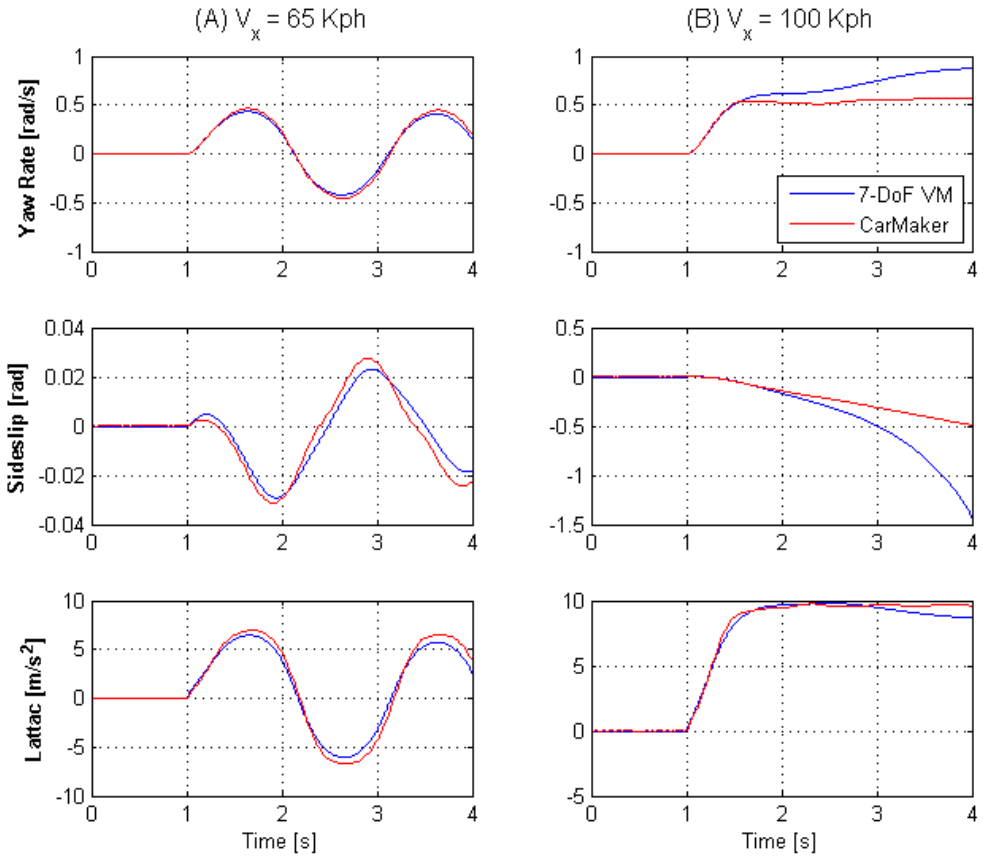

(A) (B)

Figure 3-21: Vehicle response comparison between 7-DoF Vehicle Model and CarMaker® for 60° steering Sine Inputs, μ=1.0, Off-Throttle

The comparative simulation results for sinusoidal steer input manoeuvres at high and low mu surfaces (Sin60_mu1.0_V65, Sin60_mu1.0_V100, Sin60_mu0.2_V20 and Sin60_mu0.2_V50) are shown in Figure 3-21 and Figure 3-22, respectively.

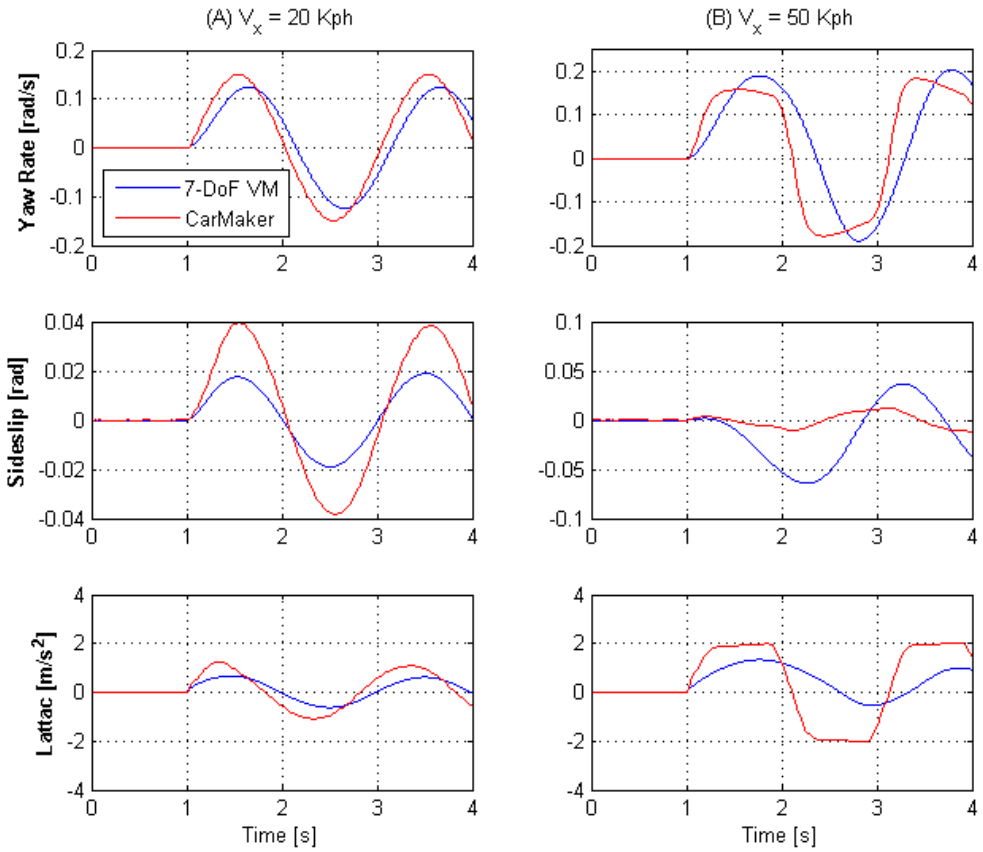

Figure 3-22: Vehicle response comparison between 7-DoF Vehicle Model and CarMaker® for 60° steering Sine Inputs, μ=0.2, Off throttle

By investigating the results for the sine steer input, the same conclusion can be made: The 7-DoF vehicle model produce good results at high mu surfaces, however, the results at low-mu surfaces (especially for sideslip response) does not match the CarMaker® results. More importantly, the CarMaker® exhibits faster response times and more overdamped behaviour than the 7-DoF vehicle model. Transient response of the system (and its subsystems) is important; especially when we are dealing with the design of several controllers and actuators in cascade control system architecture. To design a stable and high performant integrated control system, the plant bandwidth in each loop should be carefully respected as will be discussed in the next chapters.

The main drawback of CarMaker® package, is that all the system (and sub-system) models are provided in S function, so there is no access for the user to

make any changes to the structure of the model. Moreover, the software needs an extensive data input to run, which makes it less flexible for control system development. The 7-DoF vehicle model, on the other hand, provides a simple, flexible, and relatively accurate platform for control system validation. In this thesis, we employ the 7-DoF vehicle model for control system validation in different development stages. The final control system tuning and validation step, however, will be performed on the integrated EPAS&ESP HiL setup with real driver in the loop, real steering and brake smart actuators, and by employing CarMaker/HiL® model running in a real time environment, as explained in Chapter 7.

4 High-Level Control System Development

4.1 Introduction

The proposed IVCS system employs stability control in case of stability conditions[10]. Stability control block consists of high-level vehicle motion controls, control allocation and low-level smart actuators (in this work, steering and brake) controls, as explained in Chapter 2. The Simulink® block diagram of the integrated stability control system is shown in Figure 4-1.

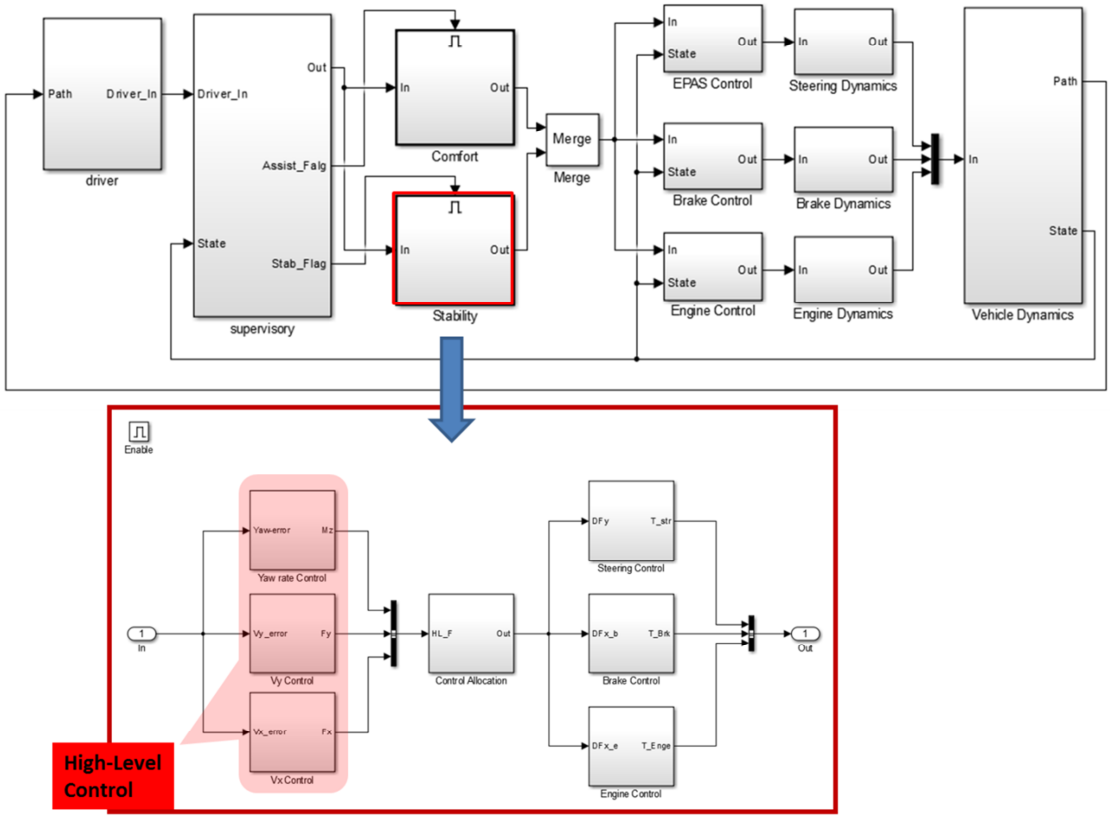

Figure 4-1: High-Level Control Simulink® Blocks

Design of high-level control system is presented in this chapter. The proposed control allocation scheme as well as a detailed design of low-level steering and brake controllers are discussed in Chapter 5 and 6, respectively.

---

[10] See section 2.2 for more detail description and criteria of *mild* and *hazardous* stability conditions in IVCS system.

4.2 MIMO control system

The high-level vehicle dynamics equations of motion was defined in Chapter 3 as:

$$\begin{bmatrix} \dot{V}_x \\ \dot{V}_y \\ \dot{\omega}_z \end{bmatrix} = \begin{bmatrix} V_y\omega_z \\ -V_x\omega_z \\ 0 \end{bmatrix} + \begin{bmatrix} 1/M & 0 & 0 \\ 0 & 1/M & 0 \\ 0 & 0 & 1/I_z \end{bmatrix} \begin{bmatrix} F_x \\ F_y \\ M_z \end{bmatrix} \tag{4-1}$$

In the above equation, $[F_x \quad F_y \quad M_z]^T$ is the vector of the generalised forces and moments (applied at the vehicle's centre of gravity) as system input and $[V_x \quad V_y \quad \omega_z]^T$ is the vector of vehicle planar motions as system output. Equation (4-1) is a Multi-Input Multi-Output (MIMO) system with 3 inputs and 3 outputs. It is clear that making a change in the system inputs (yaw moment M_z, for example) will affect all the outputs (vehicle motions), so there is interaction between the inputs and outputs as shown in Figure 4-2**.**

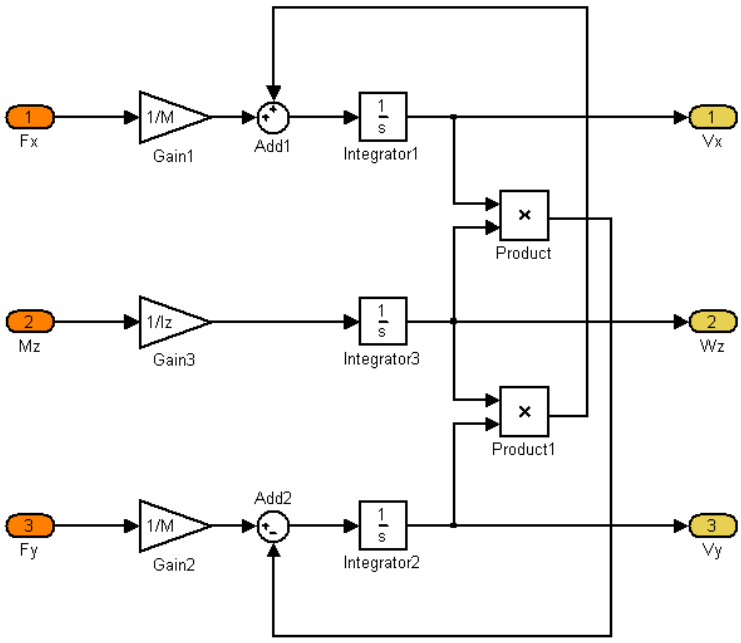

Figure 4-2: Block diagram of the high-level vehicle dynamics equations of motions

The first and second equations of the MIMO system described by Eq. (4-1) are nonlinear (because of the existence of cross product terms) and thus it is

required to design an appropriate controller that can guarantee stability (and performance, if feasible). One alternative to design such a controller for the above nonlinear system is to employ a nonlinear MIMO control design method such as MIMO sliding mode control (Wang, 2007); However, nonlinear controller designs are hard to implement in practice because of their much more complex behaviour in comparison to linear systems (Slotine & Weiping, 1991; Goodwin, 2002). In this thesis, we present a new approach for design of high level vehicle dynamics control system to come up with a simple yet robust controller which can be implemented in real time ECU with low computational cost. The proposed control design process consists of the following three steps:

1. *System linearisation*: The vehicle dynamics equations of motions equation (4-1) is linearised around an operating point.
2. *System decoupling*: It is shown that the linearised MIMO system could be decoupled into three Single-Input Single-Output (SISO) pairs at the crossover frequency[11].
3. *Decentralised (SISO) feedback control design*: at the final stage, the Q-parameterisation method[12] is employed to design three simple yet robust SISO motion controllers.

The stability and performance of the designed control system (including its robustness) will be examined by analysis as well as by simulation with the 7-DoF vehicle model.

In the following sections, the fundamentals of the system linearisation, MIMO system decoupling and the (linear) feedback control system stability and performance criteria as well as loop shaping (Youla) Q-parameterisation control design methodology are discussed. More specifically, in the proposed control design procedure, the stability requirements of the closed loop control system are met by using Youla-parameterisation method, as it provides *all the stabilising* controllers for a given plant (Youla, Jabr , & Bongiorno Jr, 1976), and

[11] For a typical passenger car, the plant bandwidth is around 1Hz, as indicated in Chapter 4.

[12] Q-parameterisation is also called Youla-parameterisation in some textbooks.

allows the performance specifications of the control system to be achieved by employing closed loop shaping technique. The procedure is then employed for design of the high-level vehicle dynamics control system.

4.2.1 Linearisation

The linearisation procedure of a nonlinear system is usually performed by employing the Taylor series expansion and on knowledge of nominal system trajectories (operating points) and nominal system inputs (Gajic, 2003). Consider the general nonlinear dynamic system in matrix form

$$\dot{\mathbf{x}}(t) = \boldsymbol{\mathcal{F}}\big(\mathbf{x}(t), \mathbf{f}(t)\big), \quad \mathbf{x}(t_0)\ given \tag{4-2}$$

where $\mathbf{x}(t)$, $\mathbf{f}(t)$ and $\boldsymbol{\mathcal{F}}(t)$ are the n-dimensional vector of system state, the r-dimensional vector of system input, and a n-dimensional vector function, respectively. Consider the system (in nominal - equilibrium) operating point $\mathbf{x}_n(t)$ is known and the nominal system input that keeps the system on the operating point is given by $\mathbf{f}_n(t)$, that is

$$\dot{\mathbf{x}}_n(t) = \boldsymbol{\mathcal{F}}\big(\mathbf{x}_n(t), \mathbf{f}_n(t)\big) \tag{4-3}$$

The linearisation procedure is based on the assumption that the actual system dynamics in the immediate proximity of the operating point can be approximated by the first terms of the Taylor series. By expanding the right-hand side of Eq. (4-2) into the Taylor series and neglecting the higher-order terms, an approximation is obtained as

$$\dot{\mathbf{x}}(t) \approx \dot{\mathbf{x}}_n(t) + \left(\frac{\partial \boldsymbol{\mathcal{F}}}{\partial \mathbf{x}}\right)\Big|_{\substack{\mathbf{x}_n(t) \\ \mathbf{f}_n(t)}} [\mathbf{x}(t) - \mathbf{x}_n(t)] + \left(\frac{\partial \boldsymbol{\mathcal{F}}}{\partial \mathbf{f}}\right)\Big|_{\substack{\mathbf{x}_n(t) \\ \mathbf{f}_n(t)}} [\mathbf{f}(t) - \mathbf{f}_n(t)] \tag{4-4}$$

The partial derivatives represent the Jacobian matrix and given by:

$$\left(\frac{\partial \boldsymbol{\mathcal{F}}}{\partial \mathbf{x}}\right)_{\substack{\mathbf{x}_n(t)\\ \mathbf{f}_n(t)}} = \begin{bmatrix} \frac{\partial \mathcal{F}_1}{\partial \mathrm{x}_1} & \frac{\partial \mathcal{F}_1}{\partial \mathrm{x}_2} & \cdots & \cdots & \frac{\partial \mathcal{F}_1}{\partial \mathrm{x}_n} \\ \frac{\partial \mathcal{F}_2}{\partial \mathrm{x}_1} & \cdots & \cdots & \cdots & \frac{\partial \mathcal{F}_2}{\partial \mathrm{x}_n} \\ \cdots & \cdots & \frac{\partial \mathcal{F}_i}{\partial \mathrm{x}_j} & \cdots & \cdots \\ \cdots & \cdots & \cdots & \cdots & \cdots \\ \frac{\partial \mathcal{F}_n}{\partial \mathrm{x}_1} & \frac{\partial \mathcal{F}_n}{\partial \mathrm{x}_2} & \cdots & \cdots & \frac{\partial \mathcal{F}_n}{\partial \mathrm{x}_n} \end{bmatrix}_{\substack{\mathbf{x}_n(t)\\ \mathbf{f}_n(t)}} \tag{4-5}$$

$$\left(\frac{\partial \boldsymbol{\mathcal{F}}}{\partial \mathbf{f}}\right)_{\substack{\mathbf{x}_n(t)\\ \mathbf{f}_n(t)}} = \begin{bmatrix} \frac{\partial \mathcal{F}_1}{\partial \mathrm{f}_1} & \frac{\partial \mathcal{F}_1}{\partial \mathrm{f}_2} & \cdots & \cdots & \frac{\partial \mathcal{F}_1}{\partial \mathrm{f}_r} \\ \frac{\partial \mathcal{F}_2}{\partial \mathrm{f}_1} & \cdots & \cdots & \cdots & \frac{\partial \mathcal{F}_2}{\partial \mathrm{f}_r} \\ \cdots & \cdots & \frac{\partial \mathcal{F}_i}{\partial \mathrm{f}_j} & \cdots & \cdots \\ \cdots & \cdots & \cdots & \cdots & \cdots \\ \frac{\partial \mathcal{F}_n}{\partial \mathrm{f}_1} & \frac{\partial \mathcal{F}_n}{\partial \mathrm{f}_2} & \cdots & \cdots & \frac{\partial \mathcal{F}_n}{\partial \mathrm{f}_r} \end{bmatrix}_{\substack{\mathbf{x}_n(t)\\ \mathbf{f}_n(t)}} \tag{4-6}$$

4.2.2 System Decoupling

By studying the vehicle dynamics equations represented by Eq. (4-1), it is clear that the yaw rate output is the sole function of one input which is the yaw moment, whereas, the longitudinal and lateral velocities outputs are functions of all the three inputs, namely, longitudinal force, lateral force and yaw moment, as shown in Figure 4-2.

If the outputs of a MIMO system are functions of two or more control inputs, there is interaction existing in the system. Interaction among different parts of a multivariable system may cause couplings in the MIMO system and makes the design of the control system more complicated. The level of interaction in a MIMO system can be defined as the degree of dependencies among various input and output of the system as a function of frequency (Salgado & Conley,

2004). In case of weak coupling between different input and output in a MIMO system, the system would be considered as decoupled and a multi-loop control strategy [13] could be employed. In decentralised control architecture, the control problem is separated into several single-loop SISO systems and then SISO control design approaches are being employed on each of the loops, see (Kinnaert, 1995) for example. It should be noted that the decentralised control strategy is only applicable for linear control system (Skogestad & Postlethwaite, 2007). Therefore, it is necessary to linearise the system before any decision about input/output pairing takes place.

The key point in decentralised architecture is to determine the right pairing of inputs and outputs. The choice of pairing channels is decisive because an inappropriate choice may make the system unstable even though each loop separately is stable. This issue might arise because of the existing interaction between the different loops. Commonly, the stronger the interactions are, the harder it is to obtain satisfactory control performance using a multi-loop strategy. Therefore, it is necessary to define a gauge to quantify the level of interaction existing in a MIMO system. Employing this measure can provide some insight to deal with the pairing problem.

Several different measures have been proposed in the literatures for quantifying the level of input/output interactions in multivariable systems (Salgado & Conley, 2004). However, one of the most commonly used interaction measures is the *Relative Gain Array* (RGA) developed by Bristol (Bristol, 1966). The RGA is a measure that can be employed in order to decide a suitable input/output pairing when applying a decentralised control structure. It also gives advice on avoiding certain pairings.

The RGA of a non-singular square complex matrix $\mathbf{G}$ is a square complex matrix defined as:

$$RGA(\mathbf{G}) = \mathbf{\Lambda}(\mathbf{G}) = \mathbf{G} \times (\mathbf{G}^{-1})^{T} \tag{4-7}$$

[13] Multi-loop control strategy is also called decentralised control architecture.

where × denotes elements-by-elements multiplication (the Hadmaarad or Schur products). RGA provides a measure of interaction: for decentralised control, we *prefer* to pair variables u_i (i-th input) and y_i (i-th output) so that Λ_{ij} is close to 1 at the frequencies around the closed loop bandwidth, because this means that the gain from u_i to y_i is unaffected by closing the other loops. More precisely, the following rules are applicable (Skogestad & Postlethwaite, 2007):

Pairing rule 1: *Prefer pairings such that the rearranged system, with the selected pairings along the diagonal, has an RGA matrix close to identity at frequencies around the closed-loop bandwidth.*

However, one should avoid pairings where the sign of the steady-state gain from u_i to y_i may change depending on the control of the other outputs, because this will yield instability with integral action in the loop, so we have:

Pairing rule 2: *Avoid (if possible) pairing on negative steady-state RGA elements.*

The RGA has other useful control properties (Skogestad & Postlethwaite, 2007), for example:

- *Plants with large RGA elements (typically, 5-10 or larger) at crossover frequency are fundamentally difficult to control because of sensitivity to input uncertainty.*
- *If the sign of an RGA element changes in the frequency range from s=0 to s=1, this means that G or some subsystem of G has a zero in the right half of the complex plane, including the imaginary axis (RHP).*

An alternative to the RGA matrix is the **RGA number** which is a simple measure for selecting pairings (Skogestad & Morari, 1987). For a diagonal pairing,

$$RGA\ number = \|\mathbf{\Lambda}(\mathbf{G}) - \mathbf{I}\|_{sum} \tag{4-8}$$

where the sum norm for a matrix $\mathbf{A}$ is defined as $\|\mathbf{A}\|_{sum} = \sum_{i,j}|a_{ij}|$. For the other pairings (i.e. off-diagonal pairings), the RGA number is obtained by

subtracting 1 for the selected pairings. The pairing rule is to select the pairs which have RGA number near to zero at crossover frequencies.

As an example, consider a 4-input, 4-output system with the plant transfer function at crossover frequency as follows:

$$\mathbf{G} = \begin{bmatrix} 1.2 & 0 & 0 & .1 \\ .03 & 1.01 & .002 & 0 \\ 0 & -0.001 & 1.005 & 0.004 \\ -.1 & 0.0002 & 0 & 0.98 \end{bmatrix}$$

The RGA matrix for this plant is:

$$RGA(\mathbf{G}) = \mathbf{\Lambda}(\mathbf{G}) = \mathbf{G} \times (\mathbf{G}^{-1})^T = \begin{bmatrix} 0.9831 & -0.0292 & -0.0008 & 0.2024 \\ 0.0248 & 0.9993 & 0.0030 & 0.0023 \\ -0.0003 & -0.0030 & 1.0000 & 0.0040 \\ -0.1653 & 0.0051 & -0.0039 & 0.9831 \end{bmatrix}$$

The diagonal elements of the RGA matrix are close to one and some of the off-diagonal elements (λ_{13} or λ_{23} for example) are near to zero. Moreover, some of the off-diagonal pairing elements (λ_{12} or λ_{41}, for example) have negative values of RGA. From pairing rule 1 and 2, one can conclude that the diagonal pairing is the best selection at this (crossover) frequency. Moreover, as the diagonal elements of the RGA at this frequency are not very large (are close to 1), therefore the plant is not sensitive to interaction of the loops..

The RGA number for diagonal elements is:

$$RGA\ number = \|\mathbf{\Lambda}(\mathbf{G}) - \mathbf{I}\|_{sum} = 0.0046$$

and the RGA number for the off-diagonal pairing is 0.9954. The RGA number for diagonal pairing is close to zero and for off diagonal pairing is close to unity, confirming that the diagonal pairing is the best selection for this MIMO plant, as concluded by RGA number analysis.

4.3 SISO Feedback Control System stability and performance

It is shown in the previous section that a MIMO system could be decoupled into several SISO systems for the pairs of input-output that have RGA elements near to 1 or alternatively have RGA number near to zero. In this section, the

stability and performance criteria of a SISO closed-loop control system are briefly reviewed and then the design methodology of a closed loop control system based on loop shaping and Q-parameterisation approaches are presented.

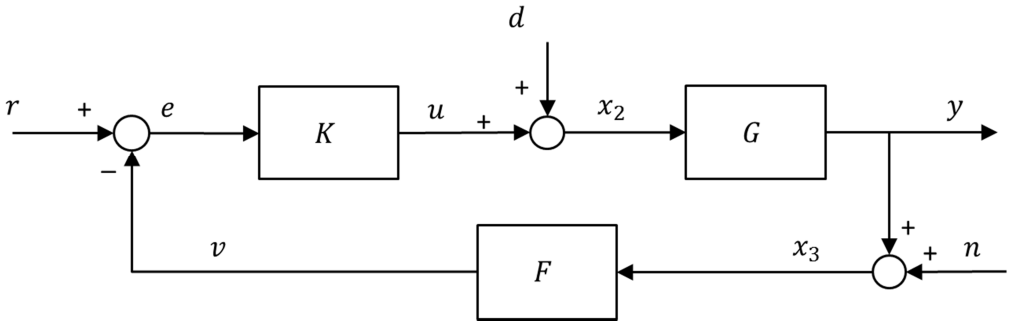

Figure 4-3: Closed loop control system

Consider the general form of a SISO negative feedback control system, consisting of a plant, a controller and a sensor, as shown in Figure 4-3, where G is the plant, K is the controller, and F is the sensor transfer functions, respectively (and are assumed to be linear and time invariant). The signals in the system are:

r reference on command input

e tracking error

v measured output

u actuating signal, controller output

d external disturbance

y plant output, measured signal

n measurement noise

The three signals from outside - r, d and n - are called exogenous inputs and u, y and v are called internal signals.

The control objective can be defined in general as: design a controller K such that the plant output y tracks the reference signal r asymptotically; even with

the existence of the disturbance d, sensor noise n and uncertainty in the plant G. Therefore, the main control design specifications are categorised as: (internal) stability and asymptotic tracking, including good disturbance attenuation, good sensor noise rejection, and low sensitivity to plant (parameter and/or model) variations (robustness). A brief discussion on the control specifications and their performance measures are presented in the following chapter.

4.3.1 Internal stability

Stability is one of the most important objectives of (linear and nonlinear) control systems design. There exists two approaches in the analysis of a dynamic system stability, known as Lyapunov stability (including asymptotic stability and exponential stability), and input-output stability (Antsaklis & Michel, 1997). In Lyapunov stability, the deviation of the system states from their desired operating points (equilibrium points), in case of applying an external disturbance, is analysed. Input-output stability is another approach to stability investigation (usually for linear systems), which takes system inputs and outputs into consideration. In an input-output stable system, it is expected that every bounded system input will produce a bounded system output. A signal $u(t)$ is defined to be bounded if there exist a constant c such that $|u(t)| < c$ for all t. System properties of this type are referred to as BIBO stability. BIBO stability is important for control systems such as tracking control, where the output of the system is expected to follow a desired input (Antsaklis & Michel, 1997). In this report, we only discuss the criterion and characteristics of BIBO stability condition, which is referred herein after as stability.

The Nyquist's stability criterion is one of the most common tests to measure the closeness of a linear system to stability:

- According to Nyquist's stability criterion, the closed loop system is stable if and only if the net number of clockwise encirclements of the point $-1 + j0$ by the Nyquist diagram $L(j\omega) = G(j\omega)K(j\omega)$ plus the number of poles of $L(j\omega)$ in the RHP is zero. For open-loop stable systems $\angle L(j\omega)$ falls with frequency such that $\angle L(j\omega)$ crosses $-180°$ only once, as shown

in Figure 4-4, a. The Nyquist stability criterion can also be expressed by logarithmic plot (Bode plot) as follows: the closed-loop system is stable if and only if the loop gain $|L|$ is less than 1 at frequency $-180°$ (see Figure 4-4, b) (Ogata, 2010).

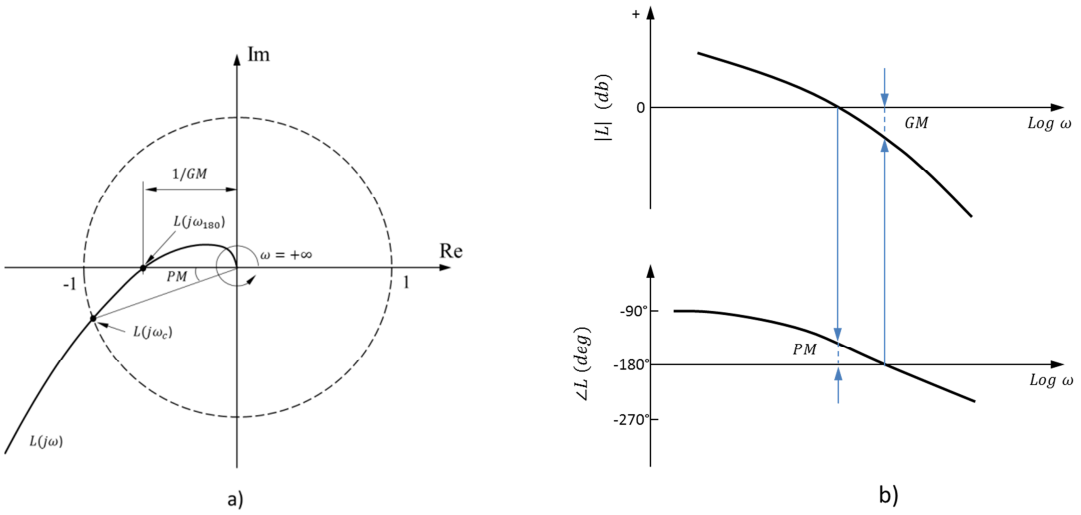

Figure 4-4: Typical plot for stable plant; a) Nyquist plot, b) Bode plot.

To test for stability of a feedback system, it is usual to employ stability criteria only for the system input-output transfer function (i.e. from r to y as shown in Figure 4-3), so called “external stability”. However, this assumes that there was no internal RHP pole-zero cancellation between the controller and the plant.

Definition 1 (Doyle, Francis, & Tannenbaum, 1992)**.** *A closed-loop system is “internally stable” if none of its components contain hidden unstable modes and the injection of bounded external signals at any place in the closed-loop system results in bounded output signals measured anywhere else in the closed-loop system.*

To investigate the internal stability of a closed-loop system, consider a negative feedback control loop as shown in Figure 4-3. By supposing that the output of the plant, the controller and the sensor are linear functions of the sums (or difference) of their inputs:

$$\begin{aligned} y &= G(d+u) \\ v &= F(n+y) \\ u &= K(r-v) \end{aligned} \tag{4-9}$$

The closed loop control system is called *well-posed* if all the nine transfer functions from the three exogenous inputs to all internal signals, namely u, y, v and the outputs of the summing junctions, namely e, x_2, x_3 are exist (Doyle, Francis, & Tannenbaum, 1992). Write the equations at the summing junctions as labelled in Figure 4-3:

$$\begin{aligned} e &= r - Fx_3 \\ x_2 &= d + Kx_1 \\ x_3 &= n + Gx_2 \end{aligned} \tag{4-10}$$

In matrix form these are:

$$\begin{bmatrix} 1 & 0 & F \\ -K & 1 & 0 \\ 0 & -G & 1 \end{bmatrix} \begin{bmatrix} e \\ x_2 \\ x_3 \end{bmatrix} = \begin{bmatrix} r \\ d \\ n \end{bmatrix} \tag{4-11}$$

Thus, the system is well-posed if the above 3x3 matrix is non-singular, that is the determinant $1 + GKF$ is not identically equal to zero. Then the nine transfer functions are obtained from the equation

$$\begin{aligned} \begin{bmatrix} e \\ x_2 \\ x_3 \end{bmatrix} &= \begin{bmatrix} 1 & 0 & F \\ -K & 1 & 0 \\ 0 & -G & 1 \end{bmatrix}^{-1} \begin{bmatrix} r \\ d \\ n \end{bmatrix} \\ &= \frac{1}{1+GKF} \begin{bmatrix} 1 & -GF & -F \\ K & 1 & -KF \\ GK & G & 1 \end{bmatrix} \begin{bmatrix} r \\ d \\ n \end{bmatrix} \end{aligned} \tag{4-12}$$

If the nine transfer functions in Eq. (4-12) are stable, then it guarantees bounded internal signals for all bounded exogenous signals (BIBO stable) and from definition 1, it is concluded that the feedback system is *internally stable.* Therefore, for a closed loop control system to be internally stable, not only the system input-output transfer function, i.e. from r to y, should be stable, but also all the internal signals should be bounded for all bounded exogenous signals. In other words, an internally stable system is always externally stable, but not conversely.

To test the internal stability in a simpler way, one can write G, K and F as ratios of coprime factorisations (i.e. polynomials with no common factors):

$$G = \frac{N_G}{M_G}\,, \quad K = \frac{N_K}{M_K}\,, \quad F = \frac{N_F}{M_F}\,. \tag{4-13}$$

The characteristic polynomial of the feedback system (i.e. $1 + GKF$) is the one found by taking the product of the three numerators plus the product of the three denominators:

$$N_G N_K N_F + M_G M_K M_F \tag{4-14}$$

The zeros of the characteristic polynomials are the *closed-loop poles, a*s seen from (4-12).

Theorem 1 *the feedback system is internally stable if there are no closed-loop poles in RHP.*

Proof: see (Doyle, Francis, & Tannenbaum, 1992). □

Therefore, by Theorem 1, internal stability can be determined by checking the zeros of polynomial (4-14).

The requirement of internal stability in a feedback system leads the following statements (Youla, et al., 1974):

1- *If $G(s)$ has a RHP-zero at z, then $L = GK$, $T = GK/(1 + GK)$ and $GS = G/(1 + GK)$, will each have a RHP-zero at z.*
2- *If $G(s)$ has a RHP-pole at p, then $L = GK$ also have a RHP-pole at p,while $S = 1/(1 + GK)$ and $Y = KS = K/(1 + GK)$, will have a RHP-zero at p.*

L, T, S and Y are so called the open loop, the closed loop, the sensitivity and the Youla (parameter) transfer functions, respectively.

Finally, from the above statements, the so called ‘interpolation condition’ could be derived:

If the plant $G(s)$ has a RHP-zero z or a RHP-pole p:

$$G(z) = 0 \quad \Rightarrow \quad L(z) = 0 \quad \Leftrightarrow \quad T(z) = 0, \qquad S(z) = 1 \tag{4-15}$$

$$1/G(p) = 0 \quad \Rightarrow \quad L(p) = \infty \quad \Leftrightarrow \quad T(p) = 1, \qquad S(p) = 0 \tag{4-16}$$

In general, if the plant has ∂p numbers of repeated poles p ,then the interpolation conditions are:

$$T(p) = 1, \qquad S(p) = 0 \quad and \quad \frac{d^k T}{ds^k}(p) = \frac{d^k S}{ds^k}(p) = 0 \qquad 1 \le k \le \partial p - 1 \tag{4-17}$$

Similarly, if the plant has ∂z numbers of repeated zeros, then the interpolation conditions are (Assadian F., 2011):

$$T(z) = 0, \qquad S(z) = 1 \quad and \quad \frac{d^k T}{ds^k}(z) = \frac{d^k S}{ds^k}(z) = 0 \qquad 1 \le k \le \partial z - 1 \tag{4-18}$$

The conditions clearly restrict the allowable S and T to achieve internal stability and also could be used as a measure for verifying internal stability of the system.

4.3.2 Closed-loop performance objectives

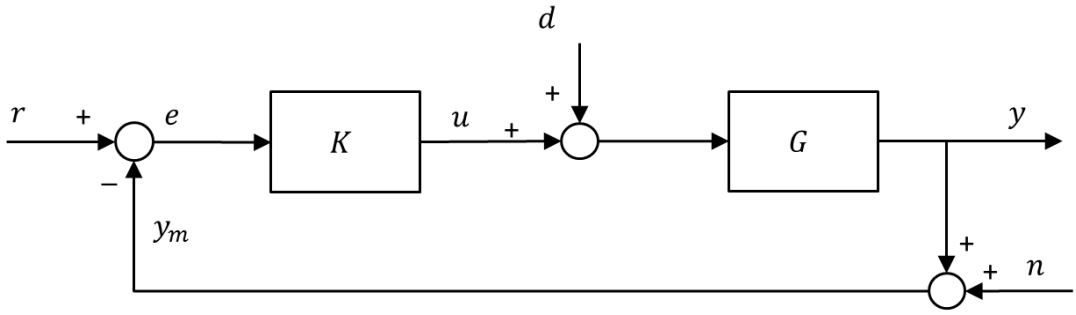

Figure 4-5: Unity-feedback control system

In addition to the internal stability, a closed-loop system should provide several other performance requirements such as robustness, asymptotic tracking, disturbance attenuation and noise rejection, as stated before. To investigate the performance objectives of a closed loop control system, one should study the relationship between a set of reference exogenous signals and their corresponding steady-state error. For simplicity assume that $F = 1$ (i.e. the unity-feedback loop) as shown in Figure 4-5. Here r is the system reference

input, y is the system output and e is the control error defined as the difference between the ideal response, r, and the measured response, y_m:

$$e = r - y_m$$

$$e = r - y - n \tag{4-19}$$

The output from the controller is

$$u = K(r - y - n) \tag{4-20}$$

and the output from the plant is

$$y = G(u + d) \tag{4-21}$$

Substitution of (4-20) into (4-21) yields

$$y = GK(r - y - n) + Gd \tag{4-22}$$

Here, Gd is the effect of the (actuator) disturbance on the output.

Hence, the closed-loop response can be written in terms of three exogenous inputs r, d ,and n as

$$y = \frac{1}{(1 + GK)}[GK\ r + G\ d - GK\ n] \tag{4-23}$$

Closed-loop performance could be investigated by focusing on the response of the system to the three exogenous inputs r, d, and n (Assadian F., 2011). For example, the closed-loop transfer function from the actuator disturbance (Gd) to the plant output y is called *sensitivity* function S.

$$S = \frac{1}{1 + GK} = \frac{1}{1 + L} \tag{4-24}$$

where L denotes the (open) loop transfer function, $L = GK$. The closed-loop transfer function from reference input r to the plant output y is called *complementary sensitivity* function T:

$$T = \frac{GK}{1 + GK} = \frac{L}{1 + L} \tag{4-25}$$

From definition of (4-24) and (4-25), one can conclude that:

$$S + T = 1 \tag{4-26}$$

One way to quantify how sensitive T is to variation in G is to take the limiting ratio of a relative perturbation in T (i.e., $\Delta T/T$) to a relative perturbation in G (i.e., $\Delta G/G$). Considering of G as a variable and T as a function of it, we get

$$\lim_{\Delta G \to 0} \frac{\Delta T/T}{\Delta G/G} = \frac{dT}{dG}\frac{G}{T} = \frac{1}{1+GK} = \frac{1}{1+L} = S \tag{4-27}$$

In this way, S is also the sensitivity of the closed-loop transfer function T which defines how T changes as a result of a change in G.

Employing the above definitions for S and T, the plant output (Eq. (4-23)) can be written in terms of S and T as:

$$y = T\,r + S\,Gd - T\,n \tag{4-28}$$

The first term in (4-28) is the closed-loop function between control reference and plant output (so called, tracking performance), while the second term is the effect of the disturbance (so called, disturbance attenuation performance) and the third term is the effect of the measurement noise (so called, noise rejection performance) on the output respectively.

Similarly, the control error e can be written as:

$$e = r - y - n = S\,r - SGd - S\,n \tag{4-29}$$

and the corresponding controller output (actuator input) signal u in terms of S and T is:

$$u = KS\,r - KSGd - KS\,n \tag{4-30}$$

The closed-loop transfer function from reference input r to the actuator input u is called *Youla parameter* Y:

$$Y = KS \tag{4-31}$$

which is the measure of actuator effort (Assadian F. , 2011). It is concluded from Eqs. (4-27), (4-28), (4-29), and (4-30) that all control performance problems can be summarised in terms of S, T, Y or some combination of them. The main control design issue is a trade-off between making S small and making T small: Ideally we want S small to obtain the benefits of feedback (good robustness as well as small control error for command and disturbances), and we want T equal to one for good command following at low frequencies and small to avoid sensitivity to noise which is one of the disadvantages of feedback at high frequencies. Moreover, from a practical point of view, we are also interested in keeping Y as small as possible. As shown in Eq. (4-26), these requirements cannot be met simultaneously, as S and T are related to each other by $S + T = 1$. Fortunately, the conflicting design objective mentioned above are generally in different frequency ranges and the objectives can be fulfilled by *using a large loop gain* $|L|$ *at low frequencies below crossover, and a small gain at high frequencies above crossover*.

To study closed-loop performance over a range of frequencies, the frequency response of the loop transfer functions $L(j\omega)$, $T(j\omega)$ and $S(j\omega)$ can be employed. One of the advantages of the frequency domain analysis compared to the time domain analysis, is that it considers the system over a broader class of signals (sinusoids of any frequency). This makes it easier to characterise feedback properties, and in particular system behaviour below the crossover (bandwidth) region.

The traditional performance measures in frequency domain are the *Gain Margin* (GM) and *Phase Margin* (PM), which can be used as control design criteria (Ogata, 2010). Defining the *phase crossover frequency* ω_{180}, to be the frequency at which the phase angle of the open loop transfer function L equals to $-180°$ (where the Nyquist curve of $L(j\omega)$ crosses the negative real axis between -1 and 0, as shown in Figure 4-4,b), the gain margin is defined as:

$$GM = \frac{1}{|L(j\omega_{180})|} \tag{4-32}$$

For a stable system, the GM indicates how much the gain $|L(j\omega)|$ can be increased before the closed-loop system becomes unstable (see Figure 4-4,b). The GM is thus a direct safeguard against steady-state gain uncertainty (error).

The phase margin is defined as:

$$PM = \angle L(j\omega_c) + 180° \tag{4-33}$$

Definition2: the gain crossover frequency ω_c is the frequency at which $|L(j\omega)|$ first crosses 1 from above, that is:

$$|L(j\omega_c)| = 1 \tag{4-34}$$

The phase margin is the amount of additional phase lag (negative phase) which can be added to the loop at frequency ω_c before the phase at this frequency becomes $-180°$ which corresponds to closed-loop instability, as shown in Figure 4-4,a. Therefore, for a minimum phase system to be stable, the phase margin should be positive (see Figure 4-4,b). The phase margin is a direct safeguard against time delay uncertainty: the system becomes unstable if we add a time delay of:

$$\theta_{max} = PM/\omega_c \tag{4-35}$$

where θ_{max} is the maximum time delay in sec (if ω_c is in rad/sec and PM is in rad).

From the above arguments, we see that gain and phase margins provide stability margins for gain and delay uncertainty. In short, the gain and phase margins are used to provide the appropriate trade-off between performance and stability. As a common rule of thumb, for achieving a satisfactory performance, the phase margin should be between $30°$ and $60°$, and the gain margin should be greater than 2 (6 dB) (Ogata, 2010).

Interestingly, the gain and phase margins are closely related to the peak values of $S(j\omega)$ and $T(j\omega)$ and are therefore useful in terms of performance (Assadian F., 2011). Define maximum peaks sensitivity and complementary sensitivity functions as

$$M_S = \max_{\omega}|S(j\omega)|; \qquad M_T = \max_{\omega}|T(j\omega)| \tag{4-36}$$

the relationship between these maximum peak and the gain and phase margins are (Skogestad & Postlethwaite, 2007)

$$GM \geq \frac{M_S}{M_S - 1}\ ; \quad PM \geq 2\sin^{-1}\left(\frac{1}{2M_S}\right) \geq \frac{1}{M_S}\ [\text{rad}] \tag{4-37}$$

$$GM \geq 1 + \frac{1}{M_T}\ ; \quad PM \geq 2\,sin^{-1}\left(\frac{1}{2M_T}\right) \geq \frac{1}{M_T}\ [rad] \tag{4-38}$$

For example, with $M_S = 2$ we are guaranteed $GM \geq 2$ and $PM \geq 29.0°$ and similarly, with $M_T = 2$ we have $GM \geq 1.5$ and $PM \geq 29.0°$. Therefore requiring $M_S < 2$ implies the common rule of thumb $GM \geq 2$ and $PM \geq 30°$. Typically it is required that M_S is less than about 2 (6dB) and M_T is less than about 1.25 (2dB). A large value of M_S and M_T (larger than about 4) indicates poor performance as well as poor robustness.

4.3.3 Control bandwidth and crossover frequency

The concept of bandwidth is very important in understanding the benefits and trade-offs involved when applying feedback control. Above we considered peaks of closed-loop transfer functions, M_S and M_T, which are related to the quality of the response (such as overshoot and so on). However, for performance one must also consider the speed of the response, and this leads to consideration of the bandwidth frequency of the control system. In general, a large bandwidth corresponds to a faster rise time, since frequency signals are more easily passed on to the outputs. A high bandwidth also indicates a system which is sensitive to noise and to parameter variation. Conversely, if the bandwidth is small, the time response will generally be slow and the system will usually be more robust.

Loosely speaking, *control bandwidth* may be defined as the frequency range $[\omega_1, \omega_2]$ over which control is *effective*. In most cases we require tight control at steady-state so $\omega_1 = 0$ and then simply $\omega_2 = \omega_B$ is the bandwidth. The word “effective” may be interpreted in different ways, and this may give rise to

different definitions of bandwidth. The interpretation we use is that control is *effective* if we obtain some *benefit* in terms of performance. For tracking performance the error is $e = r - y = Sr$ and we get that feedback is effective (in term of improving the performance) as long as the relative error $e/r = S$ is reasonably small, which we may define to be less than 0.707 in magnitude. We then get the following definition (Skogestad & Postlethwaite, 2007):

Definition 3: *the closed loop bandwidth, ω_B, is the frequency where $|S(j\omega)|$ first crosses $1/\sqrt{2} = 0.707$ ($\approx -3\ dB$) from below.*

Another interpretation is to say that control is *effective* if it significantly *changes* the output response, which leads to the tradition definition of bandwidth in terms of the closed loop transfer function T.

Definition 4: the *ω_{BT}, is the highest frequency at which $|T(j\omega)|$ first crosses $1/\sqrt{2} = 0.707$ ($\approx -3\ dB$) from above.*

The gain crossover frequency, ω_c, is also sometimes used to define closed-loop bandwidth. It has the advantage of being simple to compute and usually gives a value between ω_B and ω_{BT}. Specifically, for system with $PM < 90°$ we have

$$\omega_B < \omega_c < \omega_{BT} \tag{4-39}$$

In most cases, the two definitions in terms of S and T yield similar values for the bandwidth. In cases where ω_B and ω_{BT} differ, the sititation is generally as follows. Up to the frequency ω_B, $|S|$ is less than 0.7, and control is effective in terms of improving performance. In the frequency range $[\omega_B, \omega_{BT}]$ control still affects the response, but does not improve performance- in some cases we find that in this frequency range $|S|$ is larger than 1 and control degrades performance. Finally, at the frequencies higher than ω_{BT} we have $S = 1$ and control has no significant effect on the response.

In conclusion, ω_B (which is defined in terms of $|S|$) and also ω_c (in terms of $|L|$) are good indicators of closed loop performance, while ω_{BT} (in terms of $|T|$) may be misleading in some cases. The reason is that we want $T \approx 1$ in order to have good performance, and it is not sufficient that $|T| = 1$; we must also consider its

phase. On the other hand, for good performance we want S close to 0 , and this will be the case if $|S| \approx 0$ irrespective of the phase of S.

4.4 Controller design

In the previous sections, various control specifications such as stability and nominal performance have been presented by a set of rules (mainly on S and T). The next step is to utilise a proper control design method to achieve these specifications. In this thesis, we employ the closed-loop "Q-parameterisation" approach, which determines *all* compensators that stabilise a given plant. By *all stabilising controllers* we mean, all controllers that yield *internal stability* of the closed-loop system (Vidyasagar, 2011). Achieving internal stability is important in practical applications: it guarantees that the control input to the plant is always bounded even if the feedback loop is broken.

The control design problems can be formulated as follows: Given G, design K so that the feedback system (1) is internally stable, and (2) satisfies robust performance objectives. The method of solution is to parameterise all Ks for which (1) is true, and then to see if there exists a parameter for which (2) holds. This will be achieved by finding a general Q-parameterisation of *all* compensators that stabilise a given plant, as the first step, and then to employ the (close) loop-shaping technique to come up with the best compensator to meet the control performance objectives.

4.4.1 Youla- parameterisation method

In this section, we introduce Youla-parameterisation (also known as Q-parameterisation) of *all stabilising* controllers for a plant (Youla, Jabr , & Bongiorno Jr, 1976). The central idea in this approach is in factoring the transfer function of a system as the "ratio" of two stable rational transfer functions. Consider the closed loop unity feedback control system as shown in Figure 4-5. Let Y denote the transfer function from r to u, then the following lemma forms the basis:

Lemma 1 *for a stable plant* $G(s)$ *the negative feedback system in* Figure 4-5 *is internally stable if and only if*

$$Y = \frac{K}{1 + GK} \tag{4-40}$$

is stable.

Proof: Let G and K denote the plant and controller transfer functions respectively and $F = 1$, then all the nine transfer function in Eq. (4-12) can be written in terms of G and Y. If G and Y are stable, then it is concluded that the system is internally stable. □

By solving (4-40) with respect to the controller K, a parameterisation of all stabilising negative feedback controllers for the stable plant $\mathrm{G}(s)$ is found by

$$K = \frac{Y}{1 - GY} \tag{4-41}$$

where the " Youla parameter" Y is any stable transfer function (Zemas,1981).

As all the nine transfer functions defined in (4-12) are affine functions of the free parameter Y; (i.e. each of these nine transfer functions can be written in the form of $T_1 Y + T_2$ for some stable T_1, T_2) (Skogestad & Postlethwaite, 2007), the relation between Youla parameter Y ,sensitivity S and complementary sensitivity T functions are

$$S = 1 - GY \tag{4-42}$$

$$T = GY \tag{4-43}$$

4.4.2 Loop-shaping method

The stability requirement of the control system can be met by employing the Youla parameterisation method, as it provides all the stabilising controllers K for a given plant G. To satisfy the other control performances (such as, asymptotic tracking, robustness, disturbance attenuation and noise rejection), we can employ loop-shaping techniques. Loop-shaping is a control design procedure that involves explicitly shaping the magnitude of the (open loop or closed loop) transfer functions in frequency domain.

The *open loop shaping* method involves in constructing an open loop transfer function L to satisfy the required control system specifications and have reasonable crossover characteristics. The open loop transfer function L is the product of the feedback controller K (which has to be designed) and G which include all other transfer functions around the loop. By appropriate shaping of the L and by assuming that the plant had neither RHP poles nor zeros, and that L had at least the same relative degree as G, the controller was obtained from $K = L/G$. (Ogata, 2010). Essentially, to get the benefits of feedback control we want the loop gain, $|L(j\omega)|$, to be as large as possible within the bandwidth region. However, due to time delay, RHP-zeros, un-modelled high frequency dynamics and limitations on the allowed manipulated input, the gain has to drop below one at and above crossover frequency (Assadian F. , 2011). In the loop-shaping approach, the desired shape of the L is typically obtained by iteration and is well suited for relatively simple and stable plants. However, it needs much more effort for complicated systems and especially achieving stability may be very difficult by this method as it does not consider directly the closed-loop transfer functions such as S and T, which determine the final response of the closed loop system (Skogestad & Postlethwaite, 2007).

Another approach, the so called *closed loop shaping*, is to design K directly in terms of closed loop transfer functions S and T which can be formulated as an H_∞ optimal control problem (Zhou, Doyle, & Glover, 1996). An alternative closed loop shaping method, which is quite useful for simple plant models, is to use Y, the parameterisation of all stabilising controllers. Recall from Section 4.4.1, if the plant G is stable, then we can parameterise the set of all stabilising controllers as:

$$K = Y/(1 - GY)$$

where Y is any stable transfer function. In terms of this free parameter Y, we have that $S = 1 - GY$ and $T = GY$. As Y approaches $1/G$ (i.e., approximate inverse of the plant), then S approaches to 0 and K approaches to ∞, we can make S arbitrarily small for all frequencies. As we want S to be small at the frequencies below crossover and T to be small above crossover, therefore, Y

could be selected as $Y = F/G$ where F is a low-pass filter with a cut-off frequency equal to crossover (or other higher order filters with the frequency responses similar to low-pass filter). A similar procedure is applicable for minimum-phase but unstable plants.

If the plant is non-minimum-phase, we can use the following lemma

Lemma 1 *for each stable function G, there exists an all-pass function G_{ap} and a minimum-phase function G_{mp} such that $G = G_{ap}G_{mp}$.*

Proof: see (Doyle, Francis, & Tannenbaum, 1992).

Therefore, the non-minimum-phase plant G can be factorised as $G = G_{ap}G_{mp}$ where G_{ap} is an all-pass function (the products of all factors of the form $(s - s_0)/(s + \bar{s}_0)$ where s_0 ranges over all zeros of G in RHP and $-\bar{s}_0$ are all their reflecting poles), and G_{mp} is a minimum-phase function. One can approximately invert the minimum-phase part by letting $Y = F/G_{mp}$, where F is a low-pass filter so that Y is proper. One can then shape the low-pass F to trade-off between S and T. This approach is essentially shaping T since $T = FG_{ap}$ (Doyle, Francis, & Tannenbaum, 1992).

4.5 High-level control system design

Design of the high-level control system for the IVCS system is presented in this section. The vehicle dynamics equations of motion are represented by nonlinear MIMO Eq. (4-1) as:

$$\begin{bmatrix} \dot{V}_x \\ \dot{V}_y \\ \dot{\omega}_z \end{bmatrix} = \begin{bmatrix} V_y\omega_z \\ -V_x\omega_z \\ 0 \end{bmatrix} + \begin{bmatrix} 1/M & 0 & 0 \\ 0 & 1/M & 0 \\ 0 & 0 & 1/I_z \end{bmatrix} \begin{bmatrix} F_x \\ F_y \\ M_z \end{bmatrix}$$

Having the plant model known, the procedure of high-level control system design is based on the following steps:

1. Linearisation of the plant model
2. Control structure design (system decomposition)
3. Control system design

4. Control system validation

as are explained in the following sections.

4.5.1 Linearisation

Recall from section 4.2, the vehicle dynamics equation of motion (4-1)

$$\begin{bmatrix} \dot{V}_x \\ \dot{V}_y \\ \dot{\omega}_z \end{bmatrix} = \begin{bmatrix} V_y\omega_z \\ -V_x\omega_z \\ 0 \end{bmatrix} + \begin{bmatrix} 1/M & 0 & 0 \\ 0 & 1/M & 0 \\ 0 & 0 & 1/I_z \end{bmatrix} \begin{bmatrix} F_x \\ F_y \\ M_z \end{bmatrix}$$

can be written in the form of:

$$\dot{\mathbf{x}}(t) = \boldsymbol{\mathcal{F}}\big(\mathbf{x}(t), \mathbf{f}(t)\big)$$

where

$$\boldsymbol{\mathcal{F}} = \begin{bmatrix} \mathcal{F}_1 \\ \mathcal{F}_2 \\ \mathcal{F}_3 \end{bmatrix} = \begin{bmatrix} V_y\omega_z + F_x/M \\ -V_x\omega_z + F_y/M \\ M_z/I_z \end{bmatrix} \tag{4-44}$$

By employing definitions (4-5) and (4-6), the Jacobian matrix can be derived as:

$$\left(\frac{\partial \boldsymbol{\mathcal{F}}}{\partial \mathbf{x}}\right)\Big|_{\substack{\mathbf{x}_n(t) \\ \mathbf{f}_n(t)}} = \begin{bmatrix} \frac{\partial \mathcal{F}_1}{\partial \mathrm{V}_x} & \frac{\partial \mathcal{F}_1}{\partial \mathrm{V}_y} & \frac{\partial \mathcal{F}_1}{\partial \omega_z} \\ \frac{\partial \mathcal{F}_2}{\partial \mathrm{V}_x} & \frac{\partial \mathcal{F}_2}{\partial \mathrm{V}_y} & \frac{\partial \mathcal{F}_2}{\partial \omega_z} \\ \frac{\partial \mathcal{F}_3}{\partial \mathrm{V}_x} & \frac{\partial \mathcal{F}_3}{\partial \mathrm{V}_y} & \frac{\partial \mathcal{F}_3}{\partial \omega_z} \end{bmatrix}\Bigg|_{\substack{\mathbf{x}_n(t) \\ \mathbf{f}_n(t)}} = \begin{bmatrix} 0 & \omega_{z,n} & V_{y,n} \\ -\omega_{z,n} & 0 & -V_{x,n} \\ 0 & 0 & 0 \end{bmatrix} \tag{4-45}$$

$$\left(\frac{\partial \boldsymbol{\mathcal{F}}}{\partial \mathbf{f}}\right)\Big|_{\substack{\mathbf{x}_n(t) \\ \mathbf{f}_n(t)}} = \begin{bmatrix} \frac{\partial \mathcal{F}_1}{\partial \mathrm{F}_x} & \frac{\partial \mathcal{F}_1}{\partial \mathrm{F}_y} & \frac{\partial \mathcal{F}_1}{\partial \mathrm{M}_z} \\ \frac{\partial \mathcal{F}_2}{\partial \mathrm{F}_x} & \frac{\partial \mathcal{F}_2}{\partial \mathrm{F}_y} & \frac{\partial \mathcal{F}_2}{\partial \mathrm{M}_z} \\ \frac{\partial \mathcal{F}_3}{\partial \mathrm{F}_x} & \frac{\partial \mathcal{F}_3}{\partial \mathrm{F}_y} & \frac{\partial \mathcal{F}_3}{\partial \mathrm{M}_z} \end{bmatrix}\Bigg|_{\substack{\mathbf{x}_n(t) \\ \mathbf{f}_n(t)}} = \begin{bmatrix} 1/M & 0 & 0 \\ 0 & 1/M & 0 \\ 0 & 0 & 1/I_z \end{bmatrix} \tag{4-46}$$

where $V_{x,n}$, $V_{y,n}$,and $\omega_{z,n}$ are the values of longitudinal velocity, lateral velocity and yaw rate at the operating point respectively.

By assuming that the system is in equilibrium at the operating point (small perturbation assumption about an initial operating condition), the derivative of system states are zero

$$\dot{\mathbf{x}}_{\boldsymbol{n}} = 0 \quad \rightarrow \quad \begin{cases} \dot{V}_{x,n} = 0 \\ \dot{V}_{y,n} = 0 \\ \dot{\omega}_{z,n} = 0 \end{cases} \tag{4-47}$$

Therefore, the linearised equation of motion can be derived from Eqs. (4-45), (4-46) ,and (4-47) as:

$$\begin{bmatrix} \dot{V}_x \\ \dot{V}_y \\ \dot{\omega}_z \end{bmatrix} \approx \begin{bmatrix} 0 & \omega_{z,n} & V_{y,n} \\ -\omega_{z,n} & 0 & -V_{x,n} \\ 0 & 0 & 0 \end{bmatrix} \begin{bmatrix} V_x \\ V_y \\ \omega_z \end{bmatrix} + \begin{bmatrix} 1/M & 0 & 0 \\ 0 & 1/M & 0 \\ 0 & 0 & 1/I_z \end{bmatrix} \begin{bmatrix} F_x \\ F_y \\ M_z \end{bmatrix} \tag{4-48}$$

Eq. (4-48) can also be represented in state-space form as:

$$\begin{aligned} \dot{\mathbf{x}} &= \mathbf{A}\mathbf{x} + \mathbf{B}\mathbf{u} \\ \mathbf{y} &= \mathbf{C}\mathbf{x} + \mathbf{D}\mathbf{u} \end{aligned} \tag{4-49}$$

where $\mathbf{x} = [V_x \quad V_y \quad \omega_z]^{\boldsymbol{T}}$ is the vector of system state (and the system output) and $\mathbf{u} = [F_x \quad F_y \quad M_z]^{\boldsymbol{T}}$ is the vector of system input, and

$$\mathbf{A} = \begin{bmatrix} 0 & \omega_{z,n} & V_{y,n} \\ -\omega_{z,n} & 0 & -V_{x,n} \\ 0 & 0 & 0 \end{bmatrix}$$

$$\mathbf{B} = \begin{bmatrix} 1/M & 0 & 0 \\ 0 & 1/M & 0 \\ 0 & 0 & 1/I_z \end{bmatrix}$$

$$\mathbf{C} = \text{diag}[\,1 \quad 1 \quad 1]^{\boldsymbol{T}}$$

$$\mathbf{D} = [0].$$

It is important to note that the assumption of small perturbation (Eq. (4-47)) might be seen unrealistic, as the model does not cover the unstable behaviour of the vehicle. However, it is shown in (Milliken & Milliken, 1995) that this assumption is equivalent to the effect of small control and disturbance input and valid for the most of the vehicle's operating span (except the large amplitude safety manoeuvres) and even for the racing car when operating near the cornering limit (see also (Kiencke & Nielsen, 2005)).

It can be seen from Eq. (4-48) that the parameters of the linearised system are changing by the selection of different operating points. Therefore, there is an uncertainty that exists in the model. To deal with this issue, a simplified plant model is proposed in the next section, which is independent from operating point and valid at the frequencies above crossover. Moreover, the proposed feedback controller is robust enough to deal with unmodelled dynamics to some extent. The performance of the control system (including its robustness) is validated by MIL (simulation) and HIL testing as discussed in Section 4.6 and Chapter 7 respectively.

4.5.2 System decoupling

The next step of the control system design is to analyse the level of interaction between various inputs-outputs of the system (4-48) and to investigate the possibility of decoupling the MIMO system into several SISO systems. The procedure is then to find out the best input/output pairings for these decoupled SISO systems and then employ a SISO controller design method for each individual closed-loop control system.

RGA, as defined in Section 4.2.2, is a good indicator for investigation of the MIMO system coupling as well as for selection of the Input-Output pairing. To derive the RGA for the linearised vehicle dynamics equation of motion, the state-space equation of the system (Eq. (4-49)) could be rearranged based on the system inputs and outputs (open loop transfer function) in the Laplace domain in the form of

$$\mathbf{x} = \mathbf{G}(s)\mathbf{u} \tag{4-50}$$

where $\mathbf{G}(s)$ is the plant transfer matrix

$$\mathbf{G}(s) = \mathbf{C}(s\mathbf{I} - \mathbf{A})^{-1}\mathbf{B} + \mathbf{D} \tag{4-51}$$

Taking the Laplace transform, Eq. (4-48) can be written in expand form as:

$$\begin{cases} s\,x_1 = a_1 x_2 + b_1 x_3 + c_1 u_1 \\ s\,x_2 = -a_2 x_1 - b_2 x_3 + c_2 u_2 \\ s\,x_3 = c_3 u_3 \end{cases} \tag{4-52}$$

where $a_1 = \omega_{z,n}$, $b_1 = V_{y,n}$, $c_1 = 1/m$, $a_2 = \omega_{z,n}$, $b_2 = V_{x,n}$, $c_2 = 1/m$, $c_3 = 1/I_z$ (which are constants). Considering the first equation of (4-52), the value of x_2 can be substituted from the second equation:

$$x_1 = \frac{1}{s}\left\{a_1 \frac{1}{s}[-a_2 x_1 - b_2 x_3 + c_2 u_2] + b_1 x_3 + c_1 u_1\right\}$$

and the value of x_3 can be substituted from the third equation in (4-52):

$$x_1 = \frac{1}{s}\left\{a_1 \frac{1}{s}\left[-a_2 x_1 - b_2\left(\frac{c_3 u_3}{s}\right) + c_2 u_2\right] + b_1\left(\frac{c_3 u_3}{s}\right) + c_1 u_1\right\}$$

After some algebraic operation, the value of x_1 in terms of control input u_1, u_2, and u_3 can be derived as

$$x_1 = \frac{1}{s(s^2 + a_1 a_2)}[(c_1 s^2)u_1 + (a_1 c_2 s)u_2 + (b_1 c_3 s - a_1 b_2 c_3)u_3] \tag{4-53}$$

Similarly the value of x_2 in terms of control input u_1, u_2, and u_3 can be derived as

$$x_2 = \frac{1}{s(s^2 + a_1 a_2)}[-(a_2 c_1 s)u_1 + (c_2 s^2)u_2 - (b_2 c_3 s - a_2 b_1 c_3)u_3] \tag{4-54}$$

And the value of x_3 is only a function of u_3 :

$$x_3 = \frac{c_3}{s} u_3 \tag{4-55}$$

Combining Eq. (4-53), (4-54) and (4-55) into the matrix form of:

$$\mathbf{x} = \mathbf{G}(s)\mathbf{u}\ ,$$

the plant transfer matrix $\mathbf{G}(s)$ then become

$$\mathbf{G}(s) = \frac{1}{s(s^2 + a_1 a_2)} \begin{bmatrix} c_1 s^2 & a_1 c_2 s & b_1 c_3 s - a_1 b_2 c_3 \\ -a_2 c_1 s & c_2 s^2 & -(b_2 c_3 s - a_2 b_1 c_3) \\ 0 & 0 & (s^2 + a_1 a_2) c_3 \end{bmatrix} \tag{4-56}$$

As $a_1 = a_2 = \omega_{z,n}$, the dominator of the plant transfer matrix is $s(s^2 + \omega_{z,n}^2)$. Therefore, $\omega_{z,n}$ is the *undamped* natural frequency of the system, means that there is resonance in the system at this frequency.

To study the (idealised) plant behaviour at different driving conditions, the frequency responses of the vehicle (plant) for the nominal values of $V_{x,n} = 40\, m/s$, $V_{y,n} = 10\, m/s$, and $\omega_{z,n} = 0.3\, rad/sec$ (which corresponds to one severe driving condition) is shown in Figure 4-6[14]. It is clear that the plant frequency response for this driving condition has the undamped natural frequency equal to their corresponding nominal yaw rate, as expected. Moreover, at low frequencies the effect of off-diagonal elements of the plant are dominant (especially the yaw moment over the longitudinal and lateral velocities), i.e. $\mathbf{\Lambda}(0) \neq I$, whereas, at the medium and high frequencies, the off-diagonal elements of $\mathbf{G}(s)$ are small relative to diagonal elements, so $\mathbf{\Lambda}(\infty) = I$. This means that at low frequencies, diagonal pairing is not recommended (i.e. there are coupling exist between system inputs and outputs), whereas, at medium and high frequencies, the diagonal pairing is the best selection (i.e. the inputs and outputs of the system are decoupled).

[14] The values for the mass and moment of inertial of the vehicle are indicated in Appendix A.

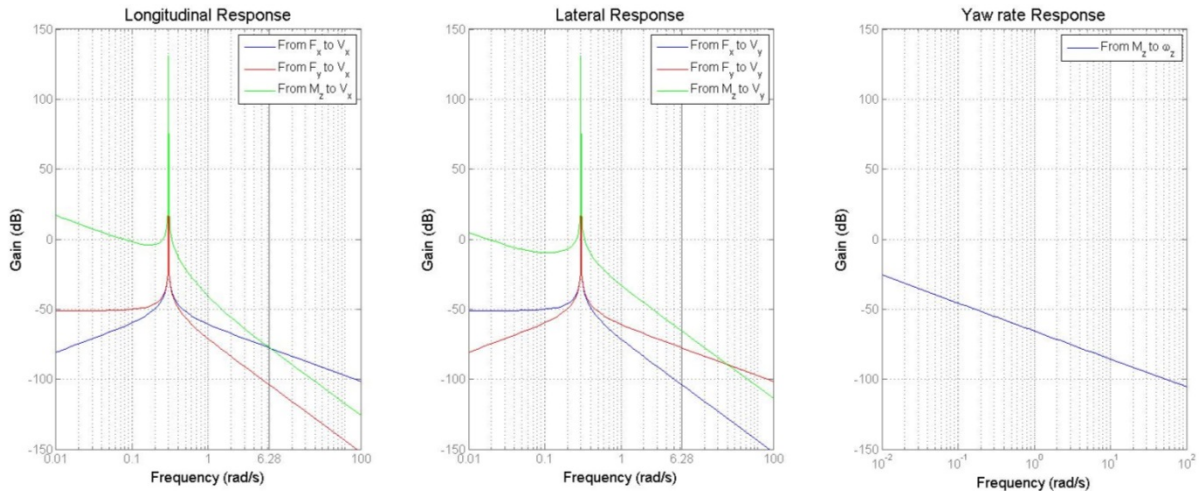

Figure 4-6: Plant Transfer Functions at one severe driving condition

To verify this conclusion on coupling behaviour of the plant, the value of RGA matrix $\mathbf{\Lambda}(s)$ (with the nominal values corresponds to one severe driving condition) is calculated from Eq. (4-7) at different frequencies as shown in Figure 4-7. According to pairing rule one[15], the preference is to pair the elements with RGA number near to one. The results confirm our previous finding that was concluded from the study of the plant frequency response: at low frequencies the off-diagonal pairings are dominant (is equal to one), whereas, at medium and high frequency ranges, the diagonal pairing is dominant.

[15] See section 4.2.2 for more detail.

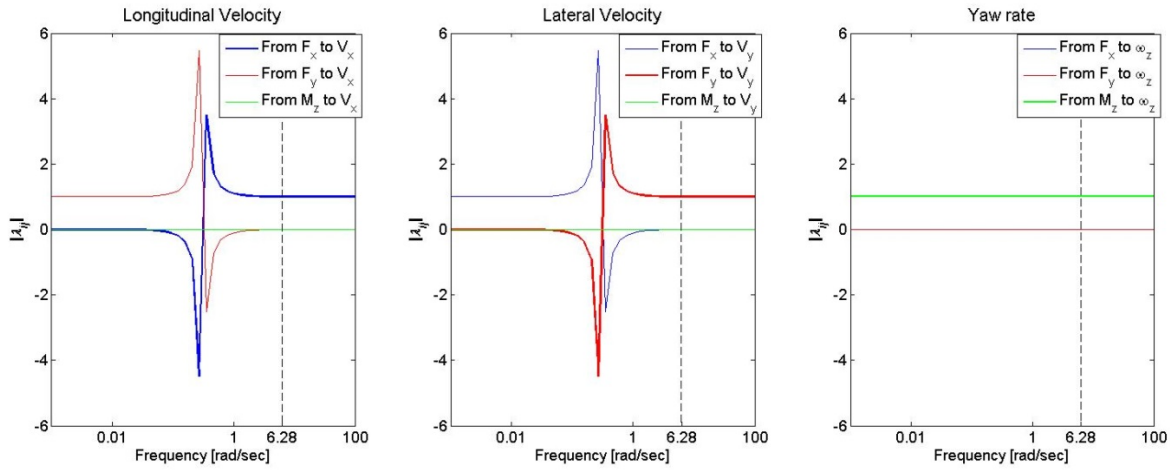

Figure 4-7: Magnitude of RGA elements

More specifically, the value of RGA matrix at the plant bandwidth frequency (6.28 rad/sec) is:

$$\boldsymbol{\Lambda} = \begin{bmatrix} 1.0023 & -0.0023 & 0 \\ -0.0023 & 1.0023 & 0 \\ 0 & 0 & 1.00 \end{bmatrix} \tag{4-57}$$

The following conclusions are justified:

- The diagonal elements of the RGA are close to one and the off-diagonal elements are near to zero. From pairing rule 1, the diagonal pairings is the best selection at this frequency. This means that at the frequencies around 1 rad/sec and above, we can use decentralised control with the following diagonal pairings: from F_x to V_x , from F_y to V_y and from M_z to ω_z.
- Moreover the off-diagonal pairing elements λ_{12} and λ_{21} (i.e., from F_y to V_x and from F_x to V_y) has negative values of RGA, so according to pairing rule 2, they are not desirable for selecting as pairing elements.
- As the diagonal elements of the RGA at the bandwidth frequency are not very large (are close to 1), therefore, the plant is not sensitive to off-diagonal coupling uncertainties. This is an important finding to declare that the simple plant model (4-56) could be confidently employed for designing a simple yet robust high-level controller.

Recall from section 4.2.2, the RGA number is another measure to find the best input/output pairing in a MIMO system. The RGA number for diagonal and off-diagonal pairing of the plant (4-56) is shown in Figure 4-8. The RGA number for diagonal paring is almost zero at frequency 1 rad/sec (and above), which confirm our finding above: the diagonal pairing is the best selection at the frequencies above crossover. Therefore, the control problem reduces to the design of three SISO controllers for three diagonal plant: from longitudinal force to longitudinal velocity, from lateral force to lateral velocity and from yaw moment to yaw rate.

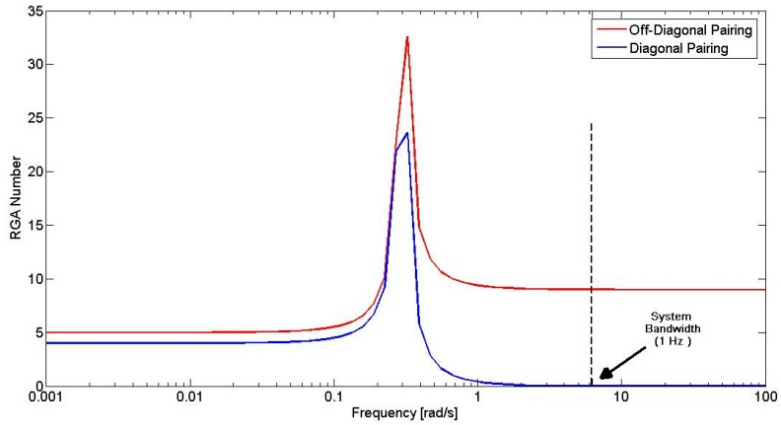

Figure 4-8: RGA number for diagonal and off-diagonal pairing

4.5.3 Control system design

4.5.3.1 Longitudinal velocity controller

Recall from Eq. (4-53), the diagonal plant transfer function along the x axis (longitudinal force input / longitudinal velocity output) is:

$$x_1 = \frac{(c_1 s^2)}{s(s^2 + a_1 a_2)} u_1$$

or

$$V_x = \frac{s}{m\left(s^2 + \omega_{z,n}^2\right)} F_x$$

Therefore the longitudinal plant transfer function is:

$$G_x = \frac{s}{m\left(s^2 + \omega_{z,n}^2\right)} \tag{4-58}$$

and the off-diagonal terms in Eq. (4-53) can be considered as disturbance to the system (which was shown to be are small in the frequency range above the plant bandwidth).

$\omega_{z,n}$ is the nominal yaw rate which normally ranges between 0 to 0.3, so the term $\omega_{z,n}^2$ is usually much smaller than the s term in Eq. (4-58) and could be ignored, then, the plant transfer function is further simplified as:

$$G_x = \frac{1}{m\,s} \tag{4-59}$$

This simplified plant model is independent from operating point (i.e. the vehicle is neutral steer (Milliken & Milliken, 1995)). To verify this simplification, the frequency response of the plant model based on the Eq. (4-58) with two different nominal yaw rates ($\omega_{z,n} = 0.3$) as well as the simplified plant model based on Eq. (4-59) is shown in Figure 4-9.

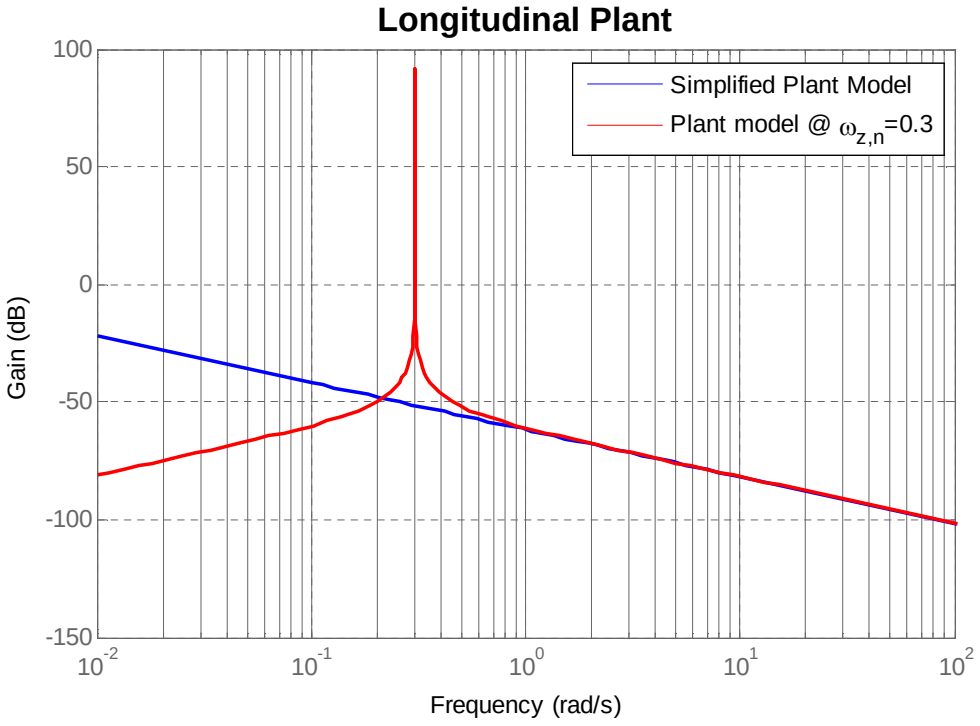

Figure 4-9: Longitudinal Plant Transfer function

By defining the plant model G_x as Eq. (4-59), the longitudinal control problem is to design a feedback controller K_x, as shown in Figure 4-10, to provide internal

stability as well as control performances in the presence of model uncertainty and disturbance. To design the high-level longitudinal (and also lateral and yaw rate) motion controllers, we employ the Youla parameterisation loop shaping method which is one of the novelties of this thesis.

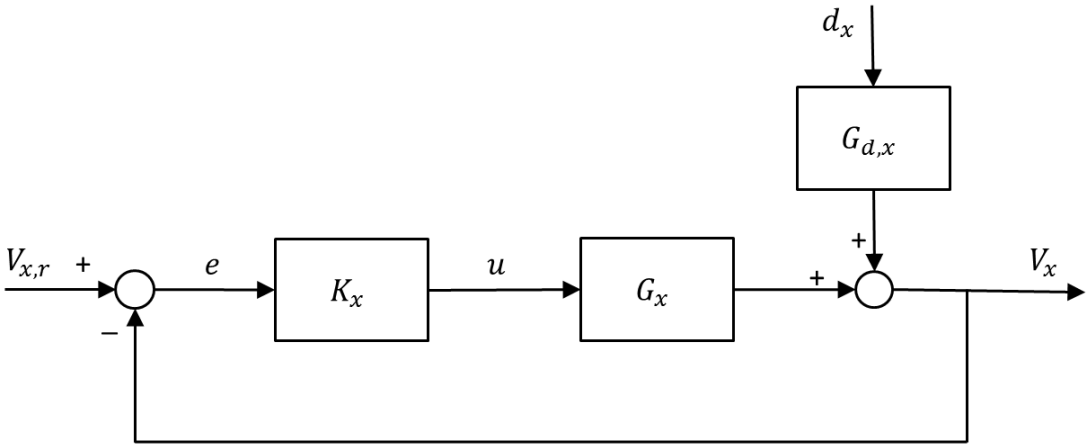

Figure 4-10: Closed loop longitudinal motion control

Considering the fact that the plant has a first order dynamics, we take the Youla parameter as the inverse of the plant multiply to one second order filter with adjustable poles and zeros such as:

$$Y_x = \frac{1}{G_x}\left[\frac{(\tau_2 s+1)}{(\tau_1 s+1)^2}\right] = \frac{m\, s\,(\tau_2 s+1)}{(\tau_1 s+1)^2}, \quad \tau_1, \tau_2 > 0 \tag{4-60}$$

The proposed Youla parameter is stable and has two tuneable parameters τ_1 and τ_2 which can be employed to shape of the loop gain $|L|$ such that to be large at low frequencies below control bandwidth, and small at high frequencies above bandwidth.

The closed loop transfer function (complementary sensitivity) is:

$$T_x = G_x Y_x = \frac{(\tau_2 s+1)}{(\tau_1 s+1)^2} \tag{4-61}$$

And the sensitivity transfer function is:

$$S_x = 1 - T_x = 1 - \frac{(\tau_2 s+1)}{(\tau_1 s+1)^2} = \frac{(\tau_1 s+1)^2 - (\tau_2 s+1)}{(\tau_1 s+1)^2} = \frac{{\tau_1}^2 s^2 + 2\tau_1 s - \tau_2 s}{(\tau_1 s+1)^2}$$

By selecting $\tau_{V_x} = \tau_2 = 2 * \tau_1$,

$$T_x = \frac{2\tau_{V_x} s + 1}{\left(\tau_{V_x} s + 1\right)^2} \tag{4-62}$$

$$S_x = \frac{{\tau_{V_x}}^2 s^2}{\left(\tau_{V_x} s + 1\right)^2} \tag{4-63}$$

The sensitivity function S_x (which is the transfer function from reference input $V_{x,r}$ to tracking error e) has two zeros at the origin, therefore the asymptotic tracking of step and ramp input is guaranteed (Doyle, Francis, & Tannenbaum, 1992).

The plant has a pole at $s = 0$, and from Eqs. (4-61) and (4-62)

$$S_x(0) = 0 \quad and \quad T_x(0) = 1$$

Therefore, from the interpolation condition, the internal stability of the system is verified.

And finally, the controller K_x can be derived from Eq. (4-41) as:

$$K_x = \frac{m\, s\, (\tau_2 s + 1)}{{\tau_{V_x}}^2 s^2} = \frac{m(2\tau_1 s + 1)}{{\tau_{V_x}}^2 s} = \frac{2m}{\tau_{V_x}} + \frac{1}{s}\frac{m}{{\tau_{V_x}}^2}$$

which is a PI controller with the proportional and integrator gain of:

$$K_p = 2m/\tau_{V_x} \quad \text{and} \quad K_I = m/{\tau_{V_x}}^2 \tag{4-64}$$

The time constant τ_{Vx} could be employed as a tuning knob to perform the required control performances. The S and T shape for two arbitrary values of $\tau_{Vx} = 1$ and $\tau_{Vx} = 0.1$ is shown in Figure 4-11. For $\tau_{Vx} = 1$, S and T cross each other at frequency below the frequency of 6.28 rad/sec (plant bandwidth) and for the value of $\tau_{Vx} = 0.1$ they crossing at the frequency above that.

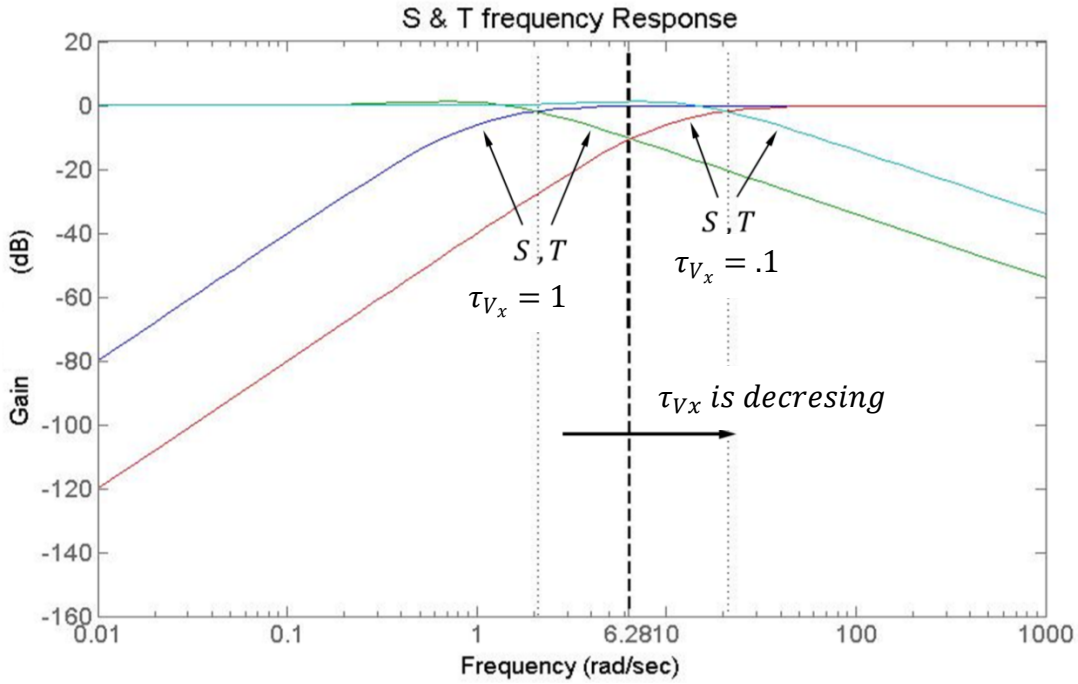

Figure 4-11: S and T variation with parameter a

A driver's steering wheel input bandwidth is measured from the number of degrees of steering wheel angle input per second. For example if a driver is capable of applying 180 degrees/second of steering, then his/her bandwidth, in hertz, is computed as follows,

$$f = 180 degrees/\sec * (\frac{\pi\, rad}{180\, degrees}) * (\frac{1}{2 * \pi}) = 0.5\, Hz$$

The average driver has a bandwidth of less than 1 Hz, however, the bandwidth of the advanced drivers could be more than 1 Hz bandwidth, whilst, the professional drivers are capable of applying steering inputs four times faster than the average drivers. The high level controllers in this work should respond quicker than the fastest drivers' inputs, hence, the bandwidths of these controllers are selected to be 3 Hz. The speed of the response of these high level controllers will be further evaluated, and if necessary, adjusted and validated in the final chapter of this thesis.

By selecting $\tau_{V_x} = 0.1$, the *control bandwidth* (crossover frequency) is set to around 20 rad/sec ($\approx 3.2\, Hz$) and the longitudinal controller K_x becomes:

$$K_x = 20m + 100m\,\frac{1}{s} \tag{4-65}$$

where m is the vehicle mass as indicated in appendix A.

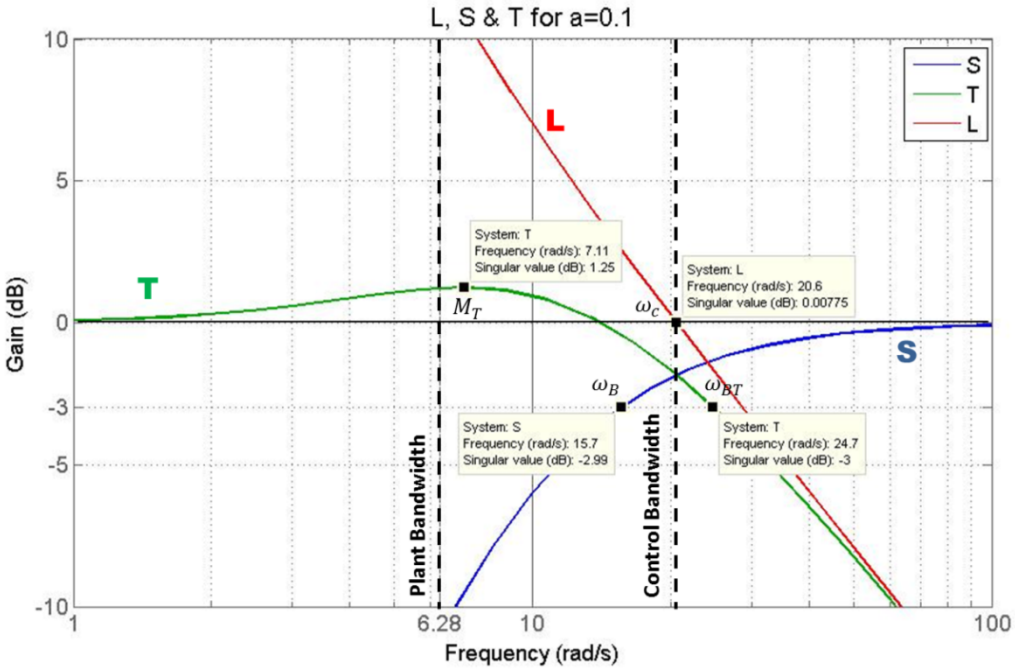

Figure 4-12: Open loop, Closed loop and sensitivity transfer functions for τ_{V_x}=0.1

To investigate the behaviour of the control system, a close-up plot of the frequency response of the open loop L, closed loop T and sensitivity S transfer functions are shown in Figure 4-12. The following conclusions are justified[16]:

1. The sensitivity transfer function $|S|$ first crosses $-3\,\mathrm{dB}$ from below at frequency around 15 rad/sec, the open loop transfer function $|L|$ first crosses 1 $(0\,\mathrm{dB})$ from above at frequency around 20 rad/sec and the closed loop transfer function $|T|$ first crosses $-3\,\mathrm{dB}$ from above at frequency around 25 rad/sec, so:

   $$\omega_B \approx 15\,rad/s < \omega_c \approx 20\,rad/s < \omega_{BT} \approx 25\,rad/s$$

   The crossover frequency ω_c is between ω_B and ω_{BT}, therefore minimum 90° phase margin is guaranteed. Moreover, during this interval the

[16] See sections 4.3 for more explanation on this course.

sensitivity transfer function S remains negative, so the control performance is not degraded while the frequency is increasing. The crossover frequency 20 rad/s ($\approx 3.2\ Hz$) is selected as the control system bandwidth.

2. The open loop gain at low frequencies (below control bandwidth) is high whereas the gain at high frequency (after control bandwidth) is low, therefore, the control system has good robustness, command tracking and disturbance attenuation performance at low frequencies and good noise rejection performance at high frequencies.
3. The value of $|S|$ and $|T|$ at crossover frequency (the point that $S = T$) are less than zero dB, therefore the stability of the closed loop system is guaranteed.
4. The maximum value of S and T (M_S and M_T) are less than 2, so the minimum of $60°$ phase margin and 6dB gain margin is also guaranteed and the control performance is met.
5. Finally, the value of $|S|$at plant (dynamics) bandwidth is less than -10 dB. This ensures a good stability margin and robustness even in the presence of plant uncertainties and disturbance.

The frequency response of the system including the plant G_x, Youla parameter Y_x, closed loop T_x, sensitivity S_x, controller K_x and open loop L_x transfer functions are shown in Figure 4-13, which confirms all the previous conclusions about the control system.

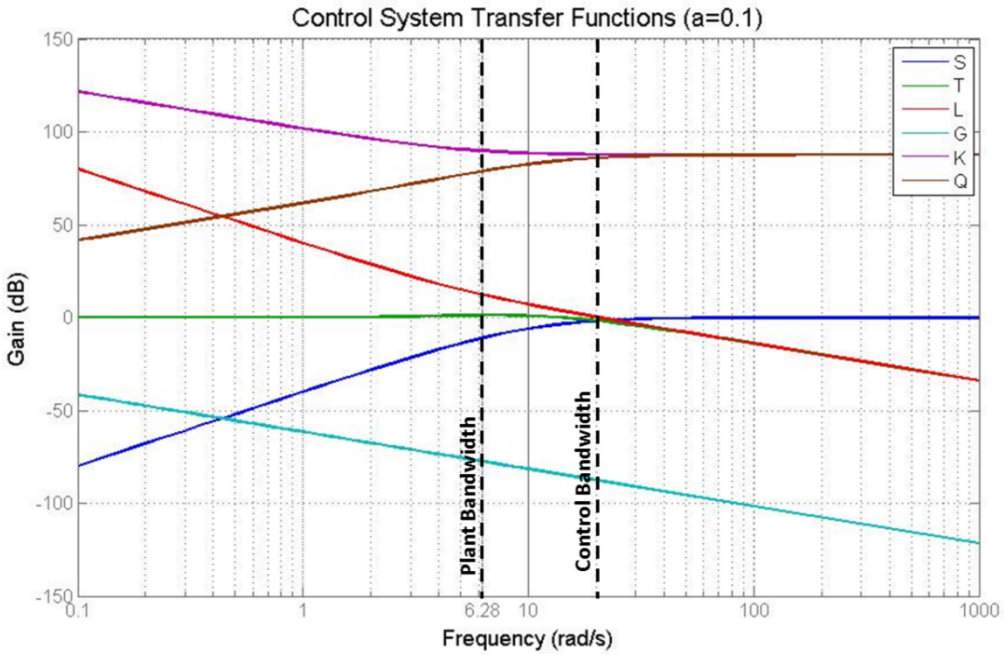

Figure 4-13: Longitudinal Control Transfer Functions

To investigate the closed loop system performance in time domain, the step response of the system with the existence of step disturbance (applied at sec 3) is shown in Figure 4-14. The magnitude of disturbance is set to %50 of reference value (which is quite high). The transient response of the system is sufficiently fast and well damped: the overshoot is less than %20 and the settling time is 0.4 sec and the disturbance is properly attenuated.

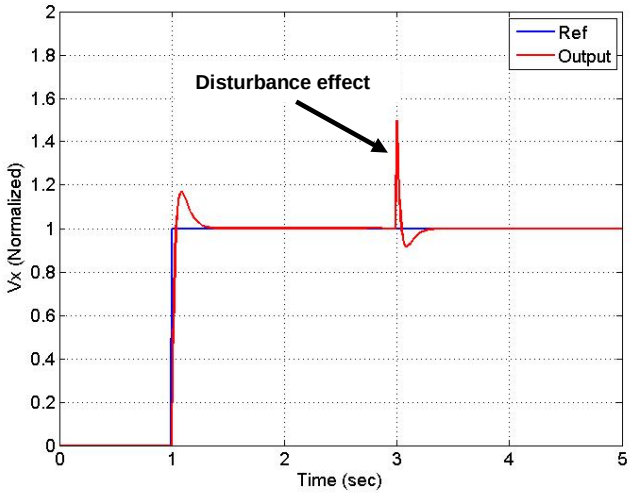

Figure 4-14: Closed loop step response with disturbance

4.5.3.2 Lateral velocity (sideslip) controller:

In a similar fashion to the longitudinal motion, the simplified lateral motion transfer function can be derived as:

$$G_y = \frac{1}{m\,s} \tag{4-66}$$

and the off-diagonal terms in Eq. (4-54) can be considered as disturbance to the system (which was shown to be small in the frequency range above the plant bandwidth).

The control design procedure is similar to the longitudinal controller design mentioned in the previous chapter, and leads to a PI controller with the proportional and integral coefficients as:

$$K_p = 2m/\tau_{V_y} \quad \text{and} \quad K_I = m/{\tau_{V_y}}^2 \tag{4-67}$$

where a is a parameter which can be used for tuning the lateral motion controller. By selecting $\tau_{V_y} = 0.1$, the lateral motion control system transfer functions is:

$$K_y = 20m + 100m\,\frac{1}{s} \tag{4-68}$$

which is similar to longitudinal motion control. Therefore, their response in the frequency domain and time domain as well as the stability and performance of the system is the same as longitudinal motion control.

4.5.3.3 Yaw rate controller

The plant transfer function as:

$$G_z = \frac{1}{I_z\,s} \tag{4-69}$$

and there is no disturbance (due to off-diagonal term) in exist the system:

$$d_z = 0$$

The control design procedure is the same as the longitudinal and lateral controllers, which lead to a PI controller with the proportional and integral coefficients as:

$$K_p = 2I_z/\tau_{\omega_z} \quad \text{and} \quad K_I = I_z/{\tau_{\omega_z}}^2 \tag{4-70}$$

where τ_{ω_z} is a parameter which can be used for tuning the yaw rate controller. By selecting $\tau_{\omega_z} = 0.1$, the lateral motion control system transfer functions is:

$$K_y = 20I_z + 100I_z \frac{1}{s} \tag{4-71}$$

which is similar to longitudinal motion control. Therefore, their response in the frequency domain and time domain as well as the stability and performance of the system is similar to the longitudinal and lateral motion controls.

4.6 Control system validation

4.6.1 Control validation with idealised plant model

The first test for validation of the control system is performed with the simple (idealised) vehicle planar model as represented by Eq. (4-1). The control objective is to track arbitrary reference values of longitudinal velocity, lateral velocity and yaw rate in the presence of different (actuator) disturbances applied to the system at different times as shown in Figure 4-15.

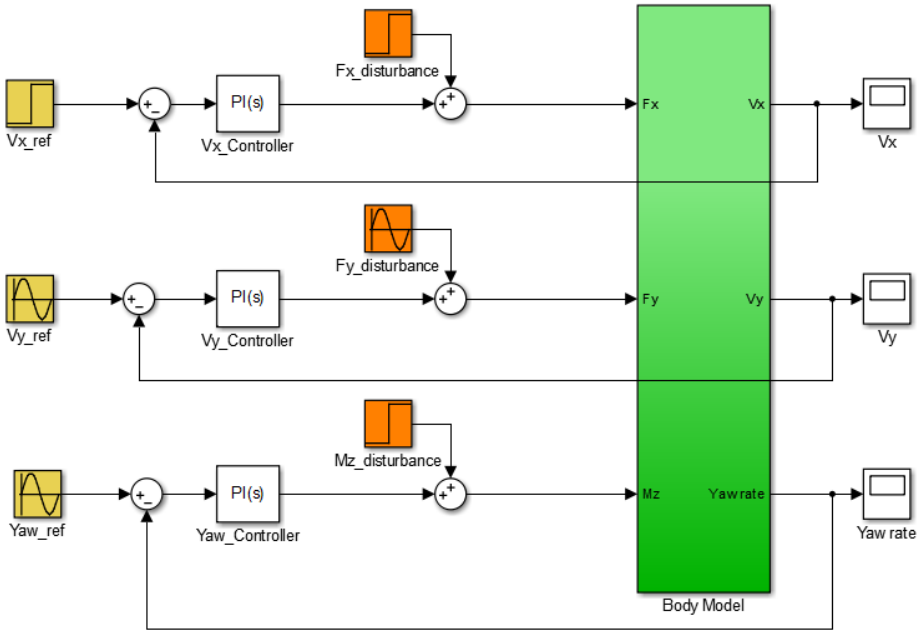

Figure 4-15: Control system with simple vehicle planar model

The chosen reference values are step input for longitudinal velocity with magnitude of 30 m/sec, sinusoidal input with amplitude of 10 m/sec and period of 10 sec for lateral velocity and sinusoidal input for yaw rate with amplitude of 1 rad/sec and period of 2 sec. The values of (actuator) disturbance inputs are: step input for longitudinal force with magnitude of 10000 N applied at time 5 sec, sinusoidal input for lateral force with amplitude of 5000 N and period of 6.28 sec applied at the beginning of the simulation, and step input for yaw moment with magnitude of 3000 Nm applied at time 3 sec. The vehicle responses (longitudinal velocity, lateral velocity, and yaw rate) and the corresponding reference values are shown in Figure 4-16. As one can see, all the three control systems are stable, follow their corresponding reference values and attenuate the applied (actuator) disturbances very well.

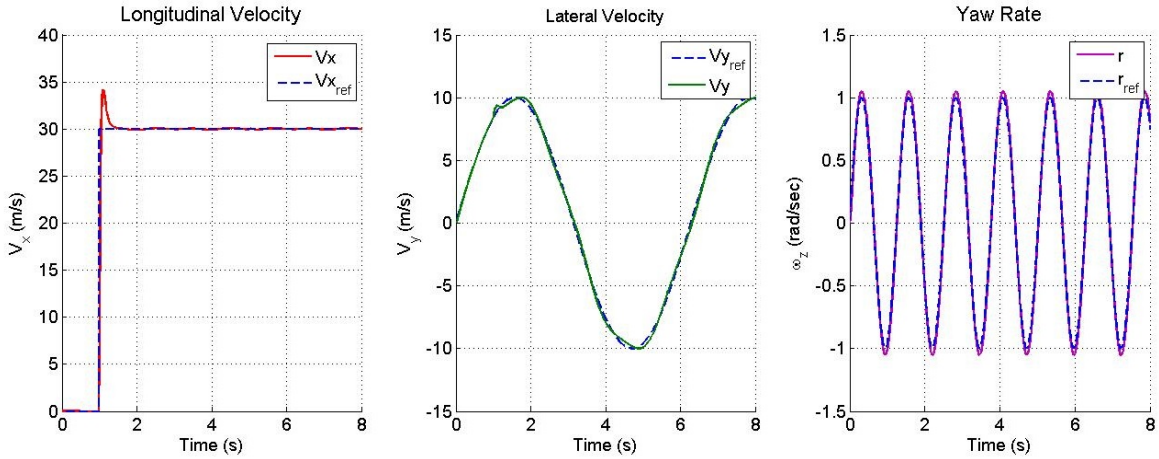

Figure 4-16: response of the control system with simple vehicle model

4.6.2 Control validation with 7-DoF vehicle model

The next step of control system validation is to employ the proposed control system in the 7-DoF nonlinear vehicle model as introduced in Chapter 3. The vehicle will be subject to the same manoeuvres as defined in section 3.7, and have the same parameters as indicated in Appendix B. The vehicle model is more comprehensive than the simplified model being employed for control design; therefore, it provides a more realistic virtual test platform to evaluate the stability, robustness and performance of the controllers with respect to un-modelled dynamics, parameter variations and also with the existence of nonlinearities such as tyre forces. We also utilise the CarMaker® as a high fidelity validated vehicle dynamics model to verify the controller stability and performance through real time HIL testing in the final stage of development, as discussed in the Chapter 7 of the thesis.

Figures 4-18 to 4-20 show the vehicle states (i.e. longitudinal velocity, lateral velocity and yaw rate) with and without the effect of control system, subject to step steer manoeuvre (Step60_mu1.0_V100, as described in Chapter 3). Here the reference value for the longitudinal velocity is set to $V_x = 27.78\, m/s$ ($100\, Kph$), and the reference lateral velocity (sideslip) is set to zero i.e. $V_y = \beta = 0$ (corresponding to a neutral steer vehicle), whereas, the reference value for the yaw rate is derived from the steady state bicycle model as discussed in Chapter 3.

After the steering action, the uncontrolled vehicle spins-out and becomes unstable (corresponding to an oversteering situation) as confirmed in the last chapter.

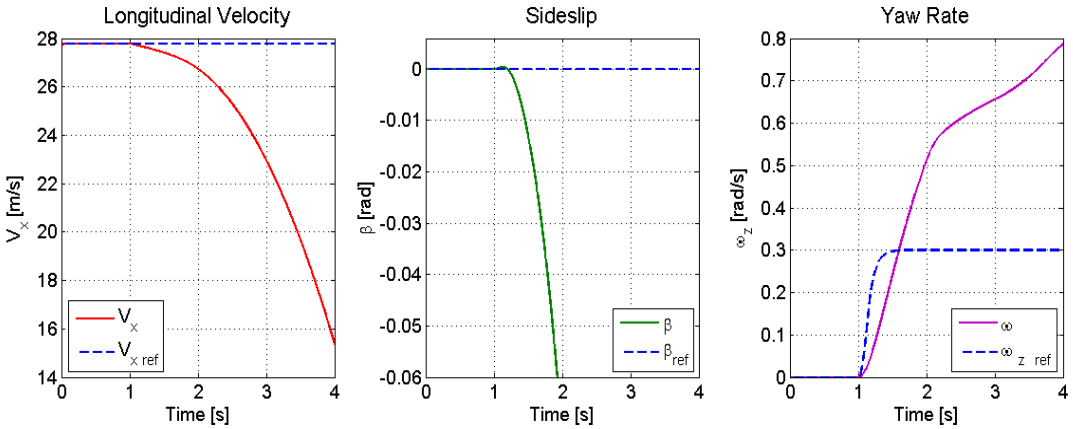

Figure 4-17: simulation results of 7-DoF vehicle model , Control Off, Off-throttle (after 2 sec)

The effectiveness of control system to track the reference commands and to stabilise the vehicle are shown in Figure 4-18.

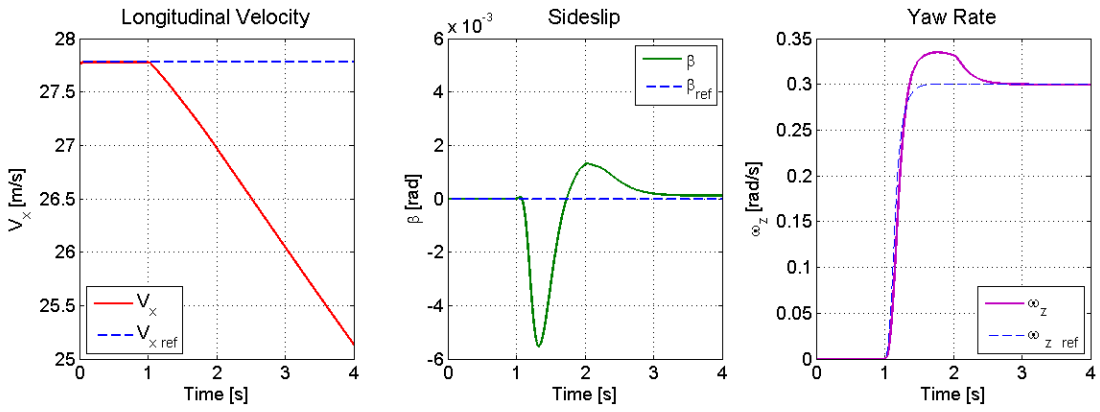

Figure 4-18: 60° Step Input, Control On, Off-throttle (after 2 sec)

Figure 4-19 shows the results of the control action for the same manoeuvre as before except the engine is always on (on-throttle). The simulation results shows that all the system states (i.e. longitudinal velocity, lateral velocity and yaw rate) follow the reference values perfectly with minimum error.

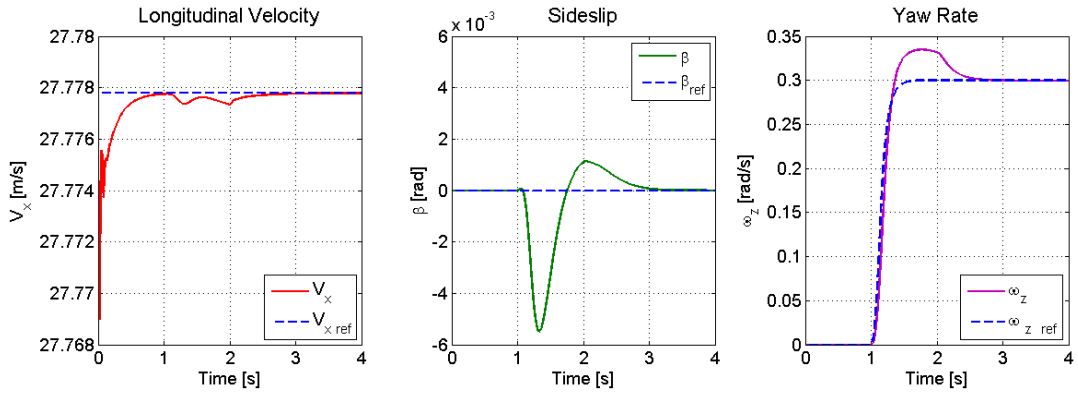

Figure 4-19: 60° Step Input, Control On, On-throttle

In the second manoeuvre, the vehicle is subject to sinusoidal steering input as defined in the previous chapter by Sin60_mu1.0_V65. Figure 4-20 shows the uncontrolled behaviour of the vehicle: after first steering action, the vehicle starts to spin and is no longer steerable, as confirmed in Chapter 3.

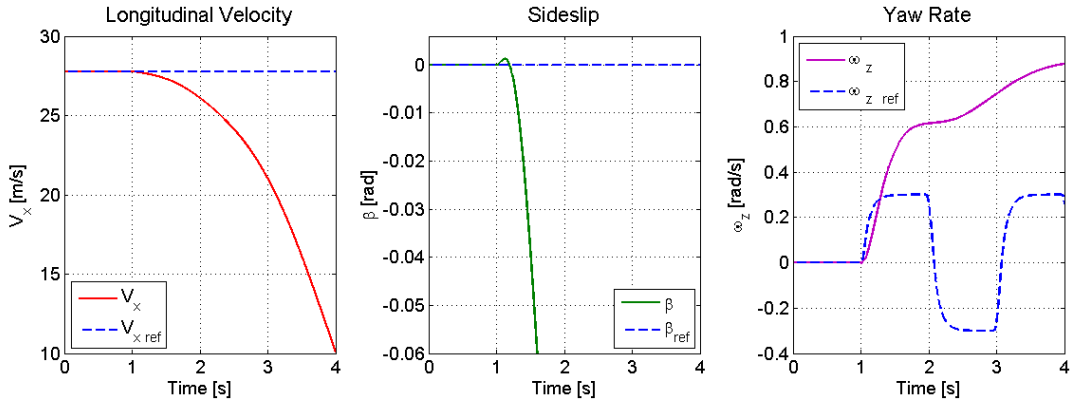

Figure 4-20: 60° Sine Input, Control Off, Off-throttle (after 2 sec)

The results of the controlled state variables are shown in Figure 4-21. In this manoeuvre, all the states follow the reference values and in spite of the engine being turned off after 2 sec, the longitudinal velocity just drops from 27.78 m/sec to 25.3 m/sec after 10 seconds of simulation. The vehicle is stable and steerable, however, the vehicle body sideslip cannot precisely be bounded to the desired value (this is due to interaction between sideslip and yaw rate) but its deviation is very small.

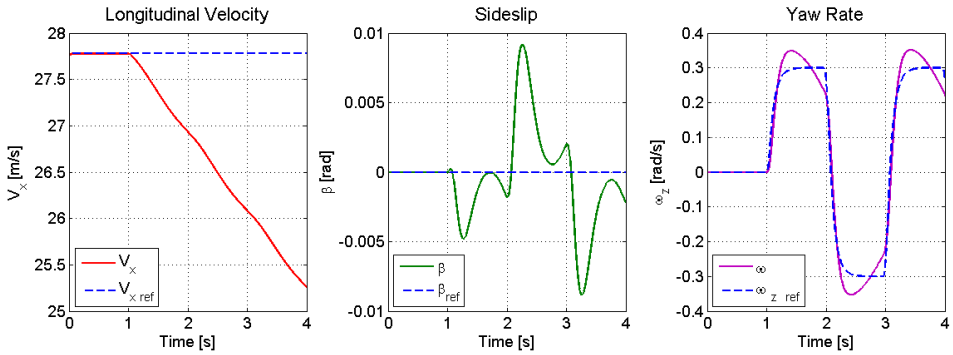

Figure 4-21: 60° Sine Input, Control On, Off-throttle

Similar successful simulation results were also carried on for the vehicle manoeuvring on low mu surface (corresponding to wet and icy roads). The uncontrolled vehicle becomes understeered while the controlled vehicle is stable and steerable as well.

It should be noted that the above simulation results were obtained by assuming that the calculated longitudinal force, lateral force and yaw moment are (virtually) directly applied to the vehicle centre of gravity (see the vehicle dynamics planar equations of motion, i.e. Eqs. (3-34), (3-35) and (3-36)). In a real vehicle, these forces and moments are generated in the tyres through steering, brake (and engine) actuation. Allocation of the derived high-level control outputs (forces and moments) to the vehicle's tyres (longitudinal and lateral) forces is the subject of the next chapter.

5 Control Allocation

5.1 Introduction

According to the proposed V-diagram (see Figure 1-2), and the multi-layer integrated vehicle dynamics control (IVCS) structure[17], the next step after designing the high–level controllers is to employ a control allocation scheme as shown in Figure 5-1. Different techniques for allocation, blending or mixing existing actuators to achieve the desired control tasks are known as the *Control Allocation* (CA) problem (Tjønnås, 2008).

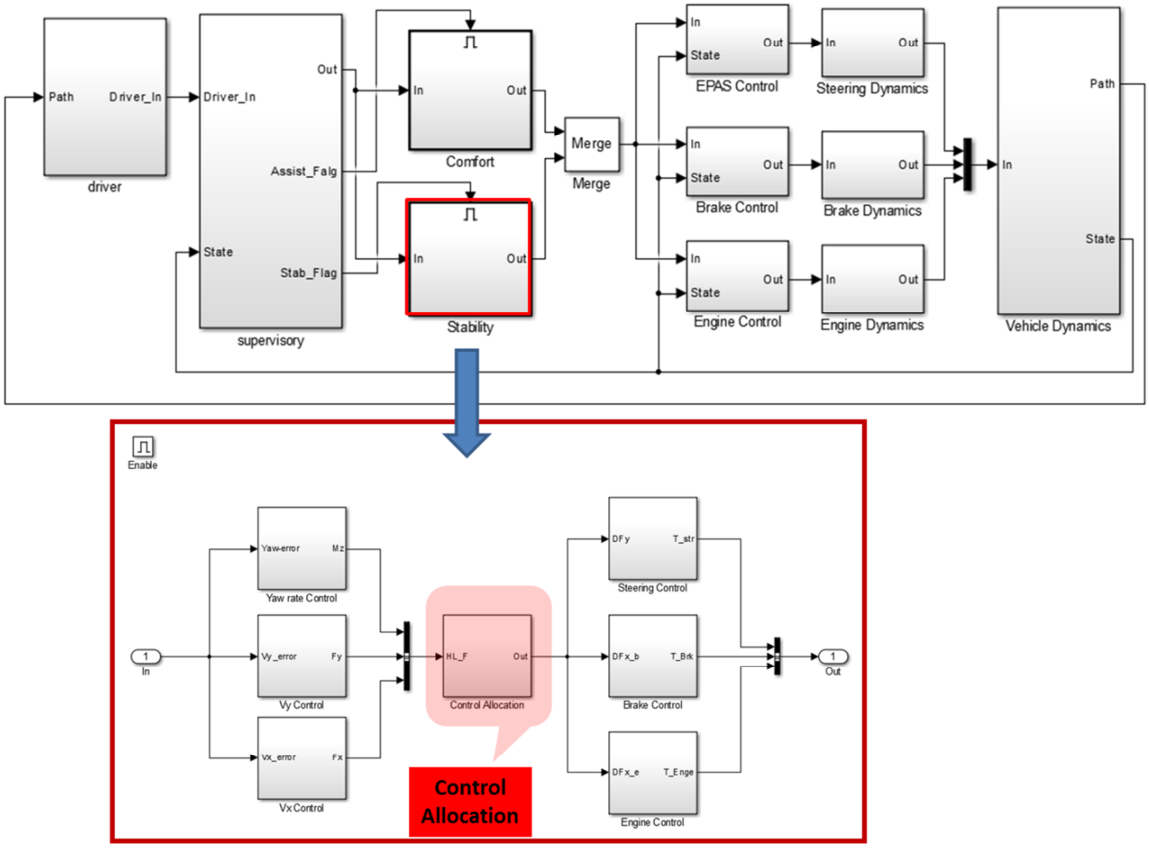

Figure 5-1: Control Allocation Simulink® Block

By increasing the number of actuators in modern vehicles, it is very common that the numbers of existing actuators are more than the number of the states that are being controlled by the high-level vehicle dynamic control system.

[17] See Chapter 3 for more detail in this course.

When the numbers of actuators are more than the number of target trajectories intended for control (controlled states), the system is called over-actuated (or redundant), and there is no unique solution available for the control problem (Valášek, 2003). The objective of CA scheme is to "*optimally*" distribute the calculated generalised forces and moments into each available actuator, considering both actuation amplitude and rate constraints.

Implementations of optimal CA scheme in control of over-actuated systems provide several benefits, including:

Performance: As the number of available actuators is more than the number of controlled states in an over-actuated system, it is possible to define different design objectives to improve the designed system performance such as: cost, size, efficiency, accuracy, dynamic response, etc. by increasing the attainable set of actuators envelop and/or prioritizing them. These design objectives could be well addressed in the optimal CA formulation (Bodson, 2002).

Reconfigurable control: Implementation of CA scheme in a redundant system can provide fault tolerance to the control system; therefore, control reconfiguration requirements could be achieved. Here, the control reconfiguration refers to a property of a control system in which the control loop is restructured to prevent failure/degradation of the system when a fault, such as actuator failures, results in a break-up of the control loop (Steffen, 2005).

Actuators saturation and bandwidth: Magnitude and rate saturation are the two fundamental limitations in fully utilising the actuators. In this thesis, actuator saturation is referred to the maximum (and/or minimum) value of force or moment which can be generated by the actuators, whereas, the rate saturation is referred to the dynamic response (bandwidth) limitation of the actuator. Saturation is one the main sources of nonlinearities in a control system, which could degrade the control system performance or even destabilise it (Slotine & Weiping, 1991). Rate saturation is especially very important when we have several actuators with different dynamics response (bandwidth) in a redundant system. Inappropriate combination of actuators, which have different bandwidths, may cause oscillation and instability in the control system. A well

formulated CA scheme is capable to address not only the actuators magnitude saturation but also the actuators rate limit by employing a constrained optimisation solution (Nocedal & Wright, 2006).

Adaptation: The actuators priority or their (amplitude and rate) saturation limits may vary with changes of environment and system operating point. For example, changing the road surface condition (tyre-road coefficient of friction) or tyre normal force, will affect the maximum achievable tyre forces. Adaptive (dynamic) CA methods, can adapt the effectiveness and/or priority of the actuators based on probable changes in the system states or conditions (Tjønnås, 2008).

Modularity: By employing CA schemes for a general over-actuated vehicle dynamics system, one could offer a modular control design framework for any type of IVDC design problems in spite of having different desired tasks and/or existing actuator types. This modular framework could be integrated into the proposed multilayer IVCS structure, as discussed in Chapter 3. The block diagram of the modular (adaptive) IVCS control structure including CA is presented in Figure 5-2.

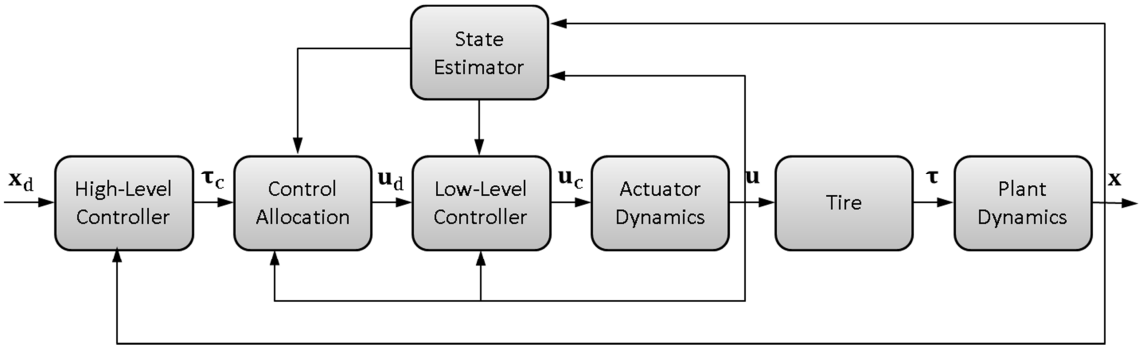

Figure 5-2: Modular IVCS control structure including control allocation.

The general formulation for control design of an over-actuated system based on the above mentioned CA scheme is discussed in this Chapter. More specifically, the formulating of CA scheme for the customised IVCS system (as an over-actuated vehicle dynamic system) is presented. Several (explicit and implicit) solutions to the CA problem, including daisy-chain and redistributed weighted pseudo-inverse as well as linear programming and quadratic

programming methods are presented and some of them are being employed in the customised IVCS system. The results of different solutions methods to CA problems are being compared in terms of accuracy and required processing time. Validation of the proposed low cost CA scheme is presented at the end of the chapter.

5.2 Control Allocation (CA) Formulation

Recall from Chapter 3, the relation between the generalised forces and moments on the vehicle level (body coordinate system) and the forces and moments on the tyre level (tyre coordinate system) are derived from the vehicle/tyre kinematic relation (Kiencke & Nielsen, 2005) and could be represented in the form of:

$$\boldsymbol{\tau} = \mathbf{B}\mathbf{u} \tag{5-1}$$

where $\boldsymbol{\tau} \in \mathbb{R}^m$ is the vector of generalised forces and moments at the centre of gravity, $\mathbf{B} \in \mathbb{R}^{\mathrm{m}\times\mathrm{p}}$ is the control effectiveness matrix and $\mathbf{u} \in \mathbb{R}^p$ is the vector of control inputs at the tyre level (actuators input); m is the number of controlled states and p is the number of the available actuators in the system. The linear CA can be formulated as follows: *given the value of generalised forces and moments,* $\boldsymbol{\tau} \in \mathbb{R}^m$ *,and effectiveness matrix ,* $\mathbf{B} \in \mathbb{R}^{m\times p}$*, find the value of actuator control input,* $\mathbf{u} \in \mathbb{R}^p$*.*

If the matrix $\mathbf{B}$ is square (i.e. $p = m$) and invertible (non-singular), the solution is

$$\mathbf{u} = \mathbf{B}^{-1}\boldsymbol{\tau} \tag{5-2}$$

However, the above solution has several limitations: Firstly, we should note that in reality each actuator is physically bound by upper and lower "*magnitude and rate limits"*, which are not considered in the solution. Secondly, if the number of the available actuators is greater than the number of the controlled states, which is the case for redundant (or over-actuated) systems, the effective matrix $\mathbf{B}$ will not be square but will have full row rank (i.e. $m < p$). This means that the solution is ill-posed, i.e. the number of vectors $\mathbf{u} \in \mathbb{R}^p$ that satisfy Eq. (**5**-**1**) is

infinite. Another issue arises when there are singularities existing in the system (for example, due to actuator failure), so the effective matrix is non-invertible and the solution of Eq. (**5**-**2**) does not exist.

In the case of system redundancy, the "*primary*" objective of CA scheme is to find out the "*best*" way of distributing the generalised forces and moments among several existing smart actuators. This means that, in the existence of actuators magnitude and rate limits, we want the sum of the forces and moments that are generated by the actuators be equal to the required generalised forces and moments at all time. Therefore, the control allocation problem can be posed as follows: Find a control input vector, $\mathbf{u} \in \mathbb{R}^p$, such that:

$$\boldsymbol{\tau} - \mathbf{B}\mathbf{u} = 0 \qquad subject\ to \qquad \mathbf{u}_{min} \leq \mathbf{u} \leq \mathbf{u}_{max} \ \ \& \ \ \dot{\mathbf{u}} \leq \dot{\mathbf{u}}_{max} \tag{5-3}$$

where $\mathbf{u}_{min} \in \mathbb{R}^p$ and $\mathbf{u}_{max} \in \mathbb{R}^p$ are the lower and upper limits of control input respectively (actuators magnitude limits) and $\dot{\mathbf{u}}_{max} \in \mathbb{R}^p$ is the maximum of control input rate[18]. In a discrete implementation of CA, the rate constraint can be considered as a time-varying magnitude constraint (i.e. the maximum amount of actuator movement) within each sampling interval. This gives the following combined constraints (Oppenheimer & Doman, 2006):

$$\underline{\mathbf{u}}(t) \leq \mathbf{u}(t) \leq \overline{\mathbf{u}}(t) \tag{5-4}$$

where

$$\begin{aligned} \overline{\mathbf{u}}(t) &= \min(\mathbf{u}_{max}, \mathbf{u} + \Delta t \dot{\mathbf{u}}_{max}) \\ \underline{\mathbf{u}}(t) &= \max(\mathbf{u}_{min}, \mathbf{u} - \Delta t \dot{\mathbf{u}}_{max}) \end{aligned} \tag{5-5}$$

Here, $\overline{\mathbf{u}} \in \mathbb{R}^p$ and $\underline{\mathbf{u}} \in \mathbb{R}^p$ are the most restrictive upper and lower control input limits, respectively, and Δt is the sampling interval (of the discrete solution).

There are several methods proposed for a solution of the CA problem (Zhang & Jiang, 2008). However, the most common and effective approach is to employ optimisation techniques (Johansen & Fossen, 2012; Assadian & Aneke, 2006).

[18] It is worth to note that the inequalities in Eqs. (**5**-**3**) & (**5**-**4**) are element wise.

The CA problem can be formulated as an optimisation problem as follows: Given a matrix $\mathbf{B}$, find a vector $\mathbf{u}$, such that:

$$\min_{\mathbf{u}} \; J = \|\mathbf{Bu} - \boldsymbol{\tau}\| \quad subject\ to \quad \overline{\mathbf{u}} \leq \mathbf{u} \leq \underline{\mathbf{u}} \tag{5-6}$$

where J is a cost function with the objective of minimising the difference between $\boldsymbol{\tau}$ and $\mathbf{Bu}$ (so called, error minimisation), and $\|\cdot\|$ is a norm depends on the type of algorithm used to perform the minimisation. Using l_1 norm for cost function leads to Linear Programming (LP) CA formulation, whereas employing l_2 norm results a Quadratic Programming (QP) CA approach (Frost, Bodson, & Acosta, 2009).

As mentioned before, the CA solution for an over-actuated system is not always unique and there are multiple solutions that exist where one solution may be preferred over another. This specification, provides extra control authority which can be used to define "*secondary"* objectives in a CA scheme, so called "control minimisation" problem (Bodson, 2002). The cost function for control minimisation problem may contain terms that penalise actuators wear/tear, power consumption, configuration (to avoid singularity, for example) and/or safety critical effects (e.g. fault tolerance) (Oppenheimer & Doman, 2006).

By combining error minimisation and control minimisation, the most complete and effective CA formulation, so called *mixed optimisation* problem, is derived as follows (Frost, Bodson, & Acosta, 2009) :

$$\min_{\mathbf{u}} \; J = \|\mathbf{W}_\tau(\mathbf{Bu} - \boldsymbol{\tau})\| + \varepsilon\left\|\mathbf{W}_u\left(\mathbf{u} - \mathbf{u}_p\right)\right\| \quad subject\ to \quad \overline{\mathbf{u}} \leq \mathbf{u} \leq \underline{\mathbf{u}} \tag{5-7}$$

where $\mathbf{W}_\tau \in \mathbb{R}^{m\times m}$ and $\mathbf{W}_u \in \mathbb{R}^{p\times p}$ are positive definite weighting matrixes, $\varepsilon > 0$ is a weighting factor and $\mathbf{u}_p \in \mathbb{R}^p$ is the preferred value of control inputs at the resting positions of the actuators[19]. The control weighting matrix $\mathbf{W}_u$ affects the control distribution among the actuators; whereas $\mathbf{W}_\tau$ affects the prioritisation among control components due to the actuators saturation or other

[19] $\mathbf{u}_p$ is typically set to zero in most applications (Johansen & Fossen, 2012)

physical limitations of the system. ε is a factor used to prioritise the relative importance of control error and control optimisation problem. It is desired to give the priority to primary objective error minimisation over control minimisation (secondary objective), therefore, ε is usually chosen to be small. (Petersen & Bodson, 2006).

5.3 Unconstrained Control Allocation Solution

In practice, all CA schemes are constrained in nature, because of the actuator limitation in the magnitude and/or rate. However, the solution of unconstrained CA problem is very important, as most of the CA algorithms start with unconstrained solution and finish, if the attained control inputs are within the constraints (Bodson, 2002). Otherwise, calculation continues to deal with actuators limitation by employing one of the constrained solution methods as discussed in the following sections. There exists an explicit solution for the unconstrained optimisation CA problem, known as weighted pseudo-inverse (Durham, 1993), which is presented in the following section.

5.3.1 Weighted Pseudo-inverse

By neglecting the actuators limits (i.e. no magnitude and rate constraints on the control input $\mathbf{u}$) and selecting a quadratic cost function for control input vector, (**5**-**7**) reduces to the following formulation:

$$\min_{\boldsymbol{u}} \; J = \frac{1}{2}\left(\mathbf{u}-\mathbf{u}_p\right)^T \mathbf{W}\left(\mathbf{u}-\mathbf{u}_p\right) \quad subject\ to \quad \mathbf{Bu}-\boldsymbol{\tau}=0 \tag{5-8}$$

An explicit optimal solution for this unconstrained (with respect to the actuators) least square problem is available based on Lagrangian multipliers (Rao, 2009). Lagrangian function, $\mathbf{L}$, can be defined as:

$$\mathbf{L} = \frac{1}{2}\left(\mathbf{u}^{\boldsymbol{T}}\mathbf{W}\mathbf{u} - \mathbf{u}^{\boldsymbol{T}}\mathbf{W}\mathbf{u}_p - \mathbf{u}_p^T\mathbf{W}\mathbf{u} + \mathbf{u}_p^T\mathbf{W}\mathbf{u}_p\right) + \boldsymbol{\lambda}(\mathbf{Bu}-\boldsymbol{\tau}) \tag{5-9}$$

where $\boldsymbol{\lambda} \in \mathbb{R}^m$ is a vector of Lagrange multiplier. By taking the partial derivative of $\mathbf{L}$ with respect to $\mathbf{u}$ and $\boldsymbol{\lambda}$ and set them to zero, the necessary condition[20] for J to be minimum is achieved (Rao, 2009), which is:

$$\frac{\partial \mathbf{L}}{\partial \mathbf{u}} = \mathbf{W}\mathbf{u} - \frac{1}{2}\mathbf{W}\mathbf{u}_p - \frac{1}{2}\left(\mathbf{u}_p^T\mathbf{W}\right)^T + (\boldsymbol{\lambda}\mathbf{B})^T = 0 \tag{5-10}$$

$$\frac{\partial \mathbf{L}}{\partial \boldsymbol{\lambda}} = \mathbf{B}\mathbf{u} - \boldsymbol{\tau} = 0 \tag{5-11}$$

Rearranging the above expressions gives:

$$\mathbf{W}\mathbf{u} = \mathbf{W}\mathbf{u}_\mathrm{p} - \mathbf{B}^\mathrm{T}\boldsymbol{\lambda}^\mathrm{T} \tag{5-12}$$

$$\mathbf{B}\mathbf{u} = \boldsymbol{\tau} \quad \Longrightarrow \quad \mathbf{B}\mathbf{W}^{-1}\mathbf{W}\mathbf{u} = \boldsymbol{\tau} \tag{5-13}$$

Substituting Eq. (**5-12**) into Eq. (**5-13**) yields:

$$\mathbf{B}\mathbf{W}^{-1}\left[\mathbf{W}\mathbf{u}_\mathrm{p} - \boldsymbol{\lambda}^\mathrm{T}\mathbf{B}^\mathrm{T}\right] = \boldsymbol{\tau} \tag{5-14}$$

Solving for $\boldsymbol{\lambda}^T$ yields:

$$\boldsymbol{\lambda}^T = (\mathbf{B}\mathbf{W}^{-1}\mathbf{B}^T)^{-1}\left[\mathbf{B}\mathbf{u}_p - \boldsymbol{\tau}\right] \tag{5-15}$$

Substituting Eq. (**5-15**) into Eq. (**5-12**) produces:

$$\mathbf{W}\mathbf{u} = \mathbf{W}\mathbf{u}_\mathrm{p} + \mathbf{B}^\mathrm{T}(\mathbf{B}\mathbf{W}^{-1}\mathbf{B}^\mathrm{T})^{-1}\left[\boldsymbol{\tau} - \mathbf{B}\mathbf{u}_\mathrm{p}\right] \tag{5-16}$$

Finally, simplifying Eq. (**5-16**) gives the desired result:

$$\mathbf{u} = \mathbf{u}_\mathrm{p} + \mathbf{W}^{-1}\mathbf{B}^\mathrm{T}(\mathbf{B}\mathbf{W}^{-1}\mathbf{B}^\mathrm{T})^{-1}\left[\boldsymbol{\tau} - \mathbf{B}\mathbf{u}_\mathrm{p}\right] \tag{5-17}$$

The *weighted pseudo-inverse* of $\mathbf{B}$ is defined as (Durham, 1993)

$$\mathbf{B}^\# = \mathbf{W}^{-1}\mathbf{B}^\mathrm{T}(\mathbf{B}\mathbf{W}^{-1}\mathbf{B}^\mathrm{T})^{-1} \tag{5-18}$$

Therefore the explicit solution of (**5-8**) is:

[20] It can be shown that the cost function J is convex, therefore the sufficient condition for optimality (global optimality) is also satisfied, see (Bordignon, 1996).

$$\mathbf{u} = \left(\mathbf{I} - \mathbf{B}^{\#}\mathbf{u}_{\mathrm{p}}\right) + \mathbf{B}^{\#}\boldsymbol{\tau} \tag{5-19}$$

For the special case $\mathbf{W} = \mathbf{I}$ and $\mathbf{u}_p = 0$, Eq. (**5-18**) reduces to:

$$\mathbf{B}^{+} = \mathbf{B}^{\mathrm{T}}(\mathbf{B}\mathbf{B}^{\mathrm{T}})^{-1} \tag{5-20}$$

where $\mathbf{B}^{+}$ is the well-known Moor-Penrose pseudo-inverse of $\mathbf{B}$ (Golub & Van Loan, 2012).

An alternative solution for pseudo-inverse of $\mathbf{B}$ can also be obtained by performing singular value decomposing (SVD) on $\mathbf{B}$. The approach is known as pseudo control method (Golub & Van Loan, 2012).

5.4 Constrained Control Allocation Solution

The optimal solutions to constrained CA problem can be characterised as explicit and implicit (iterative) methods (Johansen & Fossen, 2012). Explicit methods are based on modifications on the weighted pseudo-inverse solutions to take the constraints into consideration. The explicit solutions are effective, simple and fast as they need a few iterations to reach the result. This makes the explicit method attractive for real time applications. However, the main disadvantage is that full utilisation of actuators is not always guaranteed (i.e. their solution is sub-optimal) (Bodson, 2002). Redistributed pseudo-inverse method (Virnig & Bodden, 1994) and Daisy-chain method (Durham, 1993; Buffington & Enns, 1996), are among the most common explicit algorithms which have been successfully employed in aerospace applications (Johansen & Fossen, 2012).

Implicit CA solutions, including linear programming (LP) and quadratic programming (QP) techniques are iterative approaches. These methods are very powerful and the optimum solution is achieved but usually with large numbers of iteration and the rate of convergence is sometimes low, depending on the value of starting point (Petersen & Bodson, 2006). To implement an implicit CA solution in a real time application, we need to limit the number of iterations and hence we may accept some degree of sub-optimality. One can

conclude that the implicit CA optimal solutions need higher processing time and computational cost in comparison to implicit methods and therefore are not suited for "*low cost*" real time applications (Johansen & Fossen, 2012).

5.4.1 Explicit solution methods

5.4.1.1 Redistributed Pseudo-Inverse (RPI)

The redistributed pseudo-inverse (RPI) is a multi-step method which starts with the unconstrained least square (i.e. pseudo-inverse) solution of effective matrix $\mathbf{B}$ as presented by Eq. (**5-19**). If the resulted control inputs, $\mathbf{u}$, are within the bounds (limitations), no further steps are needed and the solution stops. Otherwise, the components of the control vector that exceed the limits are set to their limitations, and the pseudo-inverse is recomputed with the actuators that are still within the limits. The procedure is repeated until all components have saturated, or until the solution of the reduced least-squares problem satisfied (i.e. the control error becomes null).

More specifically, the algorithm first obtains the optimal control vector by solving the weighted pseudo-inverse of $\mathbf{B}$:

$$\mathbf{u} = \mathbf{B}^{\#}\boldsymbol{\tau}$$

If some elements of the allocated control vector exceed their limits, the control input vector and the control effectiveness matrix are decomposed into unsaturated and saturated groups as:

$$\boldsymbol{\tau} = [\mathbf{B}_s \quad \mathbf{B}_r] \begin{bmatrix} \mathbf{u}_s \\ \mathbf{u}_r \end{bmatrix} \tag{5-21}$$

where $\mathbf{u}_s$ are the elements of control input that exceed their limits and $\mathbf{u}_r$ are the rest of actuation elements which are within their limits, and $\mathbf{B}_s$ and $\mathbf{B}_r$ are their corresponding effectiveness matrix, respectively. The magnitude of $\mathbf{u}_s$ exceed their bounds, so their value is set to their limitations, $\overline{\mathbf{u}}_s$, i.e.

$$\mathbf{u}_s = \overline{\mathbf{u}}_s \tag{5-22}$$

and the remaining value of demanded force or moments (corresponding to control error) which should be generated by the rest of the actuators is:

$$\boldsymbol{\tau}_{\mathrm{r}} = \boldsymbol{\tau} - \mathbf{B}_{\mathrm{s}}\mathbf{u}_{\mathrm{s}} \tag{5-23}$$

The redistributed control input for the unsaturated group of actuators can be calculated as:

$$\mathbf{u}_{\mathrm{r}} = \mathbf{B}_{r}^{\#}(\boldsymbol{\tau} - \mathbf{B}_{\mathrm{s}}\mathbf{u}_{\mathrm{s}}) \tag{5-24}$$

The algorithm repeats until a solution within the limits is obtained or all the controls are saturated.

The redistributed algorithms is simple, fast and have been employed in many applications (Zhang & Jiang, 2008). However, it is shown in (Bodson, 2002) through an example that the method might not lead to an optimal solution in all cases.

5.4.1.2 Daisy-chain

The daisy-chain approach assumes a hierarchy of control effectors therefore the actuator control inputs $\mathbf{u}$ are decomposed into two or more groups. The method allocates redundant groups of controls in the following prioritised manner: elements of the second groups are not used until at least one element of the first group is saturated. The same procedure repeats for the rest groups of the actuators (Buffington & Enns, 1996). The algorithm starts with the pseudo-inverse solution for the first group of actuators. If the requested control commands (i.e. virtual force and moments) are not satisfied by the first group of actuators because of the actuator saturation, the control input are set to the saturation limits, therefore, there is an error existing between the commanded values and those produced by the control effectors. In the next step, the remaining demands (control error) are passed to the second group of actuators. If there are still virtual control demands that are not satisfied, those are passed to the third group and so on. The algorithms end when the control error becomes null or no more control freedom is available.

More specifically, a CA problem which is represented by:

$$\boldsymbol{\tau} = \mathbf{B}\mathbf{u} \qquad \underline{\mathbf{u}} \leq \mathbf{u} \leq \overline{\mathbf{u}} \tag{5-25}$$

can be decomposed into several control effector groups such as:

$$\boldsymbol{\tau} = [\mathbf{B}_1 \quad \mathbf{B}_2 \quad \mathbf{B}_3]\begin{bmatrix}\mathbf{u}_1\\ \mathbf{u}_2\\ \mathbf{u}_3\end{bmatrix} \qquad \begin{cases}\underline{\mathbf{u}}_1 \leq \mathbf{u}_1 \leq \overline{\mathbf{u}}_1\\ \underline{\mathbf{u}}_2 \leq \mathbf{u}_2 \leq \overline{\mathbf{u}}_2\\ \underline{\mathbf{u}}_3 \leq \mathbf{u}_3 \leq \overline{\mathbf{u}}_3\end{cases} \tag{5-26}$$

The daisy-chain algorithm starts by solving the CA problem for the first group of effectors ($\mathbf{B}_1$). Employing (unconstrained) weighted pseudo-inverse method leads to:

$$\hat{\mathbf{u}}_1 = \mathbf{B}_1^{\#}\,\boldsymbol{\tau} \tag{5-27}$$

If $\hat{\mathbf{u}}_1$ is within its allowable values (i.e. $\underline{\mathbf{u}}_1 \leq \mathbf{u}_1 \leq \overline{\mathbf{u}}_1$) this means that all the requested forces or moments can be generated by the first set of actuators: the rest of the actuators never utilized and the solution stops. Otherwise, the value of the first control inputs ($\mathbf{u}_1$) clipped at their limits, i.e.

$$\begin{aligned}&\mathbf{u}_1 = \hat{\mathbf{u}}_1 && \text{if} \quad \underline{\mathbf{u}}_1 < \mathbf{u}_1 < \overline{\mathbf{u}}_1\\ &\mathbf{u}_1 = \overline{\mathbf{u}}_1 \quad \text{or} \quad \mathbf{u}_1 = \underline{\mathbf{u}}_1 && \text{otherwise}\end{aligned} \tag{5-28}$$

The remaining value of requested force or moments which should be provided by the rest of the actuators is:

$$\boldsymbol{\tau}_2 = \boldsymbol{\tau} - \mathbf{B}_1\mathbf{u}_1 \tag{5-29}$$

Therefore, the control input for the second group of actuators can be calculated from:

$$\mathbf{u}_2 = \mathbf{B}_2^{\#}(\boldsymbol{\tau} - \mathbf{B}_1\mathbf{u}_1) \tag{5-30}$$

and the algorithm repeats. The solution ends when the control error becomes null or no more control freedom is available. Figure 5-3 shows a schematic diagram of daisy-chain allocation scheme with 3 groups of effectors. However, this process can be extended to any number of control effectors. From the above explanation, one can conclude that the maximum number of iterations in

the daisy-chain method is equal to the number of effector groups (which is three for the example shown in Figure 5-3).

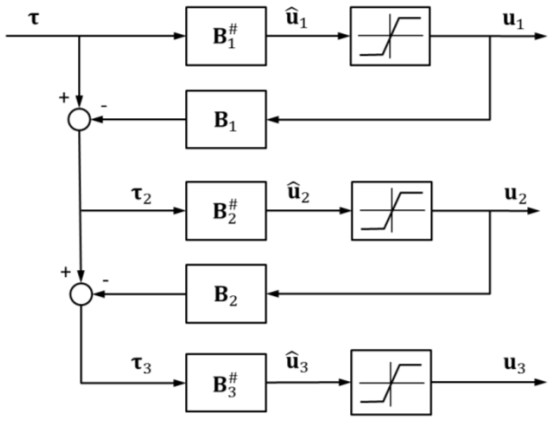

Figure 5-3: Example of daisy-chain allocation

Both daisy-chain and redistributed pseudo-inverse methods are denoted as sub-optimal or approximately optimal solutions, because the allocated actuator controls are not always obtained from the entire attainable set of actuators (Bodson, 2002). Moreover, in the daisy-chain method if, for example, the first group of actuators can provide the total amount of the requested forces or moments, the rest of the actuators never utilized, and the solution is more sub-optimal if utilisation of all the actuators are in concern.

In fact, the main difference between daisy-chain and redistributed pseudo-inverse methods is in the way that they deal with actuator saturation. In redistributed method, the control authority is distributed among all the existing actuators in each sequence, but the actuator which has the tightest limitations (i.e. has the lowest capacity) is saturated first (and therefore clipped at its limits) and the actuator which has the highest capacity will be saturated last. On the other hand, in daisy-chain method, the preference of actuators has been set in advance, based on "*a priori"* knowledge of the system. This feature is criticised as a drawback of daisy-chain method (Oppenheimer, Doman, & Bolender, 2011). However, this could be beneficial in some applications and makes the method attractive from a practical point of view. In this dissertation, we take this advantage to set the vehicle dynamics actuators preference (here brake over

steering actuations), to satisfy the system requirements (see section 3-2 for more detail).

5.4.2 Implicit (iterative) Solution Methods

Another class of solutions for the constrained CA problem is obtained by converting the CA problem into the "constraints optimisation formulation" and employ one of the standard optimisation solutions to solve the problem (Rao, 2009; Nocedal & Wright, 2006). Employing l_1 norm[21] for the cost function, will convert the CA into *linear programming (LP)* formulation whereas, with l_2 norm a *quadratic programming (QP)*[22] formulation is derived.

5.4.2.1 Linear Programming

By using l_1 norm (which is the sum of the absolute values of the component of the vector) for the cost function in (**5**-**7**), the optimisation problem statement is defined as follows:

$$\min_{\mathbf{u}} \; J = \|\mathbf{W}_\tau(\mathbf{B}\mathbf{u} - \boldsymbol{\tau})\|_1 + \varepsilon\left\|\mathbf{W}_u\left(\mathbf{u} - \mathbf{u}_p\right)\right\|_1 \quad subject\ to \quad \overline{\mathbf{u}} \le \mathbf{u} \le \underline{\mathbf{u}} \tag{5-31}$$

By introducing some auxiliary variables, the above formulation can be converted to a standard linear programming (LP) formulation (Bodson, 2002; Johansen & Fossen, 2012) such as:

$$\min_{\mathbf{x}} \; J = \mathbf{c}^T\mathbf{x} \quad subject\ to \quad \mathbf{A}\mathbf{x} = \mathbf{b}\,, \mathbf{x} \ge \mathbf{0} \tag{5-32}$$

which can be solved with one of the already developed numerical LP algorithms including simplex or interior point methods (Nocedal & Wright, 2006).

---

[21] The l_1 (1-norm) of a vector $\mathbf{u}$ is defined as:

$$\|\mathbf{u}\|_1 = \sum_i |u_i|$$

and the l_2 (2-norm) of $\mathbf{u}$ is

$$\|\mathbf{u}\|_2 = \left(\sum_i u_i^2\right)^{1/2}$$

[22] Quadratic programming also denoted as *constrained least square* problem in the literatures (Rao, 2009).

Simplex methods are usually the most practical and efficient algorithms to solve LP problems (Bodson, 2002). They belong to a general class of algorithms for constrained optimisation known as active set methods in which the actuator controls are divided into a saturated (active) set and an unsaturated (free) set. The principle of active set approach to a LP problem is based on the explicit estimation of the active and free sets which are being updated at each step of the algorithm. In other words, the search for optimality in the active set approach is done by visiting the vertices of the polytope described by the constraints of the problem (Nocedal & Wright, 2006).

Interior point methods, where the optimality search is done from the interior and/or exterior of the constraint polytope, has better theoretical convergence properties, and are often preferred for large scale problem (Nocedal & Wright, 2006). Moreover, when "warm" state initialisation (based on the previous time step solution) is not stored or available; the interior point method provides better results than active set method and is preferable even for small scale problems.

One of the disadvantages of using LP approach for solving CA problem is in the fact that when the original mixed l_1 norm optimisation problem is converted to the LP problem, the size of the problem increased significantly. For example, if we want to allocate m virtual control vector, $\boldsymbol{\tau}$, to p control inputs , $\mathbf{u}$, then the resultant matrices for the converted LP problem will be $\mathbf{A} \in \mathbb{R}^{m\times(2m+2\,p)}$, $\mathbf{c} \in \mathbb{R}^{(2m+2\,p)\times 1}$, $\mathbf{b} \in \mathbb{R}^{(2m+2\,p)\times 1}$ (Wang, 2007). This expansion of the LP problem dimension increases the required computational time and cost which is undesirable. As a rough estimation, the time required to solve a linear program may be exponential in the size of the problem (Nocedal & Wright, 2006).

5.4.2.2 Quadratic Programming

The quadratic programming formulation for mixed optimisation CA problem[23] is derived by employing l_2 norm (which is the minimum energy control effort) for the cost function in (**5**-**7**):

[23] also denoted as *weighted least-square* problem

$$\min_{\mathbf{u}} \; J = \|\mathbf{W}_\tau(\mathbf{B}\mathbf{u} - \boldsymbol{\tau})\|_2^2 + \varepsilon\left\|\mathbf{W}_u\left(\mathbf{u} - \mathbf{u}_p\right)\right\|_2^2 \quad subject\ to \quad \overline{\mathbf{u}} \le \mathbf{u} \le \underline{\mathbf{u}} \tag{5-33}$$

which can be solved by one of the standard QP solutions such as active set, interior point or gradient projection methods (Nocedal & Wright, 2006).

Several active set methods, including sequential quadratic programming (SQP) (Ono, Hattori, Muragishi, & Koibuchi, 2006), weighted least square (WLS) (Harkegard, 2002) and minimal least square (MLS) (Lötstedt, 1984) methods, has been proposed for solving CA problems, which among them, the weighted least square method was shown to be the most efficient (Harkegard, 2002). Similar to simplex method for LP problem, the active set solutions for quadratic programming starts by dividing the actuator controls into a saturated (active) set and an unsaturated (free) set, but the updates of the free sets are calculated based on the pseudo-inverse solution and the active set is reflected by calculating Lagrangian parameters (Oppenheimer, Doman, & Bolender, 2011). Note that the active set solution, as described above, is very similar to the concept of redistributed pseudo inverse (RPI) method presented in section 5.4.1.1. The difference is that an active set algorithm is more sensitive regarding which variable to saturate, and that an active set algorithm has the ability to free a variable that was saturated in a previous time step[24] (which did not happen in RPI method). The active set algorithm always converges to the optimum solution in a finite number of steps and is shown to be efficient for problems of small to medium size, but an upper bound in the number of iteration can be very large (Harkegard, 2002).

Similar to LP problems, the interior point (IP) method can also be employed to solve the quadratic CA formulations. The advantage of the IP method is uniform convergence and knowledge of the relative distance to the optimal solution. In (Petersen & Bodson, 2006) a prim-dual Interior point method, based on (Vanderbei & Shanno, 1999), is implemented in order to exactly solve a quadratic program. The method is compared with a fixed point, (Burken, Lu, &

[24] see (Harkegard, 2002) and (Petersen & Bodson, 2006) for details.

Wu, 1999), and an active set method, (Harkegard, 2002). Active set and interior point methods are now available as two standard solution algorithms within the Matlab® Control Optimization Toolbox™ (The MathWorks, 2013).

The fixed-point method is a recursive algorithm similar to a gradient search, classified as derivative free optimisation (DFO) algorithms (Nocedal & Wright, 2006). A fixed-point method was used by (Burken, Lu, & Wu, 1999) to solve a mixed optimisation problem as stated in (6-27) for aerospace applications. The method is also employed for solving IVDC problem by (Wang, 2007). Fixed-point method is very easy to code, fast for most achievable commands and reaches to the exact optimal solution within a finite number of iterations. Although, the algorithm has a theoretically proven global convergence, but it is quite slow in practice if the command values are large (unattainable) (Bodson & Frost, 2011). For that reason, the fixed-point method is usually implemented with a bounded number of iterations; this means that we accept some level of sub-optimality in the solution (Harkegard, 2002).

5.5 Control Allocation scheme for Integrated EPAS and ESP

5.5.1 The Control Allocation Formulation

Recall from Chapter 4, the relation between the generalised (virtual) forces and moments on the vehicle level, (which is the outcome of high-level control solution), and the target forces at the tyre coordinate frame, $\mathbf{u}$, (which should be generated by steering and brake actuators) could be represented in the (linear) form of:

$$\boldsymbol{\tau} = \mathbf{B}\mathbf{u} \tag{5-34}$$

For the vehicle planar motion, the generalised force and moments vector is:

$$\boldsymbol{\tau} = [\Delta F_x \quad \Delta F_y \quad \Delta M_z]^T \quad , \qquad \boldsymbol{\tau} \in \mathbb{R}^{3\times 1} \tag{5-35}$$

In the general case of four wheel steering, braking (and driving), there exists control authorities over longitudinal and lateral forces for all four tyres, i.e.

$$\mathbf{u} = \begin{bmatrix} \Delta F_{x,i} \\ \Delta F_{y,i} \end{bmatrix} \quad , \quad i = 1,2,3,4 \ , \ \mathbf{u} \in \mathbb{R}^{8\times 1} \tag{5-36}$$

where $\Delta F_{x,i}$ and $\Delta F_{y,i}$ are the amount of the (additional) longitudinal and lateral forces of the i-th tyre which should be generated by the brake and steering actuators respectively. The indices $i = 1,2,3,4$ refer to the *front left, front right, rear left and rear right* wheels respectively. The effectiveness matrix $\mathbf{B} \in \mathbb{R}^{\mathbf{3\times 8}}$ can be defined as (Jonasson, 2009):

$$\mathbf{B} = \mathbf{AT} \tag{5-37}$$

where $\mathbf{A} \in \mathbb{R}^{\mathbf{3\times 8}}$ can be derived from vehicle kinematics

$$\mathbf{A} = \begin{bmatrix} 1 & 0 & 1 & 0 & 1 & 0 & 1 & 0 \\ 0 & 1 & 0 & 1 & 0 & 1 & 0 & 1 \\ -l_w & l_f & l_w & l_f & -l_w & -l_r & l_w & -l_r \end{bmatrix} \tag{5-38}$$

and $\mathbf{T} \in \mathbb{R}^{\mathbf{8\times 8}}$ is the coordinate transformation matrix form tyre to body generalised force frame (Kiencke & Nielsen, 2005)

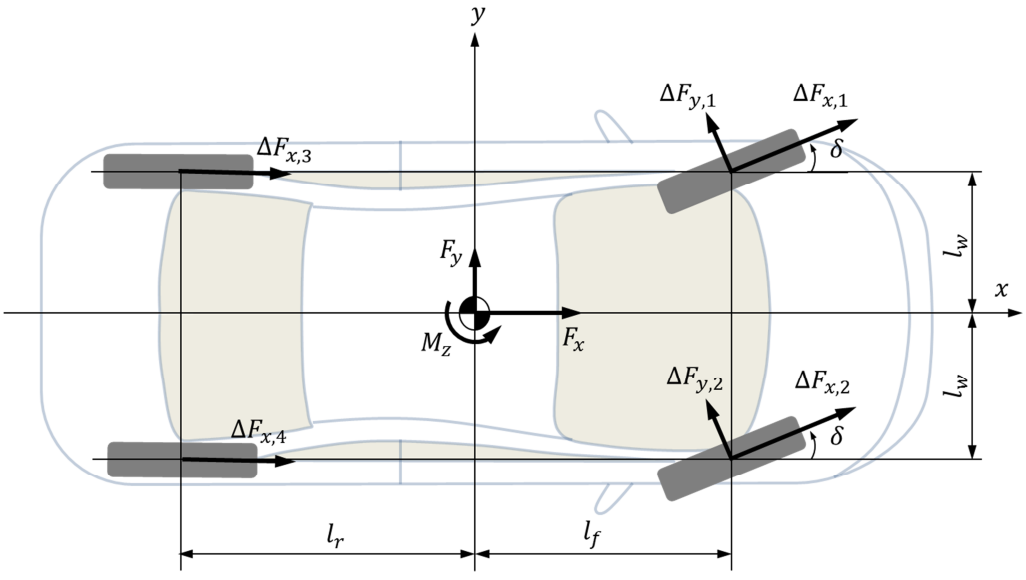

Figure 5-4: Vehicle Planar motion with front steering and 4 wheel brake actuators

$$\mathbf{T} = \mathrm{diag}(\mathbf{T_i}) \quad , \quad \mathbf{T_i} = \begin{bmatrix} \cos\delta_i & -\sin\delta_i \\ \sin\delta_i & \cos\delta_i \end{bmatrix} \quad , \quad i = 1,2,3,4 \tag{5-39}$$

In the proposed configuration (customised IVCS system), it is assumed that 4 wheel braking (through EHB hydraulic value modulation unit) and (front wheel) Electric Power-Assisted Steering (EPAS) are the only available actuators in the vehicle, as stated in Chapter 3. Therefore, the low-level control authority is available only on the front tyres lateral forces, $\Delta F_{y,i}$, $i = 1,2$ (through front steering intervention)[25] and on the four tyres longitudinal forces, $\Delta F_{x,i}$, $i = 1,2,3,4$ (through four individual wheels braking), as shown in Figure 5-4. The control input vector for this configuration is defined as:

$$\mathbf{u} = [\Delta F_{x,1} \quad \Delta F_{y,1} \quad \Delta F_{x,2} \quad \Delta F_{y,2} \quad \Delta F_{x,3} \quad \Delta F_{x,4}]^T \quad , \qquad \mathbf{u} \in \mathbb{R}^{6\times 1} \tag{5-40}$$

It should be noted that it is possible to select tyres slip and slip angle (instead of tyre longitudinal and lateral forces) as the control input variables, **u**, (see (Wang & Longoria, 2006) for example). However, this choice will lead to a nonlinear control effectiveness matrix **B** and there is a need for linearisation of **B** at each time step which adds more complexity to processing and is not a "low cost" solution from computational point of view.

In the case of front wheels steering (as shown in Figure 5-4): $\delta_1 = \delta_2 = \delta$ and $\delta_3 = \delta_4 = 0$ (therefore, $\sin\delta_3 = \sin\delta_4 = 0$ and $\cos\delta_3 = \cos\delta_4 = 1$) and by assuming $l_{wf} = l_{wr} = l_w$, the effective matrix **B** is reduced to:

$$\mathbf{B} = \begin{bmatrix} \cos\delta & -\sin\delta & \cos\delta & -\sin\delta & 1 & 1 \\ \sin\delta & \cos\delta & \sin\delta & \cos\delta & 0 & 0 \\ -l_w\cos\delta + l_f\sin\delta & l_w\sin\delta + l_f\cos\delta & l_w\cos\delta + l_f\sin\delta & -l_w\sin\delta + l_f\cos\delta & -l_w & l_w \end{bmatrix} \tag{5-41}$$

As the number of generalised forces and moments ($\boldsymbol{\tau} \in \mathbb{R}^3$) is less than the number of available actuators ($\mathbf{u} \in \mathbb{R}^6$), **B** is full row rank (has more columns than rows). The system is redundant (over-actuated) and there is no unique

[25] It is worth to note that the front tyres applied lateral forces ($\Delta F_{y,i}$, $i = 1,2$) are coupled to each other through the common steering angle δ at the front axle.

solution that exists for $\mathbf{u}$ for a given value of $\boldsymbol{\tau}$. Moreover, both the effectors (i.e. tyres) and the actuators (here: EHB and EPAS systems) are subject to magnitude and rate constraints. Therefore, the optimum allocation of generalised longitudinal, lateral forces and yaw moment (on the vehicle level) to the relevant actuators longitudinal and lateral forces (on the tyre level) can be obtained by solving a constrained optimisation CA problem, which can be stated as follows:

Knowing the demanded generalised vehicle force and moment, $\boldsymbol{\tau}$ *(which is the output of the high-level controller, as presented in the Chapter 5) and the control effectiveness matrix* $\mathbf{B}$ *as defined by (5-41); find the optimum value of control input vector,* $\mathbf{u}$ *,for the steering and brake actuators, considering actuators magnitude and rate saturation*, i.e.

$$\min_{\mathbf{u}} \; J = \|\mathbf{W}_\tau(\mathbf{B}\mathbf{u} - \boldsymbol{\tau})\|_2^2 + \varepsilon\|\mathbf{W}_u(\mathbf{u})\|_2^2 \quad subject\ to \quad \overline{\mathbf{u}} \le \mathbf{u} \le \underline{\mathbf{u}} \tag{5-42}$$

Here, $\|\mathbf{W}_\tau(\mathbf{B}\mathbf{u} - \boldsymbol{\tau})\|_2^2$ is the primary optimisation objective to minimise the error (i.e. the difference between the required high–level moment and forces, and the values of forces and moments which are generated by steering and brakes actuations on tyres); and $\|\mathbf{W}_u(\mathbf{u})\|_2^2$ is the secondary optimisation objective employed to minimise the actuator forces. The weighting matrix $\mathbf{W}_\tau$ and $\mathbf{W}_u$ can be employed for task prioritisation and actuator preference, as described before.

There are three types of constraints that exist in the system: the first type of constraint (denoted here as $\mathbf{u}_{max,E}$ and $\mathbf{u}_{min,E}$) is related to the vehicle effectors (i.e., tyres) limitations. Recall from Chapter 4, the maximum achievable tyre lateral and longitudinal forces do not exceed from the magnitude of the peak forces ($\mu_i\, F_{z,i}$) and are coupled by the friction circles expression (4-49)[26] :

$$\left(F_{x,i} + \Delta F_{x,i}\right)^2 + \left(F_{y,i} + \Delta F_{y,i}\right)^2 \le \left(\mu_i F_{z,i}\right)^2 \quad , i = 1,2,34 \tag{5-43}$$

[26] The friction circle concept is graphically shown in Chapter 3. See section 3.4 for more discussion on tyre characteristics and limits.

where $F_{x,i}$ and $F_{y,i}$ are the actual lateral and longitudinal forces of the i-th tyre, and $\Delta F_{x,i}$ and $\Delta F_{y,i}$ are the magnitude of the demanded lateral and longitudinal forces applied to the i-th tyre by the actuators (i.e., steering and brake), respectively.

The second type of constraint (denoted here as $\mathbf{u}_{max,A}$ and $\mathbf{u}_{min,A}$) is the maximum capacity of the steering and brake actuators to generate the required lateral or longitudinal force. The actuators rate constraints (denoted as $\dot{\mathbf{u}}_{max}$), associated to the actuators dynamics, is the third type of constraint existing in the system. Considering all these constraints, the upper and lower bounds of the actuator constraints are defined as:

$$\begin{aligned} \overline{\mathbf{u}}(t) &= \min\left(\mathbf{u}_{max,E}\,, \mathbf{u}_{max,A}\,, \mathbf{u} + \Delta t\dot{\mathbf{u}}_{max}\right) \\ \underline{\mathbf{u}}(t) &= \max\left(\mathbf{u}_{min,E}\,, \mathbf{u}_{min,A}\,, \mathbf{u} - \Delta t\dot{\mathbf{u}}_{max}\right) \end{aligned} \tag{5-44}$$

5.5.2 Discussion on task prioritisation and actuator preference

As the generalised force and moment vector $\boldsymbol{\tau}$ (Eq. (5-35)) has a dimension greater than one ($\boldsymbol{\tau} \in \mathbb{R}^{3\times 1}$), we need to prioritise the tasks (i.e. generalised forces and moments) in such cases where all required tasks cannot generate simultaneously, in other words, when $\boldsymbol{\tau} = \mathbf{B}\mathbf{u}$ cannot be satisfied within the constraints $\underline{\mathbf{u}} \leq \mathbf{u} \leq \overline{\mathbf{u}}$. It is also common that actuators on-board vehicle may have different characteristics, different associated costs, and/or different speed or bandwidths. The diagonal actuation preference weighting matrix $\mathbf{W}_u$ and the diagonal task prioritisation weighting matrix $\mathbf{W}_\tau$ in the control allocation cost function (5-42**)** can be adjusted to increase the corresponding weight of the less attractive actuators and thus delay their utilisations, as will be discussed below.

As one may recall from Chapter 5, the values of generalised forces and moments are the outputs of the high-level controller which have been decomposed into three SISO individual closed loop control systems corresponding to longitudinal force, F_x, lateral force, F_y , and yaw moment, M_z. The performance and stability of the controllers have been validated in Chapter 4 by employing direct implementation of the (decoupled) generalised forces and

moments into the vehicle's equation of motion. However, in reality, these high-level forces and moments are generated in a vehicle by tyre (longitudinal and lateral) forces. Here, several couplings exist in the system: firstly, the tyre longitudinal and lateral forces are dependent on each other, as described by tyre friction circle, and secondly the coupling effect of the yaw rate and sideslip as described by the vehicle governing equations of motions[27].

To investigate the coupling effect of generalised forces and moment and the tyre forces, consider the relationship between the actuated forces at the tyre level and the generated forces and moments at the vehicle level for a vehicle with 4 wheel braking and front wheel steering, as described in Chapter 3:

$$\Delta F_x = \left(\Delta F_{x,1}+\Delta F_{x,2}\right)\cos\delta - \left(\Delta F_{y,1} + \Delta F_{y,2}\right)\sin\delta + \Delta F_{x,3} + \Delta F_{x,4} \tag{5-45}$$

$$\Delta F_y = \left(\Delta F_{x,1}+\Delta F_{x,2}\right)\sin\delta + \left(\Delta F_{y,1} + \Delta F_{y,2}\right)\cos\delta \tag{5-46}$$

$$\begin{aligned}\Delta M_z = {} & l_f\left\{\left(\Delta F_{x,1}+ \Delta F_{x,2}\right)\sin\delta + \left(\Delta F_{y,1} + \Delta F_{y,2}\right)\cos\delta\right\} \\ & - l_w\left\{\left(\Delta F_{x,1}- \Delta F_{x,2}\right)\cos\delta - \left(\Delta F_{y,1} - \Delta F_{y,2}\right)\sin\delta + \left(\Delta F_{x,3}- \Delta F_{x,4}\right)\right\}\end{aligned} \tag{5-47}$$

(note that, the above expressions can be derived alternatively from Eqs. (5-34), (5-35), (5-40) and (5-41)). Considering the force and moment sign convention as indicated in Figure 5-6, one can conclude from Eq. (5-45) and (5-46) that, positive or negative longitudinal forces on vehicle will be generated by applying positive or negative longitudinal forces on each tyre ($\Delta F_{x,1}$, $\Delta F_{x,2}$, $\Delta F_{x,3}$, $\Delta F_{x,4}$) and positive or negative lateral forces on vehicle will be generated by applying positive or negative lateral force on front tyres ($\Delta F_{y,1}$, $\Delta F_{y,2}$). Similarly, it could be concluded from Eq. (5-47) that positive or negative yaw moment could be generated by applying positive or negative lateral forces on front tyres. However, the relationship between the generated vehicle yaw moment and the applied tyres longitudinal forces are not so straight forward. Positive yaw moment on vehicle will be generated by negative longitudinal forces (i.e. braking) on front left and rear left tyres ($-\Delta F_{x,1}, -\Delta F_{x,3}$), whereas, negative yaw

[27] See Chapter 3 for more detailed discussion in this course.

moment will be generated by applying negative longitudinal force on front right and rear right tyres $(-\Delta F_{x,2}, -\Delta F_{x,4})$. The above explanations are graphically presented in Figure 5-5 for positive steering as well as negative steering, which clearly shows that the requirements of high-level forces and moments generation by tyre forces are in conflict with each other in some cases.

For example, consider the situation that both the (high-level) longitudinal and yaw motion controllers request more longitudinal force and yaw moment at the same time. This corresponds to applying positive longitudinal force (driving force) on both front tyres $(\Delta F_{x,1}, \Delta F_{x,2})$ for a front wheel drive vehicle, while, the positive yaw moment can be achieved by reducing the longitudinal forces (braking) on front left and rear left tyres $(-\Delta F_{x,1}, -\Delta F_{x,3})$. In this case the "front left" tyre receives positive command from longitudinal controller and negative command from yaw rate controller at the same time.

Another conflicting situation might happen for front tyres lateral force commands during the simultaneous control of yaw moment and lateral velocity (sideslip). Consider the situation that the lateral motion controller requests for decreasing the vehicle lateral force (to reduce the lateral velocity or sideslip) and the yaw rate controller requests for increase in the vehicle yaw moment (to increase vehicle yaw rate). Reducing vehicle lateral velocity (sideslip) is achieved by reducing the front tyres lateral force (i.e. applying negative lateral forces on tyres), while, the vehicle yaw moment increase by increasing the front tyres lateral force (i.e. applying positive lateral forces).

a)

b)

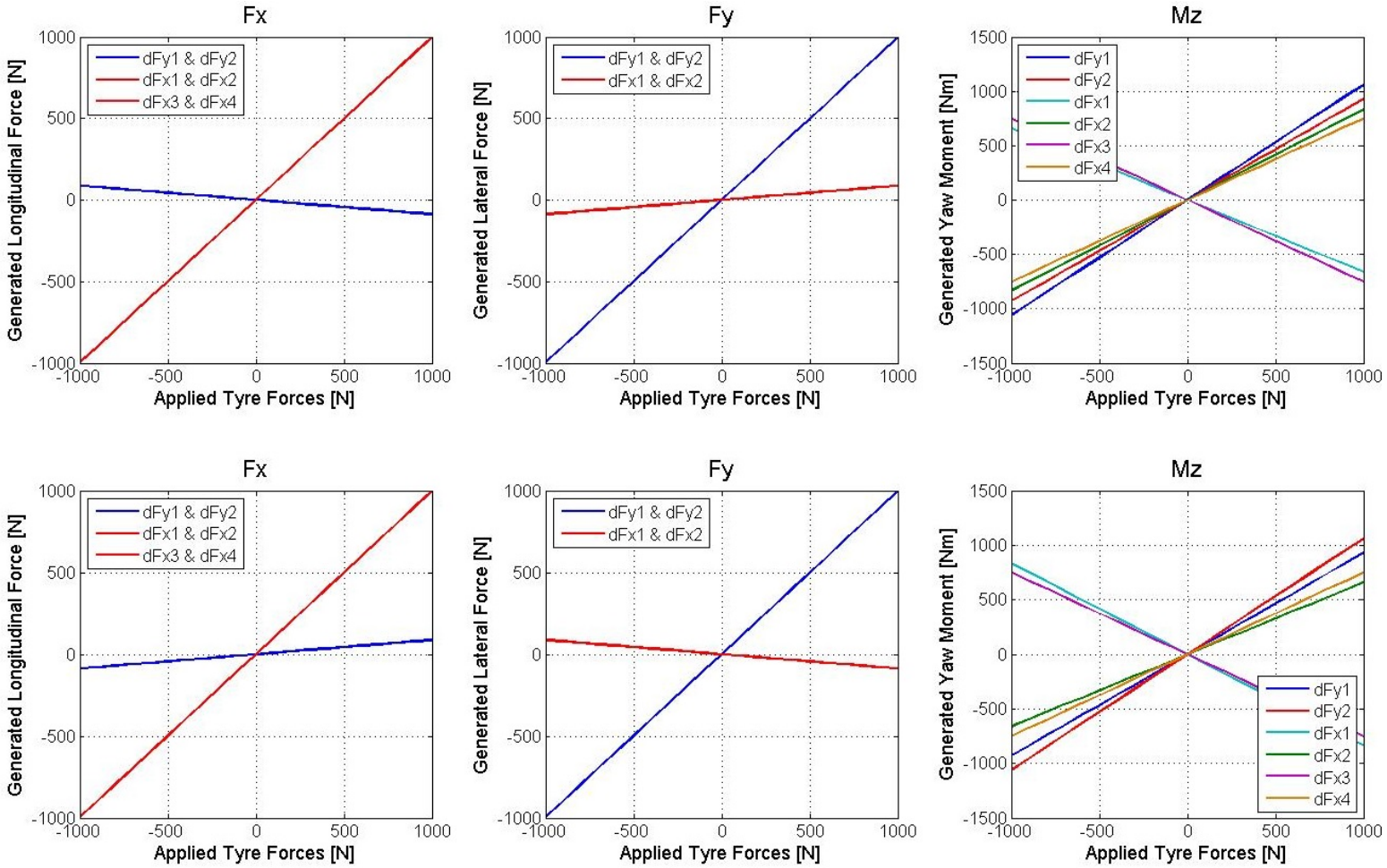

Figure 5-5: The generated vehicle forces and moments as result of applied tyre forces, a) positive steering angle ($\delta = 5°$); b) negative steering angle ($\delta = -5°$)

Moreover, in case of brake actuation, only the *inner* (front and rear) wheels brake should be activated for generating the positive moment in understeering situation. Similarly, in oversteering situation, only the *outer* (front and rear) brakes are actuating to generate negative yaw moment and stabilise the vehicle, as shown in Figure **5-6** (Smakman, 2000). The CA scheme should be able to autonomously manage these conflicting situations by prioritisation the (high-level) control tasks and/or selecting different actuators at different driving conditions.

Positive yaw moment generation (for understeering situation)

Negative yaw moment generation (for oversteering situation)

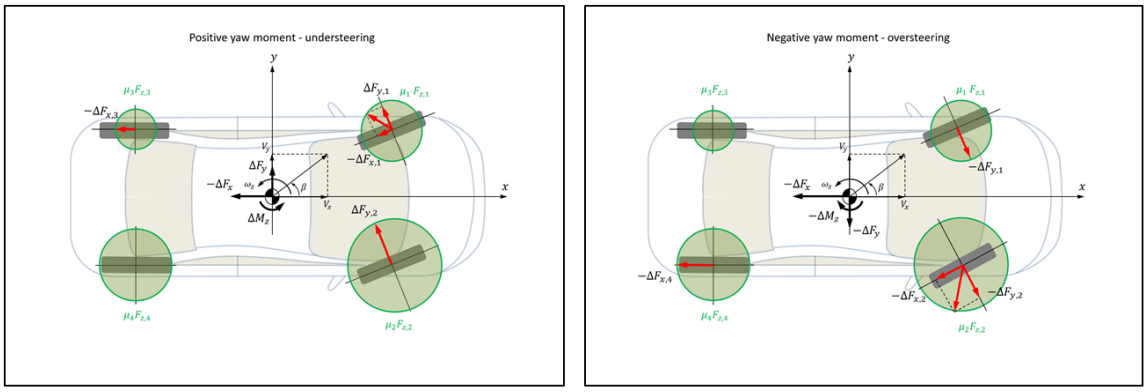

Figure 5-6: Actuators preference in understeering and oversteering situations

To address this issue, some ad-hoc or fuzzy methods of switching between the controllers have been proposed in the literatures (van Zanten A. , 2000; Karbalaei, Ghaffari, Kazemi, & Tabatabaei, 2007). Based on the CA formulation, as presented in section 5.2, the task prioritisation as well as actuator preference can be achieved by changing the corresponding elements in the diagonal weighting matrixes $\mathbf{W}_\tau$ and $\mathbf{W}_u$ in the cost function. As the object of optimisation is to minimise the value of the cost function, increasing the corresponding weighting factors will raise their priorities.

The relative importance of each task is determined from the top level IVCS system objectives and requirements[28]. For example, in stability situation, the

[28] See Chapter 3 for more discussion on the objectives (i.e. stability, comfort and agility) of the multi-layer integrated vehicle dynamics control system.

main objective of the integrated vehicle dynamics system is to recover the vehicle stability, therefore, the yaw moment has the top priority to maintain the vehicle yaw rate; the lateral force (maintaining sideslip) has the second priority, but the longitudinal motion has less priority in this situation (van Zanten A. , 2000; Rajamani, 2012). In other words, under the condition that the outcome of the motion controllers are in conflict with each other, we ignore those vehicle motions that are less important for this specific objective in favour of more important motions. This will be achieved by assigning less weighting values to those tasks.

5.5.3 The Proposed Control Allocation Scheme

A solution to the CA problem should address several requirements of the integrated vehicle dynamics control system such as, low cost computation, actuators preference, task prioritisation, fault tolerance and adaptation to vehicle state and/or environment parameters changes, as indicated in Chapter three[29]. To address these requirements, a fast, reconfigurable and adaptive CA solution based on the daisy-chain method is proposed in this dissertation.

One can conclude from the system requirements that (in hazardous stability condition) the brake actuator has priority over steering actuators. Employing the daisy-chain concept, the available actuations are divided into two groups, brake actuators and steering actuator. The control input vector $\mathbf{u}$ is then decomposed into two sub-vectors as $\mathbf{u}_1$ and $\mathbf{u}_2$, corresponding to the braking control (four wheels longitudinal forces), respectively and the steering control input (front wheels lateral forces), such that:

$$\mathbf{u}_2 = [\Delta F_{x,1} \quad 0 \quad \Delta F_{x,2} \quad 0 \quad \Delta F_{x,3} \quad \Delta F_{x,4}]^T \tag{5-48}$$

$$\mathbf{u}_1 = [\ 0 \quad \Delta F_{y,1} \quad 0 \quad \Delta F_{y,2} \quad 0 \quad 0]^T \tag{5-49}$$

The effectiveness matrix $\mathbf{B}$ is also decomposed into two matrices corresponding to the brake and steering actuators, denoted as $\mathbf{B}_1$ and $\mathbf{B}_2$, respectively,

[29] See section 3.2.1 and 3.2.2 for more discussion on the system requirements and specifications.

$$\mathbf{B}_2 = \begin{bmatrix} \cos\delta & \cos\delta & 1 & 1 & 0 & 0 \\ \sin\delta & \sin\delta & 0 & 0 & 0 & 0 \\ -l_w\cos\delta + l_f\sin\delta & l_w\cos\delta + l_f\sin\delta & l_w & -l_w & 0 & 0 \end{bmatrix} \quad (5\text{-}50)$$

$$\mathbf{B_1} = \begin{bmatrix} 0 & 0 & 0 & 0 & -\sin\delta & -\sin\delta \\ 0 & 0 & 0 & 0 & \cos\delta & \cos\delta \\ 0 & 0 & 0 & 0 & \mathrm{l_w}\sin\delta + \mathrm{l_f}\cos\delta & -\mathrm{l_w}\sin\delta + \mathrm{l_f}\cos\delta \end{bmatrix} \quad (5\text{-}51)$$

The procedure starts with the unconstrained optimal solution of the brake control input, $\mathbf{u}_1$, which is obtained by the weighted pseudo-inverse of $\mathbf{B}_1$ as presented by (**5**-**18**). If the resultant control input for braking is within the bounds and the control error ($\mathbf{Bu} - \boldsymbol{\tau}$) is zero, this means that the brake itself is capable of generating the required control commands and therefore there is no need for steering intervention.

Otherwise, if the solution of control effectiveness matrix $\mathbf{u}_1$ is exceeded its limitations, the value of the $\mathbf{u}_1$ are clipped to their saturation values and the steering is utilised for generating the rest of demanded $\boldsymbol{\tau}$. The magnitude of the longitudinal forces which should be generated by the steering actuators are achieved by employing weighted pseudo inverse solution of $\mathbf{B}_2$. The weighting matrix $\mathbf{W}_\tau$ will be employed for task prioritisation based on different driving conditions, as summarised in Table 5-1.

The actuators preference can be utilised by employing the weighting matrix $\mathbf{W}_u$. By selecting the control weighting matrix as the inverse of each tyre's peak force $\mu_i F_{z,i}$, i.e.

$$\mathbf{W}_{u,Fz} = \mathrm{diag}\left[\frac{1}{\mu_1 F_{z,1}} \quad \frac{1}{\mu_2 F_{z,1}} \quad \frac{1}{\mu_3 F_{z,2}} \quad \frac{1}{\mu_4 F_{z,2}} \quad \frac{1}{\mu_1 F_{z,3}} \quad \frac{1}{\mu_2 F_{z,4}}\right] \quad (5\text{-}52)$$

the (longitudinal and lateral) tyre forces are prioritised based on the magnitude of their peak forces, as shown in Figure **5-6**.

Table 5-1: Task prioritisation

High-level VD task	Criteria	Satisfying High-level force or moment	Weighting matrix
Driveline braking/driving	$a_y < .4\mu$	F_x	$\mathbf{W}_\tau = \text{diag}[1 \quad 0 \quad 0]$
Mild stability	$0.4\mu \leq a_y < .6\mu$	M_z	$\mathbf{W}_\tau = \text{diag}[0 \quad 0 \quad 1]$
Hazardous stability	$.6\mu \leq a_y < 1\mu$	M_z & F_y	$\mathbf{W}_\tau = \text{diag}[0 \quad .01 \quad 1]$

To make switching between various actuations, the $\mathbf{Q} \in \mathbb{R}^6$ vector with binary values can be introduced so as:

$$\mathbf{W}_u = \mathbf{W}_{u,Fz} \times \mathbf{Q} \tag{5-53}$$

In case of understeering situation (as shown in Figure **5-6**) the inner wheels braking are actuated, therefore the other side control element (i.e. outer wheels) should be set to zero:

$$\mathbf{Q} = [\ 1 \quad 1 \quad 0 \quad 1 \quad 1 \quad 0] \quad if \quad M_z > 0 \tag{5-54}$$

Similarly in case of oversteering, the outer front and rear wheels braking are actuated,

$$\mathbf{Q} = [\ 0 \quad 1 \quad 1 \quad 1 \quad 0 \quad 1] \quad if \quad M_z < 0 \tag{5-55}$$

The $\mathbf{Q}$ vector can also be used to provide the system fault tolerant as well. In case of one actuator failure, the corresponding control element is set to zero. For example, if $M_z > 0$ and rear left brake failed,

$$\mathbf{Q} = [\ 1 \quad 1 \quad 0 \quad 1 \quad 0 \quad 0] \tag{5-56}$$

Similarly, $\mathbf{Q}$ vector can be defined for different driving conditions and probable faults in the steering or brake actuators as summarised in table 4.

Table 5-2: probable fault situations and corresponding Q vector

	Steering	Front Brake	Rear Brake	
$M_z > 0$	✓	✓	✓	$\mathbf{Q} = [\ 1 \quad 1 \quad 0 \quad 1 \quad 1 \quad 0]$
	×	✓	✓	$\mathbf{Q} = [\ 1 \quad 0 \quad 0 \quad 0 \quad 1 \quad 0]$
	×	×	✓	$\mathbf{Q} = [\ 0 \quad 0 \quad 0 \quad 0 \quad 1 \quad 0]$
	×	✓	×	$\mathbf{Q} = [\ 1 \quad 0 \quad 0 \quad 0 \quad 0 \quad 0]$
	✓	×	✓	$\mathbf{Q} = [\ 0 \quad 1 \quad 0 \quad 1 \quad 1 \quad 0]$
	✓	✓	×	$\mathbf{Q} = [\ 1 \quad 1 \quad 0 \quad 1 \quad 0 \quad 0]$
	✓	×	×	$\mathbf{Q} = [\ 0 \quad 1 \quad 0 \quad 1 \quad 0 \quad 0]$
$M_z < 0$	✓	✓	✓	$\mathbf{Q} = [\ 0 \quad 1 \quad 1 \quad 1 \quad 0 \quad 1]$
	×	✓	✓	$\mathbf{Q} = [\ 0 \quad 0 \quad 1 \quad 0 \quad 0 \quad 1]$
	×	×	✓	$\mathbf{Q} = [\ 0 \quad 0 \quad 0 \quad 0 \quad 0 \quad 1]$
	×	✓	×	$\mathbf{Q} = [\ 0 \quad 0 \quad 1 \quad 0 \quad 0 \quad 0]$
	✓	×	✓	$\mathbf{Q} = [\ 0 \quad 1 \quad 0 \quad 1 \quad 0 \quad 1]$
	✓	✓	×	$\mathbf{Q} = [\ 0 \quad 1 \quad 1 \quad 1 \quad 0 \quad 0]$
	✓	×	×	$\mathbf{Q} = [\ 0 \quad 1 \quad 0 \quad 1 \quad 0 \quad 0]$

Finally, it is worth to mentioned that the pure brake actuation (i.e. conventional ESP) or pure steering actuation (EPAS only) can be easily obtained by altering the $\mathbf{Q}$ vector, such as

$$\mathbf{Q} = [\ 1 \quad 0 \quad 1 \quad 0 \quad 0 \quad 0] \qquad \text{For EPAS only} \qquad (5\text{-}57)$$

$$\mathbf{Q} = [\ 1 \quad 0 \quad 0 \quad 0 \quad 1 \quad 0] \quad if \quad M_z > 0$$

$$\mathbf{Q} = [\ 0 \quad 0 \quad 1 \quad 0 \quad 0 \quad 1] \quad if \quad M_z < 0 \qquad \text{For ESP only} \qquad (5\text{-}58)$$

Note that, to avoid singularity in the solution, all the zero terms in the $\mathbf{Q}$ vector might be replaced with a small value such as $\mathbf{1}\boldsymbol{e}-\mathbf{8}$, in practice.

5.6 The CA Scheme Validation

In this section, the performance and efficiency of two CA schemes are presented through several simulations. Implicit CA solutions (based on interior point method) are presented first and then compared with the proposed daisy-chain method. It is shown that the daisy-chain method provides a very fast solution for CA problem, while the results are very similar to the iterative optimisation methods (before actuators saturation). The effectiveness of the IVDC daisy-chain method is then compared with several traditional methods for only steering actuation (such as AFS or EPAS systems) and only brake actuation (ESP system).

Two step steer input manoeuvres at high and low mu surfaces as defined in Chapter 3 (Step60-mu1.0-V100 and Step60-mu0.2-V50) are selected for these simulations. It is shown in Chapter 3 that the passive vehicle (i.e. with no vehicle dynamics control) becomes oversteering by Step60-mu1.0-V100 manoeuvre and becomes understeering with Step60-mu0.2-V50. It is also shown in Chapter 4 that (direct) application of high-level control can bring the vehicle to the target trajectory and stabilise it if necessary. The aim of the simulations in this chapter is to confirm whether the same stabilising results can being reproduced through CA scheme application.

By applying CA scheme, we would like to investigate how the vehicle yaw moment and lateral force (output of the high-level controllers) could be generated through various allocations to steering (i.e. tyre lateral forces) and brake (i.e. tyre longitudinal forces) actuation. Note that the actuator dynamics are neglected at this stage of validation (i.e. perfect actuators assumption). The effect of adding actuator dynamics to CA scheme and the relevant low-level control systems design are discussed in Chapter 6. The performance of the CA scheme is also validated through HiL testing with the existence of real steering and brake components, as presented in Chapter 7.

5.6.1 Interior Point Solution

In this section, the optimal solution for CA problem, derived by using Interior point (IP) method, is compared with the results of the proposed daisy-chain method. As one may recall from section 5.2, the quadratic CA problem based on mixed optimisation formulation is:

$$\min_{\mathbf{u}} \; J = \|\mathbf{W}_\tau(\mathbf{B}\mathbf{u} - \boldsymbol{\tau})\|_2^2 + \varepsilon\|\mathbf{W}_u(\mathbf{u})\|_2^2 \quad subject\ to \quad \overline{\mathbf{u}} \le \mathbf{u} \le \underline{\mathbf{u}} \tag{5-33}$$

MATLAB® Optimization Toolbox™ function, *fmincon*, is employed for solution of nonlinear constrained optimisation problem (5-33). The toolbox provides different (iterative) solution algorithms including *Active-Set*, *Sequential Quadratic Programming (SQP)*, *Interior Point* (IP) and *trusted-region reflective* methods (The MathWorks, 2013). In our case, we found that the interior point method provides more accurate results (less control error) in comparison to active-set algorithm.

By setting $\varepsilon = 0$ in Eq. (5-33), the primary objective (i.e. control error minimisation) solution is obtained as shown in Figure 5-7-a. Here there is no preference over the existing actuators (steering and brakes), so the solution is obtained by considering both the steering and brake actuators. To exploit the actuator preference, the secondary objective can be employed. Therefore, ε is set to a non-zero but small value as $\varepsilon = 0.01$ to emphasise the importance of primary objective over the secondary objective. The control weighting matrixes $\mathbf{W}_{u,Fz}$ is selected as Eq. (5-52**)** so the steering and brake are mainly prioritised based on their peak forces. Note that, to emphasise the preference of steering actuator utilisation one should minimise the usage of brake actuation. Similarly in case of brake preference the steering actuation should be minimised.

The optimal CA solution based on steering and brake preferences are shown in Figure 5-7-b and c respectively. To make comparison simple, the yaw moment M_z is selected as the only high-level task to be fulfilled, in other words we set $F_x = F_y = 0$.

In spite of different actuator utilisation based on different CA prioritisations, as shown in Figure 5-7, the vehicle yaw rates follow the target yaw rate quit well. As the actuator dynamics are ignored in this simulation, there is no phase lag between the resultant yaw rates from CA.

It should be noted that each simulation run (in Matlab®/Simulink® environment) took about 769 sec to complete[30] (the manoeuvre duration is 6 sec as shown in Figure 5-7), which clearly does not meet the requirements of “low cost” real time implementation.

[30] Computer specification: Dual 1.86 GHz Intel® Core™ 2 CPU; 3 GB RAM; Windows 7 Enterprise 64-bit; MATLAB R13a.

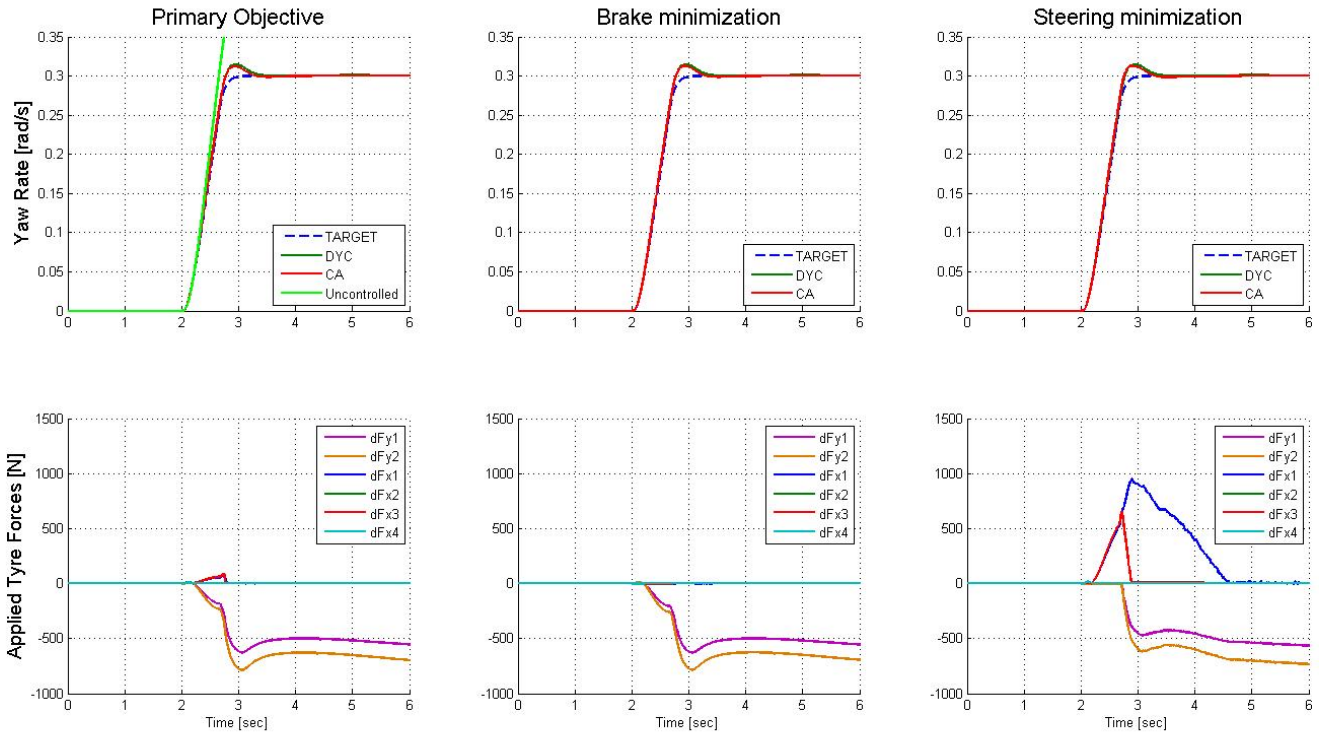

Figure 5-7: Control Allocation Optimisation Solution Using Interior Point Algorithm (Matlab® Optimization Toolbox™)

a) Primary Objective Only,

b) Primary Objective & Brake minimization (i.e. maximum steering utilisation),

c) Primary Objective & Steering minimisation (i.e. maximum brake utilisation)

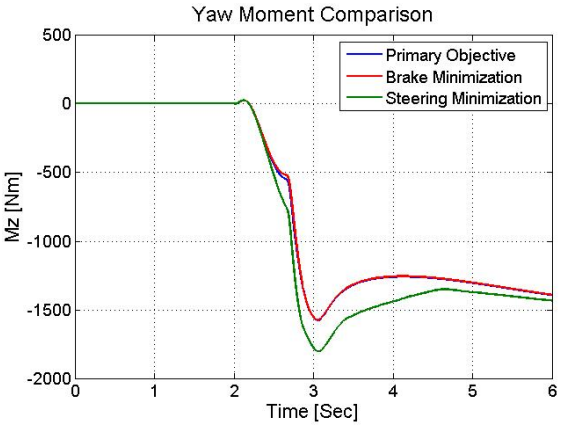

Figure 5-8: Yaw Moment Comparison (different actuators utilisation)

As the vehicle exhibits fairly similar yaw rate in all the three control allocation formulations, the vehicle requested yaw moment could be represented as the total energy that is required to keep the vehicle in the desired trajectory (through actuators utilisation). The comparison of requested yaw moment for different actuator priorities is shown in Figure 5-8, confirm the fact that the brake allocation (corresponds to Figure 5-7-c) need more energy to stabilise the vehicle than steering allocation (corresponds to Figure 5-7-a or b). This is the reason why in the case of brake prioritisation (i.e. Figure 5-7-c), the optimal solution is obtained by both allocation of steering and brake (not brake actuation itself). In other word, the only brake actuation is sub-optimal in terms of actuator utilisation, while setting the preference on steering lead to an optimal CA solution.

5.6.2 Comparison between different CA schemes

To validate the proposed daisy-chain method, different CA methods for steering and brake actuation are compared with daisy-chain solution is this section.

5.6.2.1 Daisy-chain with Interior Point Methods

As one may recall from section 5.5.3, the proposed daisy-chain algorithm is based on “absolute” priority of one set of actuators (for example brake actuation). This means that the second set of actuators will not be activated until the first set is fully utilised, which may lead to a sub-optimal solution (in case of brake priority, for example). Meanwhile, the optimal control allocation

can be obtained by solving the CA formulation by one of the iterative optimisation algorithms such as interior point (IP) method, as discussed in the previous section.

To investigate the effectiveness of the proposed CA scheme, the results of daisy-chain (steering preference) and interior point CA methods for step steer manoeuvre on high mu surfaces are compared in Figure 5-9. Both methods can stabilise the vehicle by utilising only the steering actuator and the resultant yaw rates for both methods are very similar (as the tyres are not saturated, both solutions are obtained without actuator saturation). However, daisy-chain method can stabilise the vehicle with different steering actuation force (front tyres lateral force) than IP method, which is probably due to the weighting matrixes employed in the two methods (note that in mixed CA formulation, the control weighting matrix is only applied to the secondary objective, see Eq. (5-42**)** for example). It is important to note that the requested yaw moments for both daisy-chain and IP method are similar to each other, as shown in Figure 5-9, confirming the fact that daisy-chain leads to an optimal solution when only steering actuation is being utilised.

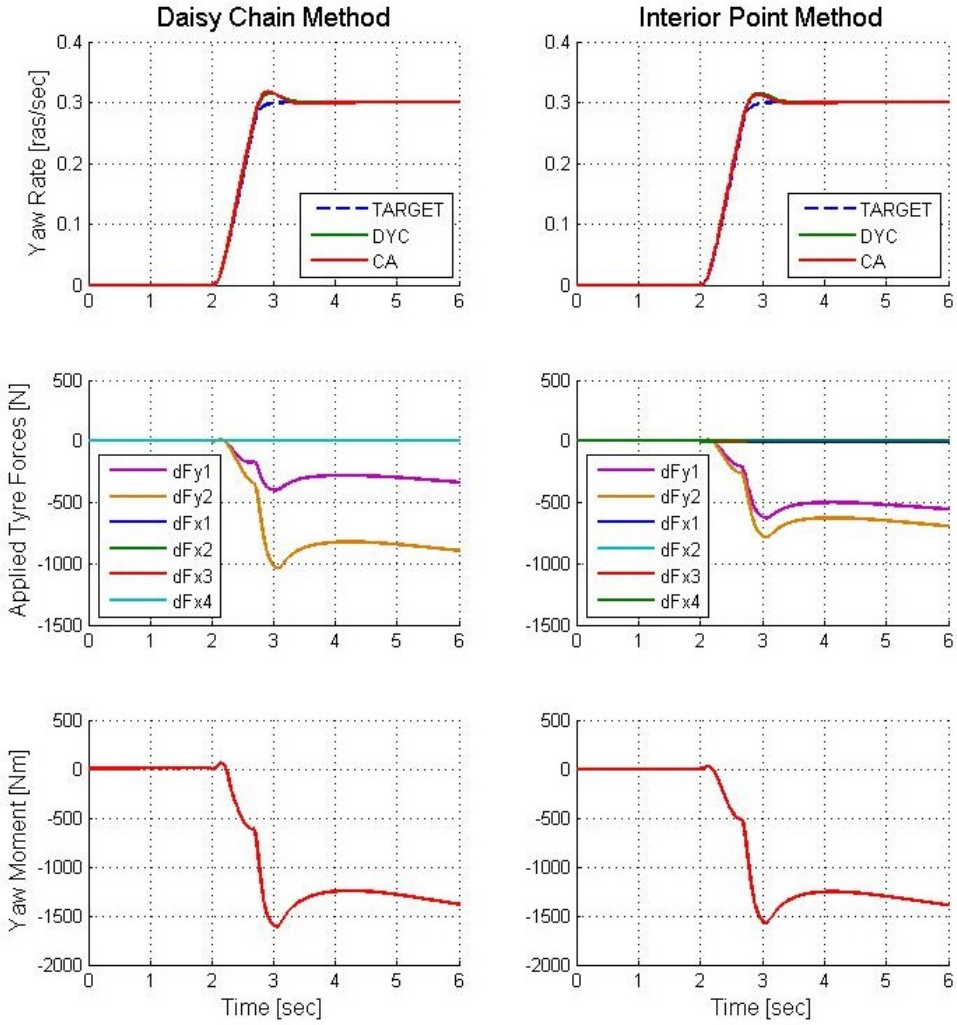

Figure 5-9: Comparison between Daisy-chain (steering priority) and IP solutions for oversteering situation

For understeering situation (i.e. Step60-mu0.2-V50 manoeuvre), both methods have good trajectory following, as shown in **Figure 5-10** However, because of the front tyres saturation, the actuator utilisation in these two methods are different. It is clear that the daisy-chain method consumes more energy than the Interior point method to follow the required target. This means that the daisy-chain solution is suboptimal in case of actuator utilisation.

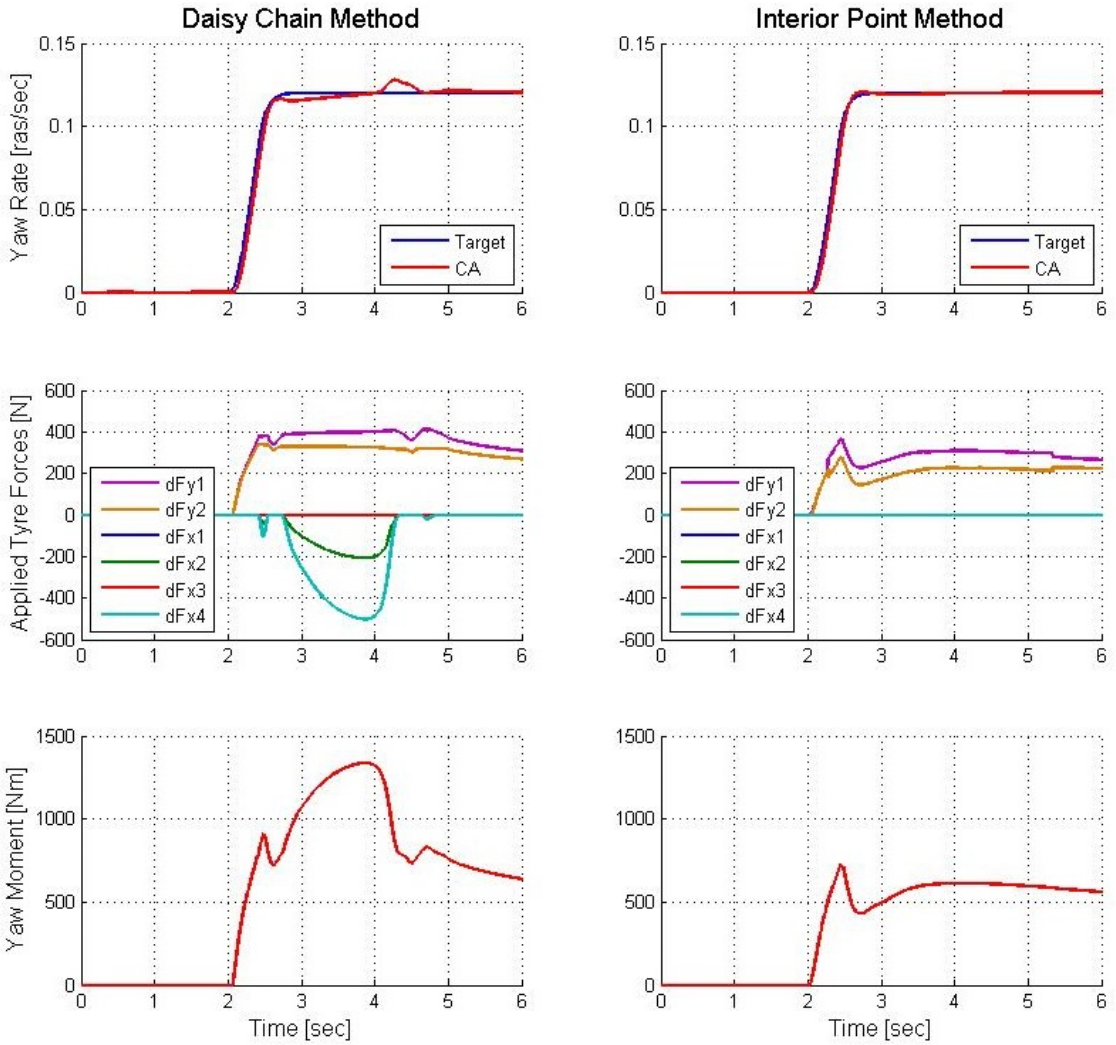

Figure 5-10: Comparison between Daisy-chain (steering priority) and IP solutions for understeering situation

Although the daisy-chain method leads to a suboptimal solution when the actuators are saturated, however, the solution is simple, flexible and very fast. More importantly, one should note that the absolute brake priority cannot obtain by any (iterative) optimal solution, because the only brake actuation is sub-optimal in its nature, as discussed before. Recall from chapter 2, in hazardous stability situation it is required that the brake actuation has ‘absolute’ priority over the steering, therefore, one can conclude that the solution of CA problem by any optimal method is clearly confronting the system specification, which is not acceptable. On the other hand, daisy-chain method provides a very flexible scheme to prioritise the actuators based on any engineering requirements,

which make the proposed scheme very attractive from practical point of view. The method is also very fast as in does not involve any iteration. Each simulation results shown in Figure 5-9 and 5-10 take about 63 sec in Matlab®/Simulink® environment to complete which is 11 times faster than IP solution (IP solution take 769 sec to complete for the similar simulation), and hence, daisy-chain could be easily implemented and run in a real time environment with low cost processors.

5.6.2.2 Daisy-chain with traditional allocation methods

Traditional ESP system is based on only brake intervention (van Zanten A. , 2000), and the active steering systems, such as AFS or EPAS, employ only steering (angle or torque) actuation to provide vehicle stability (Ackermann, 1997; Liu, Nagai, & Raksincharoensak, 2008). In this section, comparisons between only brake actuation, only steering actuation and the proposed integrated brake and steering actuation (CA) methods are performed.

In the only steering actuation systems, the applied (front) tyre lateral forces are obtained by the following relations (Furukawa & Abe, 1997) (note that the steering actuation for vehicle stability recovery is only applicable at oversteering situations):

$$\Delta \mathrm{F}_{y,1} = \frac{M_z}{(a \times \cos\delta + c \times \sin\delta)} \times \frac{\mu_1 F_{z,1}}{\left(\mu_1 F_{z,1} + \mu_2 F_{z,2}\right)}$$

$$\Delta \mathrm{F}_{y,2} = \frac{M_z}{(a \times \cos\delta - c \times \sin\delta)} \times \frac{\mu_2 F_{z,2}}{\left(\mu_1 F_{z,1} + \mu_2 F_{z,2}\right)} \quad (for\ oversteering) \qquad (5\text{-}59)$$

$$\Delta \mathrm{F}_{y,3} = 0$$

$$\Delta \mathrm{F}_{y,4} = 0$$

Similarly, for the only brake actuation, the tyre longitudinal forces can be obtained by the following equations (Furukawa & Abe, 1997; Smakman, 2000):

$$\left.\begin{aligned}
\Delta \mathrm{F}_{x,1} &= \frac{M_z}{(c \times \cos\delta - a \times \sin\delta)} \times \frac{\mu_1 F_{z,1}}{\left(\mu_1 F_{z,1} + \mu_3 F_{z,3}\right)} \\
\Delta \mathrm{F}_{x,2} &= 0 \\
\Delta \mathrm{F}_{x,3} &= \frac{M_z}{c} \times \frac{\mu_3 F_{z,3}}{\left(\mu_1 F_{z,1} + \mu_3 F_{z,3}\right)} \\
\Delta \mathrm{F}_{x,4} &= 0
\end{aligned}\right\} \; for\ M_z > 0 \qquad (5\text{-}60)$$

and

$$\left.\begin{aligned}
\Delta \mathrm{F}_{x,1} &= 0 \\
\Delta \mathrm{F}_{x,2} &= \frac{M_z}{(-c \times \cos\delta - a \times \sin\delta)} \times \frac{\mu_2 F_{z,2}}{\left(\mu_2 F_{z,2} + \mu_4 F_{z,4}\right)} \\
\Delta \mathrm{F}_{x,3} &= 0 \\
\Delta \mathrm{F}_{x,4} &= \frac{M_z}{-c} \times \frac{\mu_4 F_{z,4}}{\left(\mu_2 F_{z,2} + \mu_4 F_{z,4}\right)}
\end{aligned}\right\} \; for\ M_z < 0 \qquad (5\text{-}61)$$

where indices 1,2,3 and 4 stands for front left, front right, rear left and rear right wheels, respectively.

Figure 5-11 shows the results of: a) integrated steering and braking allocation (daisy-chain method-brake preference), b) only steering, and c) only braking interventions for the vehicle subject to Step60-mu1.0_V100 manoeuvre. The results confirm that all the three methods can stabilise the vehicle on this oversteering situation. However, by comparing the generated yaw moment, one can conclude that the brake actuation dissipates more energy in comparison to steering actuation. This fact is also clearly reflected in the resultant vehicle velocity in each case. As the tyres are not fully saturated, the daisy-chain method employs only brake actuation and the results are similar to pure brake actuation system (ESP).

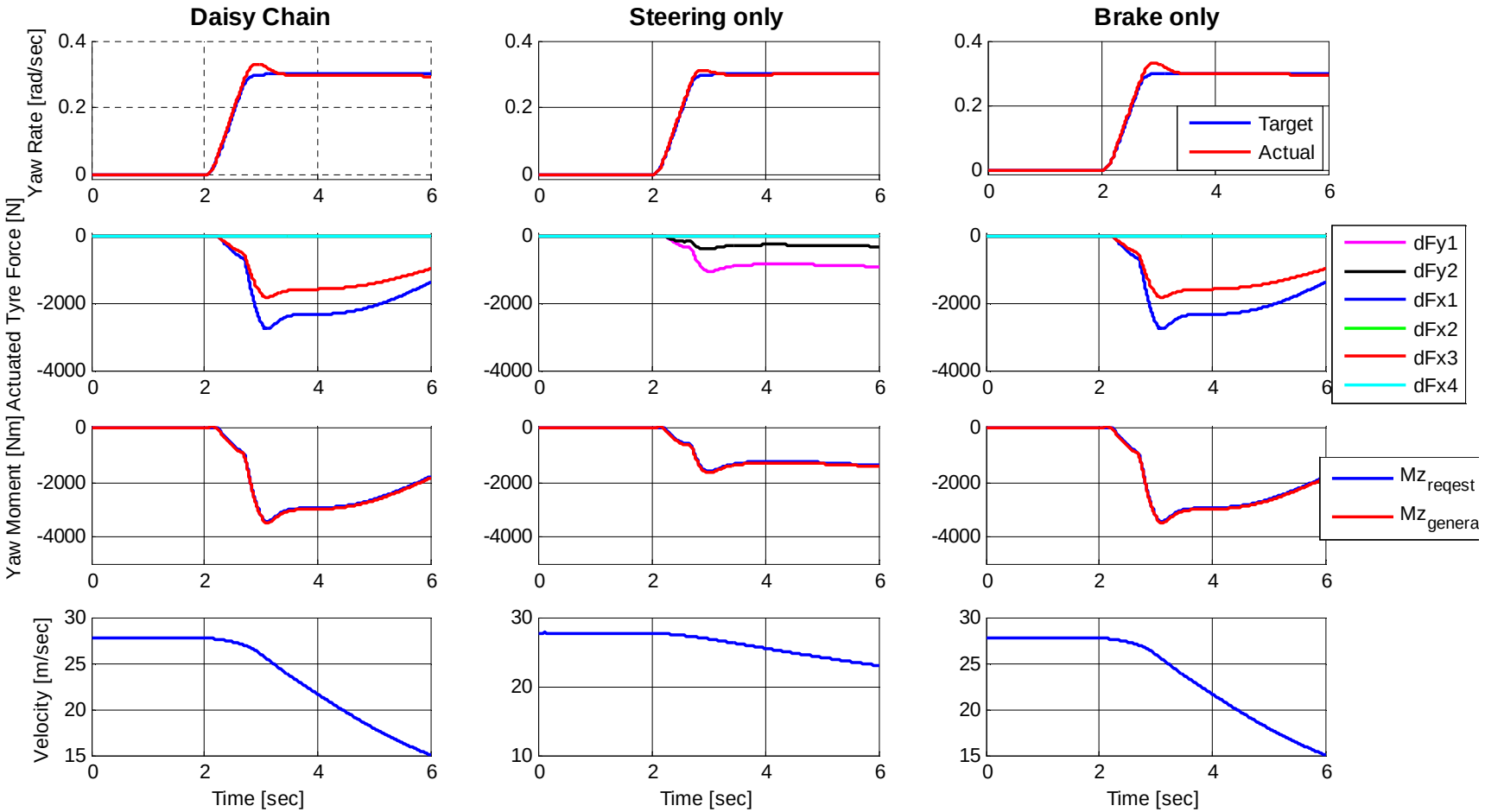

Figure 5-11: a)Integrated steering & brake actuation (daisy-chain CA); b)Only steering actuation; c)Only brake actuation

Vx=100kph, Step Steer 60° @ 1sec, $\mu = 1.0$, " without actuator constraint "

To investigate the effectiveness of the proposed integrated EPAS and ESP control system in the existence of actuator constraint, the same manoeuvre (Step60-mu1.0_V100) was performed but here the maximum achievable (longitudinal and lateral) tyre forces are bounded to 1000N, for example. Note that this imposed constraints might be due to some (unwanted) reasons such as the actuators power limitations or we may arbitrarily want to prevent the tyre forces to reach to their maximum limits (i.e. become fully saturated) because of some practical benefits, for example, to maintain vehicle steerability in case of braking. The simulation results for various actuators configurations, namely: only steering actuation, only brake actuation, daisy chain CA with steering priority and daisy chain CA with brake priority are shown in Figure 5-12. Clearly, in all these scenarios the actuated tyre (longitudinal and lateral) forces cannot exceed from 1000N, however, except the case of only brake actuation (ESP), the vehicle yaw rate can follow its target. It is shown that (in case of similar actuators constraints) the brake based stability systems (ESP) has more limited capability than the steering based stability systems (such as AFS or EPAS) to bringing the vehicle into the target path. The reason is in the fact that brake based stability systems, consumed more energy (are sub-optimal) than steering based system, as concluded before. Although, from theoretical point of view, it is preferable to employ steering based stability system, but, due to several practical reasons brake based stability system (ESP) has privilege over steering based stability systems. To name a few, the brake based stability system is based on wheel slip control dynamics which is much faster than steering based control system; they can provide much more actuation power than steering actuator (therefore they have much wider bound than steering actuators); and also it is effective in both oversteering and understeering situation (which is not the case for steering based stability systems).

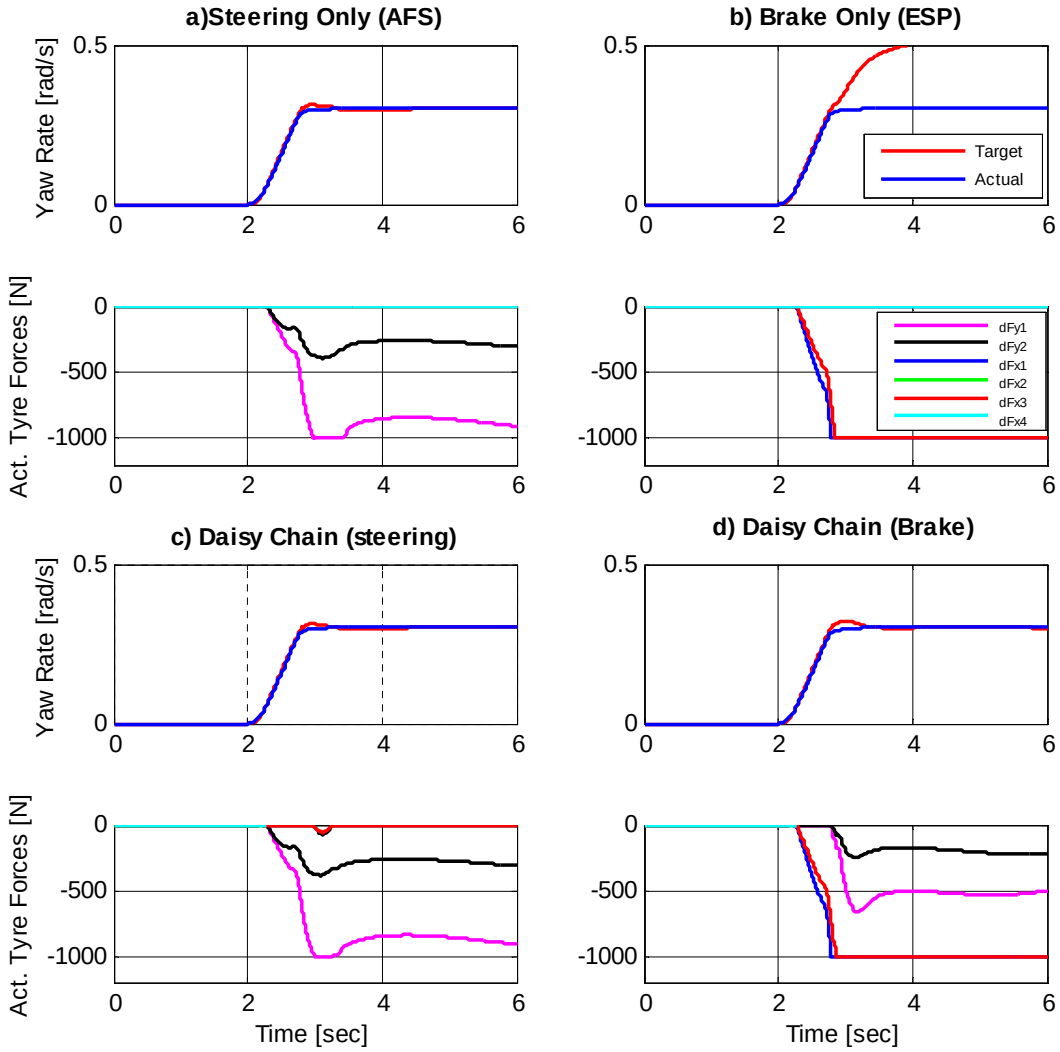

Figure 5-12: a)Only steering actuation (AFS); b)Only brake actuation (ESP) c&d)Integrated steering & brake actuation (Daisy-chain CA);

Vx=100Kph, Step Steer 60° @ 1sec, $\mu = 1.0$, " with actuator constraint

The simulation results, shown in Figure 5-12, also confirm that the proposed integrated steering and brake system (in both configurations) can maintain the vehicle stability even with the existence of actuator constraints, which exhibit advantages over the traditional stand-alone stability systems (such as ESP or AFS). One should note that, although both configurations can provide vehicle stability, the combination of tyre forces are different. Again, it confirm that the steering actuation priority has advantage over the brake actuation in terms of optimality, but because of the practical reasons, as mentioned before, the integrated stability system should be

designed and implemented based on priority of brake actuation. Interestingly, all different actuators combinations, presented in Figures 5-11 and 5-12, can be obtained simply by altering the Q vector, as introduced in section 5.5.3. Therefore, one may conclude that the proposed CA scheme provide a general reconfigurable integrated vehicle dynamics control architecture, which could be easily reduced to one of the traditional brake based or steering based stability systems. This flexible scheme has the advantage of providing fault tolerance property to the system, which means that the allocation configuration can adjust itself in case of an actuator failure.

The execution time for different allocation methods are presented in Table 5-3, which shows the preference of daisy-chain methods in comparison to solutions obtained from numerical optimisation methods such as IP in terms of processing time. It should be noted that the times indicated in Table 5-3 are presented for comparative purposes and are not indicative of the actual time required for running in a real time processor. These are the execution times of the CA algorithm simulation with the existence of the vehicle model (model in the loop simulation) in Matlab®/Simulink® environment, with several displaying and monitoring scopes (which slow down the simulation). The real time codes are usually written in low-level languages (such as C) which run much faster than Matlab®/Simulink® models.

Table 5-3: Execution time for different allocation methods (sec)

Optimal CA Solution (IP method)	Daisy-chain CA method	Steering Allocation (AFS or EPAS)	Brake Allocation (ESP)
769	63	54	54

It is worth to mention that, all the simulation results, so far, are based on assumption of ideal actuators with zero dynamics. The effect of actuator dynamics on CA scheme and design of the relevant low level (actuators) controller will be discussed in the next chapter.

6 Low-Level Control Design

6.1 Introduction

By considering the proposed architecture of the integrated vehicle dynamics system, the objective of the IVCS system is to integrate steering and brake control systems to provide driver comfort and/or vehicle safety (based on driving condition), as described in system requirements, section 2.2.

The system objective in comfort mode is to reduce the driver steering torque input by providing an electronically controlled augmentation of an assisting torque to the vehicle steering system. The required additional steering torque is derived by measuring the driver steering torque input which is forwardly fed to the EPAS electric motor controller through a variable gain , so called boost curve (see (Kim & Song, 2002), for example). Therefore, the required steering actuation (i.e. augmented steering torque) is always in the same direction of the driver input and there is no request for brake intervention (i.e. tyre longitudinal force) in comfort mode.

On the other hand, in safety mode, the total required yaw moment and lateral force of the vehicle are calculated by the high-level controller and are then allocated to the relevant tyres longitudinal and lateral forces through the control allocation scheme, as discussed in Chapters 4 and 5 respectively. Here, the requested tyres longitudinal force is always negative (i.e. brake actuation), but the requested (front) tyres lateral force might be positive or negative[31], therefore, the augmented steering torque might be in favour or against the driver input torque.

The output of the CA scheme is the tyre lateral *force*, whereas, the controlled states in EPAS is steering *torque* (Badawy, Zuraski, Bolourchi, & Chandy, 1999) and in ESP is wheel slip (Savaresi & Tanelli, 2010). Therefore, the calculated tyre longitudinal and lateral forces should be converted to the relevant wheel slip and steering torque, respectively, which will then be considered as a reference value for the low-level closed loop controller of steering and brake smart actuators.

[31] See Chapter 5 for more detailed discussions in this course.

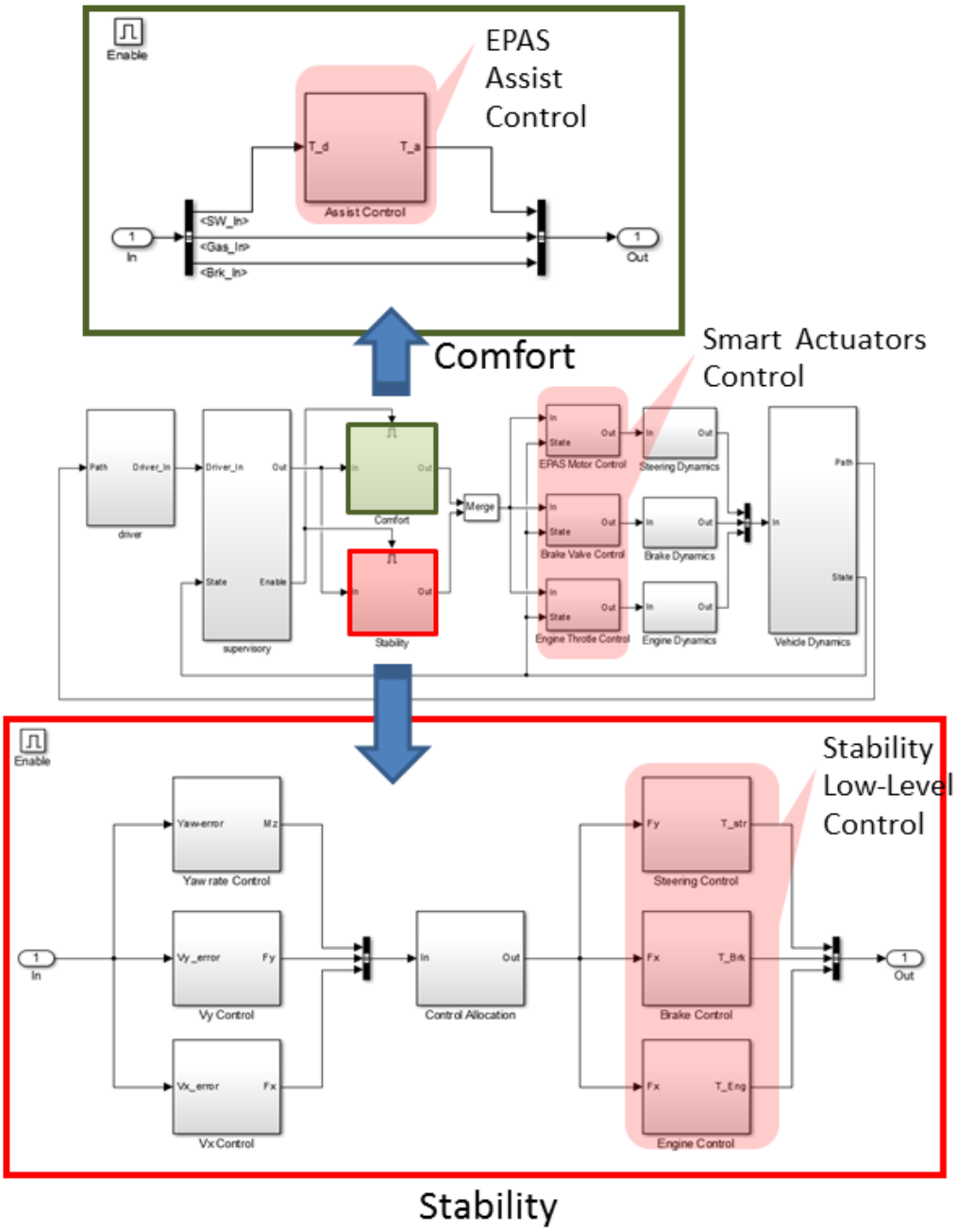

Figure 6-1:Simulink® blocks of Low-level and smart actuator control

One should note that the control system consists of three cascade closed loop controllers, so called, high-level control, low-level and smart-actuators controllers as shown in Figure 6-1. To maintain the stability in a cascade closed loop control system, the inner loops should have appropriately faster dynamics than the corresponding outer loops (Doyle, Francis, & Tannenbaum, 1992). Recall from Chapter 5, the high-level control bandwidth was selected as 3 Hz. Therefore, the (steering and brake) low-level control bandwidths as well as their smart actuators

(i.e. EPAS electric motor and brake hydraulic valve) control bandwidths should be faster than 3 Hz.

Design of the smart actuators and low-level control systems for steering and brake actuations in stability mode as well as the EPAS control system for comfort mode are discussed in this chapter.

6.2 Steering Low–Level and Smart Actuator Control Design

6.2.1 EPAS modelling

Electric Power-Assisted Steering (EPAS) is a smart actuator which provides an electronically controlled superposition of an assisting torque to the vehicle steering system. The components, functionality and the mathematical model of a column type EAPS, as well as its main block diagrams (as shown Figure 6-2), was described in Chapter 3.

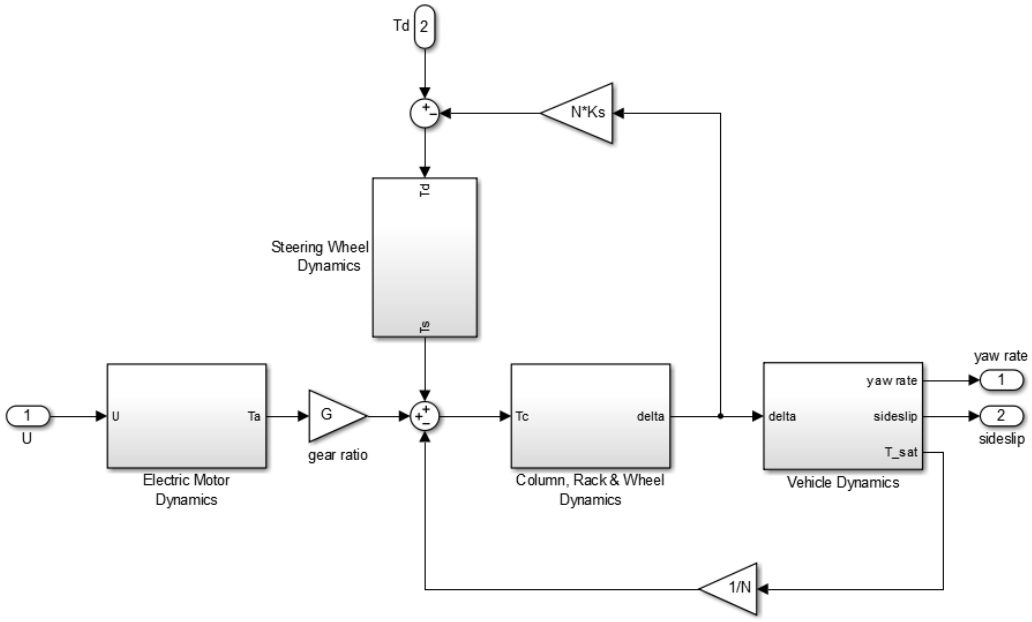

Figure 6-2:EPAS block diagram with vehicle dynamics

From Figure 6-2, it is apparent that all the system transfer functions are linked together which means that there are couplings existing between system variables or in other words, the system has high order. Note that this general model describes the main building blocks of an EPAS system, whether the employed vehicle model is linear or nonlinear. In this thesis, we employ a simple linear vehicle dynamics model (bicycle model) with variation of cornering stiffness (Mammar & Koenig, 2002) as

described in the following sections. However, one can use more complicated nonlinear vehicle models, but either the model needs to be linearised to be able to design a linear controller or nonlinear control design techniques should be employed. Both of these approaches increase the complexity of the controllers which is not suitable for a “low cost” control system solution. The validation results through MiL simulation and HiL testing, as presented at the end of this chapter and also Chapter 7, confirm the stability and robustness of the proposed control system even in severe driving conditions.

Another conclusion from Figure 6-2 is that the applied torque to the EPAS steering rack originated from two separate sources (path): 1-driver input torque and 2-electric motor torque. In comfort driving condition, the EPAS electric motor requested torque is mainly determined by amplifying the driver input torque (through a look-up table, so called, boost curve), as described in section 6.2.4. On the other hand, in case of mild and hazardous stability conditions[32], the driver steering input torque is considered as a “disturbance” which should be rejected by the closed loop stability controller and the requested electric motor torque is determined by the “High-level Controller” and “Control Allocation” scheme. This important finding is being employed in design of a novel EAPS based stability control system, as discussed in more detail in the following sections.

Design of the inner loop DC electric motor controller (3rd loop), and the low-level EPAS feedback controller (2nd loop), as well as the EPAS assist controller, are presented in this section. To design the feedback controllers, we employ the Youla parameterisation (closed loop shaping) technique as described in Chapter 5 (Assadian F. , 2011).

6.2.2 EPAS Electric Motor (Smart Actuator) Control Design

EPAS system is a *torque* actuator linked to the steering system. Assuming one has a reference torque value, the objective of EPAS motor controller is to asymptotically follow the reference torque commands by means of an electric motor (which in our

[32] See Chapter 2 for definition and criteria of normal and hazardous driving conditions in this thesis.

case is a permanent magnet DC motor). The block diagram of a closed loop current control of an EPAS electric motor[33] is shown in Figure 6-3.

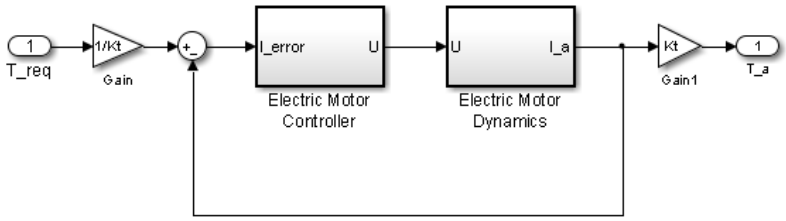

Figure 6-3: DC motor closed loop torque control

Recall from section 3.6.1, the DC motor transfer function can be derived in Laplace domain as:

$$G_m = \frac{I_a}{U} = \frac{I_m s + B_m}{(I_m s + B_m)(L_a s + R_a) + k_t k_e} \tag{6-1}$$

which is in block diagram form and can be presented as Figure 6-4 below:

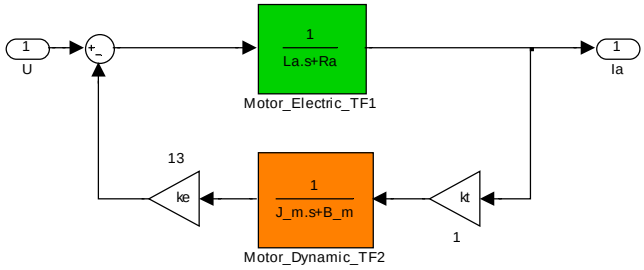

Figure 6-4: DC electric motor dynamics (plant model)

Here, the DC motor transfer functions (6-1) is the plant model, G_m, and the control objective is to design a stable closed loop controller K_m, which track the requested torque asymptotically. From Equation (6-1), the plant transfer function is:

$$G_m = \frac{s + B_m/I_m}{L_a[s^2 + (R_a/L_a + B_m/I_m)s + (R_a B_m + k_t k_e)/I_m L_a]} \tag{6-2}$$

which can be written in the form of zero-pole-gain as:

$$G_m = \frac{k_1(s + z)}{(s + p_1)(s + p_2)} \tag{6-3}$$

[33] See section 3.6.1 for more description of the EPAS system modelling.

where $k_1 = 1/L_a$ is the gain, $z = -B_m/I_m$ is the only real zero of plant model in the left half of s plane and p_1 and p_2 are the two real poles of G_m which can be found by the partial fraction expansion of the equation (6-2).

The plant is stable because all of its zero and poles are real and positive. The control problem can be posed as to define the Youla parameter, Y_m, such as the closed loop transfer function, T_m, satisfy the control performances, as described in Chapter 4. By studying the plant's poles and zero locations, the Y_m can be defined to cancel the poles and zero of the plant (inverse of the plant) and also to shape the closed loop by placing two real positive poles. Therefore, Y_m can be defined as:

$$Y_m = \frac{1}{G_m}\left[\frac{1}{(\tau_1 s + 1)^2}\right] = \frac{(s + p_1)(s + p_2)}{k_1(s + z)(\tau_1 s + 1)^2} \tag{6-4}$$

where the time constant τ_1 is a tuneable real value which can be used as controlling parameter to shape the closed loop response. Y_m is a stable function as all of its zeros and poles are real and positive. The closed loop transfer function (complementary sensitivity) is:

$$T_m = Y_m G_m = \frac{1}{(\tau_1 s + 1)^2} \tag{6-5}$$

As $T_m(0) = 1$,so the interpolation condition is satisfied. Because both the plant and Youla functions are stable, therefore the system is internally stable. The sensitivity function of the system is:

$$S_m = 1 - T_m = \frac{(\tau_1 s + 1)^2 - 1}{(\tau_1 s + 1)^2} \tag{6-6}$$

The DC motor torque controller transfer function, K_m, is obtained as:

$$K_m = \frac{Y_m}{S_m} = \frac{(s + p_1)(s + p_2)}{k_1(s + z)(\tau_1 s + 1)^2} \times \frac{(\tau_1 s + 1)^2}{(\tau_1 s + 1)^2 - 1}$$

$$K_m = \frac{1}{k_1} \times \frac{s^2 + (p_1 + p_2)s + p_1 p_2}{{\tau_1}^2 s^3 + (2\tau_1 + z{\tau_1}^2)s^2 + 2\tau_1 z\, s} \tag{6-7}$$

For the DC motor with parameters indicated in appendix 1, the controller can be parameterised as follow. From equation (6-2) the plant transfer function is:

$$G_m = \frac{s + 0.5}{0.001s^2 + 0.2005s + 350}$$

$$= \frac{1000(s + 0.5)}{(s + 198.7)(s + 1.76)} \quad (6\text{-}8)$$

The system is stable and has one zero at $s = -0.5$ and two poles at $s = -198.7$ and -1.76 respectively ($k_1 = 1000, z_1 = 0.5, p_1 = 1.76\ and\ p_2 = 198.7$). From Eq. (6-4) the Youla function is:

$$Y_m = \frac{0.001(s + 1.76)(s + 198.7)}{(s + 0.5)(\tau_1 s + 1)^2} \quad (6\text{-}9)$$

And the controller transfer function is obtained as:

$$K_m = \frac{0.001(s + 1.76)(s + 198.7)}{{\tau_1}^2 s(s + 2/\tau_1)(s + 0.5)} \quad (6\text{-}10)$$

The frequency response of T_m and S_m for different values of τ_3 is shown in Figure 6-5. The system bandwidth (intersection of S and T) is increased by lowering value of time constant τ_1. However, the maximum value of S and T (M_S and M_T) for different time constants are less than 2db, so the minimum of $60°$ phase margin and 6dB gain margin is guaranteed and the control performance is met.

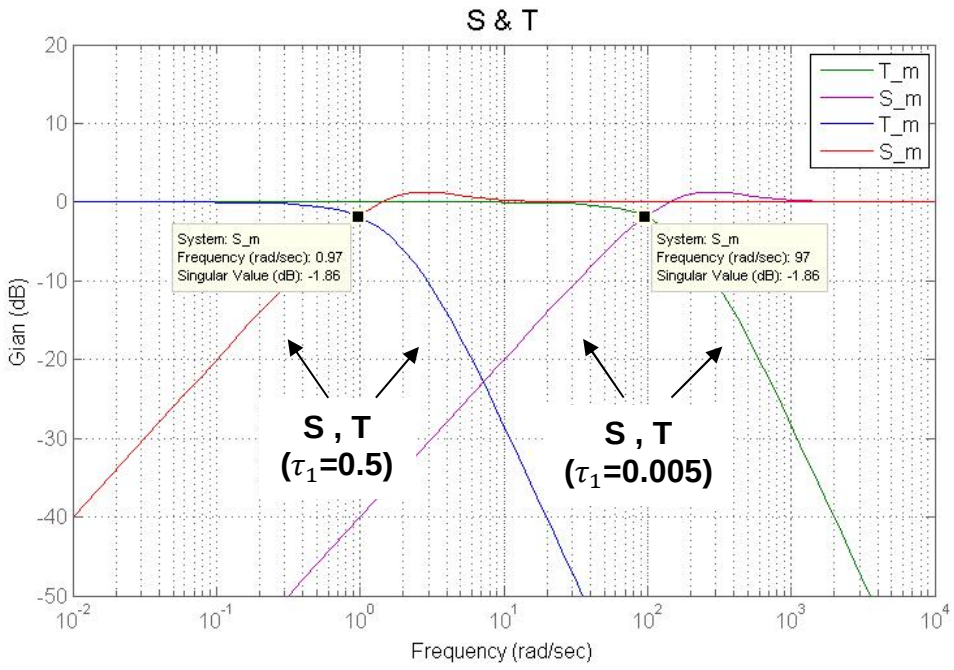

Figure 6-5: Effect of τ_1 on T and S

To investigate the performance of the system in time domain, the closed-loop unit step responses of the system for various time constants τ_1 are shown in Figure 6-6. The system does not exhibit any unstable or oscillatory behaviour for all values of time constant, however, the response time of the system is reduced by reducing the time constant, as expected.

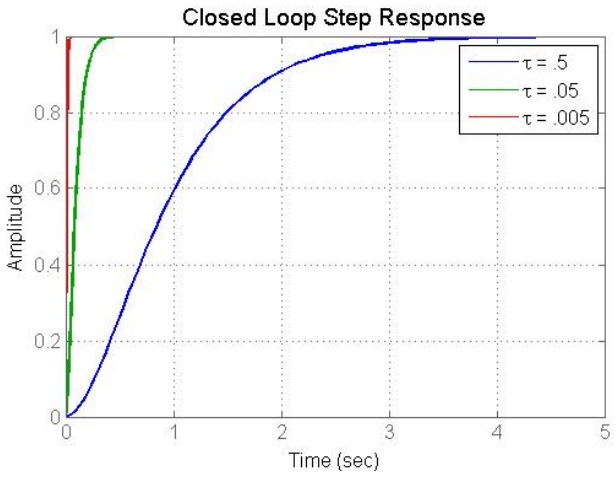

Figure 6-6: Effect of τ_1 on closed loop step response

By selecting $\tau_1 = 0.005$, the following control transfer function is obtained:

$$K_m = \frac{40(s + 198.7)(s + 1.76)}{s(s + 400)(s + 0.5)} \qquad (6\text{-}11)$$

The frequency responses of all the system's transfer functions are shown in Figure 6-7. The crossover frequency ω_c (the point that $S = T$) is about 100 rad/s ($\approx 16\,Hz$) which is selected as the control system bandwidth. This response is selected to be much faster than the high level control design response to ensure control system stability and performance.

The open loop gain at low frequencies (below control bandwidth) is high whereas the gain at high frequency (after control bandwidth) is low. Therefore, the control system has good robustness, command tracking and disturbance attenuation performance at low frequencies and good noise rejection performance at high frequencies. The value of $|S|$ and $|T|$ at crossover frequency are less than zero dB, therefore a good phase margin of the closed loop system is also guaranteed. Finally, the maximum gain of $|S|$ and $|T|$ are less than 10 db, and this ensures a good gain margin which

means a good stability margin and robustness even in the presence of plant uncertainties and disturbances.

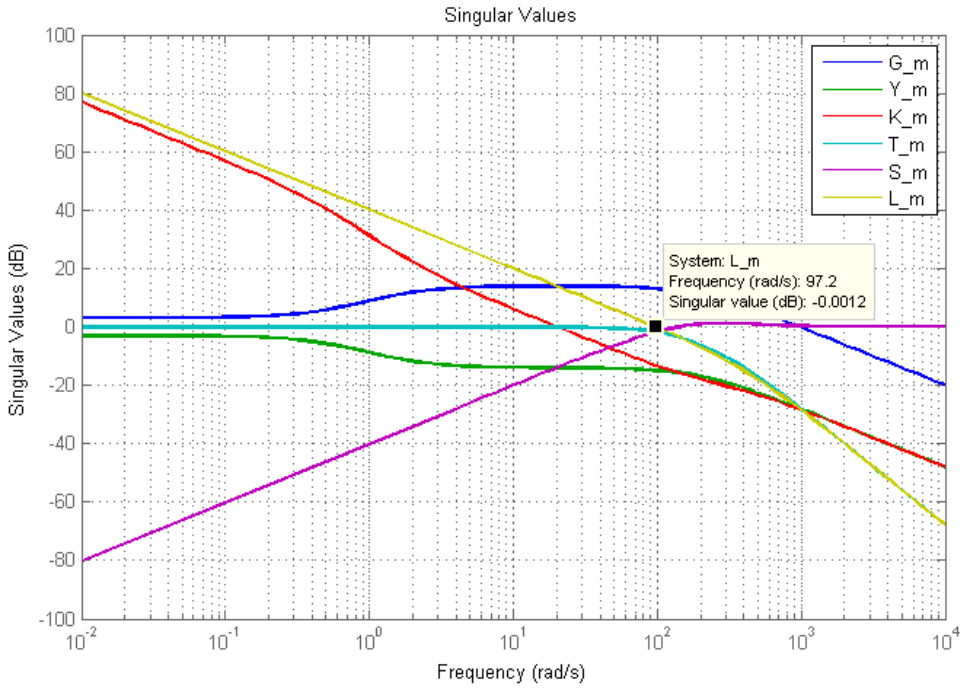

Figure 6-7: bode plot of DC motor torque control system

The closed loop step response of the proposed Youla controller is compared with a previously designed PI controller (with Kp=0.04 and Ki=10) as shown in Figure 6-8. The PI controller is slower than the proposed Youla controller. The same rise time can be obtained with PI controller with Kp=.02 and Ki=24, however, the system response exhibits a slight overshoot as well as a steady-state gain error.

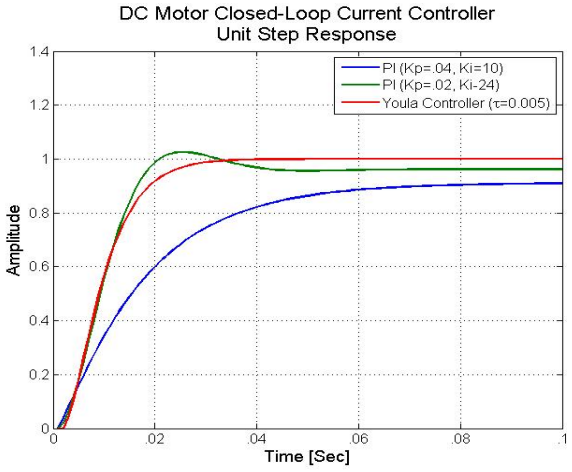

Figure 6-8: PI and Youla Controller step response comparison

6.2.3 Low-Level EPAS Stability Control Design

Design of the low-level controller for EPAS in stability mode is presented in this section. Considering Figure 6-2, the resultant steering column torque is originated from two different sources, namely, driver torque input and electric motor torque input. The generated motor torque should follow the driver input for the sake of driver comfort in comfort driving mode, whereas, the reference steering torque is the output of the control allocation scheme, in stability mode. Therefore, the driver steering inputs act as a disturbance in stability mode and should be rejected by the closed loop low-level EPAS controller.

The proposed low-level control system block diagram is shown in Figure 6-9. In this novel control architecture, the front tyres self-aligning moment, T_{sat}, is fed-back to the low-level EAPS controller. The self-aligning moment is not an available state for measurement but it could be estimated through an estimation algorithm, as proposed in (Hsu Y. , 2009), for example. The plant transfer function, G_{EPAS}, is the ratio of (front tyres) self-aligning moment, T_{sat}, (output) to request torque, T_{req}, (input) and it consist of: EPAS smart actuator dynamics (including the electric motor dynamics and controller, as presented in the previous section), steering dynamics (including column, rack and wheel dynamics), and vehicle dynamics, with several internal feedback loops as shown in Figure 6-9.

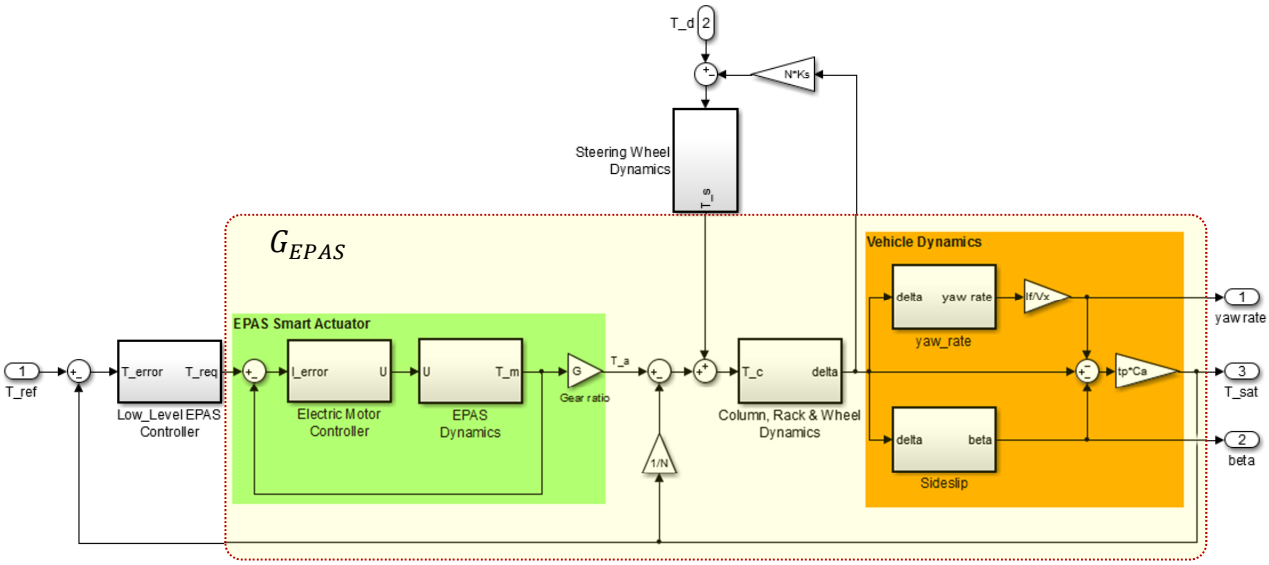

Figure 6-9: EPAS low-level control system block diagrams

From section 6.2.2, the EPAS motor controller (smart actuator) transfer function is:

$$T_a = \frac{K_m G_m}{1 + K_m G_m}\, T_{req} \tag{6-12}$$

The model of an EPAS system was introduced in section 3.6.1 as

$$I_{eq}\ddot{\delta} + B_{eq}\dot{\delta} = T_s + GT_a - \frac{1}{N}T_{sat} \tag{6-13}$$

where

$I_{eq} = \frac{1}{N}\left[N^2 I_c + (I_{z,1} + I_{z,2}) + l_d^2 m_r\right]$

$B_{eq} = \frac{1}{N}\left[N^2 B_c + l_d^2 B_r\right]$

$T_{sat} = M_{z,1} + M_{z,2}$

$N = l_d / r_p$

by considering the driver input steering wheel torque T_s as disturbance, the transfer function of column, rack and (lateral) wheel dynamics can be derived as[34]:

$$\delta = \frac{GT_a - \frac{1}{N}T_{sat}}{I_{eq}s^2 + B_{eq}s} \tag{6-14}$$

and the vehicle dynamics transfer function (bicycle model) is presented in section 3.5 as:

$$\begin{bmatrix} \beta \\ \omega_z \end{bmatrix} = \frac{1}{s^2 - (A_{11} + A_{22})s + (A_{11}A_{22} - A_{12}A_{21})} \begin{bmatrix} B_1 s + (B_2 A_{12} - B_1 A_{22}) \\ B_2 s + (B_1 A_{21} - B_2 A_{11}) \end{bmatrix} [\delta] \tag{6-15}$$

[34] See Chapter 3, for detail description of EPAS modelling and governing equations.

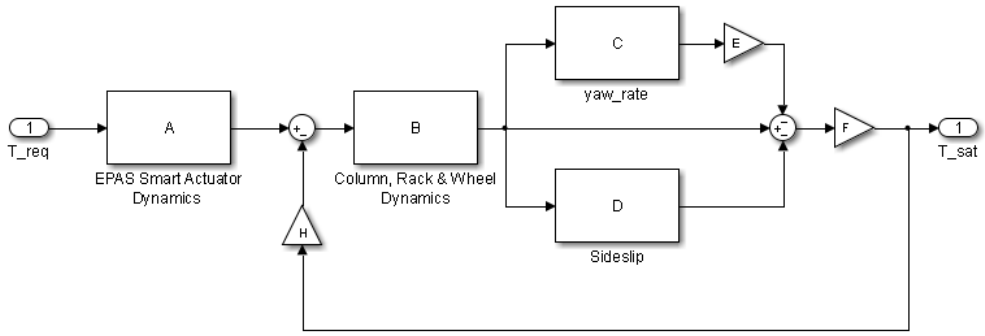

Figure 6-10: Schematic block diagram of the EPAS plant model (from T_{req} to T_{sat})

The simplified block diagrams of G_{EPAS} are shown in Figure 6-10. Employing the block diagrams manipulation rules, the plant transfer function can be derived as:

$$G_{EPAS} = \frac{T_{sat}}{T_{req}} = \frac{ABF(1 - CE - D)}{1 + BFH(1 - CE - D)} \tag{6-16}$$

Where:

$$A = G \times \frac{K_m G_m}{1 + K_m G_m}$$

$$B = \frac{1}{I_{eq} s^2 + B_{eq}}$$

$$C = \frac{B_2 s + (B_1 A_{21} - B_2 A_{11})}{s^2 - (A_{11} + A_{22})s + (A_{11} A_{22} - A_{12} A_{21})}$$

$$D = \frac{B_1 s + (B_2 A_{12} - B_1 A_{22})}{s^2 - (A_{11} + A_{22})s + (A_{11} A_{22} - A_{12} A_{21})}$$

$$E = l_f / V_x$$

$$F = t_p \times C_f$$

$$H = 1/N$$

By substituting the parameter values of vehicle, steering and DC motor ,as indicated in Appendix B, into equation (6-16), the plant transfer function (for $V_x = 120\ Kph$) can be derived as:

$$G_{EPAS} = \frac{2.505\text{e}9\, s^2 + 1.722\text{e}10\, s + 2.467\text{e}11}{s^6 + 423 s^5 + 5.348\text{e}4 s^4 + 1.522\text{e}6 s^3 + 2.409\text{e}7 s^2 + 1.428\text{e}8 s + 1.062\text{e}9} \tag{6-17}$$

The Bode plot of the EPAS plant for various longitudinal speeds is shown in Figure 6-11. The plant has a resonance frequency at around 6.8 rad/sec for all velocities, which is slightly higher than the natural frequency of the vehicle, as discussed in Chapter 3. The system damping will reduce by increasing the velocity, which exhibits a light steering feel as well as poor transient response of the vehicle at high speed manoeuvres (Mavros, 2007).

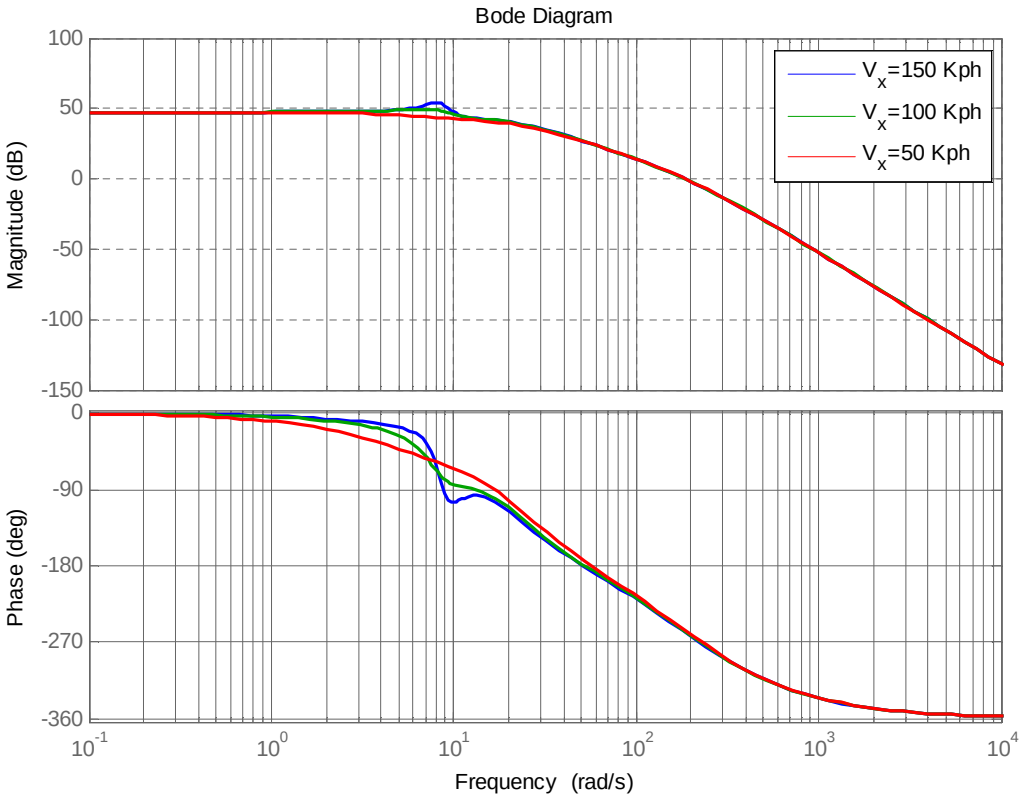

Figure 6-11: EPAS plant dynamics for different longitudinal speeds

The tyre saturation limit (normal force) and the variation of tyre-road coefficient of friction can be represented by variation of tyre cornering stiffness (Pacejka, 2006). The bode plot of the plant for various tyre cornering stiffness ($C_\alpha = [10000, 80000]$) at $V_x = 120\,Kph$ is shown in Figure 6-12. One can conclude that the plant natural frequency will not increase from 10 rad/sec even at very low values of cornering stiffness. Therefore, by selecting the low-level control bandwidth around 40 rad/sec ($\approx$ 6.4 Hz) we make sure that the variation of plant model due to changes in friction coefficient and vehicle speed will be robustly covered by the closed loop controller.

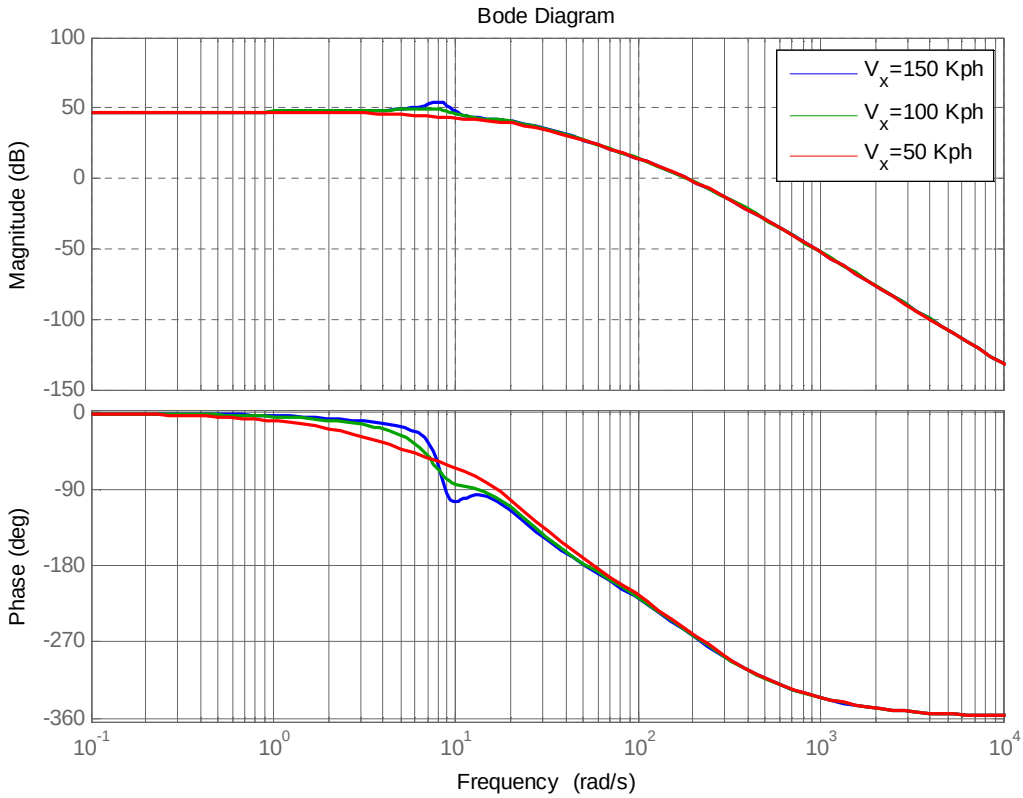

Figure 6-12: EPAS plant frequency response with different tyre cornering stiffness (Vx=120 kph)

The plant transfer function represented by Eq. (6-17) is a sixth order complicated equation and it is difficult to design a controller for this plant by Youla parameterisation method. To address this issue, it is required to reduce the order of the plant model in such a way that the major dynamic behaviour of the plant will not change. For reducing the model's order, we employ the MATLAB command '*reduce*' which invokes the 'Hankel singular value based model reduction function' (Balas, Chiang, Packard, & Safonov, 2005). The reduced 3rd order model calculated as:

$$G_{EPAS} = \frac{687.97(s + 22.98)(s + 0.1108)}{(s + 0.0887)(s^2 + 6.167s + 70.95)} \qquad (6\text{-}18)$$

The frequency response of the full order and the reduced order models are shown in Figure 6-13. The reduced order model almost matches the full order model for the frequencies up to 75 rad/sec (12 Hz) which is more than the control system bandwidth; therefore, the 3rd order reduced plant model is valid for the working frequency range of steering system.

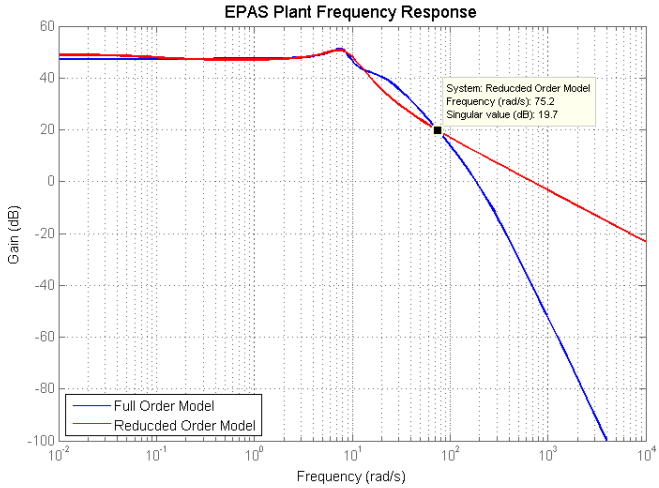

Figure 6-13: Comparison between full and reduced order model

The comparison between step response of the full order and reduced order plant models, as shown in Figure 6-14 , confirm a close match between the two models in transient response, while, the reduced order model exhibits an error in steady state. As the control task is to control the transient behaviour of the system, this steady state error could be accepted without affecting the transient behaviour of the system. The 3rd order reduced plant model (here-in-after called plant) is employed to design EPAS low-level closed loop controller based on self-aligning moment feedback.

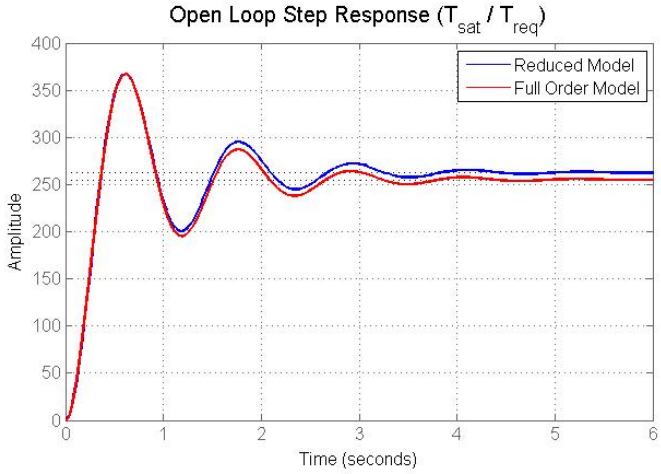

Figure 6-14: full and reduced order step response

The plant model transfer function (equation (6-18)) can be written in general form of pole-zero-gain as:

$$G_{EPAS} = \frac{k_1(s+z_1)(s+z_2)}{(s+p_1)(s^2+\gamma s+\eta)} \tag{6-19}$$

The plant has a gain of k_1 , three poles p_1 , p_2 , p_3 (one real and a pair of complex conjugate poles, denoted as γ and η); and two zeros z_1 and z_2. Note that by selection of different operating conditions (i.e. V_x and $C_{\alpha,f}$ and $C_{\alpha,r}$), the locations of plant's gain, pole and zeros are changing. If the nominal operating condition are selected such that the plant's poles and zeros located at the left hand part of the s plane, the nominal plant is stable and minimum phase. Then we can cancel poles and zeros, by defining the Youla parameter as the inverse of the nominal plant model with some extra functions to shape the closed loop transfer function (Assadian F., 2011).

Defining Youla parameter as:

$$Y_{EPAS} = \frac{1}{G_{EPAS}} \times \frac{1}{(\tau_E s+1)^2} = \frac{(s+p_1)(s^2+\gamma s+\eta)}{k_1(s+z_1)(s+z_2)(\tau_E s+1)^2} \tag{6-20}$$

The time constant τ_E is the control design parameters which will be used for shaping the T and S functions to satisfy the control system stability and performance. Because both the plant and Youla functions are stable, therefore the system is internally stable. The closed loop (complimentary sensitivity) and sensitivity transfer functions are:

$$T_{EPAS} = Y_{EPAS}G_{EPAS} = \frac{1}{(\tau_E s+1)^2} \tag{6-21}$$

$$S_{EPAS} = 1 - T_{EPAS} = \frac{(\tau_E s+1)^2 - 1}{(\tau_E s+1)^2} = \frac{(\tau_E s)^2 + 2\tau_E s}{(\tau_E s+1)^2} \tag{6-22}$$

The controller transfer function can be obtained as:

$$K_{EPAS} = \frac{Y_{EPAS}}{S_{EPAS}} = \frac{(s+p_1)(s^2+\gamma s+\eta)}{k_1(s+z_1)(s+z_2)(\tau_E s+1)^2} \times \frac{(\tau_E s+1)^2}{(\tau_E s)^2 + 2\tau_E s}$$

$$K_{EPAS} = \frac{(s+p_1)(s^2+\gamma s+\eta)}{k_1(s+z_1)(s+z_2)[(\tau_E s)^2 + 2\tau_E s]} \tag{6-23}$$

By substituting the vehicle parameters (including tyres cornering stiffness), as indicated in Appendix B, and selecting the nominal velocity of $V_x = 33.3\, m/s$ $(120\ Kph)$, the (nominal) plant transfer functions G_E takes the form of:

$$G_{EPAS} = \frac{687.97(s + 22.98)(s + 0.1108)}{(s + 0.0887)(s^2 + 6.167s + 70.95)} \tag{6-24}$$

with the following gain, poles and zeros:

$$k_1 = 687.97$$

$$p_1 = 0.0887\ ,\ \ p_2 = 3.084 - 7.84i\ \ ,\ \ p_3 = 3.084 + 7.84i\ \ ,$$

$$z_1 = 22.98\ ,\qquad z_2 = 0.1108$$

The plant is stable and minimum phase (but exhibit an oscillatory transient behaviour). The Youla Y_E and controller K_E transfer functions and can be derived as below:

$$Y_E = \frac{(s + 0.0887)(s^2 + 6.167s + 70.95)}{687.97\ (s + 22.98)(s + 0.1108)(\tau_E s + 1)^2} \tag{6-25}$$

$$K_E = \frac{(s + 0.0887)(s^2 + 6.167s + 70.95)}{687.97\ (s + 22.98)(s + 0.1108)[(\tau_E s)^2 + 2\tau_E s]} \tag{6-26}$$

The frequency responses of T and S transfer functions at two different values of $\tau_E = 0.1$ and $\tau_E = 0.001$ are shown in Figure 6-15. The system bandwidth increase by decreasing the time constant, and, the peak values of S and T transfer functions (M_S and M_T) are less than 2db for the both cases, so the 6dB gain margin is guaranteed which means that good control performance is met[35]. Moreover, the crossover gain is less than zero which means that the system stability is guaranteed. In addition, as the nominal plant is stable and non-minimum phase, the internal stability of the system is verified.

[35] See Chapter 4 for more detail discussion on control performance criteria.

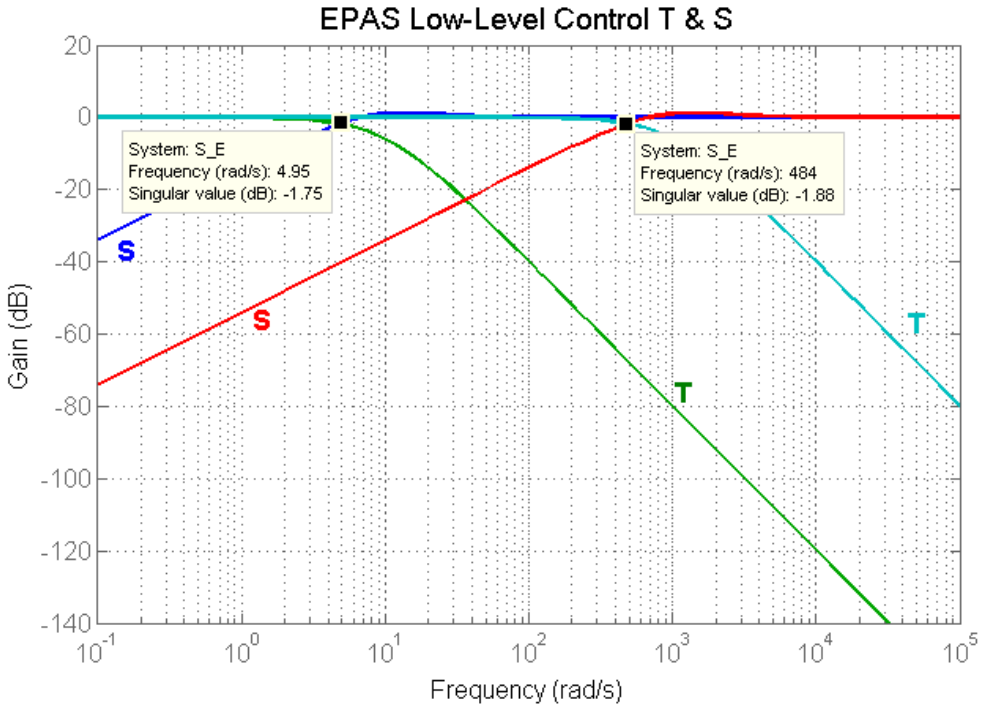

Figure 6-15: EPAS Low-Level Control T & S with different time constants

By selecting $\tau_E = 0.012$, the bandwidth of the closed loop control system of 40 rad/sec (6.37 Hz) is achieved, which is almost two times faster than the high-level control bandwidth (upper control loop) and 2.5 times slower than DC motor control (lower control loop) bandwidth and the low-level EPAS controller takes the form of

$$K_E = \frac{10.094(s + 0.0887)(s^2 + 6.167s + 70.95)}{s(s + 166.7)(s + 22.98)(s + 0.1108)} \qquad (6\text{-}27)$$

All the transfer functions of the EPAS low-level control system, including plant, Youla parameter, controller, sensitivity, open loop and closed loop transfer functions, are shown in Figure 6-16, confirm our previous conclusion for the control system performance.

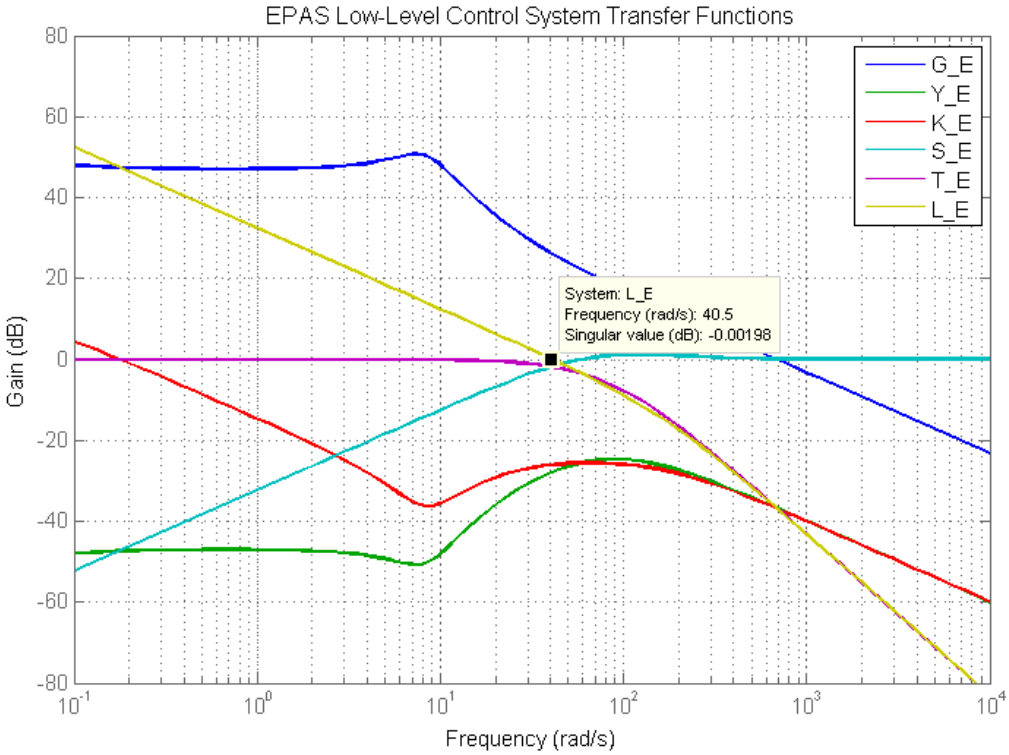

Figure 6-16: EPAS low-level control system transfer functions frequency responses ($\boldsymbol{\tau_E = 0.012}$)

To validate the performance of the control system, the comparison of uncontrolled and controller aligning moment response of the vehicle as result of unit step steering torque input at different speeds are shown in Figure 6-17. Note that the plant includes the bicycle vehicle model with steering dynamics and smart actuator DC motor controller. The vehicle exhibit a good reference following for an arbitrary aligning moment input at different speeds confirm the stability and performances of the closed loop control system.

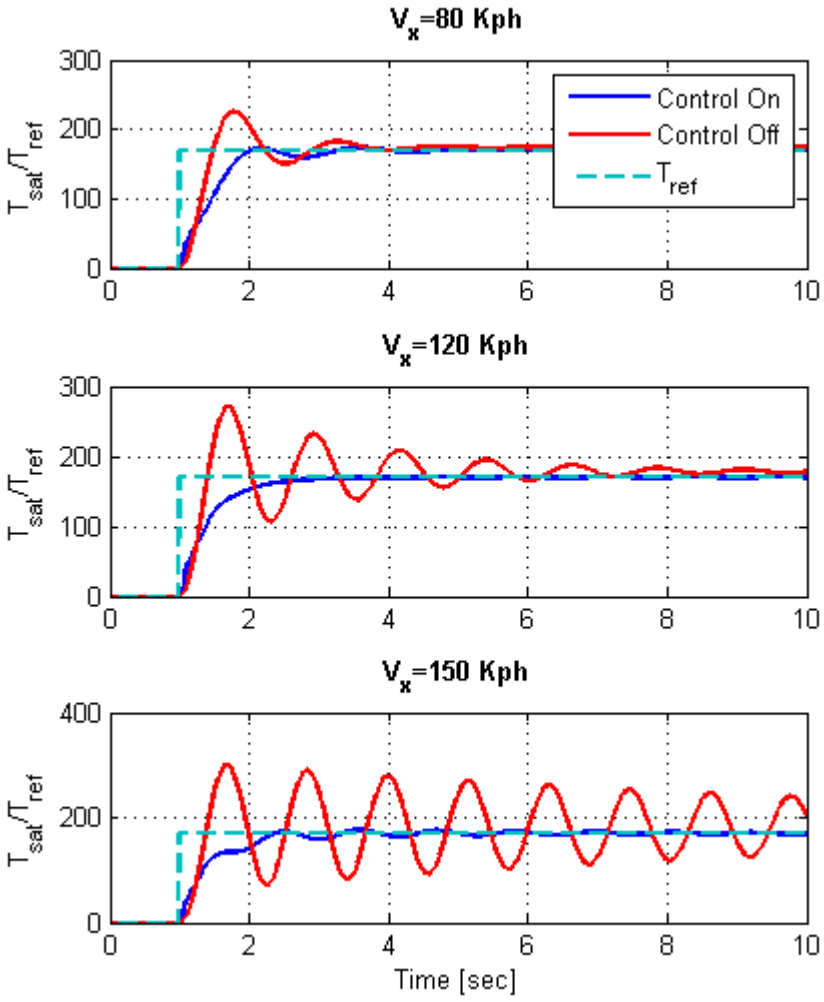

Figure 6-17: Comparison of controlled and uncontrolled T_{sat} at different speeds (nominal cornering stiffness)

6.2.4 EPAS Assist Control Design

The low-level EPAS control system, proposed in the previous section, will be utilised only in hazardous driving conditions to recover the vehicle stability by augmentation of (positive or negative) torque to the steering system. Based on the vehicle stability condition (i.e. understeering or oversteering situation), the augmented steering torque would be either in favour with or against the driver input torque, respectively. On the other hand, in normal driving conditions, the EPAS function is to provide driver comfort by reducing his/her steering torque effort, therefore, the provided assist torque is always conformed to the driver input torque.

The basic EPAS assist functionality is based on feed-forward control on driver input torque. In a production EPAS, the driver torque input is measured by a torque sensor, which is attached to the steering column and the augmented assist torque is generated by an electric motor attached to the EPAS column, rack or pinion through a reduction gear[36]. Therefore, the real EPAS assist control system should consider all the dynamics of the steering system and the attached electric motor and controller. Moreover, the value of assist gain is not fixed in a real EPAS, but it is a function of several parameters. The variable gain for assist torque is usually provided by employing a lookup table, so called EPAS boost curve (Heißing & Ersoy, 2011). Design of a boost curve is one of the important factors that determines the dynamic behaviour and feel of the Electric Power-Assisted Steering system and the vehicle (Ciarla, Cahouet, de Wit, & Quaine, 2012). A typical boost curve is a 2D lookup table, with driver steering torque and the vehicle speed as the two inputs, in which the amount of assist is reduced by increasing the vehicle speed, as shown in Figure 6-18. By reducing the amount of steering torque assist, the vehicle damping will increase, which helps the driver to maintain steering control on high-speed manoeuvring (Zaremba, Liubakka, & Stuntz, 1998).

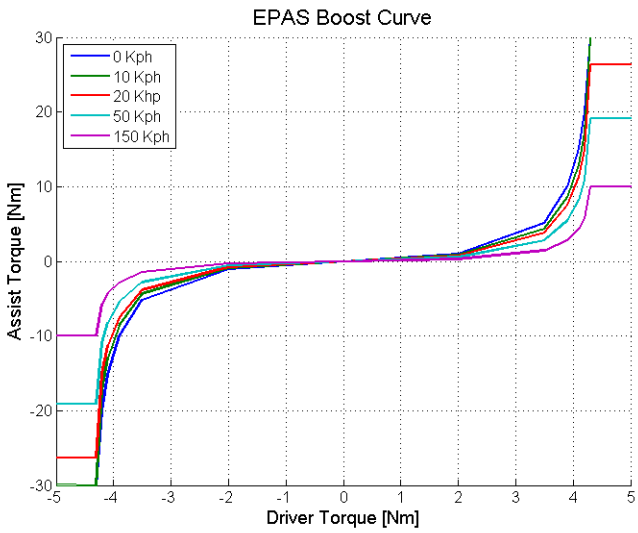

Figure 6-18: EPAS typical boost curve

In addition to the boost curve, it is possible to further alter the assist torque to enhance various steering behaviours such as returnability, damping, dynamic

[36] See Section 3.6.1 for more explanations of EPAS components and model.

response, friction compensation or steering feel improvement by employing different compensators (Badawy, Zuraski, Bolourchi, & Chandy, 1999; Kurishige, Tanaka, Inoue, Tsutsumi, & Kifuku, 2002). This can be provided by either additional Feed-forward compensation (Yih & Gerdes, 2005) or variety of feedback control loops (Sugitani, Fujuwara, Uchida, & Fujita, 1997, June) (Zaremba, Liubakka, & Stuntz, 1998) or a combination of feed-forward/feedback compensators (Mammar & Koenig, 2002).

In this thesis, a new closed looped control algorithm for EPAS assist function based on self-aligning moment feedback is proposed. Here, we employ the same control structure for low-level and electric motor closed loop controllers, as proposed in sections 6.2.2 and 6.2.3 before. However, unlike the hazardous driving condition, in which the reference torque to the low-level control system (T_{ref}) is determined by the high-level controllers and the control allocation scheme; the reference signal in normal and mild stability driving conditions is the output of the boost curve. The main block diagrams of the proposed EAPS assist control system are shown in Figure 6-19. The possibility of shaping the steering feel based on self-aligning moment feedback is one of the main advantages of the proposed control system.

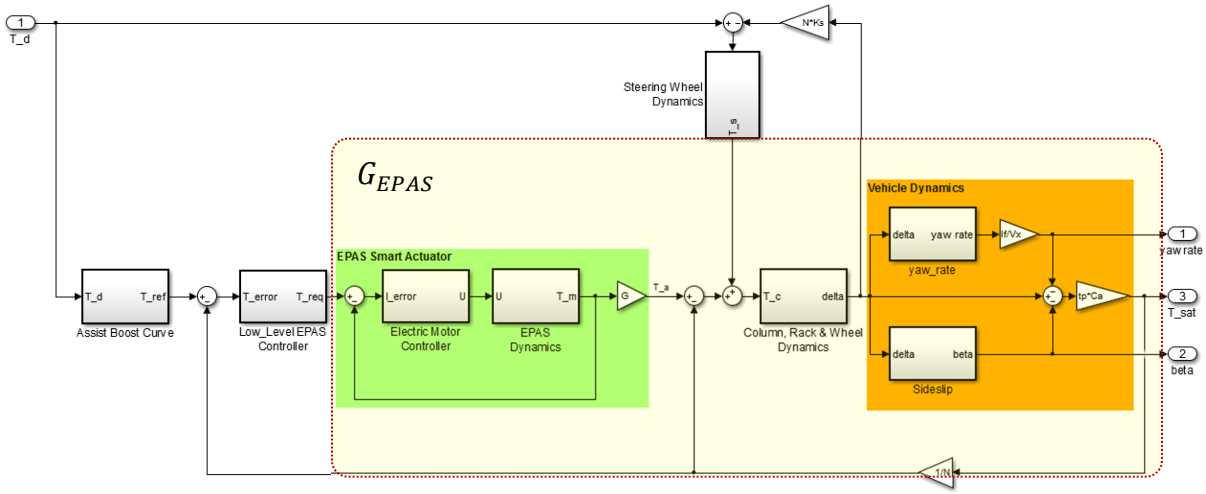

Figure 6-19: EPAS assist closed loop control system block diagram

It is worth to note that the proposed steering assist adjustment is only effective during steering turn at high-speed manoeuvres within the lateral acceleration bound between $0.4\mu g$ and $0.6\mu g$ (mild stability condition). Therefore, the mild stability requirements of the IVCS system, as specified in Chapter 2, are fulfilled.

6.2.5 EPAS Control Interface

In the normal and mild stability driving condition, the output of the boost curve could be directly fed to the EPAS low-level control system. However, in hazardous stability mode, the reference input to the low-level steering control is provided by the control allocation scheme. Recall, the output of the proposed control allocation scheme is tyre lateral force, which is not directly applicable to the low-level EPAS control system. In the proposed IVCS system, the lateral tyre force output is converted to the steering torque input via control interface block as shown in Figure 6-20[37].

As mentioned in Chapter 3, the self-aligning moment is the result of application of tyre forces at distances, so called mechanical and pneumatic trail. Mechanical trial is a function of wheel geometry and could be obtained from caster angle (Gillespie , 1992), whereas, the pneumatic trial is dependent on tyre deformation and road friction coefficient. As a first approximation, the pneumatic trail could be considered constant which is approximately equal to a quarter of the contact patch length (Pacejka, 2006). To derive a more accurate value for the pneumatic trail, one can employ the following general relation:

$$t_{p,i} = -\frac{M_{z,i}}{F_{y,i}} \tag{6-28}$$

where $M_{z,i}$ and $F_{y,i}$ are the self-aligning moment and lateral force of the tyre, respectively, and their values can be calculated from any known tyre model, such as Pacejka or brush model.[38]. In this dissertation, we select a simple model for pneumatic trial based on 'affine' formula, as introduced in section 3.4.2.1 (Hsu & Gerdes, 2008). A more precise model of the pneumatic trail may also be introduced by considering transient behaviour of the tyre (Pacejka & Sharp, 1991). It is worth to note that as this calculation will take place inside the (high-level) control loop, therefore any inaccuracy in the employed tyre model is considered as an uncertainty, and will be compensated by the robustness of the (high-level) control system.

[37] See Chapter 2 for more information about the control architecture of IVCS system.
[38] See Chapter 3 for more information about various tyre models.

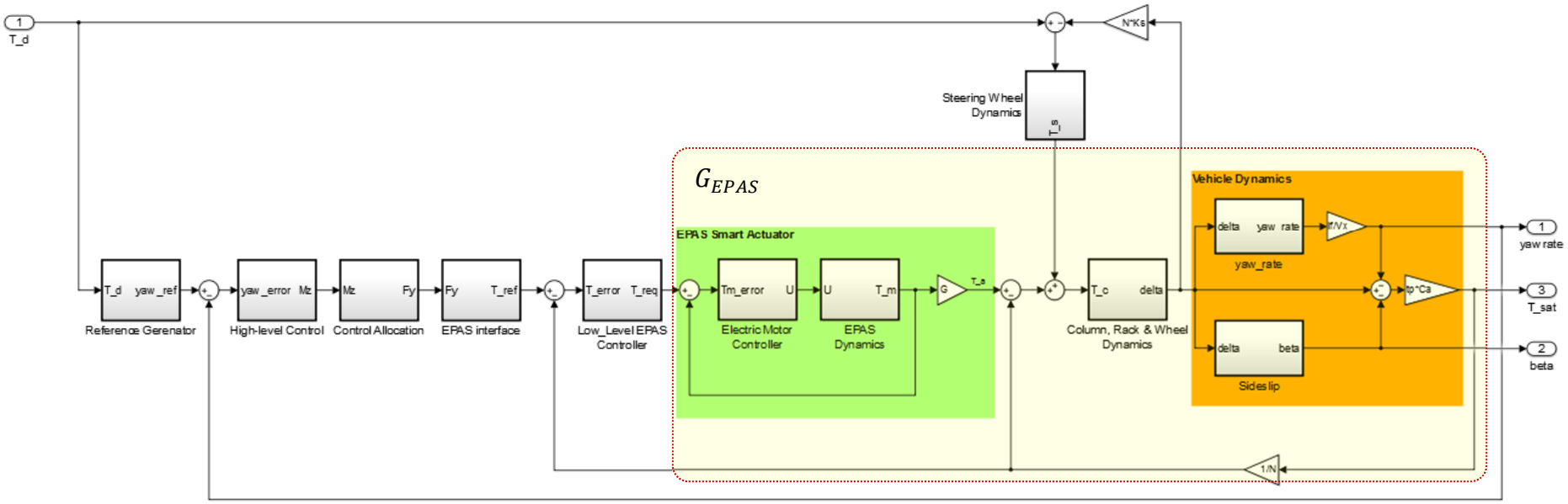

Figure 6-20: The complete EPAS control block diagram in stability mode

6.3 Brake Low-Level Control Design

In this thesis, it is assumed that the smart brake actuation (i.e. brake pressure control) is already provided by an off-the-shelf electro hydraulic brake (EHB) system, also called Sensotronic Brake Control (SBC), which has been developed by Daimler and Bosch (Gunther Plapp, 2001). By employing EHB, it is possible to continuously control the brake pressure for each individual wheel (Van Zanten, 2002). The relevant reference brake pressure for each wheel (to be generated by EHB system) is provided by the low-level control system for brake actuation.

6.3.1 EHB System Description

It is well known that in a conventional brake system, brake pressure is created by the driver pedal force via the master cylinder, amplified by vacuum booster and then distributed to the wheels by modulation of several on/off hydraulic valves (Robert Bosch GmbH, 2011). However, the EHB system concept is different from the conventional brake system, in the sense that the brake pressure is built-up by an electro-hydraulic pump to pressure between 140 and 160 Bar, stored in a gas diaphragm high-pressure reservoir and then supplied in each individual wheel by means of four continuous pressure modulators. These four pressure modulators consist of one inlet and one outlet valve, which are continuously controlled by an electronic control unit (Gunther Plapp, 2001). The main components and hydraulic circuit of EHB SBC system is schematically presented in Figure 6-21.

EHB is the first step towards complete brake by wire system (Van Zanten, 2002), as (normally) the master brake cylinder is detached from the brake circuit[39]. In normal braking, a position sensor and a pressure sensor, which is integrated to the master cylinder unit, measures how fast and how strongly the brake is actuated by the driver. The SBC control unit processes this information and generates the relevant control signals for the wheel pressure modulators. At the same time, a pedal travel simulator creates normal pedal feedback to the driver. However, in the case of stability intervention, the high-pressure reservoir supplies the required brake

[39] The Bosch SBC system is fail-safe, as the driver pedal force will be directly actuated the front brakes in case of system failure or when the system is turned off.

pressure quickly and precisely to the wheel brakes autonomously (i.e. without any driver involvement).

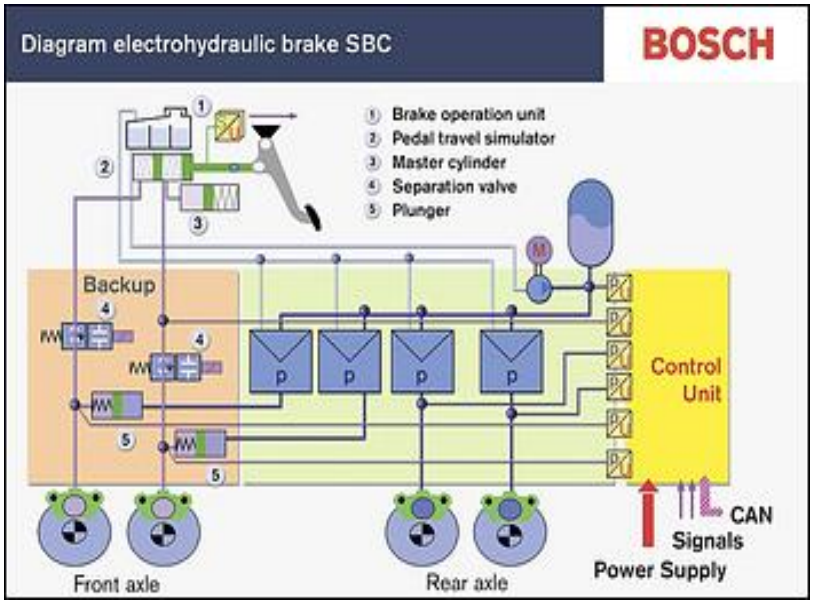

Figure 6-21: Schematic diagram of Bosch SBC system (Gunther Plapp, 2001)

In EHB system, individual wheel brake pressure (corresponding to front left, front right, rear left and rear right wheel braking) are measured by means of four pressure sensors. Either in the case of normal braking or of stability brake intervention, the desired brake pressure for each wheel is transmitted to the SBC control unit, which continually regulates the brake pressure on the individual wheels via the wheel pressure modulators. Having continuous control over brake pressure provides several advantages such as driver comfort as well as the possibility of fast and precise control over the tyres longitudinal force (and slip) (Schöner, 2004). Moreover, because there is no necessity for estimation of brake pressure at the wheels, the confidence level of the brake force estimation is higher than conventional active braking systems such as ABS or ESP (Van Zanten, 2002).

6.3.2 Low-Level Brake Control

Employing electro hydraulic brake system as smart brake actuator provides the possibility to control individual wheel brake line pressure to follow the desired target pressure continuously. This gives the opportunity of continuous control of the longitudinal slip on each wheel. In IVCS control structure, the low-level brake control

system is responsible for generating the required target pressure for each pressure control valve. As the brake pressure is regulated for each wheel individually (through EHB valve modulation unit), there are 4 independent inputs and 4 similar plants, and four similar SISO closed loop brake control systems exist in this architecture. Design of the low-level brake control system based on wheel slip feedback for one wheel ($i-th$ wheel) ,as shown in Figure 6-22, is presented in this section.

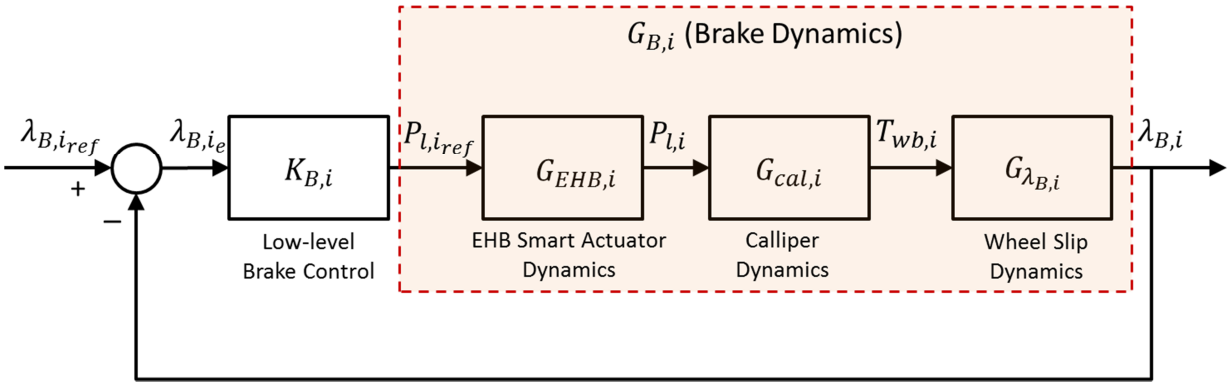

Figure 6-22: Low-Level Brake FB Control system

The starting point in designing a control system is to derive the plant dynamics model. Here the plant consists of a single corner wheel model. It consist of the ¼ of car mass[40] moving in x direction, with a single independent rotating wheel subject to braking torque $T_{wb,i}$ at the wheel hub (centre) and longitudinal force $F_{x,i}$ at the centre of tyre-ground contact patch, as shown in Figure 6-23.

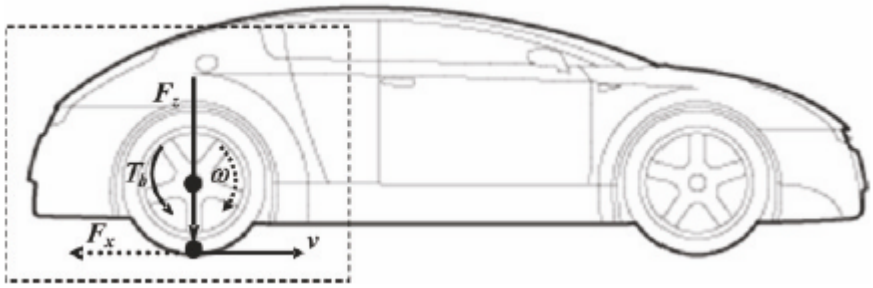

Figure 6-23: 1/4 Car Model (Savaresi & Tanelli, 2010)

[40] Single corner mass is usually assume ¼ of the total vehicle mass. However, the weight distributions on front and rear wheels are not the same in most vehicles, depending on the distance of the front and rear wheelbase from the vehicle centre of gravity and also dynamic weight transfer. See section 3.4.1 for more discussion on static and dynamics loads on each tyre. The effect of tyre normal load variation on control system performance are discussed and investigated in the following sections.

The equation of wheel dynamics, as described in section 3.6, is:

$$J_{y,i}\dot{\omega}_{R,i} = T_{wb,i} - R_{dyn,i}F_{x,i} \tag{6-29}$$

and the ¼ car dynamics in the longitudinal direction can be written as:

$$m_s\dot{V}_x = F_{x,i} \tag{6-30}$$

where m_s is the 1/4 car mass (as described above) and $\dot{V}_x$ is the vehicle longitudinal acceleration.

It should be noted that the ¼ car model relies on some simplifications. For example, the effect of suspension is ignored (i.e. coupling effect on normal loads among tyres due to pitch, roll and lateral dynamics are not considered). Furthermore, the wheel dynamic radius $R_{dyn,i}$ is assumed constant and straight-line braking is considered (i.e., the tyre lateral force due to camber angle γ and sideslip angle α is neglected); However, it is possible to include the effect of combined tyre slips into the model in a quite straightforward manner. This simple and effective model, which considers the major braking dynamics, is widely applied in active braking control system designs (Drakunov, Ozguner, Dix, & Ashrafi, 1995; Limpert, 2011).

The tyre slip ratio during braking $\lambda_{B,i}$ was defined as:

$$\lambda_{B,i} = \frac{R_{dyn,i}\omega_{R,i}}{V_{x,i}} - 1 \qquad (-1 \le \lambda_{B,i} \le 0\ ) \tag{6-31}$$

where $V_{x,i}$ is the forward speed of the tyre centre which is here assumed that is equal to vehicle longitudinal speed V_x.

Combining Eq. (6-29) with Eq. (6-31), the relationship between braking torque input and tyre slip output can be derived as:

$$\dot{\lambda}_{B,i} = -\frac{1}{V_x}\left(\dot{V}_x\left(\lambda_{B,i}+1\right) + \frac{R_{dyn,i}^2}{J_{y,i}}F_{x,i}\right) + \frac{R_{dyn,i}}{J_{y,i}V_x}T_{wb,i} \tag{6-32}$$

Substituting $\dot{V}_x$ from Eq. (6-30) into Eq. (6-32), the dynamics of the system can be formulated as a first order model of the wheel slip dynamics as:

$$\dot{\lambda}_{B,i} = -\frac{1}{V_x}\left(\frac{\left(\lambda_{B,i}+1\right)}{m_s}+\frac{R_{dyn,i}^2}{J_{y,i}}\right)F_{x,i}+\frac{R_{dyn,i}}{J_{y,i}V_x}T_{wb,i} \tag{6-33}$$

Eq. (6-33) is a nonlinear function of two state variables V_x and $\lambda_{B,i}$ (recall that the tyre longitudinal force $\left[F_{x,i}\left(\lambda_{B,i}\right)=\mu_{x,i}\left(\lambda_{B,i}\right)F_{z,i}\right]$ is a nonlinear function of slip $\lambda_{B,i}$).

To be able to design a linear control system, one could linearise Eq. (6-33) around nominal operating points $V_{x,n}$ and $\lambda_{B,i,n}$. Considering $\Delta\lambda_{B,i}=\lambda_{B,i}-\lambda_{B,i,n}$ and $\Delta V_x = V_x - V_{x,n}$ and $\Delta T_{wb,i}=T_{wb,i}-T_{wb,i,n}$; the linear transfer function for plant dynamics (from brake torque input to tyre slip output) can be derived by application of first order Taylor series expansion as (Savaresi & Tanelli, 2010)

$$G_{\boldsymbol{\lambda_{B,i}}}(\mathrm{s})=\frac{\lambda_{B,i,n}}{T_{wb,i,n}}=\frac{R_{dyn,i}}{J_{y,i}V_{x,n}}\left[\frac{1}{s+\frac{\dot{\mu}_{x,i,n}\left(\lambda_{B,i,n}\right)F_{z,i}}{m_sV_{x,n}}\left(\left(1+\lambda_{B,i,n}\right)+\frac{m_sR_{dyn,i}^2}{J_{y,i}}\right)}\right] \tag{6-34}$$

where $\dot{\mu}_{x,i,n}\left(\lambda_{B,i,n}\right)=\left.\frac{\partial\mu_{x,i}}{\partial\lambda_{B,i}}\right|_{\lambda_{B,i,n}}$,represents the slop of the $\mu_{x,i}$ curve around a nominal operating point. It should be noted that calculation of $\dot{\mu}_{x,i,n}$ in Eq.(6-34) is not dependent on any specific tyre model. It could be obtained either by differentiation of a tyre model, such as Burckhardt tyre model as cited in the literatures (see (Kiencke & Nielsen, 2005) for example), or by implementation of an online algorithm to detect the sign of the friction curve slope, which is suitable for practical applications (Van Zanten, Erhardt, Pfaff, Kost, Hartmann, & Ehret, 1996; Savaresi & Tanelli, 2010).

The linearised plant (6-34) (herein after called plant) is of first order in form of:

$$G_{\boldsymbol{\lambda_{B,i}}}(\mathrm{s})=\frac{k_i}{s+p_i} \tag{6-35}$$

with a gain of:

$$k_i=\frac{R_{dyn,i}}{J_{y,i}V_{x,n}} \tag{6-36}$$

and a single pole at:

$$p_i = -\frac{\dot{\mu}_{x,i,n} F_{z,i}}{m_s V_{x,n}} \left(\left(1 + \lambda_{B,i,n}\right) + \frac{m_s R_{dyn,i}^2}{J_{y,i}} \right) \tag{6-37}$$

To derive a control oriented linear plant model, it is essential to select an appropriate operating point, where the plant is being linearised around it. By studying the slip dynamics transfer function, Eq. (6-34), one can conclude that the tyre normal load, $F_{z,i}$, the vehicle velocity , $V_{x,n}$, and the road condition (which is reflected on $\dot{\mu}_{x,i,n}$) are the main parameters that are considerably changing during braking actuation time period[41]. Therefore, to investigate the variation of plant dynamics, it is required to derive the maximum and minimum values of longitudinal speed V_x , $F_{z,i}$and $\dot{\mu}_{x,i}$ in the plant dynamics transfer function, Eq. (6-34).

As V_x is always positive (forward driving assumption), its variation cannot make the plant unstable, but, it will impact the value of gain (k_i). On the other hand, the change of $F_{z,i}$ and $\dot{\mu}_{x,i,n}$ will move the location of pole on s plane, which will have an effect on the stability of plant. More specifically, the effect of $\dot{\mu}_{x,i,n}$ variation on the plant dynamics is significant as it can make the plant unstable, as discussed below.

Considering a typical longitudinal tyre force/slip curve, as shown in Figure 6-24, one can conclude from Eq. (6-37) that the open loop transfer function $G_{\boldsymbol{\lambda_{B,i}}}(\mathrm{s})$ is stable before slip peak (as $\dot{\mu}_{x,i,n} > 0$, therefore $p_i < 0$) , and become unstable when the slip goes beyond the peak point (as $\dot{\mu}_{x,i,n} < 0$, therefore $p_i > 0$). Moreover, when the linearisation point is close to the peak of the curve, i.e. $\dot{\mu}_{x,i,n} \cong 0$, the plant becomes a pure integrator:

$$G_{\boldsymbol{\lambda_{B,i}}}(\mathrm{s}) = \frac{k_i}{s} \tag{6-38}$$

[41] By other word, it is assumed that the vehicle mass, wheel inertia and wheel dynamic radius are constant.

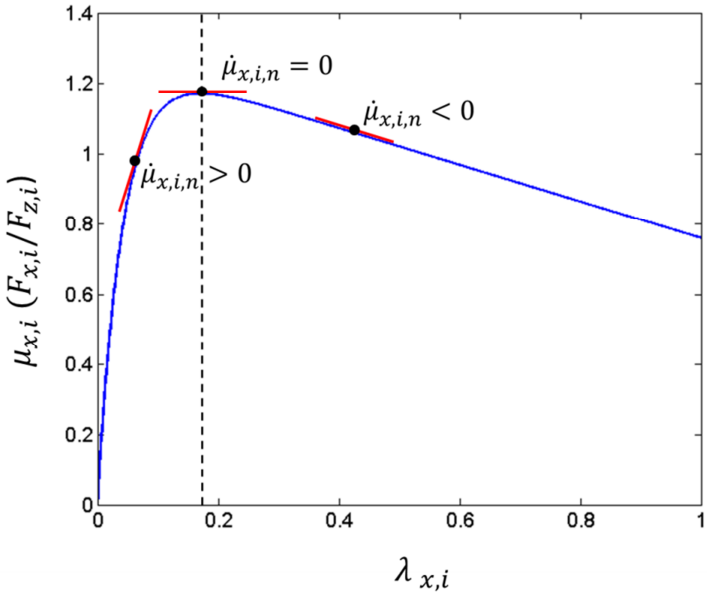

Figure 6-24: slop of $\mu(x,i)$ at different operating points

Therefore, the worse case operating points are corresponding to high longitudinal speed V_x , low normal load $F_{z,i}$ and smallest positive slope of $\mu_{x,i}$ which is equivalent to the smallest distance of stable pole from imaginary axis in s plane.

To obtain the value of tyre friction slope, $\dot{\mu}_{x,i}(\lambda_B)$, one can employ the Burckhardt tyre model. Recall from section 2.4.1, the relationship between tyre slip and normalised longitudinal tyre force (based on Burckhardt tyre model) can be defined as:

$$\mu_{x,i}(\lambda_{B,i}) = \frac{F_{x,i}(\lambda_{B,i})}{F_{z,i}} = c_1\left(1 - e^{-c_2\lambda_{B,i}}\right) - c_3\lambda_{B,i} \tag{6-39}$$

where c_1, c_2 and $c_3$are constants, defined for different road surfaces. Therefore

$$\dot{\mu}_{x,i}(\lambda_{B,i}) = \frac{\partial\mu_{x,i}(\lambda_{B,i})}{\partial\lambda_{B,i}} = c_1c_2e^{-c_2\lambda_{B,i}} - c_3 \tag{6-40}$$

By investigating different road surfaces at different slips, one can conclude that the maximum value of $\dot{\mu}_{x,i}$happens on dry asphalt at $\lambda_{B,i} = 0$ with the value of 30.2 and the minimum magnitude of $\dot{\mu}_{x,i}$ happens with the value of -0.658 on dry cobblestone at slip $|\lambda_{B,i}| = 1$,. Therefore the slip slope bound is:

$$-0.658 \leq \dot{\mu}_{x,i} \leq 30.2 \tag{6-41}$$

The variations of $\dot{\mu}_{x,i}$ as a function of tyre slip $|\lambda_{B,i}|$ for different road surfaces are shown in Figure 6-25. It is important to note that the peak point of $\mu_{x,i}$ friction curve (correspond to $\dot{\mu}_{B,i} = 0$) are different on various surfaces. This means that a tyre on snow surface reaches to its maximum achievable capacity (i.e. saturated) at a very low slip, however, it is saturated at a relatively high slip, ($\lambda_{B,i} = 0.39$) on cobblestone surface.

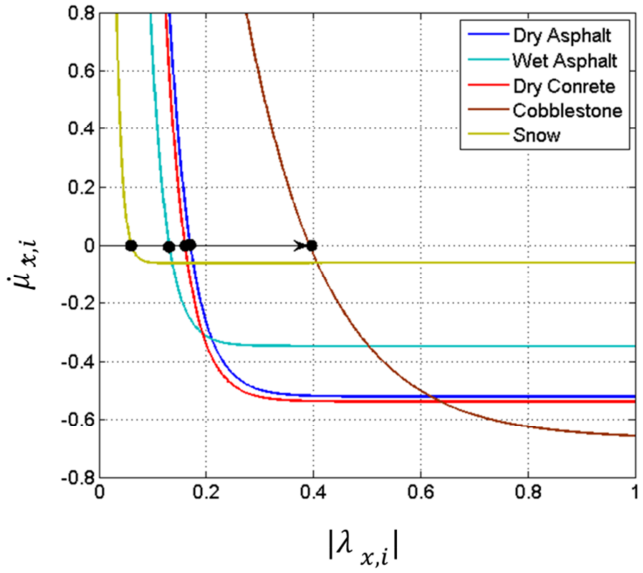

Figure 6-25: The magnitude of μ slop at different surfaces

Recall from section 3.4.1, the tyre normal load on each wheel $F_{z,i}$ is a function of the vehicle weight distribution (static load) and load transfer due to longitudinal and lateral accelerations (dynamic loads), as described by Eq. (3-50). Considering the vehicle parameters, as indicated in appendix B, and assuming the extreme magnitude of $a_x = -g$ and $a_y = g$, the maximum normal force will be applied on the front right tyre as:

$$F_{z_{max}} = F_{z,2} = 0.823\, mg = 9898.3\, N \approx 10\, KN$$

The same conclusion can be made when $a_y = -g$, however, the maximum normal force will be applied to front left tyre ($F_{z,1}$), instead. Therefore the normal force range limit is:

$$0 \leq F_{z,i} \leq 10\, KN \qquad (6\text{-}42)$$

Finally, it is assumed that the longitudinal velocity range (in which the safety brake actuation will be activated) is between 10 to 50 m/s, i.e.

$$10 \leq V_x \leq 50\ m/s \tag{6-43}$$

Employing the above operational limits of $\dot{\mu}_{x,i}$, $F_{z,i}$ and V_x, , the maximum and minimum values of gain and pole of the plant (for the vehicle with the values indicated in appendix B) can be obtained from Eqs. (6-36) and (6-37), respectively. By investigating the possible magnitudes of the plant's gain and pole locations, it is concluded that the plant dynamics is highly sensitive to its operating conditions. Therefore, selection of appropriate nominal operating point plays an important role in design of the proposed control system.

Finally, it is worth pointing out that the complete brake plant model (i.e. from pressure input to wheel slip output, as shown in Figure 6-22), includes the slip dynamics, the calliper dynamics and the EHP smart actuator dynamics. Recall from section 3.6.3, the required barking torque about the wheel spin axis and the subsequence braking force is produced by application of hydraulic brake pressure at the brake callipers. The relationship between brake line pressure $P_{l,i}$ and wheel (bake) torque $T_{wb,i}$ was defined as:

$$T_{wb,i} = K_{b,i} P_{l,i} \left(\frac{1}{\tau_{cal} s + 1} \right) \tag{6-44}$$

where $K_{b,i}$ and τ_{cal} are the calliper gain and time constant, respectively. Taking into consideration the EHB smart actuator dynamics $G_{EHB,i}(\mathrm{s})$ as a stable first order transfer functions, the calliper dynamics $G_{Cal,i}(s)$ and EHB dynamics $G_{EHB,i}(\mathrm{s})$ are:

$$G_{cal} = \frac{T_{wb,i}}{P_{l,i}} = \frac{K_{b,i}}{\tau_{cal} s + 1} \tag{6-45}$$

$$G_{EHB,i}(\mathrm{s}) = \frac{1}{\tau_{EHB} s + 1} \tag{6-46}$$

where τ_{EHB} is the EHB time constant. Therefore, The complete plant dynamics, takes the form of:

$$G_{B,i}(\mathrm{s}) = G_{\lambda_{B,i}}(\mathrm{s}) G_{EHB,i}(\mathrm{s}) G_{Cal,i}(\mathrm{s}) \tag{6-47}$$

$$G_{B,i}(s) = \left(\frac{k_i}{s + p_i}\right)\left(\frac{K_{b,i}}{\tau_{cal}s + 1}\right)\left(\frac{1}{\tau_{EHB}s + 1}\right)$$

$$= \frac{k_i \times K_{b,i}}{(s + p_i)(\tau_{cal}s + 1)(\tau_{EHB}s + 1)}$$

Bode diagram of the plant dynamics at different longitudinal slip is plotted in Figure 6-26, assuming the vehicle and brake parameters as indicated in appendix B, $\tau_{cal} = \tau_{EHB} = 0.1\ sec$, (Limpert, 2011) dry asphalt, $F_{z,i} = 10KN$ and $V_x = 50\ m/s$. It is clear that the plant is stable at the slip values before $\lambda_{x,i} = 0.16$ and become unstable at higher slips. As discussed before, the tyre slip of $\lambda_{x,i} = 0.16$ corresponds to the peak point of the tyre friction curve on dry asphalt, where $\dot{\mu}_{x,i} = 0$ (see Figure 6-24 and also Figure 6-27).

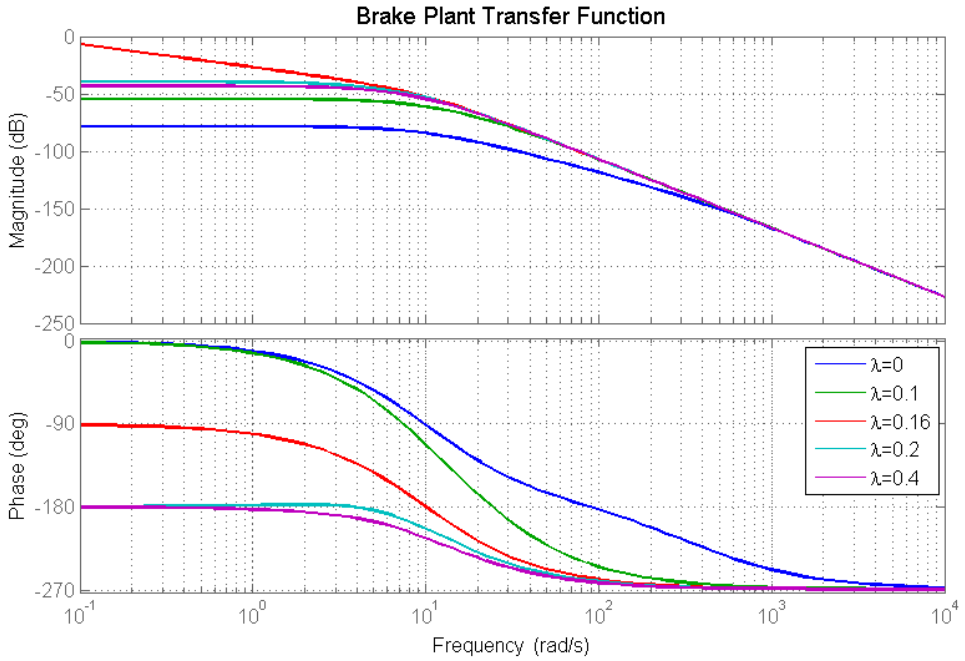

Figure 6-26: Plant dynamics $G_{B,i}$ for different slips (dry asphalt, $F_{z,i} = 10KN$ and $V_x = 50\ m/s$)

Due to the fact that the dynamics of the system is changing considerably during its operational envelope, and there are several uncertainties that exist in the system (such as brake pad coefficient of friction and so on); it is necessary to employ a feedback control system, as shown in Figure 6-22, to provide stability as well as good performance for the system at all operating conditions.

Because of the complex and variable dynamics of system, design of a slip control system is a challenging task. Several linear and nonlinear control design approaches have been proposed in the literatures, ranging from linear and nonlinear PID control system (Jiang & Gao, 2001), fuzzy logic (Mauer, 1995), gain scheduling (Johansen, Petersen, Kalkkuhl, & Ludemann, 2003) to some sort of nonlinear methodologies such as sliding mode (Drakunov, Ozguner, Dix, & Ashrafi, 1995) and Lyapunov-based (Savaresi & Tanelli, 2010) control design approaches. However, it is worth noting that most of the proposed brake controllers, which can be found in the published literatures, consider wheel slip (Eq. (6-33)) (and/or angular velocity) differential equations as the plant model, without taking the complete dynamics of the brake system (such as calliper and value dynamics and their constraints) into consideration. Interestingly, it is shown in (Savaresi & Tanelli, 2010) that it is impossible to employ a single linear controller (such as PID) for complete brake dynamics to provide stability and performance at all operational conditions.

In this dissertation, a novel closed loop wheel slip control system based on Youla parameterisation approach is proposed. One of the distinctions of the proposed controller is that, considering all the existing dynamics and constraints of the brake system, it provides stability and a reasonable control performance over the whole range of operating conditions of the system.

Investigating the complete (linearised) plant dynamics, as described by Eq. (6-47), one can conclude that the plant dynamics consists of three first order transfer functions. We take the Youla parameter as the inverse of the plant transfer function at a nominal operating point, $G_{B,i,n}$, multiply to three stable first order filters with adjustable poles corresponding to the three dynamics exist in the system, such as:

$$Y_{B,i} = \frac{1}{G_{B,i,n}}\left[\frac{1}{(\tau_1 s+1)(\tau_2 s+1)(\tau_3 s+1)}\right], \quad \tau_1, \tau_2, \tau_3 > 0 \qquad (6\text{-}48)$$

By selecting a stable nominal plant $G_{B,i,n}$, the proposed Youla transfer function is stable (and minimum phase), therefore, internal stability of the feedback system is guaranteed[42]. The tuneable parameters τ_4, τ_5 and τ_6 can be employed to shape of

[42] see section 4.4.1 for proof of this statement.

the closed loop transfer functions $S_{B,i}$and $T_{B,i}$ and control system bandwidth such that it could deal with plant dynamics uncertainties.

Recall, $G_{B,i,n}$, is the linearised transfer function of plant dynamics at a nominal operating point where the nonlinear differential equation of the slip dynamics was linearised around it. As explained before, the dynamics and stability of the plant is highly dependent on its parameters; therefore, selecting different operating points results in Youla parameters (and controllers) with very different behaviours. To obtain an appropriate plant dynamics, $G_{B,i,n}$, (for our proposed control design approach), the nominal operating point for $\dot{\mu}_{x,i,n}$ should be selected at a slip value, $\lambda_{x,i,n}$, where the tyre friction curve $\mu_{x,i}$ is near to its peak value but is in stable region (i.e $\dot{\mu}_{x,i} > 0$). Note that the wheel slip value corresponding to the abscissa of the maximum of $\mu_{x,i}$is different at various road surfaces (see Figure 6-27). For example, if we select dry asphalt $\mu_{x,i}$ curve, the maximum slip where the plant is stable is limited to $\lambda_{x,i} = 0.16$, however, employing cobblestone friction curve lead to a stable plant up to $\lambda_{x,i} = 0.39$, as marked in Figure 6-27.

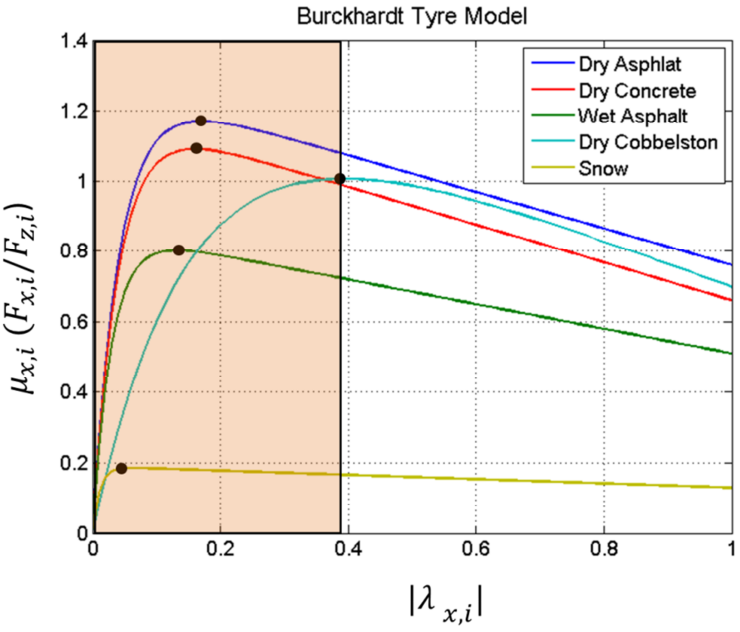

Figure 6-27: longitudinal friction curve

The complementary sensitivity $T_{B,i}$ and sensitivity $S_{B,i}$ transfer functions are:

$$T_{B,i} = Y_{B,i} \times G_{B,i,n} = \frac{1}{(\tau_1 s + 1)(\tau_2 s + 1)(\tau_3 s + 1)} \qquad (6\text{-}49)$$

$$S_{B,i} = 1 - T_{B,i,n} = \frac{(\tau_1 s + 1)(\tau_2 s + 1)(\tau_3 s + 1) - 1}{(\tau_1 s + 1)(\tau_2 s + 1)(\tau_3 s + 1)} \quad (6\text{-}50)$$

The controller transfer function can be derived as:

$$K_{B,i} = \frac{Y_{B,i}}{S_{B,i}} = \frac{1}{G_{B,i,n}[(\tau_1 s + 1)(\tau_2 s + 1)(\tau_3 s + 1) - 1]} \quad (6\text{-}51)$$

Taking the nominal operating points as: dry asphalt friction curve (Burckhardt tyre model), $\lambda_{x,i,n} = 0.09$, $F_{z,i,n} = 1/4mg\ N$ and $V_{x,n} = 10\ m/s$, , $\tau_{EHB} = \tau_{cal} = 0.1\text{sec}$ and $\tau_1 = \tau_2 = \tau_3 = \tau_B$; the control system transfer functions (for the vehicle parameters as indicated in appendix B) can be derived as:

$$G_{B,i} = \frac{5.6838}{(s + 177)(s + 10)^2} \quad (6\text{-}52)$$

$$T_{B,i} = \frac{1}{(\tau_B s + 1)^3} \quad (6\text{-}53)$$

$$S_{B,i} = \frac{s(\tau_B^3 s^2 + 3\tau_B^2 s + 3\tau_3)}{(\tau_B s + 1)^3} \quad (6\text{-}54)$$

$$Y_{B,i} = \frac{0.1759(s + 177)(s + 10)^2}{(\tau_B s + 1)^3} \quad (6\text{-}55)$$

$$K_{B,i} = \frac{0.1759(s + 177)(s + 10)^2}{s(\tau_B^3 s^2 + 3\tau_B^2 s + 3\tau_B)} \quad (6\text{-}56)$$

$$L_{B,i} = \frac{1}{s(\tau_B^3 s^2 + 3\tau_B^2 s + 3\tau_B)} \quad (6\text{-}57)$$

To shape the close loop response of the system, tuning parameter τ_B can be employed. The magnitude Bode plot of $T_{B,i}$ and $S_{B,i}$ transfer functions for two different values of τ_B time constant are shown in Figure 6-28. The system bandwidth increase by increasing the time constant, however, the peak values of S and T transfer functions (M_S and M_T) are less than 2db so the 6db gain margin is guaranteed which means that good control performance is met. Moreover, the

crossover gain is less than zero which means the minimum of 60° phase margin is also guaranteed[43].

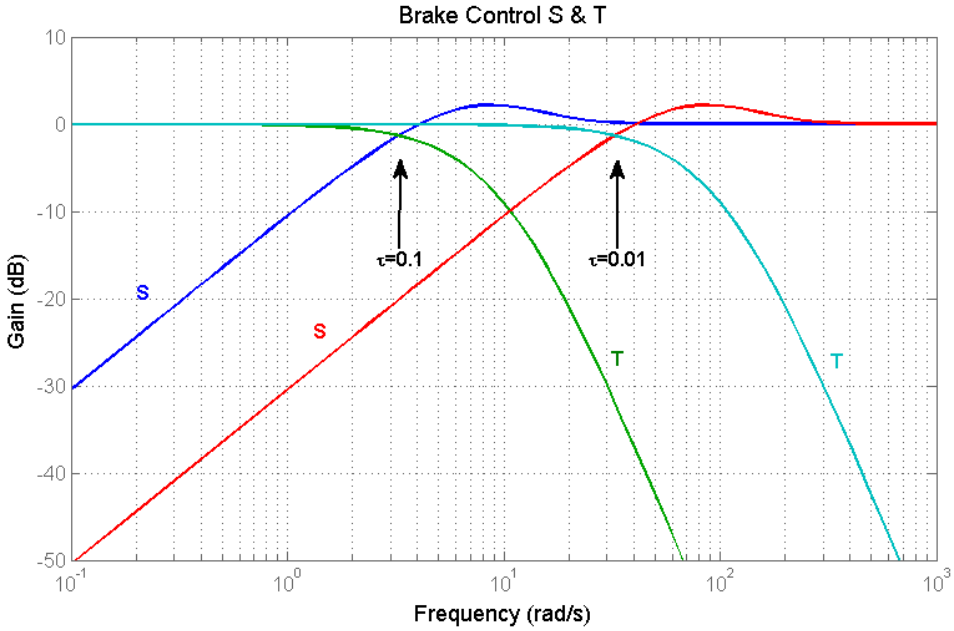

Figure 6-28: Low-Level Brake Control System S & T

By selecting $\tau_B = 0.0085$, the low-level brake controller takes the form of:

$$K_{B,i} = \frac{2.1487e5(s+9.41)(s+10)^2}{s(s^2+352.9s+4.152e4)} \qquad (6\text{-}58)$$

The bandwidth of the system is 38.5 rad/sec which is almost equal to the bandwidth of the low-level EPAS control system, as presented in section 6.2.3. By setting equal bandwidths for the two low-level control systems, we make sure that the dynamic responses of the steering and brake control systems behave coherently, when they are working simultaneously. This novel control solution addresses one of the main challenges in control allocation of overactuated systems to deal with actuators that have different dynamic behaviours. (Oppenheimer, Doman, & Bolender, 2011).

All the transfer functions of the brake control low-level control system, including plant, Youla parameter, controller, sensitivity, open loop and closed loop transfer functions, are shown in Figure 6-29, confirm our previous conclusion for the control system performance.

[43] See Chapter 4 for more detail discussion on control performance criteria.

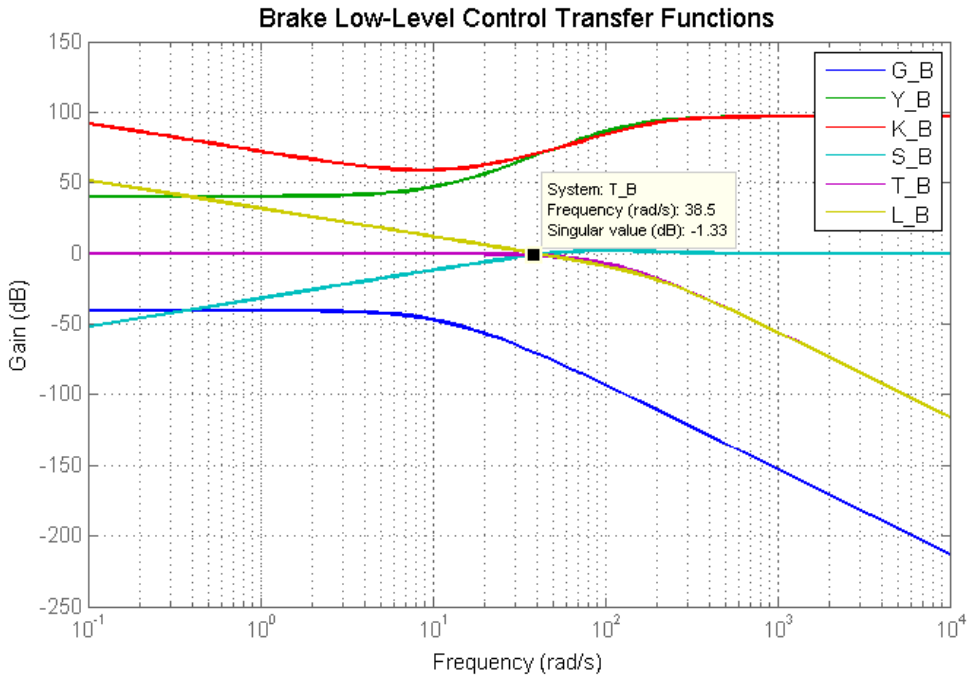

Figure 6-29: Frequency response of the low-level brake control transfer functions

To investigate the behaviour of the control system in time domain, the response of the closed loop control system subject to unit step input at nominal operating point is shown in Figure 6-30. The result confirms proper underdamped dynamic response of the control system, including its stability and performance.

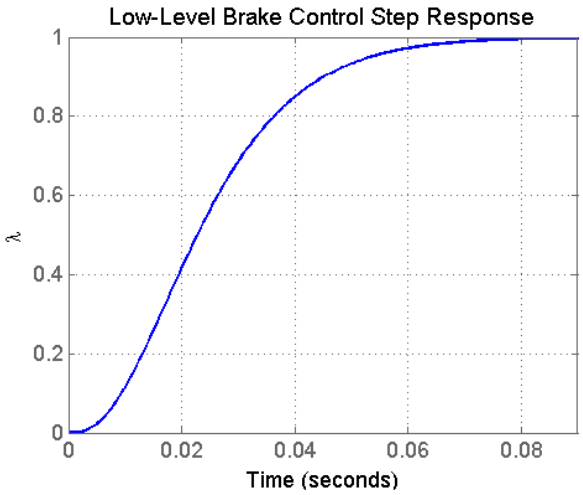

Figure 6-30: Unit step response of the brake low-level control at nominal operating point

It is worth mentioning that the proposed controller was designed based on the linearised plant transfer function at a nominal operating condition (dry asphalt friction curve (Burckhardt tyre model), $\lambda_{x,i,n} = 0.09$, $F_{z,i,n} = 1/4mg\ N$ and $V_{x,n} = 10\ m/s$). However, the dynamics of the plant is highly sensitive to variation of the parameters such as road surfaces, tyre slip, vehicle velocity and tyre normal forces, as discussed before. More importantly, increasing the tyre slip (above the peak point of tyre friction cure) make the plant unstable. To investigate the stability and robustness of the control system at all its operational envelope, the response of closed loop brake control system subject to slip step input at different operational conditions and surfaces are plotted in Figure 6-31

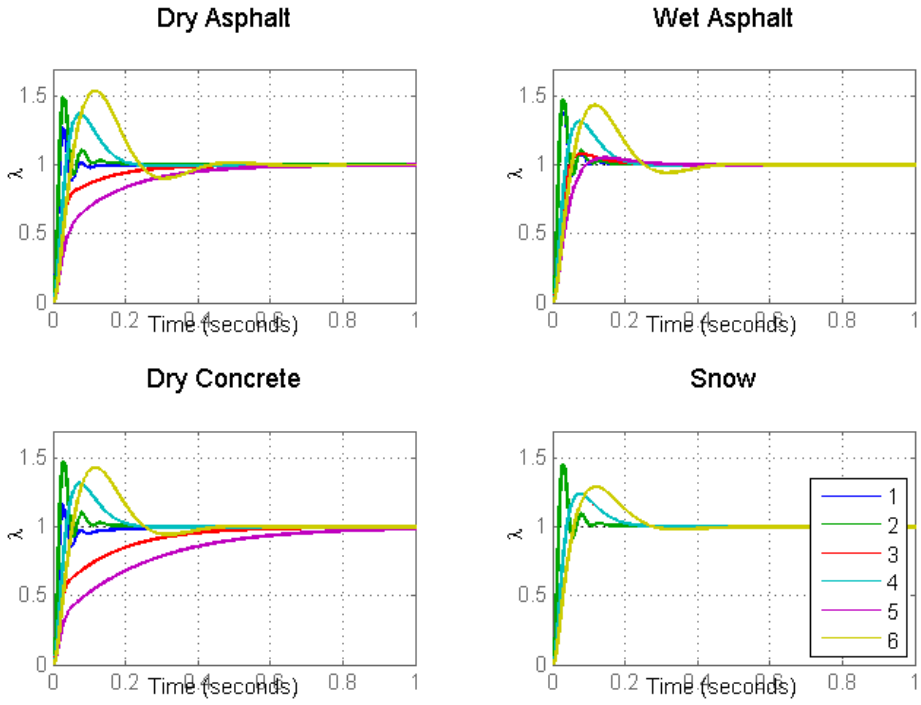

Figure 6-31: Brake control step response at various operational conditions

1) $\boldsymbol{V_x = 10\ m/s, F_{z,i} = 1\ KN, \lambda_{x,i} = 0.1}$

2) $\boldsymbol{V_x = 10\ m/s, F_{z,i} = 1\ KN, \lambda_{x,i} = 0.5}$

3) $\boldsymbol{V_x = 30\ m/s, F_{z,i} = 5\ KN, \lambda_{x,i} = 0.1}$

4) $\boldsymbol{V_x = 30\ m/s, F_{z,i} = 5\ KN, \lambda_{x,i} = 0.5}$

5) $\boldsymbol{V_x = 50\ m/s, F_{z,i} = 10\ KN, \lambda_{x,i} = 0.1}$

6) $\boldsymbol{V_x = 50\ m/s, F_{z,i} = 10\ KN, \lambda_{x,i} = 0.5}$

Interestingly, the controller can stabilise the closed loop system on different surfaces and at all nominal conditions, even in the worse-case conditions in which the plant is

unstable (i.e. at tyre high slip and high normal load, and vehicle low longitudinal velocity). Meanwhile, the performance of the control system exhibits a sizable variation (from underdamped to overdamped (oscillatory) behaviour). Moreover, the settling time of the system range from few millisecond to one second, depending also on the vehicle speed and normal load. This is due to utilising a fixed structure controller for the whole ranges of the system operations, at which the dynamics of the plant is changing considerably. However, considering the fact that the controller can stabilise the plant at all conditions and track the reference value within a few millisecond in most cases (except in worse case scenarios, which rarely happen in reality), the utilisation of one fixed structure controller could be justified.

To validate the control system in a more realistic plant dynamics, a single wheel model, as described by Eq. (6-29) and (6-30), in conjunction with the EHB and calliper dynamics is constructed in Simulink® environment. The brake actuator constraint is also included in the model, by limiting the pressure command to EHB within the range of [0,200] bar. The Simulink® model of the plant and the complete closed loop low-level brake control system are shown in Figure 6-32 and Figure 6-33, respectively.

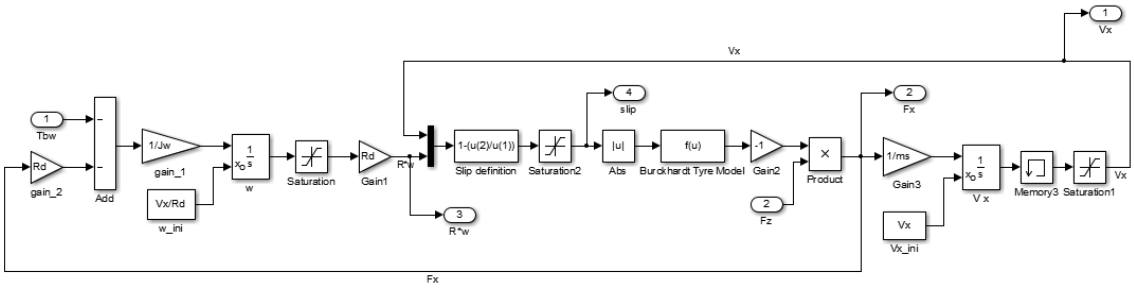

Figure 6-32: Single wheel model including wheel dynamics

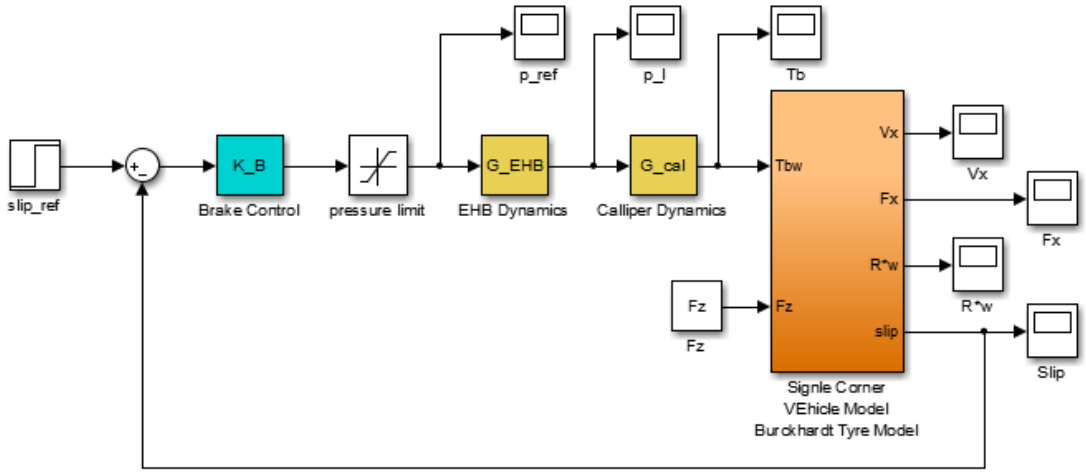

Figure 6-33: Closed loop low-level brake control with complete brake dynamics and (single wheel) vehicle dynamics

The results of simulations subject to two different driving conditions on dry asphalt surfaces are presented in Figure 6-34. The first driving condition ($V_x = 10\,m/s,\ F_{z,i} = mg/4\,N,\ and\ \lambda_{x,i} = 0.05$) corresponds to low vehicle speed and nominal tyre load where the slip is below its threshold limit, therefore the plant is stable. In this scenario, the slip reach to its target ($\lambda_{x,i} = 0.05$) within 1 sec with an overdamped response and the vehicle stops within 2.3 sec. The commanded brake pressure and the tyre longitudinal force are within their limits. The second driving condition ($V_x = 50\,m/s,\ F_{z,i} = mg/2\,N,\ and\ \lambda_{x,i} = 0.25$) corresponds to a severe driving condition where the tyre is operating beyond its saturation limit, therefore the plant is highly unstable. It could be observed that the control system can stabilise the plant even at slips greater than 0.16, however, due to actuator saturation, the system exhibits an overshoot, but it finally could track the reference value within 3 sec. The slip overshoots, which is clearly reflected from the difference between vehicle speed and tyre longitudinal speed ($R_{dyn} \times \omega_{R,i}$), is generated because of the brake pressure has reached its limit of 200 bar. In spite of the fact that the tyre slip is in unstable region and also brake pressure is saturated; the control system is stable and can reduce the vehicle speed from 25 m/s to 0 within 4 sec (without locking the wheel).

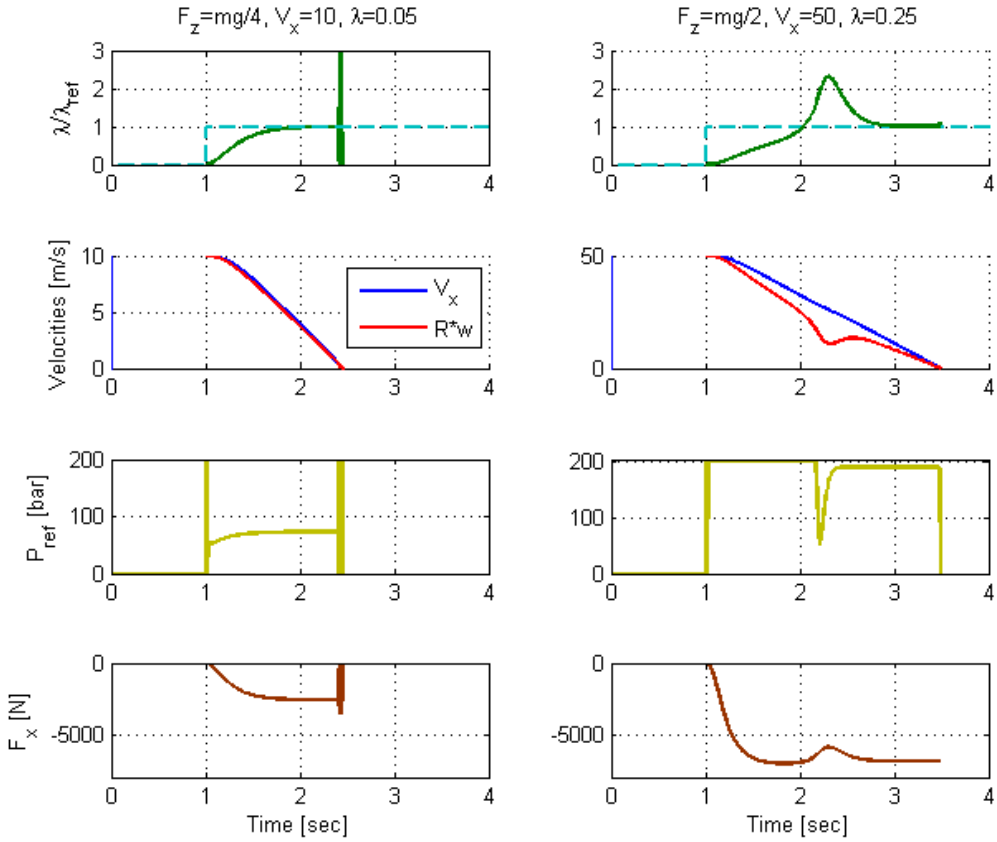

Figure 6-34: brake control step response, dry asphalt

To investigate the performance of the control system on low mu surfaces, a similar simulation is performed with the same operational conditions, but on snow. The simulation results, as shown in Figure 6-35, confirm the stability and performance of the control system at low speeds. Moreover, the control system can stabilise the plant and provide acceptable tracking (but with high overshoot) even in severe driving conditions of $Vx = 15$ m/s (54 Kph) on snow (which is far beyond an achievable driving condition in practice).

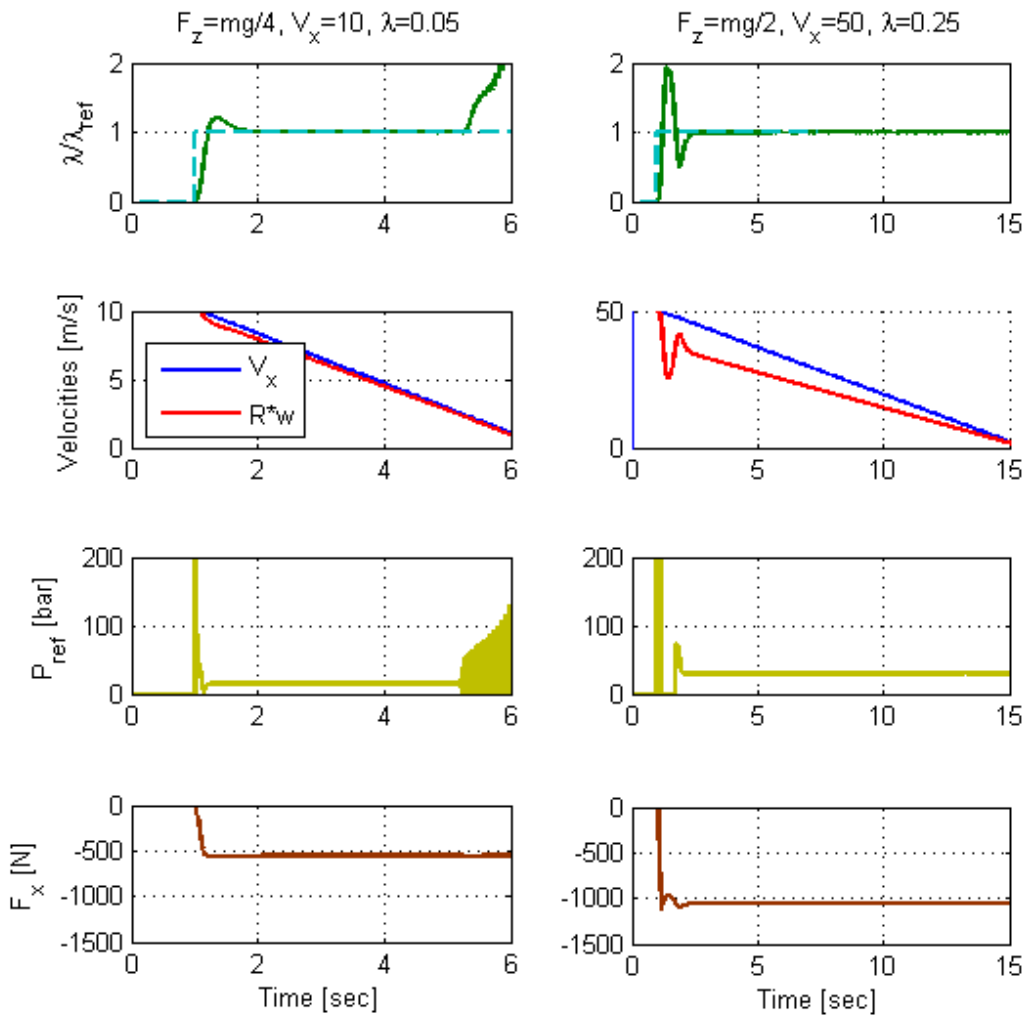

Figure 6-35: brake control step response, snow

6.3.3 Brake Control Interface

The proposed low-level brake control system is based on tyre slip as reference input, whereas the output of the control allocation scheme is the tyre longitudinal force[44]. To convert the output of the control allocation to the parameter which is suitable for low-level brake control, an inverse of tyre model could be employed. However, it should be noted that the inverse of tyre models is not monotonic, this means that for every longitudinal force (except the point where the force is maximum) one can find two slip value as shown in Figure 6-36.

[44] The proposed control allocation scheme is presented in Chapter 5.

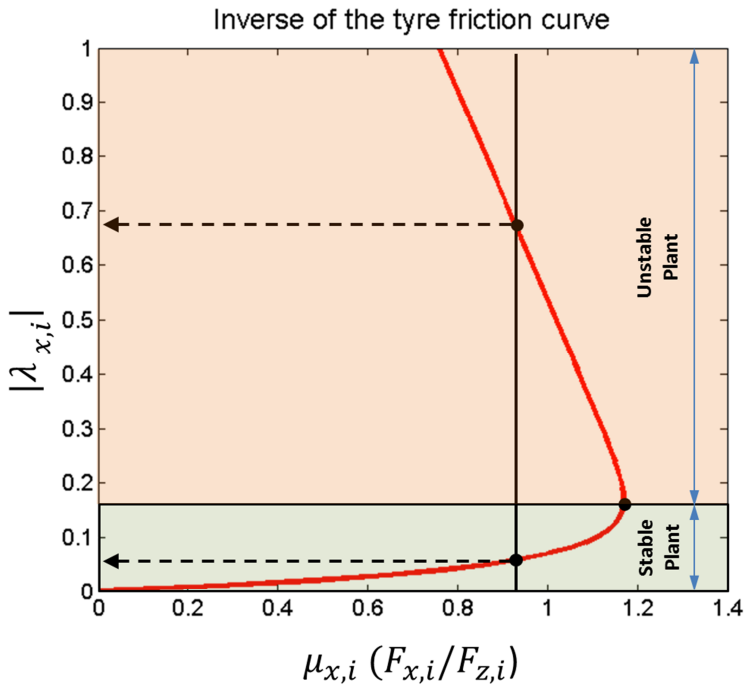

Figure 6-36: Inverse of the tyre model

To address this issue, the lower slip value (from the two possible slip values correspond to a specific tyre friction value) could be selected. Choosing the lower slip value has the extra benefit of making the brake plant stable, which is more appropriate for control system. However, working with stable plant is not very critical for the low-level brake control system as it can robustly stabilise the plant, even if the plant is unstable, as discussed in the previous section.

The other weakness of using inverse tyre is in the fact that the slope of the inverse tyre friction curve is very low at low slip values. This means that at the low values of $\mu_{x,i}$, considerable changes in the longitudinal force results in negligible difference in slip value. However, as the IVCS system in stability mode is working on higher parts of the friction curve (near stability limits) at which the slope of the inverse friction curve is high, therefore the results are more coherent.

Finally, but importantly, it is worth noting that employing inverse tyre model introduces some level of uncertainty into the control system, as the tyre models encompass several simplifications relative to the actual tyres and also it requires a good estimation of tyre-road friction of coefficient at all conditions (which is hard to achieve in practice). However, as this inversion takes place inside of the closed loop

of the high-level control system, it is expected that this level of uncertainty would be compensated by robustness of the cascade controllers.

To consider the effect of tyre slip angle on the subsequent tyre longitudinal slip, the inverse tyre curve can be derived by employing a combined tyre model, such as Pacejka combined tyre model, as introduced in section 3.4.2 (see Figure 6-37).The resultant lookup table has two inputs, tyre normalised longitudinal force and slip angle, and the one output, the tyre slip.

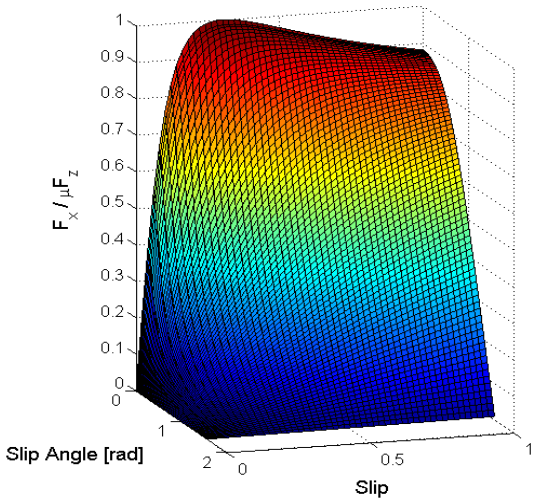

Figure 6-37: Normalised longitudinal tyre force for combined slip ad slip angle (Pacejka model)

7 Integrated EPAS & ESP HiL Design and Control System Validation

An integrated steering and brake Hardware-in-the-Loop (HiL) test rig was designed and developed as part of this thesis. The proposed integrated control system was then implemented in a real-time environment and validated through HiL testing. The concept and structure of a HiL system are discussed in this chapter. Various design aspects of Cranfield's integrated EPAS & EHB HiL setup, including the requirements and specifications setting as well as architectural, mechanical, electrical, control system and human machine interface (HMI) designs are briefly put forward. The results of the control system validation through HiL testing are presented at the end of this chapter.

7.1 HiL Testing and Validation

Model based development process of vehicle mechatronic systems starts from requirement definition and finishes by real-testing of the final product; with several Validation and Verification (V&V) feedback loops, as described by V process in chapter 2 (Isermann R. , 2008). By increasing the number of ECUs and growing the complexity of the embedded systems in today's vehicles, Hardware-in-the-Loop (HiL) testing is becoming an integral part of active systems development in the automotive industry (Bringmann & Krämer, 2008; Broy, 2006, May). Recent advancements in automated code generation and other relevant control development tool chains increase the importance of Rapid Control Prototyping (RCP) and HiL simulation in seamless model based development process (Broy, Feilkas, Herrmannsdoerfer, Merenda, & Ratiu, 2010). HiL simulation is defined as a method in which one or more real components/sub-systems interact with components/sub-systems that are simulated in real time (real time dynamic models) (Wältermann, 2009, April). HiL system provides a fast, flexible and efficient means for verification of functional and non-functional aspects of the developed control systems (ECUs) in a real time environment in the presence of (actual and virtual) system dynamics (Mutz, Huhn, Goltz, & Kromke, 2003). The real part of the system consists mainly of one or more ECUs (controllers) and/or smart actuators which operate in a closed loop with components that are (mechanically and/or electrically) simulated in real time. If the simulated models reveal sufficient proximity to how the system behaves in reality,

then the control performance can be evaluated through HiL testing with a high level of confidence and the risk and cost associated with experimental validation will reduce considerably.

HiL systems are generally employed for validation of production ECUs or smart actuators (Hanselmann, 1996, September). However, integration of a HiL system with RCP tools, such as dSPACE MicroAutoBox®, yields a suitable platform for control system development and validation in real time environment (Abel & Bollig, A., 2006). Figure 7-1 shows some possible combinations between (virtual and real) plant and control systems (Isermann R. , 2008). The possible arrangements between real and virtual systems could be wide-ranging, based on different applications. In this dissertation, an integrated steering and brake HiL/RCP platform is proposed which could be employed for control system development and validation of various stand-alone or integrated active steering and brake systems. The main components of a HiL/RCP system are described briefly in the next section.

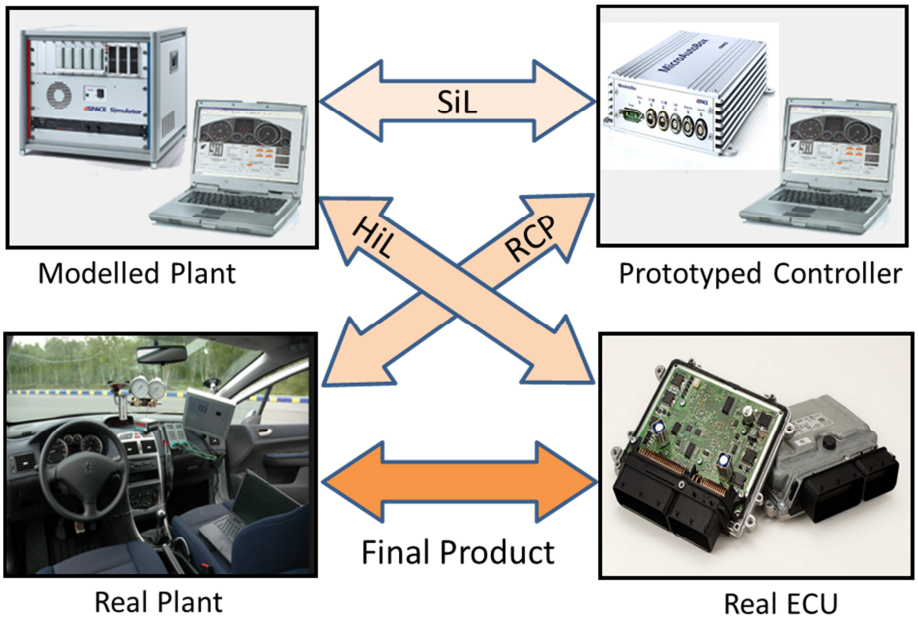

Figure 7-1: Different combination of plant and controller (adopted from (Isermann, 2008))

7.1.1 Hardware Components of a HiL System

Although the configuration of a HiL system can vary considerably based on different applications and requirements, the following are common hardware that are usually employed in a HiL (Wältermann, 2009, April):

- **Host computer:** an off-the-shelf PC, used as the user interface to real time processor (human machine interface, HMI) and also for data acquisition, test management, and storage of test results.
- **Real time processor system:** a powerful processor board for storing and executing real time applications with specialized I/O interfaces to be able to consistently handle various I/O cards and bus systems.
- **I/O boards and signal conditioning:** to generate or receive various signals such as analogue, digital, PWM or automotive specific signals (such as knock, crankshaft or wheel speed sensors signals), with sufficient level of protection (in case of overvoltage or overcurrent, for example).
- **Bus system:** to establish various automotive standard communication networks such as CAN, LIN or FexRay, to be able to receive/transmit the signals from/to other smart sensors, smart actuators or ECUs.
- **Electrical loads and load simulations:** so called “virtual actuators”, to mimic the dynamics of the actuators in the system by employing equivalent electrical circuits.
- **Electrical fault simulation:** to generate the electrical fault states, such as short circuits, open circuits, leakage resistance or loose contacts, intentionally. This feature is especially useful for investigating the fault-tolerance property of the system.
- **Real components/subsystems:** to investigate the impact of real dynamics of the plant (such as missing dynamics or existing nonlinearities) on the designed controllers through HiL testing, it is often necessary to employ the real components/sub-systems instead of virtual ones. Setting the boundaries between real and virtual components is one of the main considerations in designing a HiL system, as it determines the whole structure and functionality of the HiL as well as the associated development and implementation cost.
- **Sensors and actuators:** based on the configuration of the HiL and the specifications of the existing real components/subsystems, it is necessary to

employ several sensors and/or actuators. Selection of relevant sensors and actuators is an important stage in design of a HiL system, as they affect the overall cost as well as the performance and functionalities of the HiL. Cost, reliability, maintenance, accuracy, I/O interfaces, signal types, and static and dynamic response are some of the factors that should be considered in selection of a sensor or actuator.

- **Auxiliaries:** as the real subsystems are working in a different environment than the real vehicle, it is often required to employ some auxiliary equipment to authorise operation of the real sub-systems. For example, an electric power supply is needed to supply the existing ECUs, sensors and actuators (and other electrical consumables) or for vehicle battery simulation. By using an adjustable power supply, it would be possible to further test the system at overvoltage or undervoltage conditions. Another example is a vacuum pump, which is necessary to provide the level of vacuum required for brake booster operation (in case of using conventional brake systems).

7.1.2 Software Components of the HiL System

Considering the fact that HiL is a combined system of real and virtual (simulated) subsystems, the software components play an equally important role as the hardware components. The real time interaction between the real and the simulated subsystem make tough demands on the latter. The simulation subsystem has to perform the following actions within one sampling time:

- Read in the measurement signals (through RTI Blocksets);
- Calculate and perform numeric integration (real time simulation of the entire dynamic model);
- Output the results (through RTI Blocksets).

As there is a closed loop between the real and the simulated components/sub-systems, failure to meet the real time requirements can lead to unstable simulation results and even damage the real components (Wältermann, 2009, April).

Similar to hardware components, the type and composition of software components in a HiL vary from application to application. However, the main software packages that exist in a HiL are summarised as follows:

- **Implementation software:** to design and implement the control system in a model based environment such as Matlab®/Simulink®.Stateflow®, for rapid generation of the C code seamlessly from the designed models and functions such as Simulink® Coder™ and to provide the required I/O interfaces to/from the models via real time interfaces.
- **Experiment software:** to monitor and control the operation of the control system in a real time environment such as ControlDesk® and script language such as VBA, Matlab® or Paython® for test automation.
- **Real time software:** operating system Kernel for real time processors.
- **Dynamic model:** plant dynamic models including vehicle model, (such as Carmaker®), engine model (such as AVL CRUIS®), battery model, and so on; environment models (such as driver model, road model) and vehicle sensor models (such as radar sensor, etc.).

7.2 Integrated EPAS & ESP HiL Design

As a part of this dissertation, an integrated Steering and Brake HiL/RCP setup was designed and implemented at Cranfield University. The systematic approach to the design process of a HiL system encompasses several stages including definition of the requirements and specification and the design of system architecture, the mechanical components, the electrical systems, the controllers, and the human machine interface (HMI). Various design aspects of the Cranfield's integrated EPAS & ESP HiL setup are briefly presented in this section.

7.2.1 Requirements

The HiL is intended to perform the following tasks:

- Rapid prototyping and validation of the steering and/or brake control system.
- Functional and non-functional testing of the different stand-alone steering based active systems such as HAPS, EPAS, AFS or SBW.
- Functional and non-functional testing of the various stand-alone brake based active systems such as ABS, ESP, EHB or BBW.
- Functional and non-functional testing of the integrated steering and brake based active systems such as the customized IVCS system, as presented in this thesis.

7.2.2 Specifications

To meet the requirements, the following specifications should be considered in the design of the HiL:

- **Driver in the loop:** Most vehicle dynamics studies are performed either in an open loop fashion (i.e by ignoring the feedback loop of the driver reaction) or by employing a simplified driver model (Modjtahedzadeh & Hess, 1993). However, to achieve a realistic vehicle dynamics response, the HiL should include the driver in the loop, a so-called driving simulator (Chen & Ulsoy, 2001).
- **Steering torque feedback:** The EPAS works based on driver steering torque feedback (so called haptic feedback (Abbink & Mulder, 2010)). To be able to evaluate the EPAS control system in both comfort and stability modes, it is essential to furnish the driver with accurate feedback via steering wheel torque (Toffin, Reymond, Kemeny, & Droulez, 2007).
- **Real steering and brake systems:** To be able to receive real inputs from the driver, a steering wheel and brake and accelerator pedals equipped with the relevant sensors are required. More importantly, in order to validate the (steering and brake) control system in a more realistic environment the effect of the plant real dynamics and its nonlinearities, such as friction and backlash should be included. Therefore, the HiL should be equipped with real OEM steering and brake systems.
- **Rapid control prototyping tools:** For a fast, efficient and flexible way to calibrate and validate the developed control systems in a real time environment, the HiL should be equipped with the relevant rapid control prototyping (hardware and software) tools such as dSPACE MicroAutoBox, various dSPACE Real Time Interfaces (RTI) Blocksets and Simulink® Coder™ (automatic code generation).
- **Validated models:** To achieve reliable and validated test results, it is essential to employ high fidelity models for the simulated subsystems. Moreover, the models should be executed in a real time environment. Industry standard, off-the-shelf software such as CarMaker/HiL®, CarSim/HiL®, AVL CRUISE® are preferred as they provide validated results and facilitate straightforward data exchange among different parties in a joint project.

- **Flexible yet strong structure:** The mechanical structure of the HiL system should be properly designed to cope with a wide range of steering and brake system sizes and types. More specifically, the HiL size should be appropriate to enable installing steering and brake of different (passenger) cars from different manufacturers and its mechanical structure should be as flexible as possible to fit with variety of systems including:
    - Different steering based active systems, such as EPAS, AFS, SBW;
    - Different braking based active systems, such as ABS, ESP, EHB, BBW.

  In addition, as the steering and brake systems are subject to tough real dynamic loads during their operations, it is required that the mechanical structure of the HiL is sufficiently robust to withstand high dynamic forces from the steering system and actuators.

7.2.3 Architectural Design

Architectural design is one of the most important stages in the systematic approach toward development of a HiL system. Recall that a HiL is a hybrid system that consists of real components/subsystems which work together with modelled (virtual) sub-systems to form a virtual reality environment. By architectural design, the layout of the HiL system, in a high level of abstraction, is defined. More specifically, the main (real and virtual) elements of the system and their functionalities within the HiL platform are determined, and the boundaries between real and virtual components/sub-systems are specified. To design the architecture, one should consider the requirements and specifications together with engineering trade-off between the system performance and available resources such as cost and time.

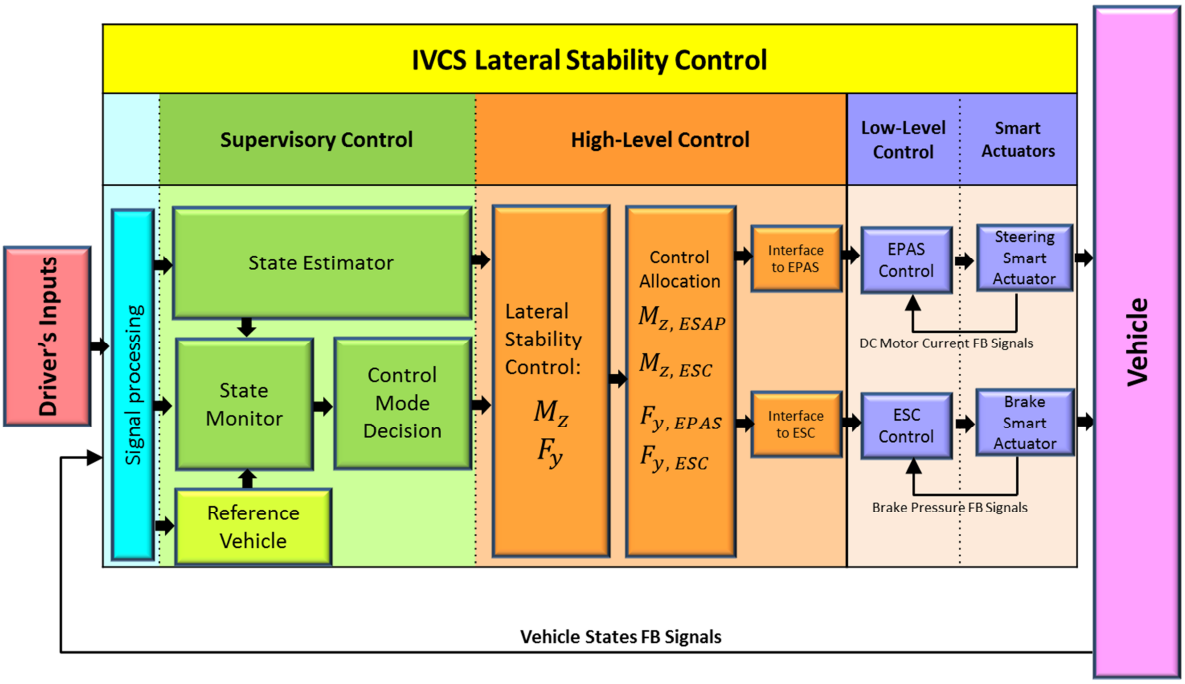

Figure 7-2: Customised IVCS control structure

Considering the customised IVCS control structure for lateral vehicle dynamics control, as shown in Figure 7-2, and the HiL requirements and specifications, as defined in the previous sections, the proposed architecture for integrated steering and brake HiL/RCP setup is presented in Figure 7-3. In this configuration, the real steering and brake smart actuator systems are linked to a virtual vehicle model. Here the existing steering and brake smart actuators are EPAS and EHB, respectively. It is, however, possible to employ different steering or brake active systems such as SBW, AFS, ABS and so on in this HiL.

The driver inputs to the system are the steering wheel (torque/angle), the brake pedal and the gas pedal positions, based on his/her responses to a computer generated road scene which is projected in front of him/her, to form a driver-in-the-loop (driving simulator) platform. The steering torque feedback to the driver is generated by the forces that are applied to the steering rack by means of two linear actuators connected to both ends of the rack. The magnitude and direction of applied forces to the rack is calculated by the vehicle model and take the form of target values for the linear actuators controllers.

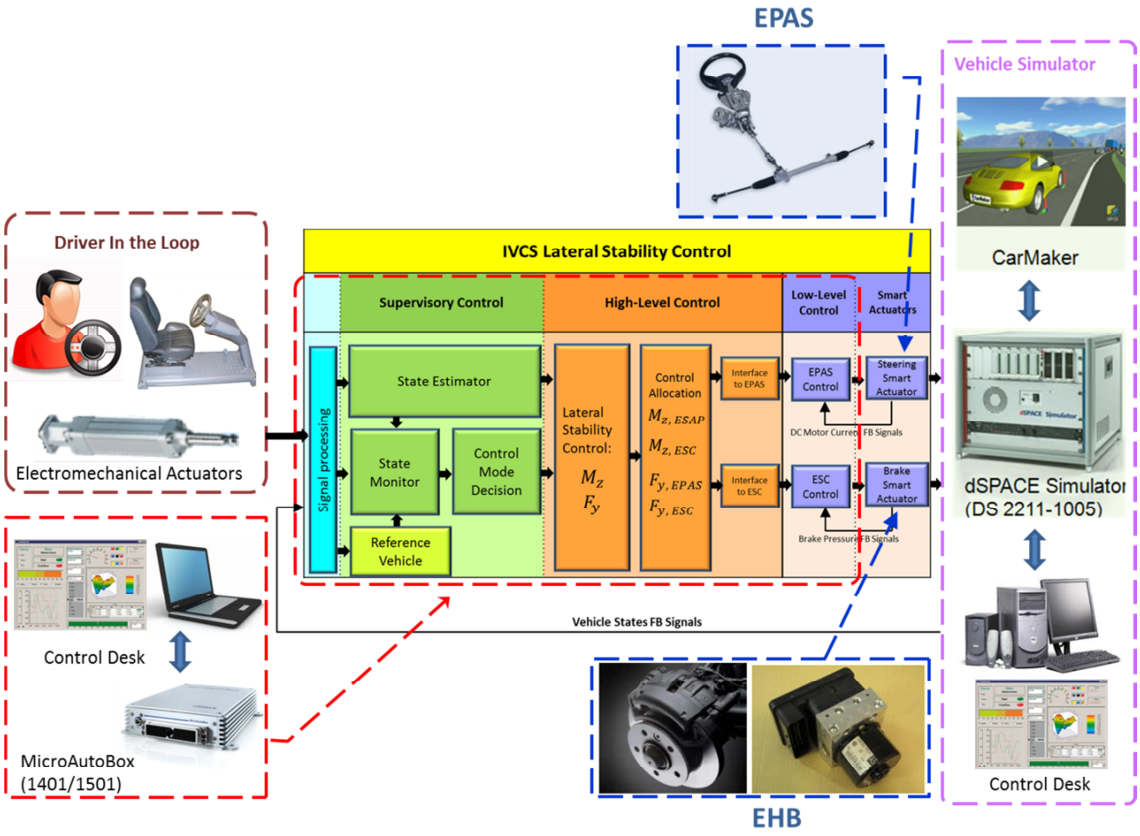

Figure 7-3: The integrated steering & brake HiL architecture

In normal driving conditions, the input to the brake (slip) control system is the driver brake pedal input. However, in case of a stability situation, the amount of brake pressure is determined for each individual wheel by IVCS control system, as described in the previous chapters. The existing real parts for brake system include: brake pedal, master cylinder, EHB (or other stand-alone brake active systems) valve modulation unit, and complete hydraulic line connected to each wheel brake callipers. In order to reduce the cost as well as the complexity of the HiL, the wheels do not rotate in this system. Therefore, the virtual parts of the brake systems are the wheel dynamics and the brake torque calculation, together with the high fidelity vehicle dynamics model. The brake torque at the wheels is estimated based on measuring the brake line hydraulic pressure by means of four pressure sensors connected to the end of the hydraulic line of each wheel. As there are no rotating wheels on the HiL, the wheel speed signals are provided by the vehicle simulator (virtual wheel speed sensor).

The vehicle simulator consists of the high fidelity vehicle model (here CarMaker/Hil), which executes in a real time processor (here dSPACE Simulator, ds 2211-1005). It performs the numerical calculations and generates the required signals of vehicle dynamics states (including the rack force) and wheel dynamics states. Concurrently, the IVCS control system, including supervisory control, high-level control, low-level control and smart actuator control blocks (as described in the previous chapters), execute in the second real time processor (here dSPACE MicroAutoBox) as the rapid control prototype ECU. The prototype ECU receives signals from (real and virtual) sensors and generates command signals for steering and brake actuation. The communication between the vehicle simulator, the prototype ECU and the existing sensor and actuators is performed via various analogue, digital and CAN buses interfaces.

A simplified schematic diagram of the HiL including the main elements and the feedback loops are shown in Figure 7-4. In should be noted that the complete relationship between the HiL elements is far more complex than represented in this Figure.

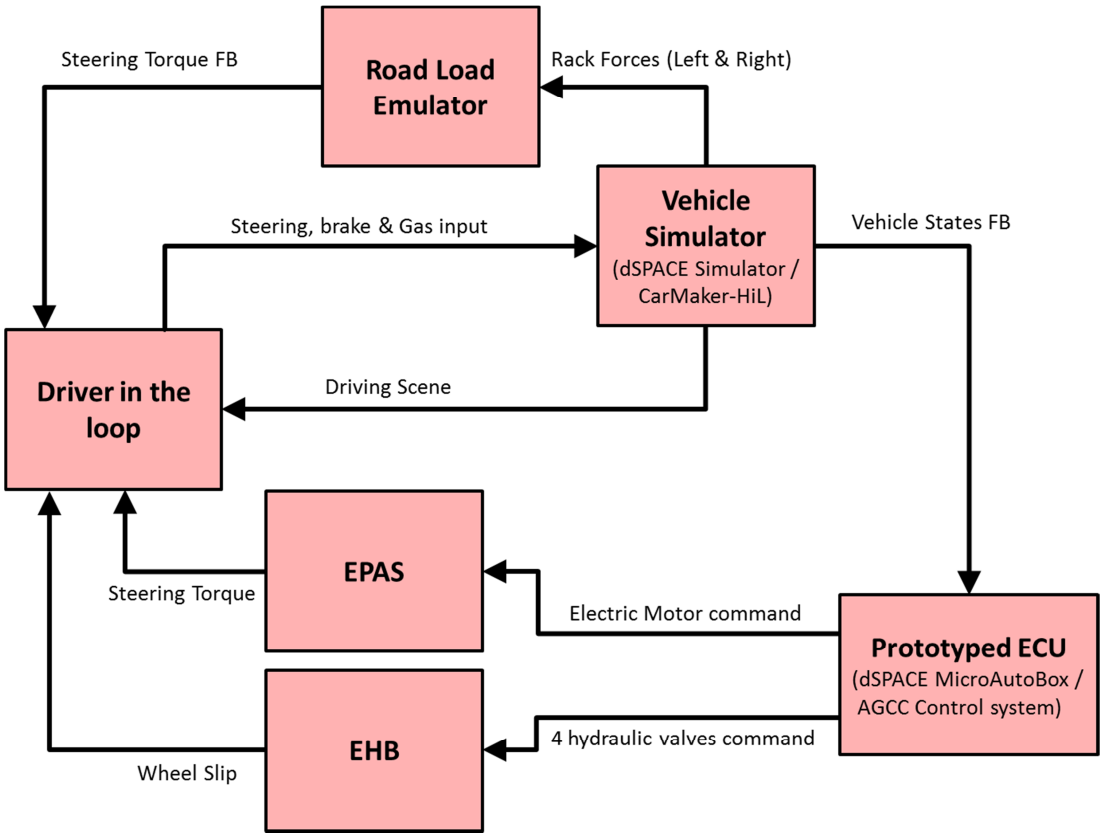

Figure 7-4: The (simplified) schematic diagram of HiL architecture

7.2.4 Mechanical Design

By employing a real steering and brake system, the mechanical structure of the HiL is subject to tough input loads from the driver, the actuators, the steering and the brake systems. For example, the steering system encounters heavy dynamic loads from driver, EPAS electric motor, and electric actuators concurrently, especially when the system is being operated in off-road and/or stability conditions. Therefore, it is required that the mechanical structure of the HiL can handle these high dynamics loads without affecting the HiL performance. Importantly, if the structure of the HiL is not solid enough, unnecessary shaking and vibration will generate and propagate through the system, which will diminish the performance of the control system and degrade the process of control tuning and validation.

The actual mechanical parts that exist in the HiL include:

- **EPAS Smart Actuator:** The complete steering system (here a column type EPAS) consisting of steering wheel, steering column, an electric motor connected to the column via a reduction gear, steering pinion and rack. Two linear actuators, which are connected to both ends of the rack's swivel pin ball joints, imitate the applied loads from front wheels (and suspension) to the steering system. The linear actuators should have enough bandwidth to produce the high dynamic steering loads that usually generated during real vehicle handling and stability tests.
- **Road Load Emulator:** The steering haptic feedback is generated from the actuators and transmitted to the driver through the steering rack, column and steering wheel to provide a real and accurate steering feel. To generate the required rack (static and dynamic) forces, two Bosch-Rexroth electro-mechanical linear (EMC100 40x5 attached to MSK060C motor) actuators have been employed. Each actuator is capable of generating up to 10kN force at frequencies of up to 10 Hz, which is fast enough to test the steering of various passenger cars at different road conditions. The specification of the Bosch-Rexroth EMC can be found in Appendix C. The electro-mechanical actuator incorporates a ball screw and ball nut in which the screw is directly coupled to an electric motor. Electro-mechanical actuators have several advantages over the hydraulic or pneumatic cylinders actuators such as: low maintenance, cleanness, lower cost, self-contained and easy to control. More

importantly, their (sound) specifications such as, high bandwidth, good repeatability, identical behaviour in extending or retracting, possibility of employing various electric motor such as DC or step motors; make them more attractive from control application point of view.

- **EHB Smart Actuator:** The complete hydraulic brake system, consists of brake pedal, brake master cylinder, EHB (or ESP) unit including valve modulation unit and 4 wheels calliper assembly and disk, all connected by hydraulic line to form a complete brake hydraulic circuit. The brake line is subject to high hydraulic pressure up to 200 bar, so all the hydraulic lines and fittings should be commissioned according to automotive standards.
- **Driver in the loop:** Driver compartment, including an adjustable seat, control panel (including emergency stop switches), steering wheel, brake and gas pedals. These are packaged with relevant fixtures, considering the driver's ergonomic requirements.

To fix all the mechanical (and electrical) components, the HiL should be furnished with a suitable baseplate. The base of the HiL should be mechanically robust to withstand high dynamic forces and be heavy enough to absorb the vibrations (generated from mechanical system operation). It should be sufficiently large to cover all the components and yet be flexible enough to enable mounting various system types and sizes with minimum effort. The best (and cheapest) solution to satisfy all these requirements is to employ a good size machine tool T slotted bedplate.

All the mechanical parts are fastened to the bedplate with proper fixtures, including: the steering column and rack; the brake and gas pedals; the brake master cylinder; valve modulation unit; hydraulic piping and 4 wheels calliper assembly and disk; the electro-mechanical actuators. More specifically, the steering column and rack, and the brake and the gas pedals are fixed by employing a unique flexible fixture. The fixture is adjustable in three spatial directions (x, y, z) which provides enough flexibility to fit with various steering systems, such as EPAS (column type, rack type or pinion type), AFS, SBW with different sizes and different braking active systems, such as ABS, ESP, EHB, BBW. Some pictures of the various components of the HiL are shown below.

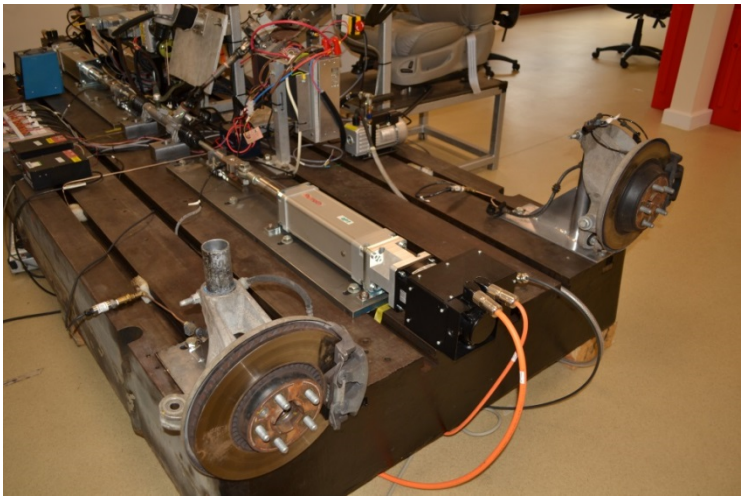

Figure 7-5: The brake disks, callipers and hydraulic line & EMC actuator (left side) attached to the bedplate

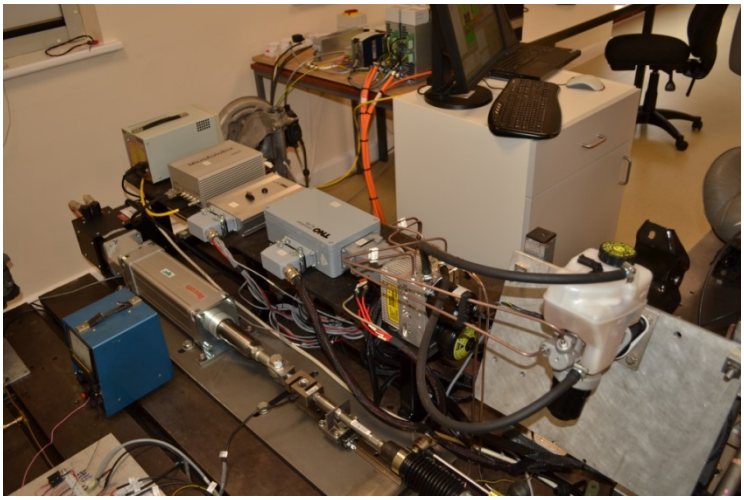

Figure 7-6: The SBC EHB module and right side EMC actuator

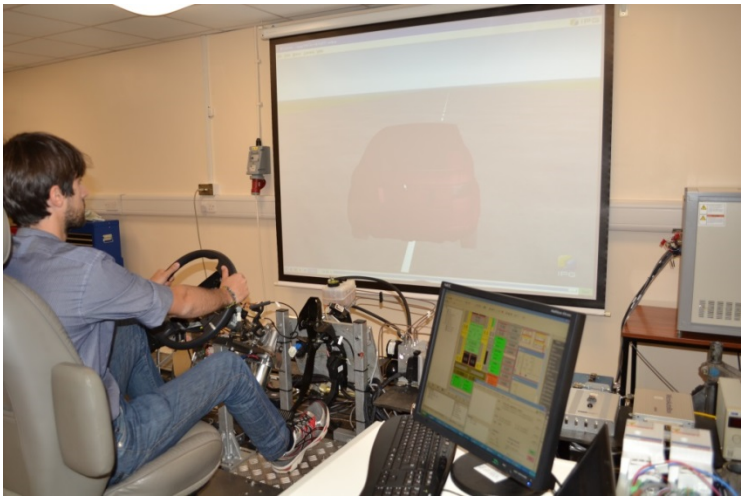

Figure 7-7: Driver compartment and steering system

7.2.5 Electrical Design

Considering the architectural design of the system, the electrical components of the HiL system can be categorised as follows:

- **Road Load Emulator:** including two 3-phase brushless DC motors (Bosch-Rexroth MSK060C) attached to each EMC actuator. Each motor incorporated with a Bosch-Rexroth IndraDrive C motor driver (Bosch-Rexroth HCS02.1E-W0028) and controller (Bosch-Rexroth CSH01.1) and a load cell to provide the force feedback signal.
- **EPAS Smart Actuator:** including a DC motor, an H-bridge, a current sensor, a steering angle sensor, and a steering torque sensor.
- **EHB Smart Actuator:** Bosch SBC electro-hydraulic brake system comprising: a valve modulation unit (including an electric pump, 4 proportional hydraulic valves, 5 pressure sensors, oil temperature sensor, EHB voltage sensor); a master cylinder (with brake pedal feedback emulator and brake pedal position/speed senor) and a brake pedal switch.
- **Vehicle Simulator:** dSPACE Simulator, ds 2211-1005, to receive driver input signals, run the vehicle model in real time and provide the vehicle state signals (as virtual sensor) to the prototype ECU and road load emulator actuator (electro-mechanical actuators, EMC).
- **Prototype ECU:** dSPACE MicroAutoBox ds 1401 for rapid control prototyping as prototype ECU to run integrated vehicle control system in real time environment and provide the relevant actuation signals to the steering and brake actuators. The proposed integrated steering and brake control system (customised IVCS system) includes: supervisory control; high-level control (with control allocation scheme); low-level control; smart actuator control blocks as described in the previous chapters.
- **Driver in the loop:** including steering wheel sensor, gas pedal position sensor, and brake pedal switch, an electric adjustable seat and a projector for projecting the road scene on a wide screen in front of the driver.

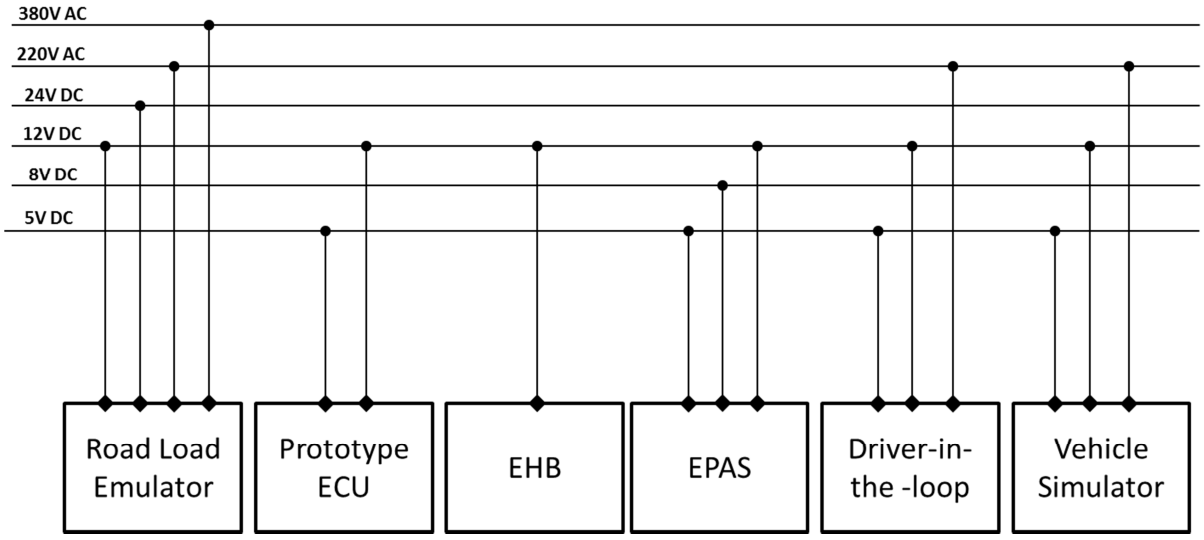

Figure 7-8: HiL electrical consumers supply voltage

The existing electrical components (including actuators, sensors and controllers) need various supply voltages, ranging from three phase 380 V AC, to single phase 220V AC, 24V DC, 12V DC, 8 V DC and 5V DC as shown in Figure 7-8. A detailed list of electrical consumers and their supply voltage are summarised in Table C.1 Appendix C.

There are several sensors fitted with the EPAS, EHB and electro-mechanical actuators to take the required measurements for control systems feedback and for the vehicle simulator. The required vehicle states and parameters (such as yaw rate, lateral acceleration, sideslip, wheel speed, tyre-road coefficient of friction and self-aligning moment, etc.) are calculated by the vehicle simulator (the vehicle model which is running in real time) and these “virtual sensor” signals are transmitted through a CAN bus to the prototype ECU. Note that in real vehicle implementation, some of the vehicle states such as yaw rate, lateral acceleration or wheel speed are available through sensor measurement. However, there exist several parameters, such a vehicle sideslip, tyre-road coefficient of friction, wheel slip or tyre self-aligning moment, for which direct measurement is difficult (or expensive) and therefore they should be estimated by employing several robust estimation algorithms (Stéphant, Charara, & Meizel, 2004; Ahn, Peng, & Tseng, 2012; Hsu Y. , 2009). The list and specifications of the existing (real) and virtual sensors can be found in Appendix D.

The command signals for steering and brake smart actuators are generated by the prototype ECU (MicroAutoBox) and transmitted to the EPAS and EHB actuators via

several analogue, digital and CAN bus interfaces. The reference signals for closed loop control of electro-mechanical actuators (i.e. rack forces – left and right sides) are derived from real time vehicle model and send to the EMC motor controller and driver (Rexroth IndraDrive C). The list and specifications of the actuator signals are also indicated Appendix D.

A schematic diagram of the signal flows among the existing components of the HiL including the vehicle simulator, the driver-in-the-loop, the steering, the brake smart actuator, the road load emulator, and the prototype ECU are shown in Figure 7-9.

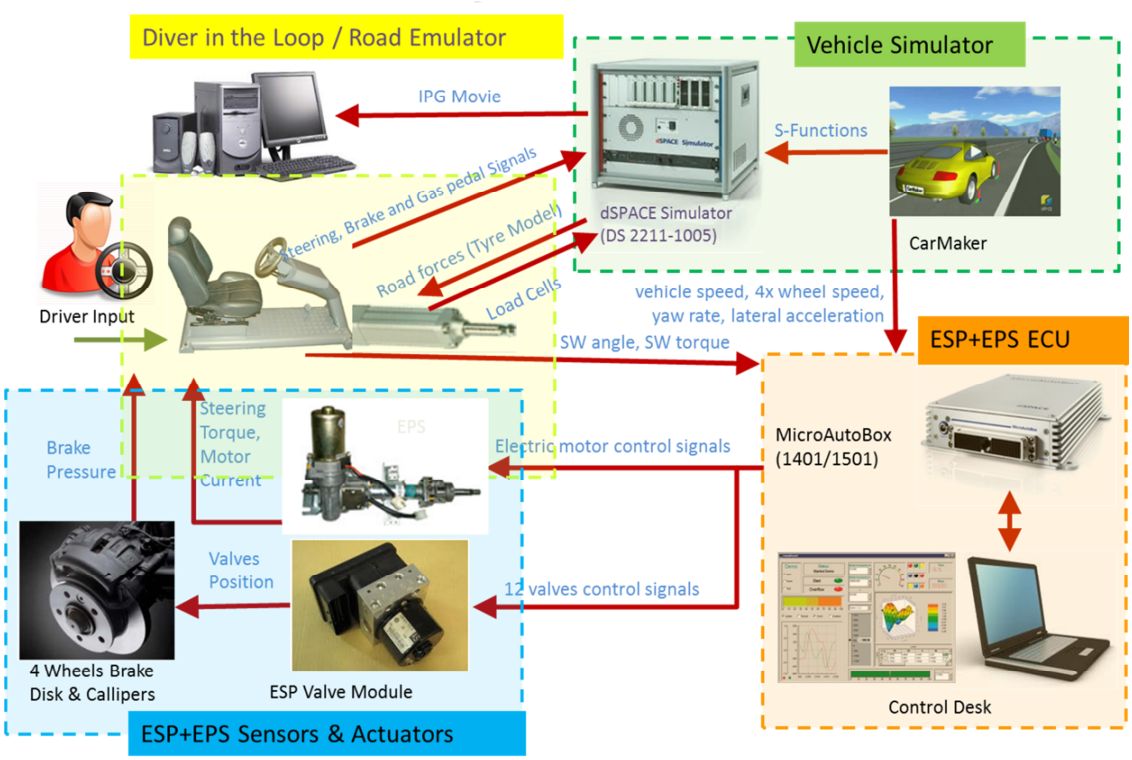

Figure 7-9: The signal flows among several HiL components

7.2.6 Control System Design

To control the magnitude of the forces generated by the two electro-mechanical actuators, two similar closed loop PI control systems based on rack force feedback were designed. The control system is a two cascade feedback system, consisting of an inner loop to control the electric motor current (torque) and the outer loop control task to follow the target rack force (calculated by the vehicle model), as shown in Figure 7-10.

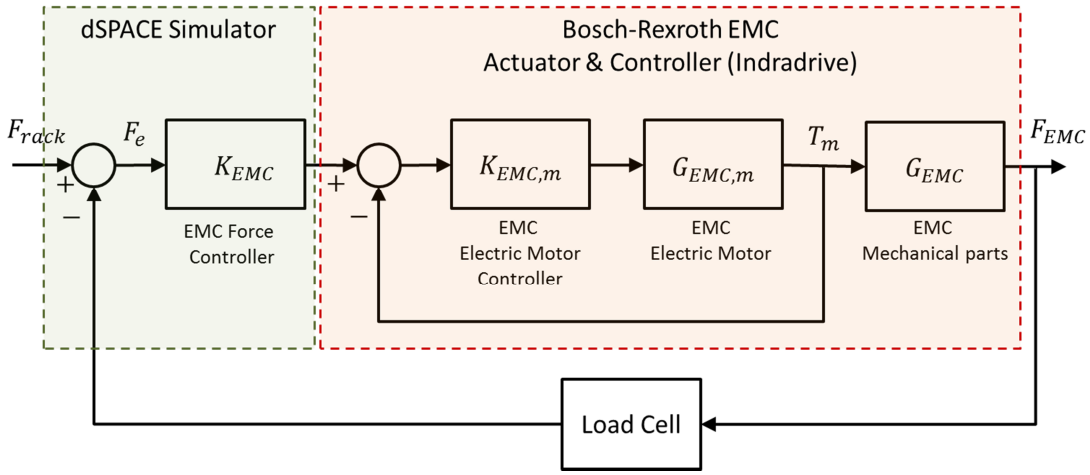

Figure 7-10: EMC actuator control loops

The control task for the inner loop is to control the magnitude of the generated torque at the output shaft of the electric motor. It consists of a PI controller and motor driver (pre-set by Bosch-Rexroth, and embedded in Indradrive®). However, due to the ball screw and cylinder dynamics and friction, the delivered force at the end point of the cylinder is not equal to the amount of the torque which is generated by electric motor. By placing a load-cell in between both ends of the EMC actuator and steering rack, an outer loop controller was designed to compensate the internal loses and dynamics of the system and ensure that the correct value of rack force is applied to the steering system.

Figure 7-11 shows a plot of reference force and actual force at two sides of the rack (measured by means of the two load cells connected in between the EMC actuators and the both two ends of the steering rack), confirming the good tracking performance of the designed controller. Note that the graphs show a steady-state error between reference trajectory and the generated force in some occasions, which is mainly because of the (load cells) measurement inaccuracy. The maximum observed deviation between the reference and measured forces is around 100 N, this is equal to maximum 2% error if a 5 KN force applied from wheel to the steering rack.

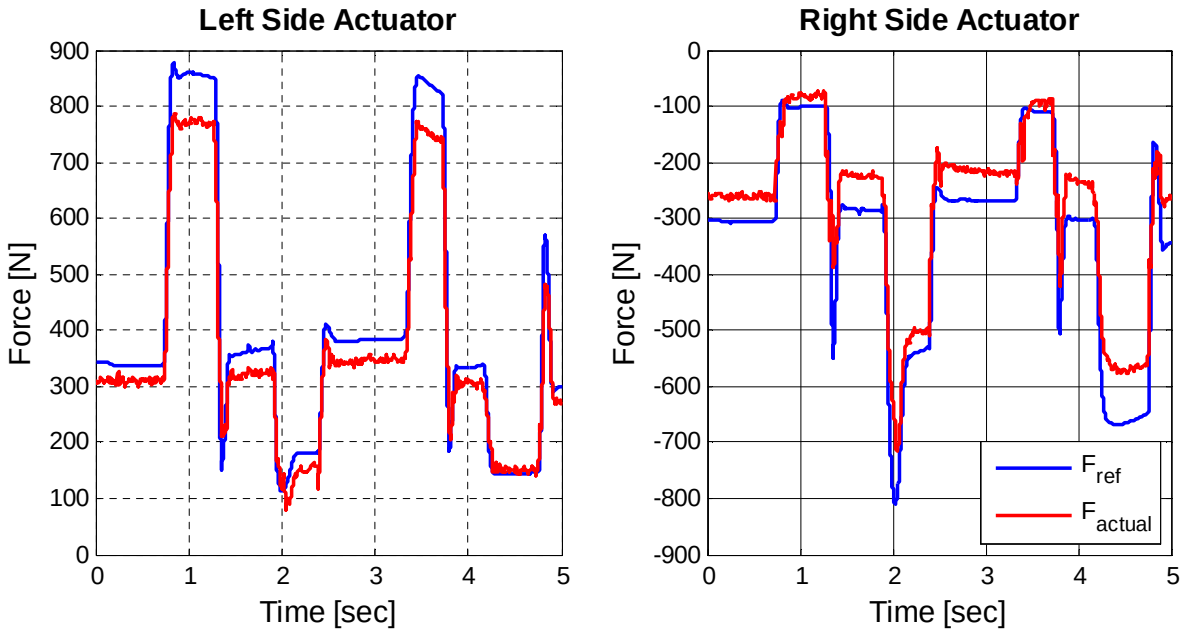

Figure 7-11: EMC actuator control response

7.2.7 Human Machine Interface (HMI)

To establish a communication between the HiL operator and all the existing active systems, several human machine interfaces are designed in ControlDesk® environment to perform the following (real time) tasks:

- To command and monitor the vehicle simulator (dSPACE Simulator) operation;
- To command and monitor the prototype ECU (dSPACE MicroAutoBox) operation;
- To tune the IVCS integrated control system parameters (RCP), for achieving the best control performances in real time environment with the existence of the actuators real dynamics, nonlinearities, saturation, and so on.
- For data acquisition and logging of the test results;

The screenshots of the designed Controldesk® layouts are presented in Appendix E.

A picture of the implemented HiL/RCP setup with the driver in the loop is shown in Figure 7-12.

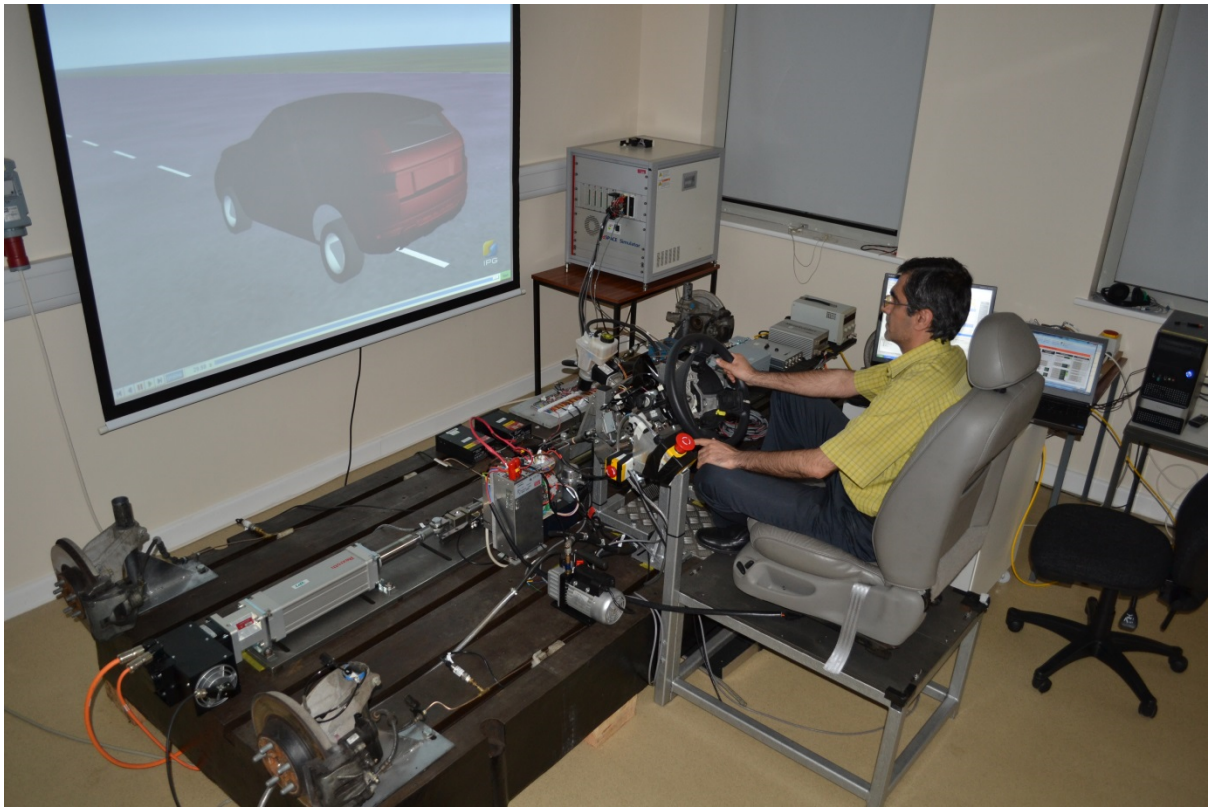

Figure 7-12: Cranfield's HiL/RCP setup with the driver-in the-loop

7.3 Control System Validation Through HiL Testing

To validate the integrated control system, several tests were performed in Cranfield University's integrated steering and Brake HiL setup. The objective of these tests is to validate the stability and performances of the proposed closed loop control system in a real time environment., and to make any further control calibrations in the existence of real driver inputs, actual dynamics of the steering and brake system (including their smart actuators), the high fidelity vehicle model (CarMAker/HiL®), the actuators saturation, the sensor noises, and CAN bus message latencies. Considering the fact that the IVCS system is a cascade closed loop control system, it is important to investigate the dynamic responses of the control loops, to confirm the consistency of control system bandwidths, which is essential for the stability of the integrated control system. Moreover, as the IVCS system is an over-actuated system, it is also important to assure a smooth switching between dissimilar actuators.

To implement the control system in the real time environment, the following steps was performed:

- All the designed continuous-time control transfer functions that exist in the IVCS integrated control system were converted to discrete time by employing the Matlab® command "*c2d*", the sampling time is 0.001 sec.
- All the Matlab®/Simulink®/Sateflow® models was compiled into C code by Simulink® Coder™ toolbox.
- The communication between HiL Simulator and MicroAutoBox was established via a CAN bus running at baud rate of 500 Kbit/sec.
- To avoid integrator wind-up (especially during the start-up), which cause the controller saturation and degrade the control performance, several anti-windup strategies schemes implemented. The schemes were also employed for bumpless transfer and resetting the controllers, when switching between actuators happens.

Recall from Chapter 2, the systematic stages for the control system validation, as proposed by the V diagram, starts from subsystem testing toward the complete system validation. In our case, the validation process starts from the smart actuators control system as the most inner loop and continues to the low-level control loop as the second loop and ends up by validation of the high-level control system as the third loop. At the final stage, the complete integrated IVCS system including the all the cascade control loops, control allocation scheme and control mode decision is verified by performing several manoeuvres.

7.3.1 Smart actuators control system validation

The first set of tests, focus on validation of smart actuator control system as the most inner loop. The objective of these tests is to investigate the stability and dynamic response of the closed loop control system for the EPAS electric motor and EHB hydraulic valves.

7.3.1.1 EHB Smart Actuator

The responses of the EHB smart actuators are investigated in this section. Recall, the SBC EHB valve modulation unit consist of a high pressure hydraulic reservoir and four proportional hydraulic valves (and controllers) to control the hydraulic

pressure of the of the Front Left (FL), Front Right (FR), Rear Left (RL) and Rear Right (RR) calliper. The tests were performed in two stages. In the first step the responses of the closed loop control of EHB hydraulic valves subject to step input was investigated. In the second step, the responses of the complete braking system were examined.

The response of the closed loop control of EHB hydraulic valves subject to step (pulse) input are shown in Figure 7-13. The target pressure for each line was set to 50 bar and measurements were performed by means of the pressure sensors embedded in the EHB valve unit. The results confirm the good performance of the EHB smart actuator system: the behaviour of all the four valves are similar, the hydraulic pressure in each line can track the reference trajectory very well, and the response time of the whole closed loop control system (including, the hydraulic valve and controllers response time) in less than 1.5 ms. The pressure at rear lines (i.e. real left and rear right lines) exhibit an overshoot, which might be due to the fact that the rear valves are weaker than the front valves as they were designed to handle lower pressures (the rear wheels brakes are generally produce less braking torque than the front brakes). Also there is a pressure reduction to hold the pressure after 2.5 seconds, which might be due to the activation of the ENB reservoir and hydraulic pump to build up the pressure.

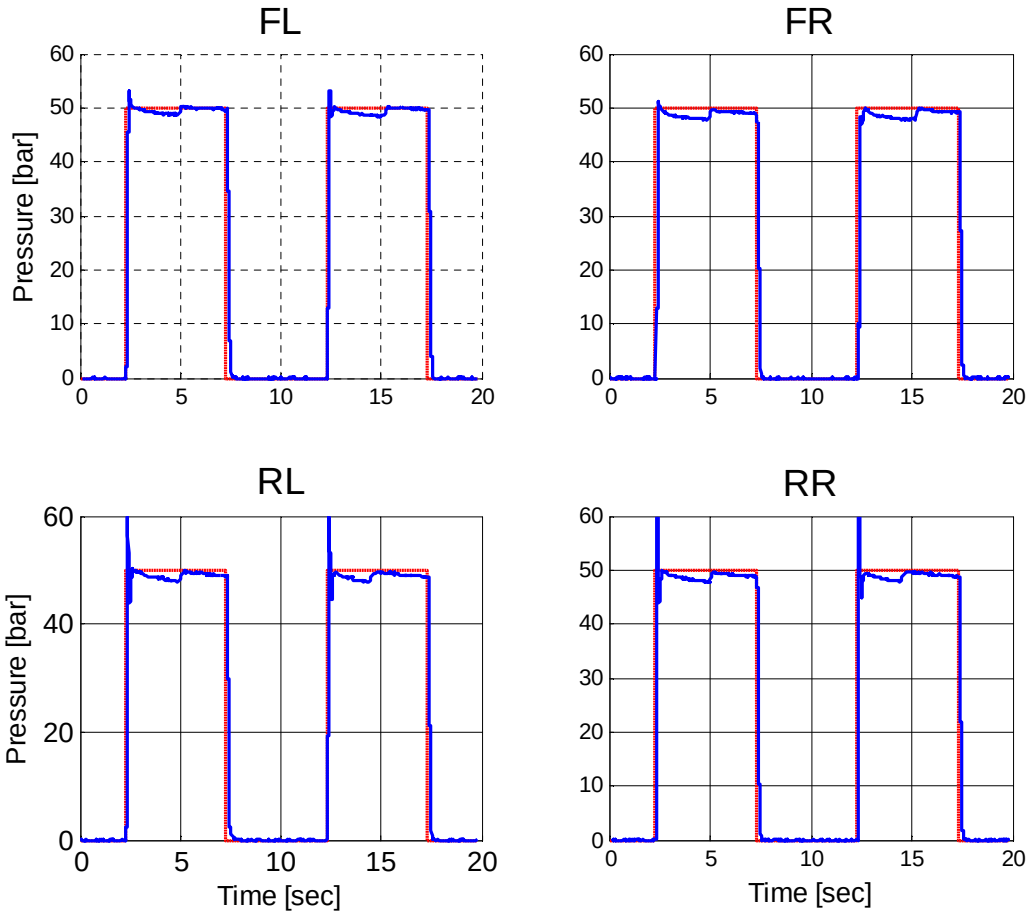

Figure 7-13: EHB Hydraulic valves responses to step input

The next step is to investigate the response of the entire brake hydraulic line (from driver brake pedal input to calliper pressure output). This includes the dynamics of the driver pedal input, master cylinder, EHB hydraulic unit and also the brake hydraulic lines (for each wheel). The input is the driver brake pedal stroke which is measured by the brake pedal position sensor (embedded in the EHB master cylinder unit) as shown in Figure 7-14 (a). The equivalent driver pressure input is calculated based on the pedal position input and considered as the reference value for the EHB valve smart actuator. The comparison between the commanded pressure and the build-up pressure at the at the EHB unit and at the calliper for the front left wheel is shown in Figure 7-14 (b).

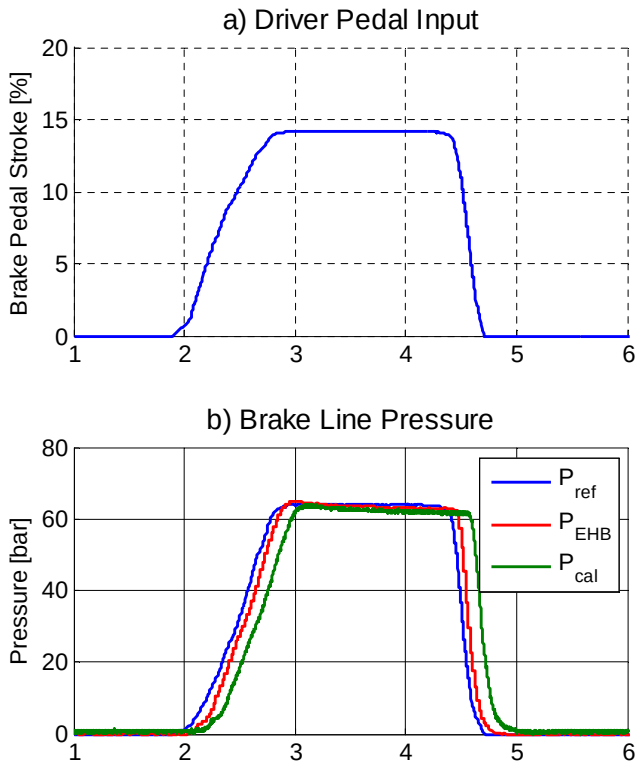

Figure 7-14: Drive pedal input and the build-up hydraulic pressures at different points in the brake (front left) line

The EHB smart actuator follows the commanded pressure very well and also the following observation can be made:

- The EHB smart actuator dynamics (including the valve dynamics and the closed loop pressure controller dynamics) can be fairly modelled as a first order transfer function. The time constant between reference input (to the EHB unit) and the build-up pressure at the output of EHB is about 0.05 sec.
- The hydraulic line dynamics can be modelled as a first order transfer function. The time constant between the pressure build-up at the EHB and the pressure sensed at the calliper is about 0.15 sec.

The above findings, justify our previous assumptions on defining the brake plant dynamics, as mentioned in section 6.3.2.

7.3.1.2 EPAS Smart Actuator

Similar to the EHB smart actuator, the control validation of the EPAS smart actuator (i.e. the torque controlled DC motor) was performed in two stages. In the first step,

the stability and performance of the closed loop current (torque) control system was evaluated by testing the DC motor only. In the second step, the DC motor is attached to the steering system; hence, the control system is validated in the presence of the steering dynamics. Moreover, the test results can also be used to justify the proposed model for the steering plant dynamics. The closed loop response of the DC motor current (torque) controller for the motor is shown in Figure 7-15[45]

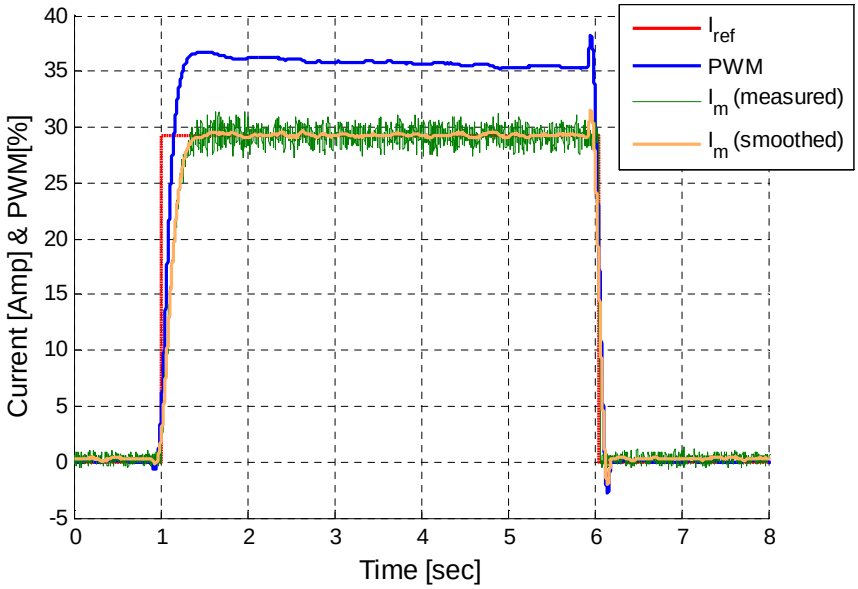

Figure 7-15: DC motor closed loop current control step response

The closed loop step response can be approximated with a first order transfer function with the time constant of 0.14 sec. Note that this actual time constant is obtained with the existence of hardware (motor driver) including the H-bridge MOSFETS, current sensor, and power supply dynamics.

To get a more realistic result, the step input response of the DC motor closed loop current controller with the existence of steering dynamics was measured and the results are shown in Figure 7-16. Here the input is a reference torque to the electric motor, and the output is the forces at the both ends of the rack which are measured by means of the two load cells attached in between the both ends of the rack and the

[45] For clarity of the plots, all the measuremed data shown in the following figures was smoothed by employing Savitzky-Golay smoothing filter with the polynomial degree of 3 and the data span of 250 (Matlab® command yy = smooth(y,250,'sgolay',3)). An overlay plot of unfiltered and filtered current measurement is shown in Figure 7-15. However, in the subsequent plots, only the filtered data are presented.

EMC actuators. In order to compare the results, the motor current is converted to the equivalent rack force by the following relation

$$F_{rack} = I_m \times K_t \times G \times r_p$$

where $I_m$is the measured motor current, $K_t = 0.05$ is the DC motor torque constant, $G = 41/3$ is the motor gear ratio and $r_p = 0.0081$ is the steering pinion radius.

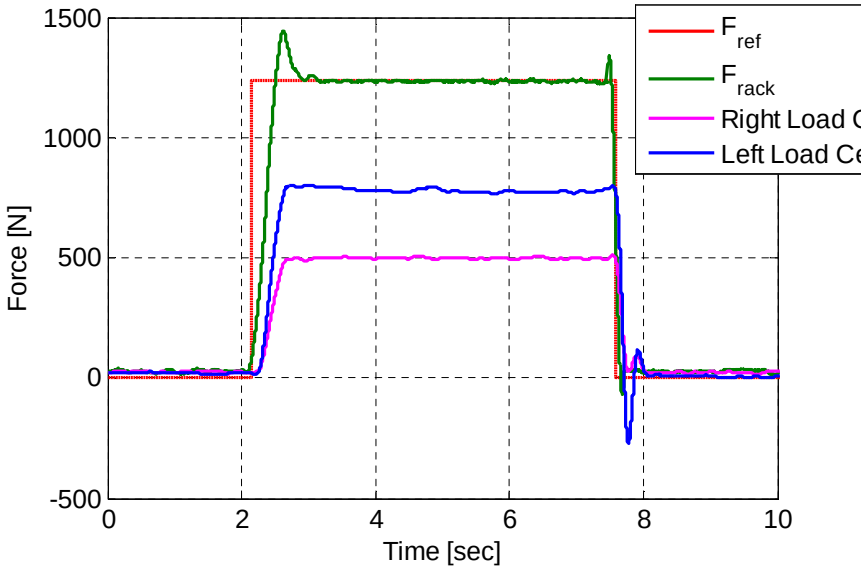

Figure 7-16: DC motor closed loop current control step response, steering dynamics included

By investigating the step response of the complete steering dynamics, the following conclusion can be made:

- There is a transport delay with the magnitude of 0.1 sec between the inputted motor torque and what is observed at the end of rack. This delay is mainly due to the imperfection in the mechanical structure of the existing EPAS.
- The response of closed loop control exhibits an overshoot, because of the column, and rack compliance.
- The time constant between reference input and motor current is 0.14 sec, as concluded before.

One should note form Figure 7-16 that the measurements of the rack forces by the left and right load cells are dissimilar. It was observed during several tests that the right load cell amplifier add a dc gain error to the measurement, and need to be

replaced in the future. However, this steady-state error does not effect the transient response measurements.

7.3.2 Low-level control system validation

In this section, the response of the low-level brake control (slip control) and low-level steering control (based on self-aligning torque feedback) subject to step input are investigated.

7.3.2.1 Low-level slip control

To examine the stability and performances of the proposed closed loop slip control system, the complete brake system (including the EHB unit) was integrated with the virtual vehicle simulator to form a complete vehicle dynamic loop. The vehicle is driving at speed of around 33 m/s (120 Kph) was subjected to step slip input (slip target was set to 0.03) at rear wheels. The test results, as shown in Figure 7-17, confirm the good stability and performance of the slip control system. The brake pressure increases to 40 bar and the wheel slip reaches its target within 0.5 sec, and as a result, the vehicle longitudinal speed reduces (from 33 m/s) to 10 m/s within 1 sec without wheel locking. At low speeds, the slip controller exhibits an oscillatory behaviour and therefore discarded. One should note that the issue of controlling the slip at low vehicle velocities was already reported in the literatures (Savaresi & Tanelli, 2010). It is worth to mention that as the proposed slip control is for employing at stability situations, therefore, the low vehicle velocities are normally not considered in the operating condition of the (slip control) system.

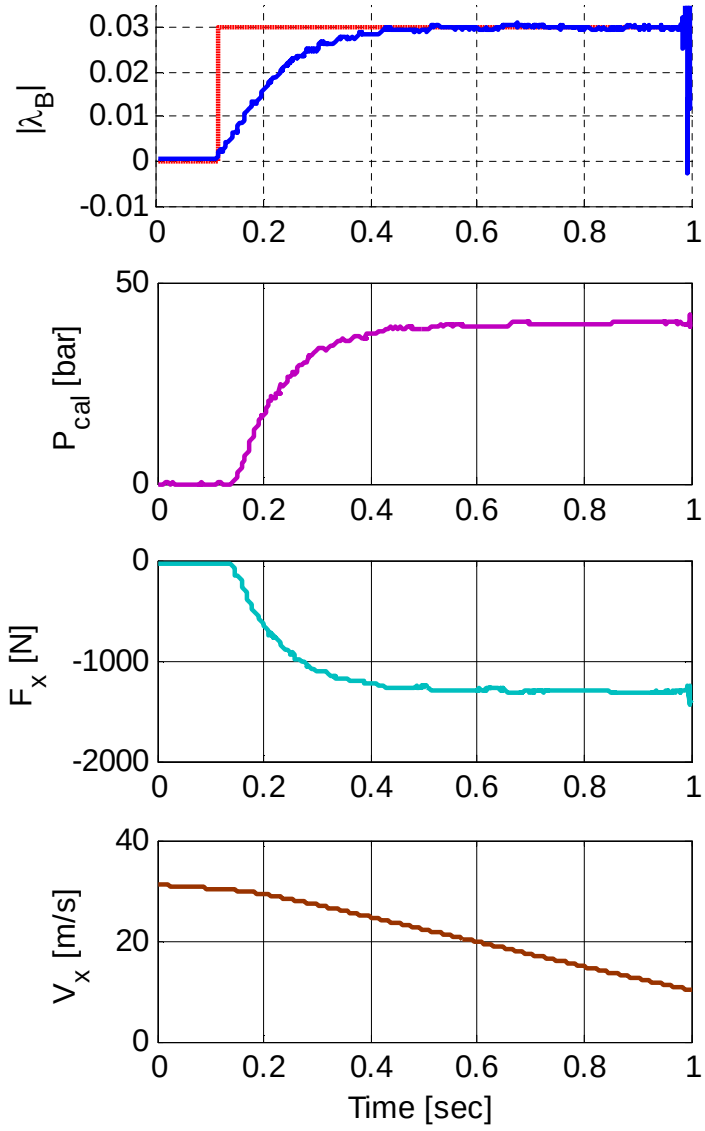

Figure 7-17: Closed loop slip control responses

In spite of good stability and performance of the proposed slip controller, it was realised during several test manoeuvres that this response time is still slow for controlling the wheel slip at stability situation. One solution to address this issue is to increase the closed loop slip control bandwidth; however, by increasing the bandwidth, the (closed loop) control system exhibits an oscillatory behaviour. In fact the closed loop control system is slow in its nature as it has to respect the feedback time delay which is received from the (whole) plant .The other solution is to add a feedforwrad compensator to the control system, while reducing the closed loop bandwidth (i.e. slow down the feedback response). In this configuration, the objective

of the feedforward compensator is to provide a fast response for the control system, while, the stability of the control system and disturbances rejections (due to the feedforward term) are provided by the feedback loop. The proposed feedforward compensator consists of inverse of the plant model. Here the normalised longitudinal tyre force is derived from the target slip passing through a tyre model, which is then multiplied by the tyre normal force to give the longitudinal tyre force. The target pressure is then calculated from the inverse of the caliper and EHB dynamics, as shown in Figure 7-18.

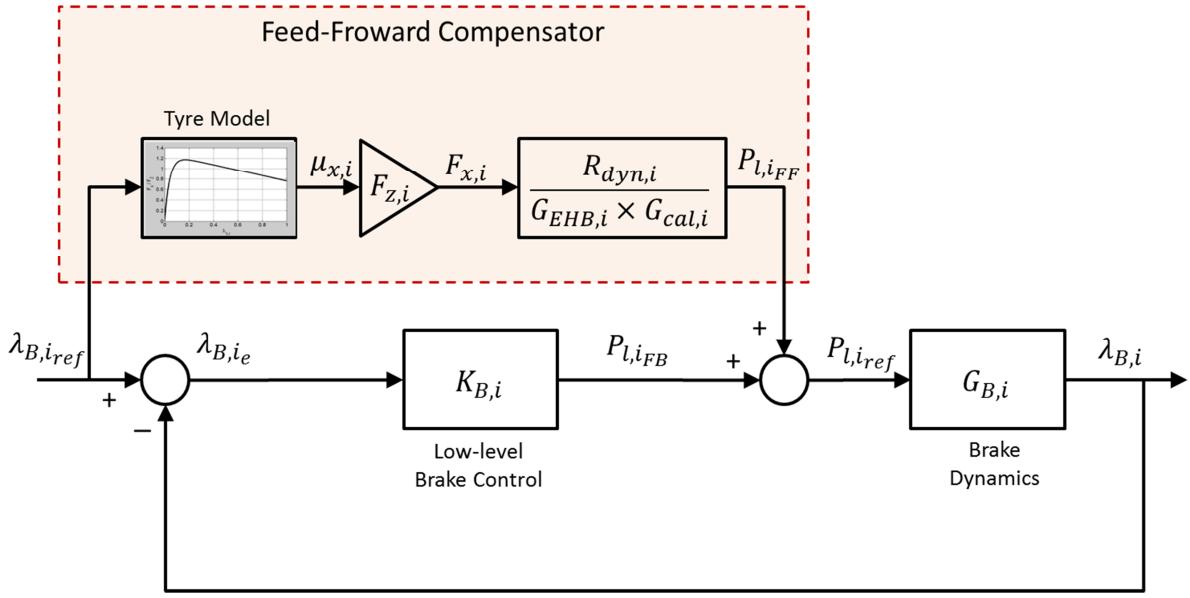

Figure 7-18: Combined Feedback and Feedforward slip control system

To validate the modified control system in a real situation, four slip control systems were implemented for each 4 wheels individually. The brake distribution strategy (target slip) is based on the magnitude of peak force at each tyre (normal force multiplied by road-tyre coefficient of friction, $\mu_i F_{z,i}$). The vehicle was being tested by braking on surfaces with different coefficient of frictions (so called mu-split manoeuvre) as shown in Figure 7-19. Here, the left side has $\mu = 1.0$ and the right side has $\mu = 1.0$, vehicle velocity at the time of braking is 120 Kph. To exclude the reaction of the driver in this test, the steering wheel set to autonomous by activating the built-in IPG CarMaker® driver model (instead of real driver).

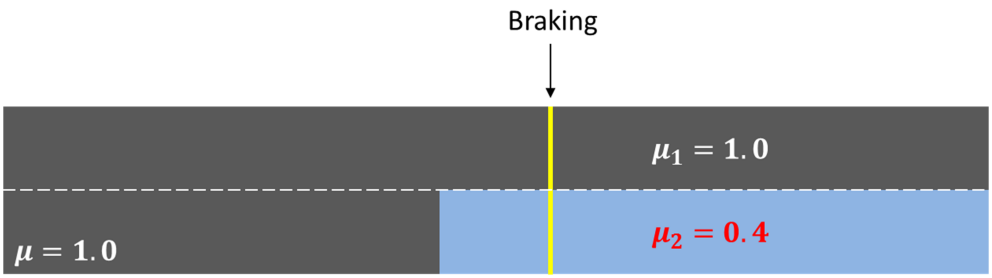

Figure 7-19: Road surfaces for the mu-split test

The test results for vehicle without slip control subject to mu-slip test are presented in Figure 7-20 (a). Here, the wheels are suddenly locked after braking and as the longitudinal forces on the left side tyres are much lower than the longitudinal forces on the right tyres, the vehicle becomes highly oversteer and spin-out. The responses of the vehicle with the slip control subject to the same manoeuvre are shown in Figure 7-20 (b), which confirm the performance and effectiveness of the proposed slip control system. The vehicle speed reduces to zero within 10 sec quite stably and it need much lower brake pressure (than the case of uncontrolled slip braking). Note that the slip build-up quite fast (in around 0.05 sec) and to produce the same longitudinal force, the slip values for the left side (low-mu surface) become higher than the slips at right side tyres (high mu surface).

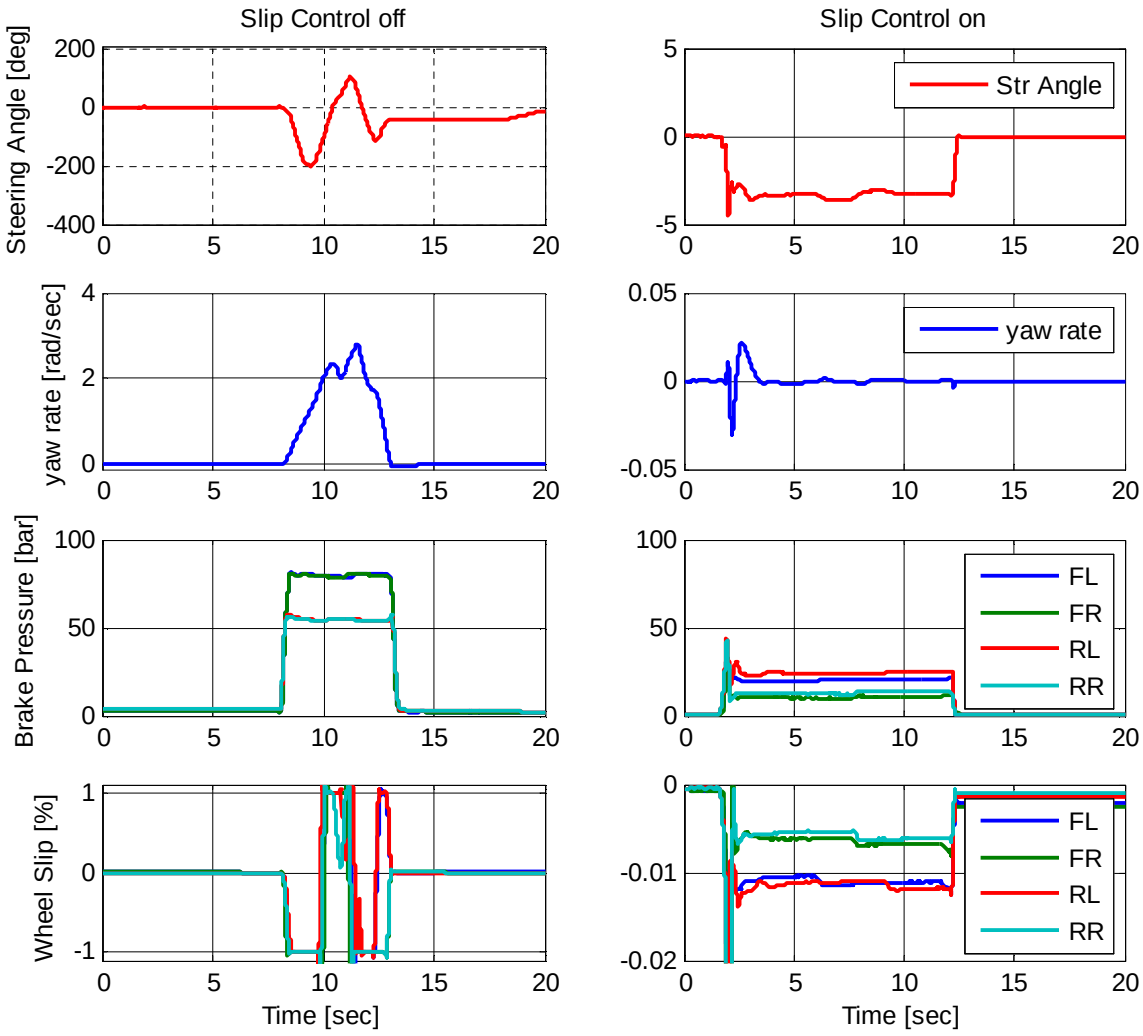

Figure 7-20: vehicle response subject to mu-split manoeuvre, a) without slip control b) with slip control

7.3.2.2 Low-level self-aligning moment feedback control

The validation results of the low-level steering control system based on self-aligning moment feedback is presented in this section. Similar to slip control system, the response of the control system, in the presence of complete dynamics of the plant, subject to step self-aligning moment input is investigated. The test starts when the vehicle is moving in a straight line (steering angle=0) at steady velocity of 100 Kph, and the steering wheel is not touching by the driver. The input is an arbitrary step input to the low-level control system, so called T_{sat_ref}, and the output is the vehicle self-aligning moment, so called T_{sat}. To have more detailed information about the system behaviour, the current of the electric motor I_m is also measured[46]. In order to compare the responses, the equivalent motor torque is calculated by the following relation

$$T_{sat\_m} = I_m \times k_t \times G \times N$$

where $N = {}^{l_d}/_{r_p} = 17$ is the ratio of drop link to the pinion radius.

During the tests, the control system exhibit an oscillatory behaviour and therefore the control bandwidth reduced to 2 Hz[47]. The test results are shown in Figure 7-21 confirm the good stability and performance of the (modified) control system. The vehicle self-aligning moment reach to its target within about 0.2 sec, containing a transport delay between input to the low-level control system and output of the motor torque (as observed before). As in this test, the steering wheel was free to turn, therefore, by applying the motor torque to the column, the steering wheel turns until the vehicle reach to the equilibrium point (i.e the generated self-aligning moment at the vehicle tyres become equal to the reference self-aligning moment), as shown in Figure 7-21.

[46] See Figure (6-9) for more information about the low-level EPAS control system block diagram.
[47] The original bandwidth of the low-level EPAS control system was 6.37 Hz, see section 6.2.3 for more information.

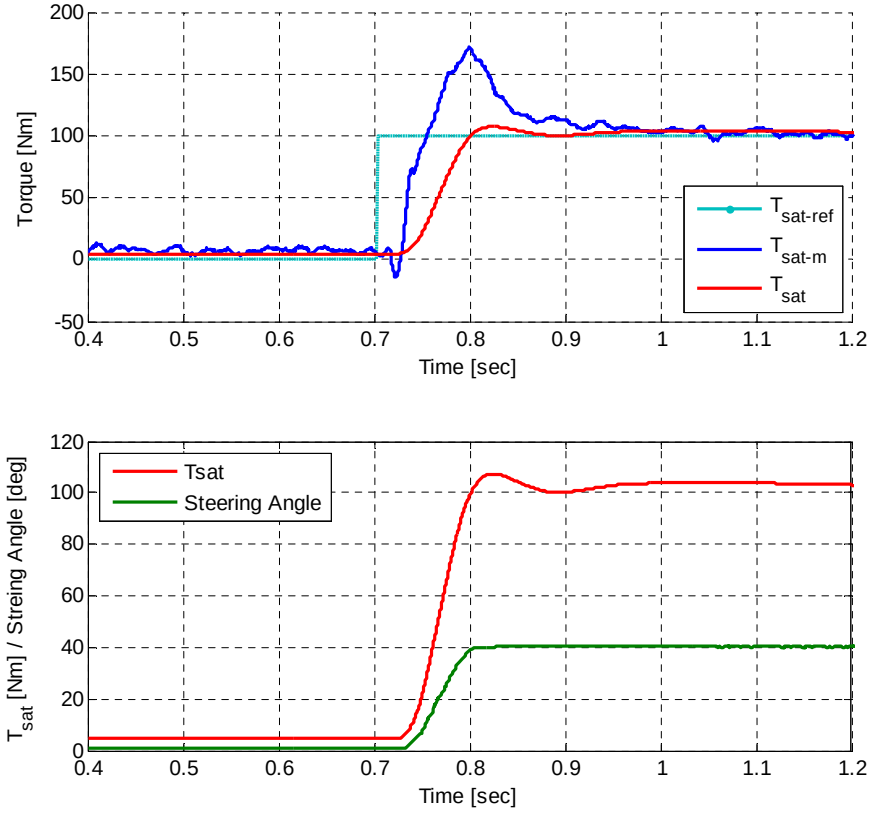

Figure 7-21: Low-Level EPAS control step response

7.3.3 Integrated steering and brake control system validation

By applying the required modifications on the low-level steering and brake controllers (as discussed in the previous sections), the next step toward the final tuning and validation of the proposed integrated vehicle dynamics control system, is to implement the designed high-level controllers, as the most outer control loop, in real time environment and to test the complete IVCS system with the existence of real driver in the loop through various driving scenarios. It is worth to mentioned that, as the bandwidth of the low-level EPAS control system was already reduced to 2 Hz, therefore, to maintain the stability of the whole cascade control system, the bandwidth of the high-level control system (as the outer loop) should also be reduced accordingly. During several tests, it was concluded that the best control performance could be achieved with the high-level control bandwidth of 1 Hz.

In this section, the performance of the proposed integrated vehicle dynamics systems is validated through several actual manoeuvres. It should be noted that in

the following tests, the complete IVCS system was active, both EPAS and EHB actuators were switched on and the tests were performed by the real driver.

To demonstrate the effectiveness of the control system in mild stability situation, the vehicle was subject to mu-split test (as presented in the previous section). As in this manoeuvre the target is to keep the controlled vehicle in straight line path after braking, therefore, it is expected that lateral acceleration would remain below $0.6 \times \mu g$ (which correspond to mild stability condition, as defined in section 5.5.3).[48] Recall, in mild stability condition, the vehicle stability is maintained by only steering (EPAS) actuation.

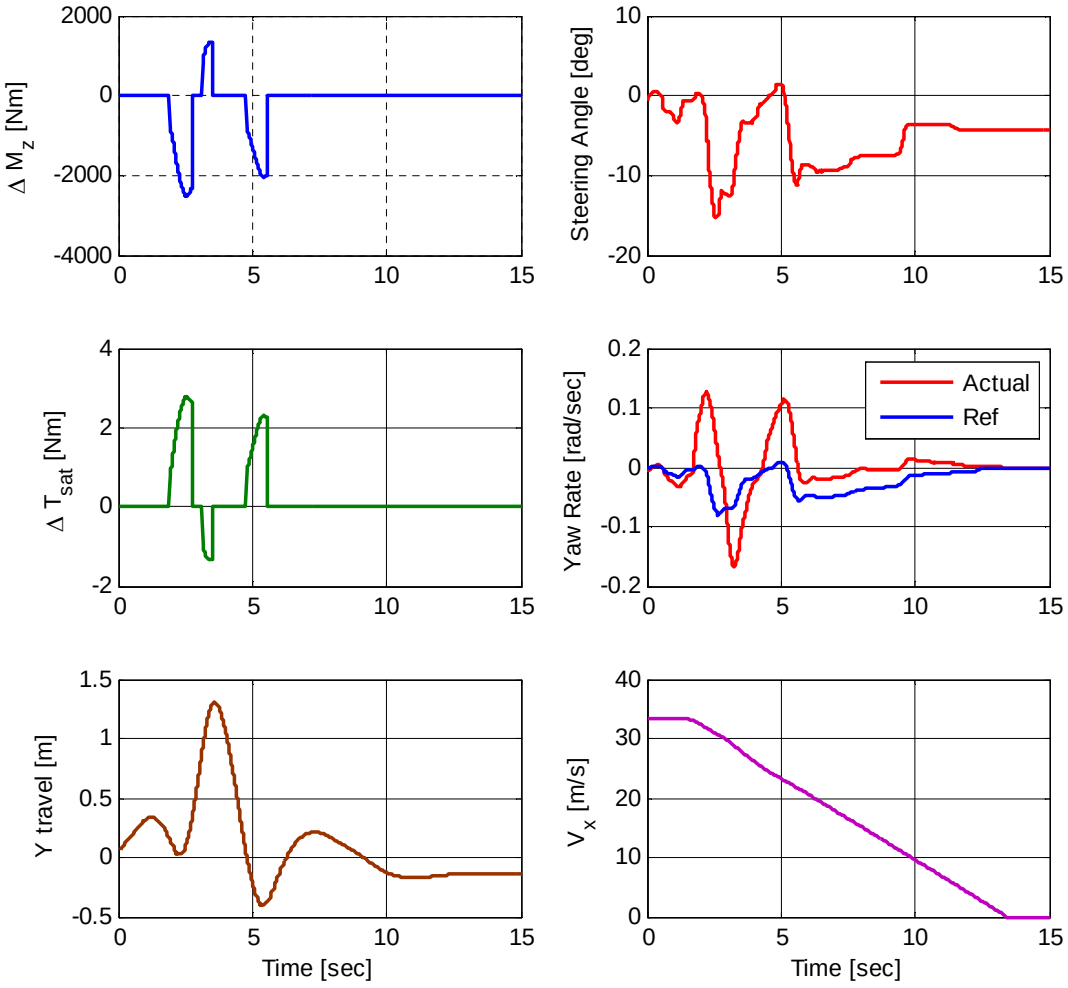

Figure 7-22: mu-split test, EPAS Control, Vx=120 Kph, $\mu_1 = 1.0$, $\mu_2 = 0.4$

[48] Note that in this manoeuvre, the tyre-road coefficients of friction at the left tyres are 0.4 where at the right tyres are 1.0. Here, μ is considered as the average of coefficients of friction at the four tyres.

The result of mu-split test, as shown in Figure 7-22, confirm the good performance of the control system in real situations. The vehicle velocity reduced from 120 Kph to zero within less than 10 sec quite steadily. To maintain the lateral stability of the vehicle, the steering angle is automatically adjusted by applying the corrective ΔT_{sat} to the steering wheel. As the test was performed with real driver steering input, therefore, the vehicle behaviour was affected by the driver haptic feedback. However, the maximum lateral deviation of the vehicle, which was happened at the beginning of the braking, not more than 1.2 meter.

To examine the performance of the proposed control system in more severe driving condition, the vehicle was tested subject to VDA lane change manoeuvre (has now been published as ISO 3888-2 standard). The object of this (closed loop) test is to investigate the lateral dynamics performance of the vehicle in sever driving conditions (ISO 3888-2). The test is based on 3 cone lanes with a total length of 61 meters to define a double lane change (see Figure 7-23), which must be completed with maximum speed. The entry speed (measured in the entry lane) is increased step by step, starting from 60 Kph until the car skids, hits cones, or spins around. This usually happens at speeds of about 70-80 Kph in the best cases (Constant, 2012).

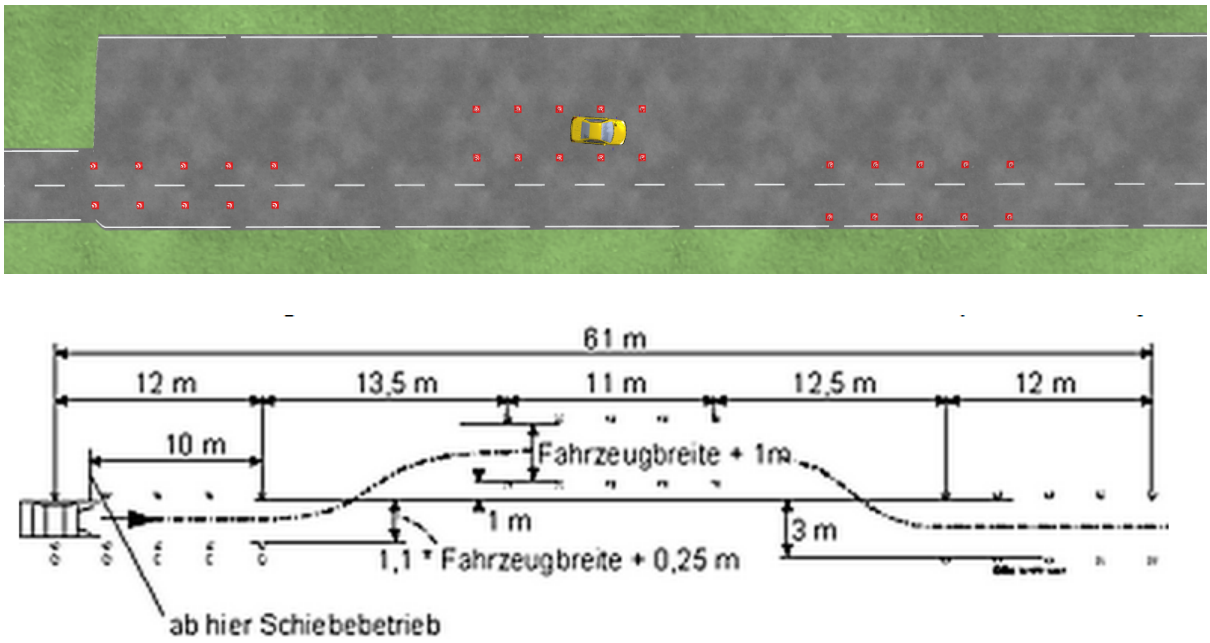

Figure 7-23: VDA Lane change manoeuvre (ISO 3888-2)

The result of the VDA lane change test for the vehicle at entry speed of 75 Kph with and without control system activation is compared in Figure 7-24. As the front tyres of the passive vehicle become saturated on lateral force, the vehicle exhibits understeer behaviour; therefore, it could not follow the path and hits the cones. Meanwhile, the vehicle with control system can nicely follow the target yaw rate and pass through the cones. As the vehicle lateral acceleration exceeded $0.6g$ $(\mu = 1.0)$ the situation is recognised as hazardous stability condition by the IVCS system, therefore the brake actuation is activated and the system perform the same functionality as conventional ESP systems.

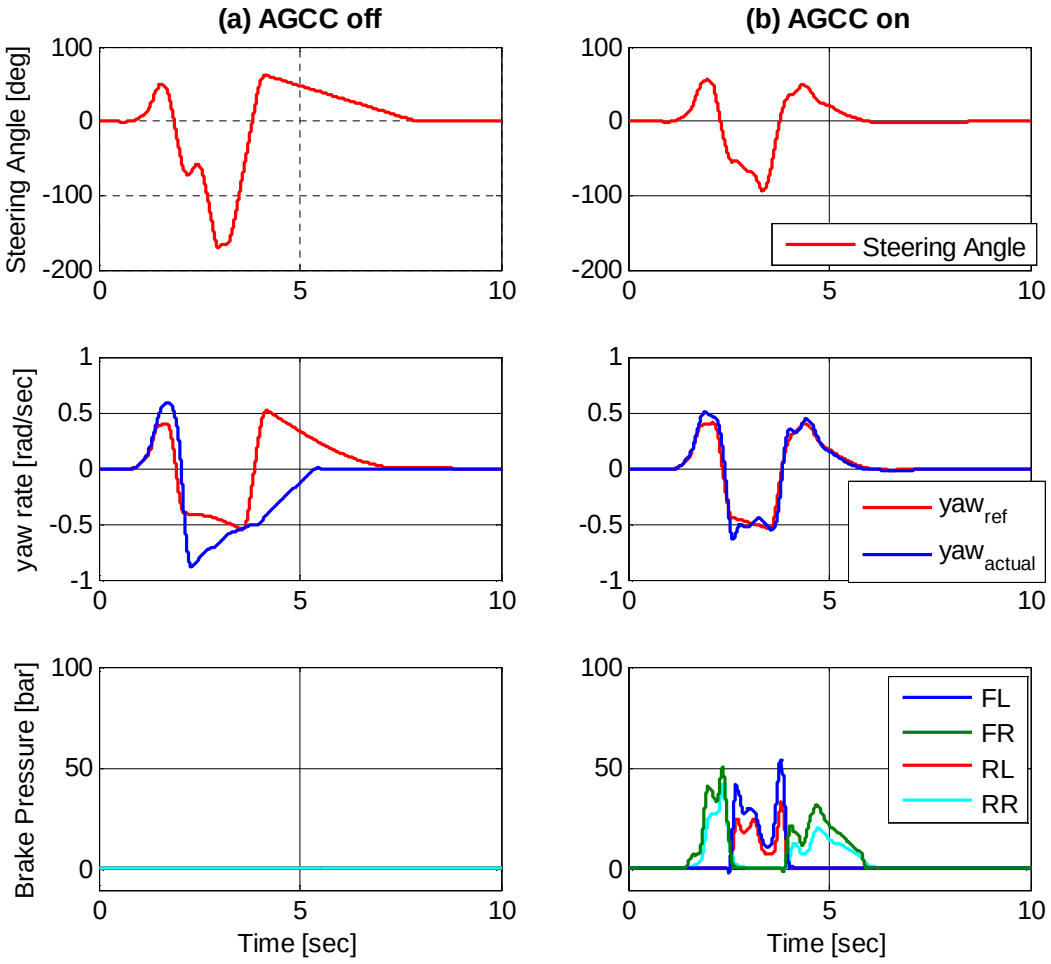

Figure 7-24: VDA lane-change manoeuvre, V=75 Kph

To demonstrate the effectiveness of the IVCS system in case of actuator saturation, a J-turn manoeuver was performed. In this manoeuvre the vehicle is driving on high mu surface $(\mu = 1.0)$ at speed of 120 Kph, was subject to step steer input of 100

degree within one second, as shown in Figure 7-25 (a). Here the tyre longitudinal and lateral forces were arbitrarily limited to 1000N (because of actuator limitations, for example).

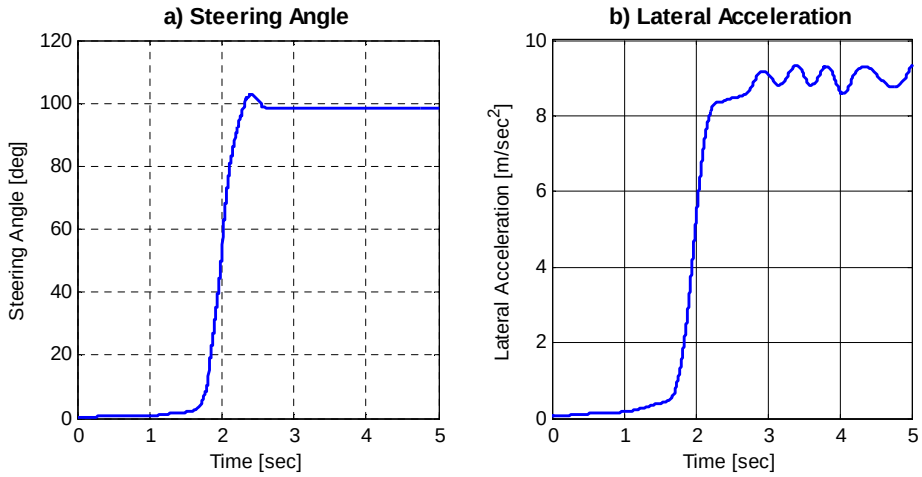

Figure 7-25: Step-Steer manoeuvre, mu=1.0, Vx=120 Kph, Off-throttle

During the manoeuvre, the vehicle lateral acceleration exceeded $0.6g$ ($\mu = 1.0$) as shown in Figure 7-25 (b), therefore, the situation is recognised as hazardous stability condition by the IVCS system. As a result, the brake actuation is activated to maintain the vehicle stability, however, as the requested longitudinal force surpassed the saturation limit, the commanded longitudinal forces (for front right and rear right wheels) were clipped to their saturation limit and the steering (EPAS) actuator will be activated to accommodate the required yaw moment, as shown in Figure 7-26.

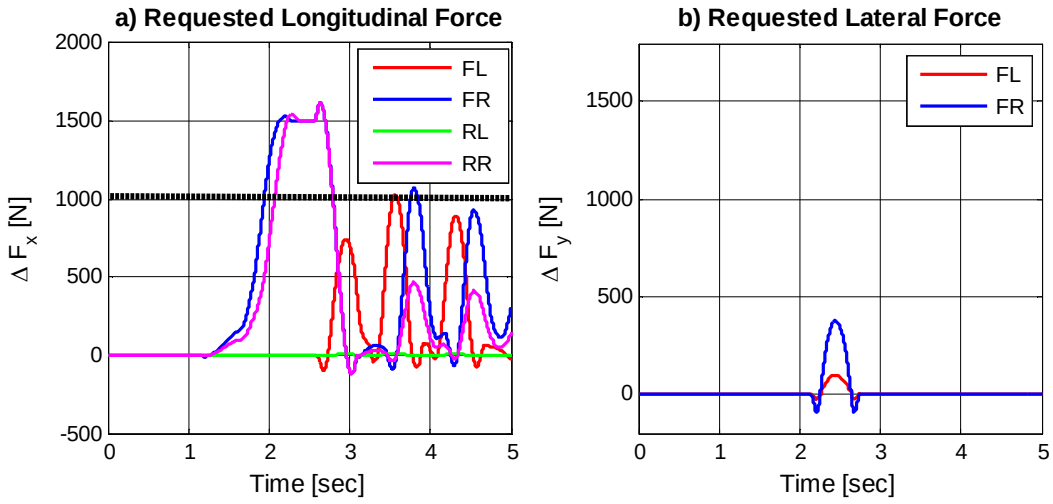

Figure 7-26: The requested longitudinal and lateral tyre forces

The magnitude of brake lines pressure of each wheel and the EPAS motor current and the resultant yaw rate of the vehicle are shown in Figure 7-27. The yaw rates of the passive vehicle subject to the same manoeuvre is compared with the controlled vehicle in Figure 7-27, confirm the fact that the control system prevent the vehicle to spin-out and finally could manage the vehicle to follow the target yaw rate.

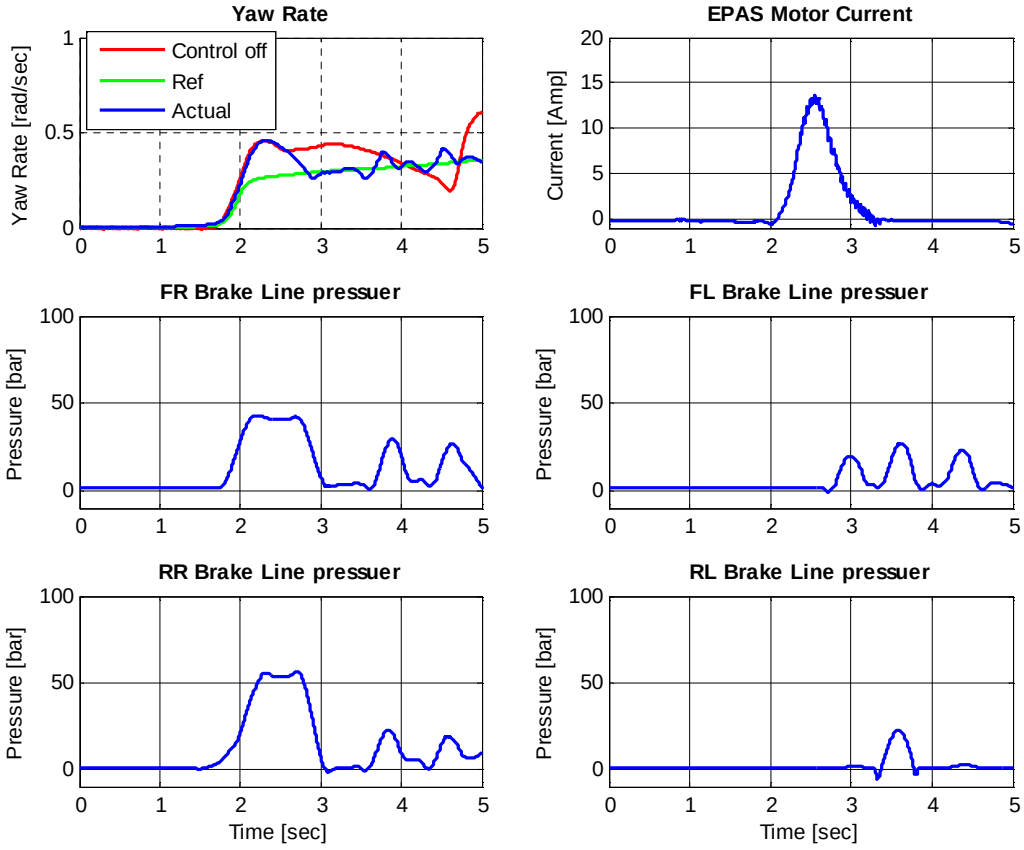

Figure 7-27: Yaw rate, Brake line pressures & EPAS motor current

Finally, it is worth to mention that the proposed CA scheme provide a general flexible framework to adjust any combinations of the existing actuators based on different requirements. For example by altering the Q vector, the system can simply change from pure steering based actuation, to pure based brake actuation or integrated steering and brake actuation. This property of the system is especially very beneficial to provide the system fault tolerant in case of any actuator degradation.[49].

[49] See section 5.5.3 for more information about the role of Q vector in the proposed CA scheme.

8 Conclusion and Future Works

8.1 Conclusion

This dissertation is aimed at proposing a systematic approach for development of a “low-cost”, coordinated and reconfigurable IVDC system. Here, “low-cost” refers to low “processing” cost, so the aim is to design an integrated control system that could be executed in real time by employing low cost processor (ECU). The proposed integrated control system has several interesting features such as flexible, modular, coordinated, adaptive and reconfigurable (active) fault-tolerant. Furthermore, the proposed control architecture is not limited to any specific control design method. It is possible to employ various (linear or nonlinear) control design methods in each control loop in a systematic manner. Modular means the proposed control architecture is not limited to any specific actuators and/or control objectives. It provides a flexible framework for designing several customised IVDC systems within the existing (general) architecture. Coordination refers to the possibility of controlling of all the available actuation resources towards the same overall control objectives, while (active) fault-tolerance is the property of the control system that ensures control objectives are best achieved even in case of some of the actuators failure. Last but not least, adaptive means the control system could be adjusted for better performance if some external conditions such as road surface coefficient of friction are changed.

To prove this concept, a customised control system for integration of two stand-alone VDC systems, namely EPAS and ESP was proposed The system objective is to provide driver comfort as well as vehicle safety. Several high-level and Low-level control loops were designed based on Youla-Parameterisation (closed-loop shaping) method. A fast control allocation algorithm based on daisy-chain method is proposed for steering and brake allocation. Performance of the designed control system was validated through simulation in each design stage. To validate the performance of the integrated control system in real time environment, a Hardware-in-the-Loop (HiL) system was designed and developed. The integrated EPAS & ESP HiL configuration includes real steering and brake actuators in conjunction with a high fidelity real time vehicle model (run in a dSPACE ds1006 simulator), real driver in the loop, and dSPACE MicroAutoBox as rapid control prototyping platform. The proposed control

architecture was implemented in real time and its performance was validated through HiL testing.

The HiL test results confirm the flexibility and effectiveness of the proposed integrated vehicle dynamics control system to fulfil the system requirements and specifications. More importantly, it demonstrates that the control system could be implemented in real time environment

It was demonstrated that by employing the customised IVCS is possible to integrate steering and brake based active systems in a coordinated and reconfigurable manner and interestingly it is possible to reduce the integrated system to each of the traditional stand-alone vehicle dynamics control systems (such as ESP, AFS, EPAS) just by altering few parameters.

It should be noted that although the steering based stability systems (such as AFS or EPAS) provide an optimal solution for control actuation, but from practical point of view, the brake based stability systems (such as ESP) has several privileges. Hazardous stability is featured as a critical driving situation in which the stability system needs a very fast, autonomous and powerful actuation response. Considering the fact that steering dynamics is slow in its nature, could not be utilised in terminal understeer situation (because of the tyre saturation) and it should respect the driver reaction, one can conclude that, in case of severe stability situation the brake based stability system (ESP) should have absolute priority over the steering based stability systems. It was demonstrated that ‘absolute’ priority of the brake actuation cannot obtain by solving the optimal solution algorithms, as the brake based stability system is sub-optimal in its nature. Therefore the system requirements cannot be satisfied by employing any (iterative) optimal algorithms. On the other hand, by daisy chain method absolute priority could be achieved (although it may lead to a sub-optimal solution, especially in case of actuator saturation), which might be desirable from practical pint of view.

The general limitation of employing steering systems to provide vehicle stability is even getting worth in case of EPAS employment. Note that the EPAS system is directly linked to the driver via steering wheel and continuously interact with him/her through steering wheel haptic feedback, therefore any change to the steering wheel torque is immediately felt by the driver and he/she will react to it accordingly. The

question of employing the EPAS system to maintain vehicle stability (in oversteering situation) seems paradoxical: in order to recover the vehicle stability we have to employ a counter steering torque to the steering wheel, this in turn reduce the vehicle manoeuvreability which has adverse effect on driver handling capability. Moreover, the reference yaw rate (and sideslip) is directly derived from steering wheel angle[50], therefore, any change to the steering wheel (as a result of EPAS/driver interaction) will have negative impact on the performance of the stability system (as it degrade the control target)

On the other hand, the effectiveness of the EPAS system to prevent the vehicle to enter to the hazardous stability situation was demonstrated through mu-split manoeuvre. Therefore one may conclude that the EPAS stability system is effective in mild stability situations and also could be employed as a backup for brake based stability system (ESP) to provide extra stabilising moment (and side force) in case of brake actuators saturation or degradation. Again, all these required specifications can be easily formulated via daisy chain CA scheme, as proposed in this thesis.

8.2 Future works

A systematic approach toward the development of integrated vehicle dynamics control system is proposed in this thesis. To complete the current achievements and also to broaden the applicability of the proposed system, several research subjects are proposed, as follows:

- The role of reference generator is crucial in every vehicle dynamics control system, as it has influence on the performance of the control system and also dictate the behaviour of the (controlled) vehicle. Development of more advanced reference generator is one the important research topics which could improve the performance of any vehicle dynamics control system, including the proposed IVCS system.
- The customised IVCS system was designed to improve the vehicle *comfort* and *stability* as two high-level vehicle dynamics objectives. It is possible to further extend this work by including other objectives such as agility or manoverability to the IVCS system. This especially important for improving the

[50] See section 3.5 for more discussion on

performance of the controlled vehicle in the whole range of the vehicle driving conditions.

- The proposed system was designed based on daisy chain control allocation scheme. Investigating and implementing other control allocation methods which might lead to better results in terms of optimality, yet any proposed solution should consider the practical requirements (and limitations) and also should be able to be implemented in real time ECUs with low processing cost.
- In this thesis a novel, neo-classical methodology was employed for design of the low-level and high-level control systems. The proposed control design methodology is the first step toward the more advanced robust control design methodologies such as H_∞ (Assadian F. , 2011). Considering the fact that the vehicle dynamics system (and its subsystems) have high level of (structural and unstructural) uncertainties, it is possible to further improve the performances of the proposed control systems by employing other control design approaches, especially the robust H_∞ method.
- The flexibility of the proposed control structure (and the designed HiL test rig) enable ones to expand the functionality of the customised IVCS system by considering the employment of other (steering and/or brake based) vehicle dynamics active systems, such as AFS, SBW and BBW (or even TCS).
- The proposed IVCS system provides a systematic approach toward development of integrated vehicle dynamics control system. One of the important extensions to the current work is to include other chassis control systems such as active suspension or active roll control to the current structure. This would be the next step toward the idea of development of a complete global chassis control systems.
- The IVCS system was mainly developed for integration of various vehicle dynamics active systems, however, considering the generality and flexibility of the proposed control structure, it is possible to expand the application of the system by adapting it to other (over-actuated) vehicle domains such hybrid power trains. One of the interesting research areas would be the implementation of the proposed CA scheme in design of hybrid-electric powertrains.

- Last but not least, the aim of this thesis was to develop a low cost integrated control system solution that could work in vehicles. The excellent results that have been achieved through HiL testing foster us for the next development step which is the implementation of the proposed IVCS system in a vehicle and its validation through field testing. This will not happened without a strong support from an OEM company. I hope that this dream will come through very soon by the help of Jaguar Land Rover Company, as they did before for this project.

REFERENCES

Loucopoulos, P., & Karakostas, V. (1995). *System Requirements Engineering.* N.Y.: McGraw-Hill, Inc.

Nicolescu, G., & Mosterman, P. (2010). *Model-Based Design for Embedded Systems.* CRC Press.

(2004). *VDI 2206, Design methodology for mechatronic systems.*

Abbink, D. A., & Mulder, M. (2010). Neuromuscular analysis as a guideline in designing shared control. *Advances in haptics, 109*, 499-516.

Abel, D., & Bollig, A., A. (2006). Rapid control prototyping. Springer Berlin Heidelberg.

Ackermann, J. (1997). Robust control prevents car skidding. *Control Systems, IEEE, 17*(3), 23-31.

Ahn, C., Peng, H., & Tseng, H. (2012). Robust estimation of road friction coefficient using lateral and longitudinal vehicle dynamics. *Vehicle System Dynamics: International Journal of Vehicle Mechanics and Mobility, 50*(6), 961-985.

Amberkar, S., Bolourchi, F., Demerly, J., & Millsap, S. (2004). A control system methodology for steer by wire systems . *SAE 2004-01-1106*.

Antsaklis, P. J., & Michel, A. N. (1997). *Linear Systems.* Boston: Birkhauser.

Asarin, E., Bournez, O., Dang, T., Maler, O., & Pnueli, A. (2000). Effective Synthesis of Switching Controllers for Linear Systems. *Proceedings of the IEEE, 88*(7), 1011.

Aslaksen, E., & Belcher, W. (1992). *Systems Engineering.* Prentice Hall.

Assadian, F. (2011). Neo-Classic Control Approach. *Unpublishe Lecture Notes*. Cranfield University.

Assadian, F. (2012). *Chassis Control Systems.* Cranfield University.

Assadian, F., & Aneke, E. (2006). Two distinct methods for integration of active differential and active roll control systems. *Int. J. Vehicle Design, 42*(3/4), 348-369.

Automotive SIG. (2010). *Automotive SPICE® : Process Reference Model, Release v4.5.* Automotive Special Interest Group (SIG).

Badawy, A., Zuraski, J., Bolourchi, F., & Chandy, A. (1999). Modeling and analysis of an electric power steering system. *SAE Technical Paper 1999-01-0399*.

Balas, G., Chiang, R., Packard, A., & Safonov, M. (2005). *Robust Control Toolbox™ 3.* MathWorks.

Bitar, N., Bolourchi, F., Colosky, M., Colosky, M. P., & Etienne, C. (1999). *Patent No. U.S. Patent No. 5,919,241.* Washington, DC: U.S. Patent and Trademark Office.

Blundell, M., & Harty, D. (2004). *Multibody Systems Approach to Vehicle Dynamics.* Oxford: Elsevier Butterworth-Heinemann.

Boada, B. L., Boada, M. J., & Diaz, V. (2005). Fuzzy-logic applied to yaw moment control for vehicle stability. *Vehicle System Dynamics: International Journal of Vehicle Mechanics and Mobility, 43*(10), 753-770.

Bodson, M. (2002). Evalution of Optimization Methoda for Control Allocation. *Journal of Guidance, Control, and Dynamics, 25*(4), 703-711.

Bodson, M. (2002). Evalution of Optimization Methoda for Control Allocation. *Journal of Guidance, Control, and Dynamics, 25*(4), 703-711.

Bodson, M., & Frost, S. A. (2011). Load Balancing in Control Allocation. *Journal of Guidance, Control, and Dynamics, 34*(2), 380-387.

Bordignon, K. A. (1996). *Constrained Control Allocation for Systems with Redundant Control Effectors.* PhD Dissretation, Virginia Tech.

Brach, R., & Brach, R. (2000). Modeling Combined Braking and Steering Tire Forces. *2000-01-0357*.

Brach, R., & Brach, R. (2009). Tire models used in accident reconstruction vehicle motion simulation. *SAE 2009-01-0102*.

Bringmann, E., & Krämer, A. (2008). Model-based Testing of Automotive Systems. *International Conference on Software Testing, Verification, and Validation.*

Bristol, E. (1966,). On a new measure of interaction for multivariable process control. *Automatic Control, IEEE Transactions on, 11*(1), 133-134.

Broy, M. (2006, May). Challenges in automotive software engineering. *In Proceedings of the 28th international conference on Software engineering* (pp. 33-42). ACM.

Broy, M., Feilkas, M., Herrmannsdoerfer, M., Merenda, S., & Ratiu, D. (2010). Seamless model-based development: From isolated tools to integrated model engineering environments. *Proceedings of the IEEE, 94*(8), 526-545.

Buffington, J. M., & Enns, D. F. (1996). Lyapunov stability analysis of daisy chain control allocation. *Journal of Guidance, Control, and Dynamics, 19*(6), 1226-1230.

Burckhardt, M. (1993). *Fahrwerktechnik: Radschlupf-Regelsysteme.* Germany: Vogel-Verlag.

Burken, J., Lu, P., & Wu, Z. (1999). *Reconfigurable flight control designs with application to the X-33 vehicle.* National Aeronautics and Space Administration, Dryden Flight Research Center.

Burton, A. W. (2003). Innovation drivers for electric power-assisted steering. *Control Systems, IEEE, 23*(6), 30-39.

Chang, S. (2007). *A Flexible Hierarchical Model-Based Control Methodology for Vehicle Active Safety Systems.* USA: The University of Michigan.

Chen, C., Dao, T., & Lin, H. (2010). A compensated yaw-moment-based vehicle stability controller. *Int. J. of Vehicle Design, 53*(3), 220-238.

Chen, L. K., & Ulsoy, A. G. (2001). Identification of a driver steering model, and model uncertainty, from driving simulator data. *Journal of dynamic systems, measurement, and control, 123*(4), 623-629.

Chen, W., Xiao, H., Liu, L., Zu, J. W., & Zhou , H. (2011). Integrated Control of Vehicle System Dynamics: Theory and Experiment. In *Advances in Mechatronics* (pp. 3-30). InTech.

Chen, X., Yang, T., Chen, X., & Zhou, K. (2008). A generic model-based advanced control of electric power-assisted steering systems. *Control Systems Technology, IEEE Transactions on, 16*(6), pp. 1289-1300.

Chen, Y., & Wang, J. (2012). Fast and global optimal energy-efficient control allocation with applications to over-actuated electric ground vehicles. *Control Systems Technology, IEEE Transactions on, 20*(5), 1202-1211.

Ciarla, V., Cahouet, V., de Wit, C. C., & Quaine, F. (2012, September). Genesis of booster curves in electric power assistance steering systems. *In Intelligent Transportation Systems (ITSC), 2012 15th International IEEE Conference on* (pp. 1345-1350). IEEE.

Constant, C. (2012, 12 15). Retrieved 06 08, 2014, from Car Engineer: http://www.car-engineer.com/the-moose-test-or-vda-test/

Davidson, J. B., Lallman, F. J., & Bundick, W. T. (2001, July). Real-time adaptive control allocation applied to a high performance aircraft. *In 5th SIAM Conference on Control & Its Application*, (pp. 1211-1229).

De Wit, C. C., & Tsiotras, P. (1999). Dynamic tire friction models for vehicle traction control.

Desoer, C. A., & Vidyasagar, M. (1975). *Feedbak System: Input-Output Properties.* New York, NY: Academic Press.

Desoer, C., Liu, R. W., Murray, J., & Saeks, R. (1980). Feedback system design: The fractional representation approach to analysis and synthesis. *Automatic Control, IEEE Transactions on, 25*(3), 399-412.

Doyle, J. C., Francis, B. A., & Tannenbaum, A. (1992). *Feedback Control Theory.* New York: Macmillan Publishing Co.

Drakunov, S., Ozguner, U., Dix, P., & Ashrafi, B. (1995). ABS control using optimum search via sliding modes. *Control Systems Technology, IEEE Transactions on, 3*(1), 79-85.

Durham, W. C. (1993). Constrained control allocation. *Journal of Guidance, Control, and Dynamics, 16*(4), 717-725.

Eppinger, S. D., & Salminen, V. (2001). Patterns of Product Development Interacting. *Proceedings of the international conference on engineering.* Glasgow.

Ertas, A. (1996). *The Engineering Design Process* (2nd ed.). N.Y.: John Wiley & Sons, Inc.

Fehrenbach, A., Hoetzel, J., Tschiskale, E., & Weber, J. (2000). *Patent No. U.S. Patent No. 6,061,002.* Washington, DC: U.S. Patent and Trademark Office.

Frost, S. A., Bodson, M., & Acosta, D. M. (2009). Sensitivity analysis of linear programming and quadratic programming algorithms for control allocation. *In Proc. AIAA Infotech and Aerospace Conf. and Exhibit.* Seattle, WA.

Furukawa, Y., & Abe, M. (1997). Advanced Chassis Control Systems for Vehicle Handling and Active Safety. *Vehicle System Dynamics: International Journal of Vehicle Mechanics and Mobility, 28*(2-3), 59-86.

Gajic, Z. (2003). *Linear dynamic systems and signals.* Prentice Hall/Pearson Education.

Gerdes, J., & Hedrick, J. (1999). Brake System Modeling for Simulation and Control. *Journal of Dynamic Systems, Measurement, and Control, 121*, 496-503.

Gillespie , T. D. (1992). *Fundamentals of Vehicle Dynamics.* SAE.

Glinz, M. (2007, October). On non-functional requirements. In *Requirements Engineering Conference, 2007. RE'07. 15th IEEE International* (pp. 21-26). IEEE.

Golub, G. H., & Van Loan, C. F. (2012). *Matrix Computations* (4 ed.). JHU Press.

Goodwin, G. C. (2002). *A brief overview of nonlinear control.* Centre for Integrated Dynamics and Control, Department of Electrical and Computer Engineering, The University of Newcastle, Australia.

Gordon, T., Howell, M., & Brandao, F. (2003). Integrated Control Methodologies for Road Vehicles. *Vehicle System Dynamics, 40*(1), 157-190.

Gross, D. (1999). Report from the Fidelity Implementation Study Group. *Spring Simulation Interoperability Workshop.*

Gunther Plapp. (2001, Nov. 20). *Electronic Brake Control Systems*. Retrieved April 22, 2014, from Auto Speed: http://www.autospeed.com/cms/article.html?&title=Electronic-Brake-Control-Systems&A=1202

Hanselmann, H. (1996, September). Automotive control: from concept to experiment to product. *In Computer-Aided Control System Design, 1996., Proceedings of the 1996 IEEE International Symposium on* (pp. 129-134). IEEE.

Harkegard, O. (2002). Efficient active set algorithms for solving constrained least squares problems in aircraft control allocation. *Decision and Control, 2002, Proceedings of the 41st IEEE Conference on, 2*, 1295-1300.

Härkegard, O., & Glad, S. (2005). Resolvingactuator redundancy—optimal control vs. control allocation. *Automatica, 41*, 137-144.

Heißing, B., & Ersoy, M. (Eds.). (2011). *Chassis Handbook: Fundamentals, Driving Dynamics, Components, Mechatronics, Perspectives.* Vieweg+Teubner Verlag.

Hirano, Y., Harada, H., Ono, H., & Takanami, K. (1993). Development of an Integrated System of 4WS and 4WD by H∞ Control. *SAE Technical Paper 930267*.

Holtmann, J., Meyer, J., & Meyer, M. (2011). A Seamless Model-Based Development Process for Automotive Systems. In *Software Engineering (SE) 2010 - Workshopband, LNI volume P-184* (pp. 79-88). Bonner Kollen Verlag.

Horiuchi, S., Okada, K., & Nohtomi, S. (1999). Improvement of vehicle handling by nonlinear integrated control of four wheel steering and four wheel torque. *JSAE Review, 20*(4), 459-464.

Hsu, Y. (2009). *Estimation and Control of Lateral Tire Forces using Steering Torque (PhD Thesis).* USA: Stanford University.

Hsu, Y. H., & Gerdes, J. C. (2008). The Predictive Nature of Pneumatic Trail: Tire Slip Angle and Peak Force Estimation using Steering Torque. *9th International Symposium on Advanced Vehicle Control.*

Hu, C.-H. (2008). Modelling and Simulation of Automotive Electric Powers Steering Systems. *Intelligent Information Technology Application, 2008. IITA '08. Second International Symposium on, 3*, 436 - 439.

IPG Automotive GmbH. (2013). *CarMaker® Reference Manual Version 4.0.6.*

Isermann, R. (2005). *Mechatronic systems: fundamentals.* Springer.

Isermann, R. (2008). Mechatronic systems—Innovative products with embedded control. *Control Engineering Practice, 16*, 14-29.

Ishida, S., & Gayko, J. E. (2004, June). Development, evaluation and introduction of a lane keeping assistance system. *In Intelligent Vehicles Symposium, 2004 IEEE* (pp. 943-944). IEEE.

ISO Technical Committee TC 22/SC9. (1998). Tansient open-loop response test method with one period of sinusoidal input. *ISO/TR 8725-1998*.

ISO Technical Committee TC 22/SC9. (2003). Lateral transient response test methods. *ISO 7401-2003*.

ISO Technical Committee TC 22/SC9. (2004). Steady-state circular driving behaviour. *ISO 4138-2004*.

ISO Technical Committee TC 22/SC9. (2011). Passenger cars - Test track for a severe lane-change manoeuvre - Part 2: Obstacle avoidance. *ISO 3888-2:2011*.

ISO Technical Committee TC 22/SC9. (2011). Vehicle dynamics and road-holding ability - vocabulary. *ISO 8855-2011*.

Jazar, R. N. (2008). *Vehicle Dynamics:Theory and Application.* NY: Springer.

Jiang, F., & Gao, Z. (2001). An Application of Nonlinear PID Control to a Class of Truck ABS Problems. *Decision and Control, 2001. Proceedings of the 40th IEEE Conference on. 1*, pp. 516-521. IEEE.

Johansen, T. A., & Fossen, T. I. (2012). Control Allocation - A survey. *IEEE*, 1-10.

Johansen, T. A., Petersen, I., Kalkkuhl, J., & Ludemann, J. (2003). Gain-scheduled wheel slip control in automotive brake systems. *Control Systems Technology, IEEE Transactions on, 11*(6), 799-811.

Jonasson, M. (2009). *Exploiting individual wheel actuators to enhance vehicle dynamics and safety in electric vehicles (PhD Thesis).* Stockholm, Sweden: KTH Royal Institute of Technology.

Karbalaei, R., Ghaffari, A., Kazemi, R., & Tabatabaei, S. (2007). A new intelligent strategy to integrated control of AFS/DYC based on fuzzy logic. *International Journal of Mathematical, Physical and Engineering Sciences, 1*(1), 47-52.

Karnopp, D. (2013). *Vehicle Dynamics, Stability, and Control* (2nd ed.). CRC Press.

Kathrin, S., Andreas, R., Thomas, B., Christian, S., & Daouda, S. (2012). Maneuver-Based Testing of Integrated, Highly Interconnected Safety Systems. *FISITA F2012-E14-019*.

Kiébré, R. (2010). *Contribution to the modelling of aircraft tyre-road interaction (PhD thesis).* Université de Haute-Alsace.

Kiencke, U., & Nielsen, L. (2005). *Automotive Control Systems For Engine, Driveline, and Vehcile* (2 nd ed.). Springer.

Kim, J. H., & Song, J. B. (2002). Control logic for an electric power steering system using assist motor. Mechatronics, 12(3), 447-459. *Mechatronics, 12*(3), 447-459.

Kinnaert, M. (1995). Interaction measures and pairing of controlled and manipulated variables for multiple-input multiple-output systems: A survey. *Journal A, 36*(4), 15-23.

Klier, W., & Reinelt, W. (2004). Active front steering (part 1): Mathematical modeling and parameter estimation. *SAE Technical Paper 2004-01-1102*.

Koehn, P., Eckrich, M., Smakman, H., & Schaffert, A. (2006). Integrated Chassis Management: Introduction into BMW's Approach to ICM. *SAE TECHNICAL PAPER SERIES, 2006-01-1219*.

Komoto, H., & Tomiyama, T. (2012). A framework for computer-aided conceptual design and its application to system architecting of mechatronics products. *Computer-Aided Design, 44*, 931-946.

Kurishige, M., Tanaka, H., Inoue, N., Tsutsumi, K., & Kifuku, T. (2002). An EPS control strategy to improve steering maneuverability on slippery roads. *SAE paper, (2002-01), 0618*.

Kurishige, M., Tanaka, H., Inoue, N., Tsutsumi, K., & Kifuku, T. (2002). An EPS control strategy to improve steering maneuverability on slippery roads. *SAE paper, (2002-01), 0618*.

Laine, L. (2007). *Reconfigurable motion control systems for over-actuated road vehicles.* Chalmers University of Technology.

Laws, S., Gadda, C., Kohn, S., Yih, P., Gerdes, J. C., & Milroy, J. C. (2005, July). Steer-by-wire suspension and steering design for controllability and observability. *Proceedings of IFAC World Congress.* Prague.

Leen, G., & Heffernan, D. (2002). Expanding automotive electronic systems. Computer. *Computer, 35*(1), 88-93.

Limpert, R. (2011). *Brake Design and Safety* (3rd ed.). USA: SAE International.

Liu, L., Nagai, M., & Raksincharoensak, P. (2008). On Torque Control of Vehicle Handling and Steering Feel for Avoidance. Maneuver with Electric Power Steering. *Proceedings of the 17th IFAC World Congress.* Seoul, Korea.

Lötstedt, P. (1984). Solving the minimal least squares problem subject to bounds on the variables. *BIT Numerical Mathematics, 24*(2), 205-224.

Mammar, S., & Koenig, D. (2002). Vehicle handling improvement by active steering. *Vehicle system dynamics, 38*(3), 211-242.

Manning, W. J., & Crolla, D. A. (2007). A review of yaw rate and sideslip controllers for passenger vehicles. *Transactions of the Institute of Measurement and Control, 29*(2), 117-135.

Mauer, G. F. (1995). A fuzzy logic controller for an ABS braking system. *Fuzzy Systems, IEEE Transactions on, 3*(4), 381-388.

Mavros, G. (2007). On the objective assessment and quantification of the transient-handling response of a vehicle. *Vehicle System Dynamics, 45*(2), 93-112.

McCann, R. (2000). Variable Effort Steering for Vehicle Stability Enhancement Using an Electric Power Steering System. *SAE Technical Paper 2000-01-0817*.

Milliken, W. F., & Milliken, D. L. (1995). *Race Car Vehicle Dynamics.* SAE International.

Minoiu Enache, N., Netto, M., Mammar, S., & Lusetti, B. (2009). Driver steering assistance for lane departure avoidance. *Control engineering practice, 17*(6), 642-651.

Modjtahedzadeh, A., & Hess, R. A. (1993). A model of driver steering control behavior for use in assessing vehicle handling qualities. *Journal of dynamic systems, measurement, and control, 115*(3), 456-464.

Mokhiamar, O., & Abe, M. (2004). Simultaneous optimal distribution of lateral and longitudinal tire forces for the model following control. *Journal of dynamic systems, measurement, and control, 126*(4), 753-763.

Mokhiamar, O., & Abe, M. (2004). Simultaneous Optimal Distribution of Lateral and Longitudinal Tire Forces for the Model Following Control. *Journal of Dynamic Systems, Measurement, and Control , 126*(4), 753-763.

Morari, M. (1983). Design of resilient processing plants—III: A general framework for the assessment of dynamic resilience. *Chemical Engineering Science, 38*(11), 1881-1891.

Motoyama, S. (2008). Development of EPS+. *Mitsubishi Motors Technical Review, 20*, pp. 97-98.

Mutz, M., Huhn, M., Goltz, U., & Kromke, C. (2003). Model based system development in automotive. *SAE SP*, 1-10.

Nagai, M., Shino, M., & Gao, F. (2002). Study on integrated control of active front steer angle and direct yaw moment. *JSAE review, 23*(3), 309-315.

Navet, N., & Simonot_Lion, F. (. (2008). *Automotive embedded systems handbook.* CRC press.

Nazareth, D., & Siwy, R. (2013). Development of an AUTOSAR Software Component Based on the V-Model. In *Proceedings of the FISITA 2012 World Automotive Congress* (pp. 407-416). Springer Berlin Heidelberg.

Nocedal, J., & Wright, S. J. (2006). *Numerical optimization* (2 ed.). New York: Springer.

Ogata, K. (2010). *Modern Control Engineering.* Prentice-Hall.

Ono, E., Asano, K., & Koibuchi, K. (2004). Estimation of tire grip margin using electric power steering system. *Vehicle System Dynamics, 41*, 421-430.

Ono, E., Hattori, Y., Muragishi, Y., & Koibuchi, K. (2006). Vehicle dynamics integrated control for four-wheel-distributed steering and four-wheel-distributed traction/braking systems. *Vehicle System Dynamics: International Journal of Vehicle Mechanics and Mobility, 44*(2), 139-151.

Oppenheime, M. W., Doman, D. B., & Bolender, M. A. (2006, June). Control allocation for over-actuated systems. *In Control and Automation, 2006. MED'06. 14th Mediterranean Conference on* (pp. 1-6). IEEE.

Oppenheimer, M. W., Doman, D. B., & Bolender, M. A. (2011). Control Allocation. In W. S. Levins, *Control System Applications* (pp. 8-1,8-24). CRC Press.

Oppenheimer, W. M., & Doman, D. B. (2006). *Control Allocation for Overactuated Systems.*

Pacejka, H. B. (2006). *Tyre and Vehicle Dynamics* (2nd ed.). Oxford: Butterworth-Heinemann.

Pacejka, H. B., & Sharp, R. S. (1991). Shear force development by pneumatic tyres in steady state conditions: a review of modelling aspects. *Vehicle system dynamics, 20*(3-4), 121-175.

Pacejka, H. B., Bakker, E., & Nyborg, L. (1987). Tyre modelling for use in vehicle dynamics studies. *SAE Paper, 870421*.

Pagea, a. b., & Steinberg, M. L. (2000, August). A closed-loop comparison of control allocation methods. *In Proceedings of the 2000 Guidance, Navigation and Control Conference.*

Petersen, J. A., & Bodson, M. (2006). Constrained quadratic programming techniques for control allocation. *Control Systems Technology, IEEE Transactions on, 14*(1), 91-98.

Pick, A., & Cole, D. (2003). Neuromuscular dynamics and the vehicle steering task. *Vehicle Syst. Dyn., 41*, 182-191.

Post, J. (1995). *Modeling, Simulation and Testing of Automobile Power Steering Systems for the Evaluation of On-center Handling.* Clemson University.

Pretschner, A., Broy, M., Kruger, I. H., & Stauner, T. (2007, May). Software engineering for automotive systems: A roadmap. *In 2007 Future of Software Engineering* (pp. 55-71). IEEE Computer Society.

Rajamani, R. (2012). *Vehicle Dynamics And Control, 2nd ed.* Springer Verlag.

Rao, S. S. (2009). *Engineering Optimization, Theory and parctice* (4 ed.). New Jersey: John Wiley & Sons.

Robert Bosch GmbH. (2011). *Automotive Handbook* (8th ed.). (K. Reif, Ed.) Cambridge, USA: Bentley Publishers.

Robert Bosch GmbH. (2011). *Bosch Automotive Handbook: 8th Edition.* John Wiley & Sons Inc.

(n.d.). *Robust estimation of road friction coefficient using lateral and longitudinal vehicle dynamics.*

Salgado, M. E., & Conley, A. (2004). MIMO interaction measure and controller structure selection. *Int. J. Control, 77*(4), 367-383.

Savaresi, S. M., & Tanelli, M. (2010). *Active braking control systems design for vehicles.* Springer.

Schöner, H. P. (2004). Automotive mechatronics. *Control engineering practice, 12*(11), 1343-1351.

Shibahata, Y. (2005). Progress and future direction of Chassis control technology. *Annual Reviews on Control, 29*(1), 151-158.

Shibahata, Y., Shimada, K., & Tomari., T. (1993). Improvement of vehicle maneuverability by direct yaw moment control. *Vehicle System Dynamics, 22*(5-6), 465-481.

Shladover, S. E. (1995). Review of the state of development of advanced vehicle control systems (AVCS). *Vehicle System Dynamics, 24*(6-7), 551-595.

Skogestad, S., & Postlethwaite, I. (2007). *Multivariable feedback control: analysis and design* (2 ed.). New York: Wiley.

Slotine, J. E., & Li, W. A. (1991). *Applied Nonlinear Control* (Vol. 199). New Jersey: Prentice Hall.

Slotine, J. E., & Weiping, L. (1991). *Applied nonlinear control.* New Jersey: Prentice hall.

Smakman, H. (2000). *Functional Integration of Slip Control with Active Suspension for Improved Lateral Vehicle Dynamics.* Utz.

Soltani, A. (2011). *1st year progress report.* Cranfield University.

Steffen, T. (2005). *Control reconfiguration of dynamical systems: linear approaches and structural tests* (Vol. 320). Springer.

Stéphant, J., Charara, A., & Meizel, D. (2004, April). Virtual Sensor: Application to Vehicle Sideslip Angle and Transversal Forces. *IEEE TRANSACTIONS ON INDUSTRIAL ELECTRONICS, 51*(2), 278-289.

Sugitani, N., Fujuwara, Y., Uchida, K., & Fujita, M. (1997, June). Electric power steering with H-infinity control designed to obtain road information. *In American Control Conference, 1997. Proceedings of the 1997. 5*, pp. 2935-2939. IEEE.

Svendenius, J., & Wittenmark , B. (2003). Brush Tire Model with increased Flexibility. *European Control Conference.*

Takahashi, T. (2004). Modeling, Analysis and Control Methods for Improving Vehicle. Dynamic Behavior (Overview). *R&D Review of Toyota CRDL, 38*(4), 1.

Tanaka, H., & Matsunaga, T. (2008, March). Torque Controlled Active Steering for Electric Power Steering. *Mitsubishi Electric ADVANCE*, pp. 11-13.

Tanaka, H., Hitosugi, K., Kurishige, M., & Kifuku, T. (2007). Development of Torque Controlled Active Steering with Improving the Vehicle Stability for Brushless EPS. *SAE Technical Paper 2007-01-1147*.

The MathWorks. (2013). *Optimization Toolbox: User's Guide version 6.4.* The MathWorks, Inc.

Tjønnås, J. (2008). *Nonlinear and Adaptive Dynamic Control Allocation.* Norway: NTNU, Trondheim.

Toffin, D., Reymond, G., Kemeny, A., & Droulez, J. (2007). Role of steering wheel feedback on driver performance: driving simulator and modeling analysis. *Vehicle System Dynamics, 45*(4), 375-388.

Trachtler, A. (2004). Integrated vehicle dynamics control using active brake, steering and suspension systems. *International Journal of Vehicle Design, 36*(1), 1-12.

Tseng, H., Ashrafi, B., Madau, D., Brown, T., & Recker, D. (1999). The development of vehicle stability control at Ford. *IEEE/ASME transactions on mechatronics, 4*(3), 223-234.

Uematsu, K., & Gerdes, J. (2002, September). A comparison of several sliding surfaces for stability control. *In Proceedings of International Symposium on Advanced Vehicle Control,(AVEC)*, (pp. 601-608).

Valášek, M. (2003). Design and control of under-actuated and over-actuated. *Vehicle System Dynamics, 40*, 37-49.

van Zanten, A. (2000). Bosch ESP Systems: 5 Years of Experience. *SAE Technical Paper 2000-01-1633*.

Van Zanten, A. T. (2002). Evolution of electronic control systems for improving the vehicle dynamic behavior. *In Proceedings of the 6th International Symposium on Advanced Vehicle Control*, (pp. 1-9).

van Zanten, A. T., Erhardt, R., Pfaff, G., Kost, F., Hartmann, U., & Ehret, T. (1996). Control aspects of the Bosch-VDC. *AVEC' 96.* Achen.

Van Zanten, A. T., Erhardt, R., Pfaff, G., Kost, F., Hartmann, U., & Ehret, T. (1996). Control aspects of the Bosch-VDC. *AVEC' 96.* Achen.

Vanderbei, R., & Shanno, D. (1999). An interior-point algorithm for nonconvex nonlinear programming. *Computational Optimization and Applications, 13*(1-3), 231-252.

VDI 2206. (2004). *Design methodology for mechatronic systems.* Berlin: Beuth Verlag.

Vidyasagar, M. (2011). *Control system synthesis: a factorization approach.* Morgan & Claypool Publishers.

Virnig, J. C., & Bodden, D. S. (1994). Multivariable control allocation and control law conditioning when control effectors limit(STOVL aircraft). *In AIAA Guidance, Navigation and Control Conference, Scottsdale, AZ*, (pp. 572-582).

Wältermann, P. (2009, April). Hardware-in-the-loop: The technology for testing electronic controls in automotive engineering. *In 6th Paderborn Workshop" Designing Mechatronic Systems" Paderborn.*

Wang, J. (2007). *Coordinated and Reconfigurable Vehicle Dynamics Control (PhD Thesis).* University of Texas.

Wang, J., & Longoria, R. G. (2006). Coordinated vehicle dynamics control with control distribution. *American Control Conference, 2006*, (p. 6).

Wong, J. (2008). *Theory of Ground Vehicles* (4th Revised ed.). John Wiley & Sons.

Yi, K., Chung, T., Kim, J., & Yi, S. (2003). An investigation into differential braking strategies for vehicle stability control. *Proceedings of the Institution of Mechanical Engineers, Part D: Journal of Automobile Engineering, 217*(12), 1081-1093.

Yih, P., & Gerdes, J. C. (2005). Modification of vehicle handling characteristics via steer-by-wire. *Control Systems Technology, IEEE Transactions on, 13*(6), 965-976.

Youla, D., Jabr , H., & Bongiorno Jr, J. (1976). Modern Wiener-Hopf design of optimal controllers--Part II: The multivariable case. *Automatic Control, IEEE Transactions on, 21*(3), 319-338.

Yu, F., Li, D. F., & Crolla, D. A. (2008, September). Integrated Vehicle Dynamics Control—state-of-the art review. *In Vehicle Power and Propulsion Conference, 2008. VPPC'08. IEEE* (pp. 1-6). IEEE.

Yu, Z., Zinger, D., & Bose, A. (2011). An innovative optimal power allocation strategy for fuel cell, battery and supercapacitor hybrid electric vehicle. *Journal of Power Sources, 196*(4), 2351-2359.

Yuhara, N., Horiuchi, S., Iijima, T., Shimizu, K., & Asanuma, N. (1997). An advanced steering system with active kinesthetic feedback for handling qualities improvement. *Vehicle System Dynamics, 27*((5-6)), 327-355.

Zaremba, A., Liubakka, M., & Stuntz, R. (1998). Control and steering feel issues in the design of an electric power steering system. *Proceedings of the 1998 American Control Conference, 1*, 36-40.

Zhang, Y., & Jiang, J. (2008). Bibliographical review on reconfigurable fault-tolerant control systems. Annual reviews in control, 32(2), 229-252. (n.d.).

Zhang, Y., & Jiang, J. (2008). Bibliographical review on reconfigurable fault-tolerant control systems. *Annual Reviews in Control, 32*(2), 229-252.

Zhou, K., Doyle, J. C., & Glover, K. (1996). *Robust and optimal control.* New Jersey: Prentice Hall.

APPENDICES

Appendix A : Linear 2 D.o.F. vehicle model (Bicycle Model)

The investigations of vehicle stability can perform by stability analysis of the differential equations of vehicle motion (3-19). Unfortunately, there is no any general analytical method available for stability criteria of nonlinear systems (Slotine & Li, 1991). One of the simplest yet widely acceptable linear vehicle model to describe vehicle lateral motions, is a two degree of freedom model called bicycle model (Karnopp, 2013; Milliken & Milliken, 1995). Bicycle model provide a suitable mathematical formulation to study the basic aspects of vehicle handling and stability as well as the steady-state response to steering input and the stability of the resulting motion.

To drive the bicycle model, the following assumption is made:

1. The vehicle four wheels are lumped into two 'virtual' wheels in the centreline of the vehicle (i.e. the vehicle is symmetric about its longitudinal plane), so the effects of body roll, normal load transfer and road bank angle are neglected.
2. There is only front wheel steering ($\delta_f = \delta,\ \delta_r = 0$) as shown in Figure A-1.
3. The vehicle longitudinal velocity V_x is constant over a limited period of time, so the derivative $\dot{V}_x = 0$.
4. Slip angle is small so the tyre lateral forces are working in the linear region and approximated to be proportional to the tire slip angle as defined by Eq. (3-46) (i.e. $F_{y,i} = C_{\alpha,i}\,\alpha_i$)
5. The value of cornering stiffness $C_{\alpha,i}$ is considered as twice of its value for one tyre in each axle.

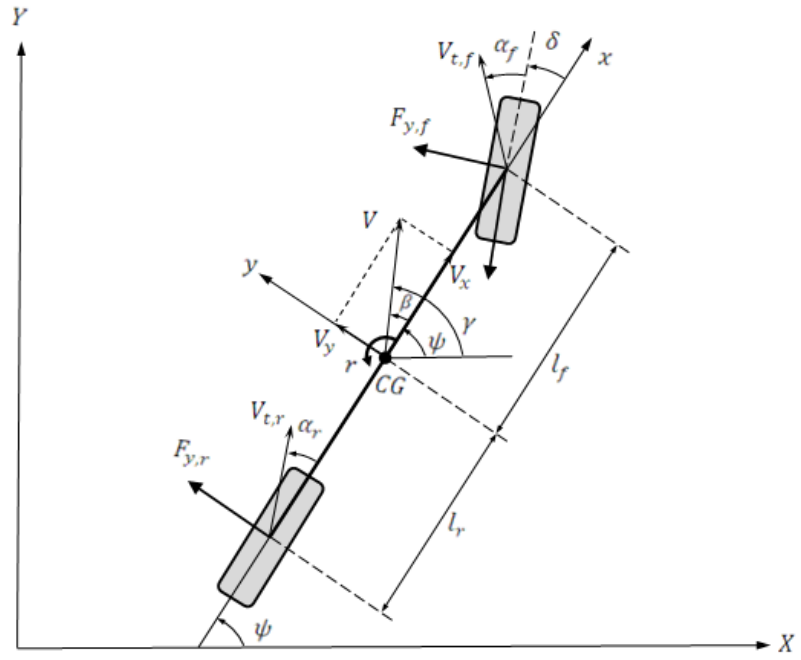

Figure A-1: Bicycle (Dynamic) Model

Considering the above assumptions, Eqs. (3-35) and (3-36) for the lateral translational and rotational yaw moment motions then simplifies to

$$\dot{V}_y = -V_x\omega_z + \frac{1}{m}\left(C_{\alpha,f}\,\alpha_f + C_{\alpha,r}\,\alpha_r\right) \qquad \textbf{(A-1)}$$

$$r = \frac{1}{I_z}\left(l_f\,C_{\alpha,f}\,\alpha_f + l_r\,C_{\alpha,r}\,\alpha_r\right) \qquad \textbf{(A-2)}$$

where $r = \dot{\omega}_z$ is the vehicle yaw rate, $C_{\alpha,f}$ and $C_{\alpha,f}$ are the tyre cornering stiffness's and α_f and α_r are the slip angles of the front and rear tyres respectively. While the cornering stiffness is a parameter which can be measured from the tyre properties, the tyre slip angle should be calculated from vehicle states. From Eq. (3-44) the slip angle for the front and rear wheels can be simplified as

$$\alpha_f = \delta_f - \tan^{-1}\left(\frac{V_y + \omega_z\,l_f}{V_x}\right)$$

$$\alpha_r = -\tan^{-1}\left(\frac{V_y - \omega_z\,l_f}{V_x}\right) \qquad \textbf{(A-3)}$$

And by assuming small angle approximations (i.e. $\tan^{-1}\varphi \approx \varphi$)

$$\alpha_f = \delta_f - \frac{V_y + \omega_z\, l_f}{V_x}$$

$$\alpha_r = -\frac{V_y - \omega_z\, l_f}{V_x} \qquad \textbf{(A-4)}$$

The above approximation works well for small angle, for example the error is within 2% for sine function at $20°$ or for cosine function up to about $10°$.

Vehicle slip angle β is defined as

$$\beta = \frac{V_y}{V_x} \qquad \textbf{(A-5)}$$

The longitudinal velocity was assumed constant, therefore

$$\dot{\beta} = \frac{\dot{V}_y}{V_x} \qquad \textbf{(A-6)}$$

Using the above formulation, Eqs. (A-1) and (A-2) can be written in the following form

$$\dot{\beta} = -\left(\frac{C_f + C_r}{mV_x}\right)\beta - \left(\left(\frac{C_f l_f - C_r l_r}{m\, V_x^2}\right) + 1\right) r + \left(\frac{C_f}{mV_x}\right)\delta \qquad \textbf{(A-7)}$$

$$\omega_z = -\left(\frac{C_f l_f - C_r l_r}{I_z}\right)\beta - \left(\frac{C_f l_f^2 + C_r l_r^2}{I_z V_x}\right) r + \left(\frac{C_f l_f}{I_z}\right)\delta \qquad \textbf{(A-8)}$$

These equations can also be represented in state-space form as

$$\begin{aligned} \dot{\mathbf{x}} &= \mathbf{A}\mathbf{x} + \mathbf{B}\mathbf{u} \\ \mathbf{y} &= \mathbf{C}\mathbf{x} + \mathbf{D}\mathbf{u} \end{aligned} \qquad \textbf{(A-9)}$$

where $\mathbf{x}$, $\mathbf{u}$ and $\mathbf{y}$ are the system state, input and output vectors respectively

$$\mathbf{x} = \begin{bmatrix} \beta \\ \omega_z \end{bmatrix} \quad , \quad \mathbf{u} = [\delta] \quad , \quad \mathbf{y} = \begin{bmatrix} \beta \\ \omega_z \end{bmatrix}$$

and $\mathbf{A}$ is the system, $\mathbf{B}$ is the input, $\mathbf{C}$ is the output and $\mathbf{D}$ is the feed-forward matrixes:

$$\mathbf{A} = \begin{bmatrix} A_{11} & A_{12} \\ A_{21} & A_{22} \end{bmatrix} = \begin{bmatrix} -\left(\frac{C_f + C_r}{mV_x}\right) & -\left(\frac{C_f l_f - C_r l_r}{m\,V_x^2}\right) - 1 \\ -\left(\frac{C_f l_f - C_r l_r}{I_z}\right) & -\left(\frac{C_f l_f^2 + C_r l_r^2}{I_z V_x}\right) \end{bmatrix}$$

$$\mathbf{B} = \begin{bmatrix} B_1 \\ B_2 \end{bmatrix} = \begin{bmatrix} \left(\frac{C_f}{mV_x}\right) \\ \left(\frac{C_f l_f}{I_z}\right) \end{bmatrix}$$

$$\mathbf{C} = \begin{bmatrix} 1 & 0 \\ 0 & 1 \end{bmatrix} \quad , \quad \mathbf{D} = [0]$$

Appendix B : Vehicle, Steering & Brake parameters

	Parameters	Abbreviation	value	Unit
Vehicle	Vehicle Mass	m	1226	kg
	Front Tyre distance to Centre of Gravity	l_f	0.863	m
	Rear Tyre distance to Centre of Gravity	l_r	1.567	m
	Half track	l_w	0.71	m
	Height of CG from the ground	h	0.519	m
	Vehicle Inertia	I_z	1458.76	$kg\ m^2$
	Pneumatic trail	t_{p0}	0.015	m
	Front Tyre Cornering Stiffness	$C_{\alpha f}$	48701.4	N/rad
	Rear Tyre Cornering Stiffness	$C_{\alpha r}$	45836.6	N/rad
	Gravitational Acceleration	g	9.8	m/s^2
Electric Power-Assisted Steering	Steering Wheel Inertia	I_{sw}	0.022	$kg\ m^2$
	Steering Wheel Damping	B_{sw}	0.1661	$N\ m/rad/sec$
	Torque Sensor Stiffness	K_s	134.07	$N\ m/rad$
	Column Inertia	I_c	0.01	$kg\ m^2$
	Column Damping	B_c	0.361	$N\ m/rad/sec$
	Column stiffness	K_c	115	$N\ m/rad$
	Rack and pinion Radius	r_p	0.0081	m
	Steering Arm	l_d	0.1377	m

	Steering Ratio	N	17	
	Rack Mass	M_r	10	kg
	Rack Damping	B_r	653.2	$N\ m/s$
	Wheel Inertia	$I_{z,i}$	1.17	$kg\ m^2$
	DC Motor Inertia	I_m	0,01	$kg\ m^2$
	DC Motor Damping	B_m	0.005	$N\ m/rad/sec$
	DC Motor Stiffness	K_m	125	$N\ m/rad$
	DC Motor Electric Constant	k_e	0.05	$V\ s/rad$
	DC Motor Torque Constant	k_t	0.05	$N\ m/A$
	Motor Gear Ratio	G	13.667	
	DC Motor Armature Resistance	R_a	0.2	Ω
	DC motor Armature Inductance	L_a	0.001	H
Brake	Wheel inertia	$I_{y,i}$	1.17	$kg\ m^2$
	Wheel dynamic radius	R_{dyn}	0.266	m
	Brake gain factor (front)	$K_{b,i} = 10$ $i = 1,2$	10	Nm/bar
	Brake gain factor (rear)	$K_{b,i} = 10$ $i = 3,4$	5	Nm/bar
	line pressure build up time lag	τ_{cal}	.1	sec

Appendix C dSPACE ControlDesck layout

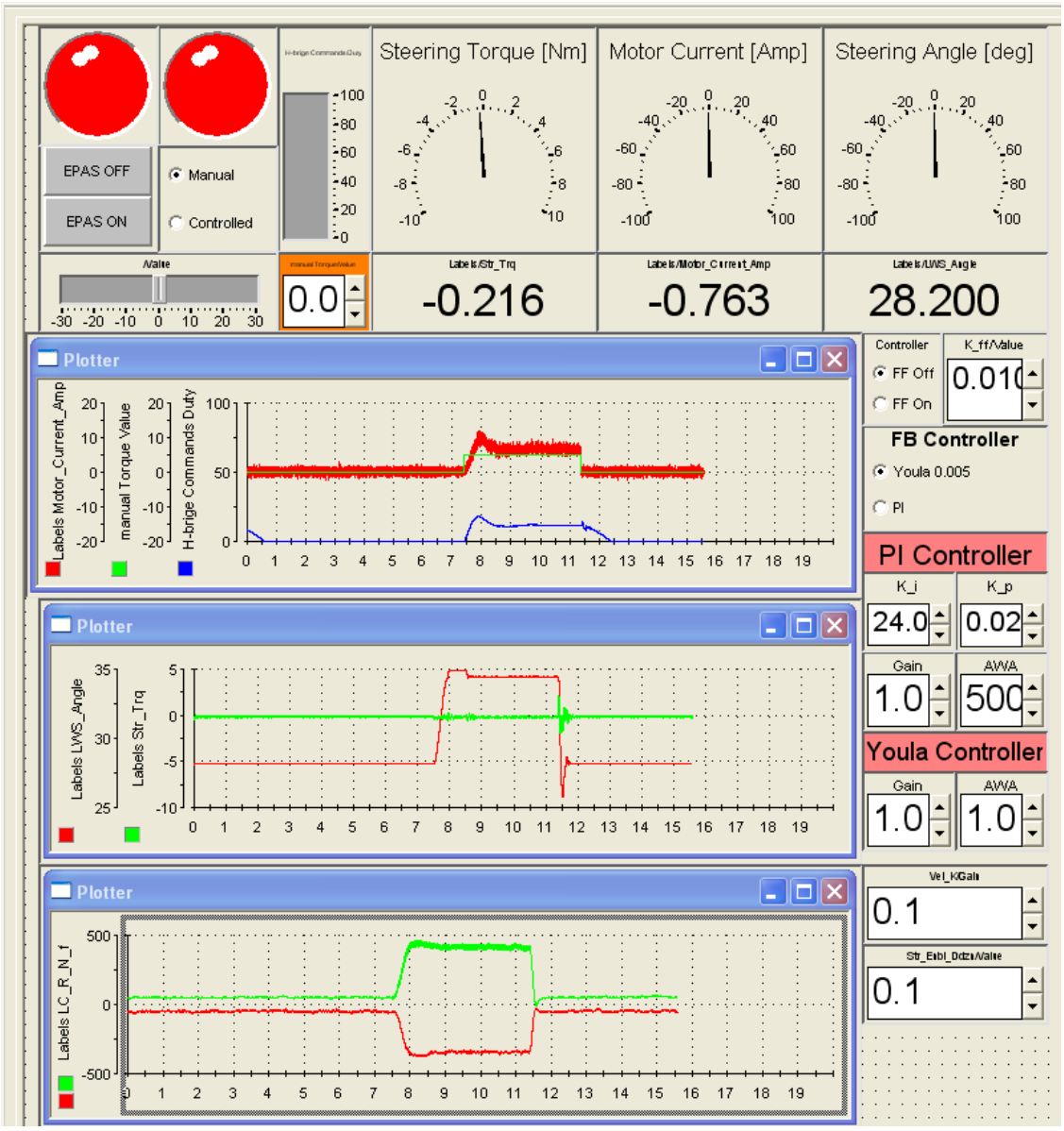

Figure A-2: An example of designed control desk layout (for EPAS Control system)